AGARD

ADVISORY GROUP FOR AEROSPACE RESEARCH & DEVELOPMENT

7 RUE ANCELLE, 92200 NEUILLY-SUR-SEINE, FRANCE

AGARD Conference Proceedings 597

Impact Head Injury: Responses, Mechanisms, Tolerance, Treatment and Countermeasures

(les Traumatismes crâniens consécutifs aux impacts : les mécanismes, la tolérance, le traitement et les contremesures)

Papers presented at the Aerospace Medical Panel Specialists' Meeting held in Mescalero, New Mexico, USA, 7-9 November 1996.

North Atlantic Treaty Organization
Organisation du Traité de l'Atlantique Nord

19980808 037

The Mission of AGARD

According to its Charter, the mission of AGARD is to bring together the leading personalities of the NATO nations in the fields of science and technology relating to aerospace for the following purposes:

— Recommending effective ways for the member nations to use their research and development capabilities for the common benefit of the NATO community;

— Providing scientific and technical advice and assistance to the Military Committee in the field of aerospace research and development (with particular regard to its military application);

— Continuously stimulating advances in the aerospace sciences relevant to strengthening the common defence posture;

— Improving the co-operation among member nations in aerospace research and development;

— Exchange of scientific and technical information;

— Providing assistance to member nations for the purpose of increasing their scientific and technical potential;

— Rendering scientific and technical assistance, as requested, to other NATO bodies and to member nations in connection with research and development problems in the aerospace field.

The highest authority within AGARD is the National Delegates Board consisting of officially appointed senior representatives from each member nation. The mission of AGARD is carried out through the Panels which are composed of experts appointed by the National Delegates, the Consultant and Exchange Programme and the Aerospace Applications Studies Programme. The results of AGARD work are reported to the member nations and the NATO Authorities through the AGARD series of publications of which this is one.

Participation in AGARD activities is by invitation only and is normally limited to citizens of the NATO nations.

Printed on recycled paper

Impact Head Injury: Responses, Mechanisms, Tolerance, Treatment and Countermeasures

(AGARD CP-597)

Executive Summary

The Aerospace Medical Panel (AMP) of the Advisory Group for Aerospace Research and Development (AGARD) held a Specialists' Meeting on "Impact Head Injury: Responses, Mechanisms, Tolerance, Treatment and Countermeasures" in Mescalero, New Mexico, USA, 7-9 November 1996. The meeting was a joint venture with the Stapp Car Crash Conference Advisory Committee (SCCCAC) and the Society of Automotive Engineers (SAE) to honour Col John Paul Stapp, (USAF Ret) for his lifetime achievements in biodynamics and crash protection.

Impact head injury is a major concern of both military and civilian health care workers. Significant advances have been made in understanding the causes and treatment of severe head injury, and in the design and proper use of countermeasures to increase survivability in vehicular accidents. This Specialists' Meeting provided a forum for addressing these issues; the results of which are directly relevant to the NATO Forces and concerned civilian agencies. Benefits derived include:

— new insights into the nature of the biomechanical strains that develop in the skull/brain during impact;

— new understandings of brain injury mechanisms and thresholds associated with diffuse axonal injury, a leading cause of brain death;

— new physical and computer models that relate head/brain impact responses to injury severity;

— improved ways of establishing valid head injury criteria;

— information on the use of brain imaging and signal detection techniques for assessing injury and status for return to flight duties;

— knowledge of the merits of antioxidant drug therapy for controlling secondary brain injuries;

— baseline data on the epidemiology of head injuries in both civilian and military mishaps;

— considerations for improvement, harmonization and enforcement of standards for protective head gear;

— knowledge of new developments in inflatable restraint systems and other energy absorptive concepts as personal protective systems in aircraft and other vehicles;

— description of computer models and design techniques that simulate the human body and the safety system for designing optimal impact head protection.

This venture between AGARD/AMP, the SCCCAC and the SAE is consistent with AGARD's goal of becoming more aware of the dual-use research and technology of other organizations. It marks the first time that these aviation and automotive organizations have jointly addressed a topic of common concern: impact head injuries in vehicular accidents. The success of this meeting suggests that the AMP should continue this process at joint opportunities in other areas of common interest.

Les traumatismes crâniens consécutifs aux impacts : les mécanismes, la tolérance, le traitement et les contremesures

(AGARD CP-597)

Synthèse

Le Panel de médecine aérospatiale de l'AGARD (AMP) a organisé une réunion de spécialistes sur "Les traumatismes crâniens consécutifs aux impacts: Les mécanismes, la tolérance, le traitement et les contremesures" à Mescalero, New Mexico, USA, du 7 au 9 novembre 1996. L'organisation de la réunion a été une entreprise conjointe avec le Stapp Car Crash Conference Advisory Committee (SCCCAC) et la Society of Automotive Engineers (SAE) pour honorer la contribution du Colonel John Paul Stapp à la biodynamique et à la protection contre les accidents de voiture.

Les traumatismes crâniens consécutifs aux impacts sont l'une des préoccupations majeures du personnel soignant civil et militaire. D'importants progrès ont été réalisés dans le domaine de la détermination des causes et du traitement des lésions cérébrales graves, ainsi que dans la conception et la mise en œuvre judicieuse des contremesures pour augmenter les chances de survie en cas d'accident de la circulation. Cette réunion de spécialistes a servi de forum pour la discussion de ces questions dont les résultats sont directement applicables aux forces de l'OTAN et aux agences civiles concernées, à savoir:

— de nouveaux aperçus sur la nature des souches biomécaniques qui se développent dans le crâne/cerveau lors des impacts;

— une meilleure compréhension des mécanismes et des seuils des lésions cérébrales associés aux lésions axonales diffuses, qui sont l'une des principales causes de la mort cérébrale;

— de nouveaux modèles physiques et informatiques qui permettent d'établir le lien entre les réactions aux impacts crâne/cerveau et la gravité des lésions;

— des méthodes améliorées pour l'établissement de critères de lésions crâniennes valables;

— des enseignements sur l'emploi de l'imagerie cérébrale et sur les techniques de détection du signal pour l'évaluation des blessures et de l'aptitude au service;

— une meilleure compréhension des mérites de la pharmacothérapie aux antioxydants pour le contrôle des lésions cérébrales secondaires;

— des données de référence en ce qui concerne l'épidémiologie des lésions crâniennes résultant d'accidents civils et militaires;

— des considérations concernant l'amélioration, l'harmonisation et l'application de normes relatives aux casques de protection;

— des nouveaux développements en ce qui concerne les systèmes de retenue gonflables et d'autres concepts d'absorption d'énergie en tant que systèmes de protection personnels pour avions et autres véhicules;

— des descriptions de modèles informatiques et de techniques de conception qui simulent le corps humain, ainsi que le système de sécurité pour la conception optimisée des casques de sécurité.

Cette entreprise conjointe entre AGARD/AMP, le SCCCAC et la SAE est compatible avec l'objectif que l'AGARD s'est donné, à savoir se tenir mieux informé des travaux de recherche sur les technologies à double usage entrepris par d'autres organisations. Pour la première fois, ces organisations de l'aéronautique et de l'automobile ont examiné ensemble un sujet de préoccupation commune: les traumatismes crâniens consécutifs aux accidents véhiculaires. L'accueil très favorable qui a été réservé à cette réunion suggère que l'AMP devrait poursuivre ce processus, lorsque l'opportunité se présente, dans d'autres domaines d'intérêt commun.

Contents

SESSION I: DYNAMIC HEAD IMPACT RESPONSES

SESSION II: BRAIN INJURY MECHANISMS

SESSION III: MODELLING HEAD AND BRAIN IMPACT RESPONSES AND INJURY

SESSION IX: MODELLING HEAD INJURY COUNTERMEASURES

Paper 27 withdrawn

Preface

Severe head injury resulting from vehicular accidents is a major concern to military and civilian health care workers. In the developed world, 50% or more of highway fatalities are due to head injury. Of injured crewmen involved in fixed-wing propeller and rotary-wing accidents, some 20 to 30% will experience head injuries. Moreover, of aircrew in these accidents experiencing a fatal head injury, some 25 to 30% could have survived had appropriate countermeasures been taken.

Significant advances have been made in the understanding of the causes of severe brain injury and in the factors, both direct and indirect, that contribute to the pathophysiological changes that follow from a severe head injury. Moreover, advances in design and the proper use of countermeasures can significantly reduce head injuries causing death. This Specialists' Meeting addressed the issues of severe head injury from the point of view of:

- the dynamic response of the head during impact;
- brain injury mechanisms in diffuse axonal injury;
- physical and computer models for assessing injury severity;
- human tolerance and injury criteria;
- head injury assessment and treatment:
    - brain imaging and signal detection,
    - antioxidant drug therapy;
- epidemiology in head injury mishaps;
- harmonization and enforcement of standards for protective head gear;
- personal protective systems in aircraft:
    - inflatable restraint systems,
    - other energy absorptive concepts;
- computer simulations for optimizing head impact protective designs.

Aerospace Medical Panel

Chairman: Dr P. VANDENBOSCH
Loriesstraat, 44
B-1500 HALLE
Belgium

Deputy Chairman: Lt.Col E. ALNAES
(Chairman as of   Oslo Military Clinic
12 October 1996)   Oslo Mil/Akershus
                      N-0015 OSLO
                      Norway

TECHNICAL PROGRAMME COMMITTEE

Chairmen

Dr J.P. LANDOLT
DCIEM
1133 Sheppard Avenue West
PO Box 2000
North York, ON M3M 3B9
Canada

Dr R.R. BURTON
Armstrong Laboratory
2509 Kennedy Circle
Brooks AFB, TX 78235-5118
USA

Members

Prof A.I. KING
Wayne State University
818 W Hancock
Detroit, MI 48202
USA

Dr I. KALEPS
Armstrong Laboratory
2610 7th Street
Wright-Patterson AFB, OH 45433-7901
USA

Dr D.H. GLAISTER
RAF School of Aviation Medicine
Farnborough, Hants GU14 6SZ
United Kingdom

Dr A. LEGER
Sextant Avionique
Rue Toussaint Catros, B.P. 91
33166 Saint Médard en Jalles, Cedex
France

Col D.F. SHANAHAN
US Army Aeromedical Research Laboratory
Fort Rucker, AL 36362 - 0577
USA

SAE COORDINATOR

Mr M.J. ASENSIO, Jr
Society of Automotive Engineers
3001 West Big Beaver Road
Suite 320
Troy, MI 48984-3173
USA

PANEL EXECUTIVE

Mail from Europe and Canada:
Major R. POISSON, CF
AGARD/NATO
7, rue Ancelle
92200 Neuilly-sur-Seine, France

Tel: (Paris) 1 55 61 22 60
Telefax: 1 55 61 22 99

Mail from USA:
AGARD/NATO/AMP
PSC 116
APO AE 09777

Acknowledgements

TECHNICAL EVALUATION REPORT

by

Jack P. Landolt, PhD
Defence and Civil Institute of Environmental Medicine
1133 Sheppard Ave. West, P.O. Box 2000
North York, Ontario, Canada M3M 3B9

1. INTRODUCTION

The Aerospace Medical Panel (AMP) held a Specialists' Meeting on "Impact Head Injury: Responses, Mechanisms, Tolerance, Treatment and Countermeasures" at Inn of the Mountain Gods, Mescalero, New Mexico, USA, 7-9 November 1996. The Meeting was sponsored by NATO Advisory Group for Aerospace Research and Development (AGARD) in cooperation with the Stapp Car Crash Conference Advisory Committee (SCCCAC) and the Society of Automotive Engineers (SAE) to honour Col John Paul Stapp (USAF Ret.), MD, PhD, and address a topic of importance to the organizers. The SCCCAC, led by Prof Albert I King, Director, Bioengineering Center, Wayne State University, Detroit, Michigan, USA, strongly supported the venture and contributed eleven solicited papers to the Meeting. In total, twenty-three invited papers were given from four NATO countries. A Special Luncheon Address: Doing Safety Research Safely was given by Col Stapp. There were 170 registrants for the Meeting including nationals from Australia, China, India, Iraq, Israel, Japan, Pakistan and Sweden.

There was also a half-day technical tour that started with a visit to see the "Sonic Wind I", a test sled at the Space Center in Alamogordo, New Mexico on which Col Stapp conducted many of his early studies on the effects and limitations of mechanical forces on the human body. The tour concluded with a trip to 46th Test Group, Holloman Air Force Base to observe the capabilities of the High Speed Test Track. This facility, having a track length of almost 10 miles, simulates flight trajectories, including seat ejection sequences to test life support systems, by means of rocket sleds operating on heavy duty crane rails.

2. THEME

The theme of the Specialists' Meeting concerned the recurring operational problem of impact head injury resulting from vehicular accidents. This is a major concern of both military and civilian health care workers. In the developed world, 50% or more of highway fatalities are due to head injury. Of injured aircrew in survivable fixed-wing-propeller and rotary-wing accidents, some 20 to 30% will experience head injuries. Moreover, of those aircraft occupants experiencing a fatal head injury, some 25 to 30% could have survived had appropriate countermeasures been taken. (Head injury is not as pervasive a problem in jet aircraft, escape system accidents, accounting for less than 5% of all injuries.)

Significant advances have been made in the understanding of the causes of severe brain injury and in the factors, both direct and indirect, that contribute to the pathophysiological changes that follow a severe head injury. Moreover, advances in design and the proper use of countermeasures can significantly reduce head injuries causing death. Papers were invited that discussed these advances.

3. PURPOSE AND SCOPE

There is a continuing requirement in NATO to reduce fatalities from, and improve survivability to, head injuries from accidents in

both fixed- and rotary-wing aircraft. The purpose of this Specialists' Meeting was to bring together experts in a variety of disciplines to discuss new directions and findings that are relevant to reducing and controlling severe head injuries.

Speakers were invited to address impact head injury from the following perspectives:

- the dynamic response of the head resulting from direct and indirect impacts,
- injury mechanisms of the head and brain,
- human tolerance and injury criteria,
- head injury assessment and treatment,
- physical and analytical modelling,
- epidemiology of head injury mishaps, and
- injury countermeasures.

The participants included military and civilian experts in biomechanics, cognitive psychology, neuropsychiatry, neurology, neuropathology, neurosurgery, orthopedic surgery, trauma medicine, epidemiology, mathematical modelling, biomedical and other engineering disciplines, and those concerned with operational requirements. Presentations were solicited from industry, defence and other governmental research laboratories, universities, and military and civilian health care centres.

4. SYMPOSIUM PROGRAM

The focus of this Specialists' Meeting was impact head injury. Papers were solicited that addressed issues in nine sessions as follows:

a. Session I - Dynamic Head Impact Responses
    Chairmen: Prof A.I. King, US and
            Dr R.R. Burton, US
Three papers discussed injury patterns of head structures to impact.

b. Session II - Brain Injury Mechanisms
    Chairmen: Prof A.I. King, US and
            Dr R.R. Burton, US
Two papers described the mechanical loading

and thresholds for diffuse axonal injury.

c. Session III - Modelling Head and Brain Impact Responses and Injury
        Chairmen: Dr J.P. Landolt, CA and
        Prof A.I. King, US
Three papers addressed physical and finite-element modelling of the effects of impact acceleration on the head/brain.

d. Session IV - Human Tolerance and Injury Criteria
        Chairmen: Dr J.P. Landolt, CA and
        Dr I. Kaleps, US
Two papers discussed traumatic injury measures for determining head injury risk.

e. Session V - Head Injury Assessment and Treatment
        Chairmen: Dr R.R. Burton, US and
        Dr D.H. Glaister, UK
Two papers provided some insight into secondary injury assessment and prevention following a severe head impact. Another paper discussed modern neuropsychological assessment for determining brain damage to impact.

f. Session VI - Head Injury: Epidemiology in Mishaps
        Chairmen: Dr R.R. Burton, US and
        Dr D.H. Glaister, UK
Two papers reported on the epidemiology of head injuries; one in civilian accidents, the other on US Army rotary-wing mishaps.

g. Session VII - Standards and Improvements in Protective Helmets
        Chairmen: Dr D.H. Glaister, UK and
        Dr R.R. Burton, US
Three papers reported on helmet components designed for head protection, and spoke for the harmonization and enforcement of standards for protective headgear.

h. Session VIII - Head Impact Protective Systems and Issues
        Chairmen: Dr J.P. Landolt, CA and

Dr I. Kaleps, US

Three papers described the use of air bags, wall padding, articulating seats and energy absorptive structures as protective systems in helicopter and commercial aircraft. A fourth paper discussed head/neck loads on Indy car drivers during high speed crashes.

i.   Session IX - Modelling Head Injury Countermeasures
     Chairmen: Dr I. Kaleps, US and
     Dr J.P. Landolt, CA

One paper described the use of computer models for simulating both the human body and the safety system to determine optimal head impact protection.

5. TECHNICAL EVALUATION

5.1 Dynamic Head Impact Responses

A good knowledge of the biomechanically-induced strains imparted on the skull/brain complex during controlled impacts under laboratory conditions is essential for correlating physical processes to biological (dys)function. This information may then be used to develop computational models, including three-dimensional, finite element models of the human head with which to conduct parametric studies under traumatic loading to predict the risk of injury and prepare safer protective devices.

Kallieris and colleagues (Paper #1) reported on some injury patterns and the associated severity of skull/brain trauma that results from head impact. The findings of autopsies from accident cases, and experiments in cadavers to frontal, lateral and occipital head impacts at velocities of 20 km/h against rigid and padded obstacles were compared. Skull and brain injury patterns were similar in the two methods, and comparable to head impacts occurring from a sudden fall on the road. The brain injuries of both the cadavers and the accident findings included contrecoup subarachnoidal hemorrhages which may have

been caused by skull-brain interactions including contributions resulting from rotational head motions. These hemorrhages were more severe in accident cases than in experimental exposures, maybe because of differences in impact intensities delivered and/or possibly because of deficiencies in filling the capillary beds with blood during cadaveric repressurization. Padding prevented skull fractures but not brain injuries which would tend to support the notion of a skull-brain interaction during impact. This study demonstrated the potential of using appropriately-prepared cadavers for assessing brain tissue responses in impact conditions.

Nonembalmed specimens of nonpathological human cadaveric skulls were studied by Sances, Jr., and colleagues (#2) to determine the nondestructive and destructive biodynamical properties of the head under static and dynamic loading. Force-deformation curves for the nondestructive tests returned to normal conditions following the tests. For the destructive tests, each specimen was dynamically loaded once to failure. Force-deflection responses for these tests were strictly nonlinear, showing significant amounts of hysteresis. A wide variety of complex injury patterns appeared, including bilateral and multiple fractures. Skull fracture widths were consistently wider at sites remote from the loading region. The biomechanical parameters of force, deformation, stiffness and energy obtained in these tests provided further fundamental data with which to develop valid computer models for establishing injury risk.

Few experimental studies have quantified the loads required to produce basilar skull fractures resulting from compressive neck loading. Paper #3 by Myers, Richardson and Nightingale described basilar skull fractures resulting from a near vertex head impact in a human cadaver model. Ligamentous head-neck specimens were coupled to a 16-kg simulated torso mass and dropped onto impact surfaces at a height of 53 cm. Of 16 injuries occurring, basilar skull

fractures resulted from one drop onto a padded impact surface, and from two drops onto a rigid surface. Interestingly, the drop height that produces this type of injury is lower than corresponding ones required to cause cranial vault fractures resulting solely from head inertial loading. In fact, these injuries occurred as a result of neck impact surface loading and were not related to head impact acceleration. This means that criteria, such as the Head Injury Criterion (HIC), which are based on head acceleration are not applicable. This being the case, it is unlikely that the addition of surface padding will mitigate basilar skull fractures resulting from compressive neck forces. The authors believed that such injuries actually may be potentiated by the addition of surface padding. They also suggested that compressive neck injury force tolerance might be a more suitable criterion for predicting basilar skull fracture.

5.2 Brain Injury Mechanisms

Diffuse axonal injury is one of the most common types of severe brain damage observed in closed head injury. It is thought to be associated with the progressive biomechanical tearing over time of axons in the cerebral hemispheres following a severe head impact. Loss of consciousness and brain swelling followed by loss of life or severe mental and motor deficits are common sequellae to this type of brain injury.

The dynamic loading conditions causing diffuse axonal damage patterns are not well characterized. Miller et al. (#4) provided some experimental evidence demonstrating that an abrupt, biphasic rotational head acceleration/deceleration contributes to the distribution and severity of diffuse axonal injury. Results obtained in miniature swine showed that axonal injury was revealed throughout the cerebral hemispheres and brainstem. The injury pattern displayed correlated well with the inertial loading conditions. Injury onset thresholds were estimated in terms of peak loading parameters. Injury severity versus load conditions was not significant because of the small sample size. Although incomplete, further trends such as these may provide a basis for determining brain injury criteria that relate head motion to diffuse axonal injury.

Bain et al. (#5) used guinea pig optic nerve bundles to determine traumatic thresholds for diffuse axonal injury. A mechanical device delivered a controlled amount of elongation , in vivo, to the optic nerve. A range of displacements was used to characterize the continuum of deformations leading to axonal injury. Standard immunohistochemical techniques were used to assess the severity of axonal injury. A frequency distribution function was determined to represent the degree of axonal stretch imparted by the force applied to the optic nerve bundle. By combining this information with concepts in quasi-linear viscoelastic theory, a mathematical basis was established for relating the material. properties of stress-strain to injury thresholds in the individual axons. (In other words, the model enabled the extent of damage to be correlated with the mechanical parameters to establish injury thresholds.) Although requiring complex mathematical formulations, this framework shows promise for characterizing tissue level criteria in human head injury. It also lends itself readily to computational constructs for predicting severity of diffuse axonal injury.

5.3 Modelling Head and Brain Impact Responses and Injury

Computer models, some employing finite element structures, are being used extensively to relate experimental head impact response data to injury potential. Novel physical models have also been developed to gain knowledge of the complex interaction of skull and brain components for the abrupt decelerations encountered during impact. Session III dealt with both types of model.

Nusholtz, Glascoe and Wylie (#6) used a water-filled aluminum cylinder as a physical head model to investigate the significance of brain material on the development of pressure gradients in the brain during head impact. Previous studies using the same model had shown that the complex nature of skull-brain interaction during severe head impact resulted in contrecoup cavitation followed by a sudden, sometimes violent, vapour cavity collapse which could be, potentially, a mechanism for brain injury. In this study, the authors assessed the effects of a pre-existing brain stress such as neck loading on brain cavitation. This stress could be induced by either a long duration, low acceleration or by an angular motion prior to head impact. Results from this model were then employed in two computational models designed to further investigate this effect. The computational models suggested that, in closed head impacts, pre-existing stresses in the brain potentiate cavitation. This cavitation, in the form of micro-voids in the brain material itself, may be a contributory cause of diffuse axonal injury. If more extensive studies support these findings, then the implications for reducing neck loading in the vehicle environment may be quite profound!

Paper #7 was to have discussed the simulation of the effects of angular and linear acceleration on a silicon gel 'brain'. The results of this were to be used to refine finite element models of brain displacement and deformation during head impact. Mechanisms of associative brain injury were also to have been discussed. However, the authors were unable to make the presentation.

Finite element modelling also has application to accident reconstruction and the assessment of occupant injury mechanisms. Zhou et al. (#8) used such techniques to identify areas of high shear strain in the brain of a crash victim who had succumbed to an automotive side impact. In addition to the usual components of the head (scalp, skull, cerebellum, brain stem, etc.), this finite element model featured the different viscoelastic properties of the cerebral gray and white matter, the ventricles and the parasaggital bridging veins. Injury mechanisms resulting from pure translational and pure rotational impact accelerations were studied. The finite element results were compared to brain autopsy data showing diffuse axonal injuries. In particular, the shear stress contours exhibited by the finite element model corresponded well with autopsy results of diffuse axonal injury in the corpus callosus. The crash reconstruction also indicated a possible head contact with the hood of the striking vehicle, even though there was no such sign at autopsy. This study demonstrated the effectiveness of three-dimensional, finite element analysis as an adjunctive tool in predicting and diagnosing brain injuries, such as diffuse axonal injury, in complex human-systems interactions resulting from a motor vehicle accident.

Ueno and Melvin (#9) are developing tissue-level criteria to predict brain injury during impact. They have produced experimental brain injury in an animal model that is compatible with the mechanical state of the tissue at the injury site. A method for directly impacting the cortex was devised which generated reproducible graded levels of injury severity. A three-dimensional, finite element model was produced to assess the dynamic stresses and strains in the human brain during head impact. This model is being validated against the experimental biomechanical responses obtained from the animal studies. When finalized, the model may be able to predict the potential for head injury to both contact and noncontact loading of the head. In the paper given at this Specialist's Meeting, the authors utilized three nonlinear, finite element codes - Dyna3D, Pamcrash and Abaqus - to validate the displacements and stresses in the brain following a bilateral cortical impact. Although results were comparable in the three methods, Dyna3D and Pamcrash were better from the point of view of efficiency and economy. Both are explicit time integration

codes, meaning that results are determined according to the immediate past history of the dynamic state of the brain under impact. Abacus is an implicit code; i.e., it uses both current and past time histories. It is more accurate but very time consuming and costly to implement.

5.4 Human Tolerance and Injury Criteria

To adequately describe a brain injury criterion that is predictive and reliable, one must relate brain deformations and strains resulting from an impact to tissue-level dysfunction. Bandak et al. (#10) described techniques, using a finite element model and experimental data from the miniature pig brain in combination with dummy test measurements, for developing quantitative measures to assess traumatic brain injuries observed in automotive crashes. These measures are:

- the Cumulative Strain Damage Measure - an index of diffuse axonal injury - which monitors the cumulative magnitude (volume) of brain tissue experiencing tensile strains greater than some specified level under dynamic loading,
- the Dilatation Damage Measure, which calculates the volumetric fraction of brain tissue that reaches a specified pressure threshold, and
- the Relative Motion Damage Measure, which assesses brain movements resulting from both rotational and angular accelerations of the head.

Head impact dummy tests were analyzed to obtain loading conditions for the finite element analysis of a human brain simulation. Some of the quantitative measures obtained were computationally related to the values of the HIC. The authors asserted that preliminary indications are that these techniques appear feasible for assessing traumatic brain injury. However, tissue material properties and injury threshold values to impact will need to be improved or refined, and different loading conditions have to be studied before the feasibility of these measures is assured.

Moreover, although these early results are promising, more complex brain models will need to be developed and validated under rigorous test conditions before these measures become truly meaningful.

The HIC takes into consideration the average resultant acceleration of the centre of mass of the rigid head during an impact for a time interval which maximizes the value to the HIC. Historically, the value of HIC was chosen to not exceed 1000. Any time interval for which HIC exceeded 1000 would risk a head injury. The US Federal Motor Vehicle Safety Standard 208 has set a limit of 36 ms for that time duration. It was noted by Mertz and colleagues (References 1 & 14 in Paper #11 by Mertz, Prasad and Nusholtz) that such a limit gave unrealistic values of the HIC in dummy testing for air bag interactions and three-point restraint system applications where there was no head contact. They recommended a time interval of 15 ms or less to predict risk of head injury in these instances. The risk of significant closed head (brain) injury as a function of the 15-ms HIC has been further developed in terms of a probabilistic model; the Head Injury Risk Curve (HIRC). Mertz, Prasad and Nusholtz (#11) modified the HIRC by including an expanded cadaver data base of non-skull-fracture, 15-ms HIC values to develop a new statistical index of risk; the Skull Fracture Risk Curve (SFRC). The efficacy of the SFRC was demonstrated by comparing its predictions to results of simulated fracture impacts from a finite element model of the head. The HIRC was not changed as no additional brain damage data were analyzed.

Both HIC and the HIRC/SFRC have been criticized as methods of predicting closed head injury risk (see ISO/TC22/SC12/WG6/N453). Some of the criticisms include:

- the relative motion of the brain to the skull is not considered, therefore, it is erroneous to assume equivalence of dummy and cadaver head acceleration responses to impact,
- the effects of rotational acceleration are

ignored,
- skull fracture is not a necessary and sufficient condition for the occurrence of a closed head injury, and
- the historical HIC is a poor approximation to the original data from which it was derived.

Notwithstanding these criticisms, Mertz and colleagues show the efficacy of the HIRC in predicting head injury reductions stemming from the introduction of air bags in automobiles and from the improvements implemented in football helmets. There is also the fact that, at the moment, there are no satisfactory alternatives to using HIC or its derivative forms when assessing head injury risk. It must also be recognized that current biomechanical data are not really adequate for assessing low injury risks of approximately 1%. The continuing struggle to establish a satisfactory correlation between head/brain injury and HIC emphasizes the need to develop good tissue-level criteria that realistically predict injury during impact as well as being practical to implement.

5.5 Head Injury Assessment and Treatment

Post-mortem examinations show that cerebral ischemia/infarction, both local and diffuse, is the most common form of secondary damage resulting from an acute brain injury. The concept is that this occurs as a result of a mismatch between the brain's ability to maintain an adequate blood supply to the whole brain and regions within it, and the stresses that precipitate ischemia. Such stresses include arterial hypotension, hypoxia, high fever, raised intracranial pressure (ICP), mediators of secondary injury such as toxic amino acids and free radicals, etc. The mechanisms of secondary brain cell damage frequently last only for a few minutes and their detection and subsequent sequelae require advanced methods in real-time monitoring and analysis. Pickard and colleagues (#12) argued for the use of functional brain imaging and multimodal bedside monitoring at these critical times to reveal the consequences

of ischemia in the acute brain-injured patient. The authors hoped that the outcome from such efforts would lead to useful 'end points' in patients for assessing the therapeutic and side effects of novel neuroprotective agents. Functional brain imaging will aid in identifying such regional aspects as tissue viability and swelling, blood flow, and drug penetration and binding. To expedite functional brain imaging on critically ill patients, Pickard et al. recommended incorporating such systems - positron emission tomography (PET) and functional magnetic resonance (fMR) scanners - directly within the Critical Care Unit to reduce logistic problems which could increase the risk of secondary deterioration. He strongly advocated long-term, clinical bedside monitoring employing information gathered from several different sensors together with suitable computer analysis to provide an improved and immediate diagnostic interpretation of patient health status. Multimodal monitoring would include such continuous measurements as ICP, brain temperature, blood oxygen saturation, and blood flow.

Paper #13 was to have discussed differences between elecroencephalographic and magnetoencephalographic endogenous and evoked activity to auditory, visual and somatic stimuli for localizing the sources of functional deficits following brain injury. However, the authors were unable to make the presentation.

Drew and Patterson (#14) addressed the issue of the association of closed head injury with observation time before clearance for return to flight duty. The two primary concerns in returning the seemingly fully-recovered aviator to flight status after receiving a closed head injury are:
- the presence of subtle cognitive deficits that are not apparent on clinical examination, and
- the risk of late post-traumatic seizure.

Both conditions are becoming increasingly important for flight safety as aviation missions

are requiring more and more of '... the highest levels of cognitive functioning and psychomotor skills ...' to operate the aircraft. The USAF returns closed head injured aviators to flying duties according to their status as mildly, moderately or severely injured. A mild injury implies a return in thirty days if the neurological examination is normal and cognitive dysfunction is not evident. Seizure risk, which is found mostly in moderately or severely injured patients, is more problematic. Moderate and severe cases undergo an extensive examination and may require a period of observation up to five years before there is a return to flying. Drew and Patterson are designing a ten-year study that will evaluate closed head injury serially at thirty days, six months, two years and five years post-accident in a cohort population. Those who perform satisfactorily at any of these epochs will return to flying. The investigators will employ standard neurological methods with neuroimaging techniques (computerized tomography, magnetic resonance imaging, electroencephalography, etc.) and modern neuropsychological testing (Cogscreen, Multidimensional Aptitude Battery, etc.) to see if a more realistic assessment can be made of the medical disposition of aviators having closed head injuries at each of the epochs cited above. A computerized data entry and reporting system is being constructed that will allow others to participate: Hopefully, with the help of others, this will increase the number of reported injuries and, accordingly, increase the likelihood of providing statistically significant results in as short a time as possible.

Participating in the compilation of such a data base is well suited to the capability and needs of NATO/AGARD/AMP. Participation by a multi-national organization such as the AMP would certainly enhance collection of data should the authors and the Laboratory feel compelled to try this approach. Recent experiences by the AMP in a study on the effects of +Gz on subclinical disorders (Working Group 18) are testimony to the

effectiveness of such an approach. Working Group 18 utilized information from fifteen hundred cases from thirteen NATO countries to develop a database from which it was determined that there was no damage to the heart from high Gz forces as assessed by echocardiograhic techniques. No single country had sufficient data to undertake such a study on its own.

Muizelaar (#15) spoke to the issue of secondary (or delayed) injury prevention following severe brain trauma. He indicated that these injuries are of two types: One is caused by cerebral ischemia and/or hypoxia, the other by biochemical cascades resulting from mechanical trauma. Ischemia occurs when the cerebral blood flow decreases to the extent that oxygen and glucose supplies cannot accommodate tissue energy demands. Ischemia that occurs under conditions of normal blood pressure and ICP can be prevented by not treating spontaneous arterial hypertension, by rapidly removing hematomas to decrease ICP, by not hyperventilating the patient in the early stages of trauma, and by giving mannitol to increase vascular filling and decrease blood viscosity. Biochemical cascades result from an impairment of cellular homeostasis. There may be several cascades, they may run in parallel and they may be interconnected. During the post-traumatic period, endogenous mediators are released, including oxygen free radicals, arachidonic acid and its metabolites (eicosanoids), excitatory amino acids (mainly glutamate), etc., all of which are suspected of causing delayed brain damage. The cascades also include the release of Ca- and Na-ions, and water influx into the cell which disrupt major metabolic pathways and membrane permeabilities. Interestingly, these cascades are similar to those encountered in stroke; thereby, leading investigators to try similar therapeutic intervention strategies. To protect against secondary injuries occurring, treatment intervention would have to be initiated within 8 hours after injury. Muizelaar noted that drug therapy aimed at controlling a number of these

cascades has been successful in animal studies; however, the benefit of drugs in human clinical trials has been limited.

5.6 Head Injury: Epidemiology in Mishaps

A very systematic study of head injuries in motorcycle accidents was conducted by Doyle and Sturrock (#16). Non-fatal accidents were assessed through brain imaging and fatal ones by extensive neuropathological assessments. The predominant pathology observed was focal brain damage, although true contrecoup injuries were difficult to prove. Difficulties were encountered in assessing brain damage in immediate deaths and those after very short survival periods. In some instances where little obvious brain damage was evident, there were indications, nevertheless, of severe impact by studying the damage to the protective helmet. In these cases, a careful brain examination would reveal small patches of subarachnoid hemorrhage and/or hemorrhage from ruptured ventricles. The authors argued for a concept of diffuse vascular injury resulting from blood vessel loading to describe the intracerebral contusions and hemorrhages. They stated further that vascular distortions may be responsible for the generation of diffuse axonal injury. The implications of improved helmet designs to alleviate some of these injuries were discussed. The authors recommended the wearing of protective helmets by occupants of all types of vehicles.

Shannon, Albano and Licina (#17) reported in a very comprehensive retrospective study, over the three time intervals: 1980-84, 1985-89 and 1990-94, the trends in head injury patterns occurring in US Army helicopter accidents in terms of survivability. (A mishap was considered to be survivable if the mechanical forces sustained by a crew member were within human tolerances and the cockpit structure maintained a minimal livable space.) Since 1980, sixty percent of cockpit crew members involved in a ground-strike mishap had sustained an injury. One-third of these injuries

were fatal. One-half of the injuries included injury to the head. More significantly, even with improvements in crashworthiness and personal protective equipment, well over half of all fatalities were from an injury to the head. The risk of injury to all parts of the head (i.e., face, skull and brain) decreased by about twenty-five percent in potentially survivable mishaps between 1980-84 and 1990-94. No similar differences in traumatic injury reductions to the neck, torso and upper extremities were demonstrated, although lower extremity injuries were significantly reduced. No causative factor was identified to account for the decrease in head injury. However, the authors noted that a new aircrew helmet, the SPH-4B having improved protective capability, was put into service in 1990 (see comments in **5.7** regarding paper on subject topic by McEntire). The authors estimated that seventeen lives have been saved by reducing the mortality rate over the fifteen-year period: 1980-94.

5.7 Standards and Improvements in Protective Helmets

Glaister (#18) spoke to the matter of standards for protective head gear, noting that the protection provided by manufacturers is close to the level - a minimal level at that - defined by the standards. He stated that standards-making bodies are obligated to ensure that maximal protection for the public at risk is given even though this may be difficult to achieve because of the cultural, climatic, philosophical and other demands of member nations. Particular areas for standardization of protective helmets include resistance to penetration, absorption of linear impact forces, reduction in angular impact forces, helmet retention and aging. Glaister noted the need for a better definition of brain injury mechanics and brain injury thresholds to expedite the process of standardization. He elaborated on efforts for the harmonization and enforcement of helmet standards. He requested the continued compilation and application of accident data, the use of new materials as protective helmet

components, the development of effective test methods and noted the public acceptance of the wearing of helmets. All of these different ways will enable standards makers to enforce helmet manufacturers to improve their helmets. He gave examples of standards that are applicable to military applications, reviewing, in particular, Standard BS 6658 on protective helmets for vehicle users.

A directly related paper by McEntire (#19) described the improvements made in US Army aircrew helmets, since the introduction of the SPH-4 in 1969. That helmet, of fiberglass construction, provided increased sound attenuation but a negligible increase in head impact protection over previous models. Subsequently, significant changes were made to improve head impact protection, resulting in the Kevlar-based SPH-4B. Now, additional functional requirements for weapon targeting, a night vision capability, flight symbology, and nuclear flash protection necessitate further helmet improvements. A new helmet, the HGU-56/P, which offers some of these features in addition to improved impact protection, was introduced in 1995 to US Army aircrew. Improved protective features include a hybrid nylon-graphite helmet-shell construction, a thermoplastic liner, crushable ear cups, a fitted liner and decreased mass. The feasibility of using the HGU-56/P as a US Army standard mounting platform for securing helicopter avionics is currently being explored.

Recommendations for helmet mass and centre-of-mass location requirements to reduce neck loading in operations employing helmet mounted devices were presented in a paper by McEntire and Shanahan (#20). Based on limited data available, these authors determined a maximal allowable helmet mass of 2.5 kg, and maximal allowable vertical and longitudinal centre-of-mass locations of 5.2 cm and 9.5 cm, respectively. Between these limits, the centre-of-mass location is defined as an algebraic function of helmet mass and expressed as a curve. Exceeding the vertical limits as defined

by this function places the operator at risk of severe neck injury, while surpassing the longitudinal limits imposes user fatigue and performance decrements. The authors cautioned on using these results however, indicating that further data need to be collected for verification. In particular, the neck strength to loading, and user tolerance and the fatigue effects of the mass properties of head supported devices need to be determined. Obtaining such information is important as it may impact on selection standards and the training of future helicopter aircrew.

5.8 Head Impact Protective Systems and Issues

Air bags are widely used in automobiles to guard against injury in frontal impacts, and, now, are being introduced for side impact protection. Zimmerman and Yaniv (#21) described current research and development programs at Simula Government Products Inc., Phoenix, AZ that have demonstrated the feasibility of designing a variety of safe and effective inflatable restraint systems for both military and civilian vehicles. These are of four types:

- the Passenger Air Bag System (PABS), which is mounted on partitions such as bulkheads for occupant protection in adjacent facing seats in commercial aircraft,
- the Cockpit Air Bag System (CABS) for attack (three bags - front and two sides) and utility (four bags) helicopter crew stations,
- the Inflatable Body and Head Restraint System (IBHRS), a five-point restraint system with air bags attached to the shoulder straps, for protecting against lethal cockpit projections in attack helicopters, and
- the Inflatable Tubular Structure (ITS), a novel side impact device for head protection that is applicable to small helicopters and automobiles.

Safety issues of concern such as non-impact deployment and its subsequent obstruction of the field of view, appropriate air bag shape, size and number, and speed of deployment were

some of the factors considered in the designs. With completion of the developmental process, kits will be furnished by Simula for installation in a variety of aircrafts and automobiles.

Using mathematical simulations, Alem et al. (#22) assessed the benefits of using air bags in reducing head and neck injuries in helicopter crashes. Additionally, the roles of the restraint system and the energy absorbing seat stroke were also investigated. The crash kinematics from a potentially survivable US Army AH-64 Apache helicopter crash in which a pilot was killed were used as input to the simulations. Pilot death was caused by a fatal basilar skull fracture thought to have occurred when the pilot's helmet struck and became jammed under the glare shield mounted on the cockpit instrument panel. It was conjectured that a delay in inertia reel locking together with an inadequate seat stroking due to a cockpit structural distortion contributed to the head strike. In all simulations, whether an air bag was used or not, when the restraint system and seat stroking functioned properly, peak neck loads were reduced by as much as 68%. Most importantly, however, when air bags were used in the absence of a working harness, neck load levels were confined well within acceptable injury assessment corridors. These simulations demonstrated the potential of air bags for reducing the severity of head and neck injury resulting from contact with cockpit interior structures, such as the glare shield, instrumentation panel, gun sights, etc. Furthermore, they showed the utility and cost effectiveness that good biodynamic models used in conjunction with sound (yet simple) simulations can offer the design engineer or accident investigator involved in these types of issues.

The US Federal Aviation Administration (FAA) amended the airworthiness requirements for impact protection in newly-designed transport aircraft in 1988. Head impact protection entails, as a minimum requirement, no evidence of head contact with an interior aircraft structure or a HIC of less than 1000 determined on a test dummy during contact. The initial focus of research and development within the airline industry was directed at the potential for head injury in forward-facing seating positions located directly behind bulkheads or partition walls. Designs proposed to meet these new requirements for head impact protection included:

- air bags,
- articulating seats and other seat design modifications,
- modified lap-belt anchoring positions, and
- energy-absorptive interior structures including wall padding.

Paper #23 was to have reviewed how compliance with these regulations is being met. However, it was not given.

McCarthy and colleagues (#24) described an elaborate design done at Wayne State University that meets the HIC requirements of the FAA regulation. The design utilizes an articulating seat pan to minimize the forward head-path trajectory in front-row seats in such a way that head contact with a contiguous wall-like structure such as a bulkhead could be eliminated. A concern was raised in the audience that implementing such a design could lead to decapitation and bilateral leg fractures in any subsequent aircraft accident. The argument was made that studies have shown that a brace position with head on knees or as low as possible down the back of the seat in front and stabilized by hands locked over the head and heels aft of the knee panel, will give as much protection as any envisioned technology (Aviat. Space Environ. Med. 64: 103-109, 1993). Bracing limits head flailing which decreases brain acceleration and, consequently, subsequent brain injury on impact, and it also reduces the chance of being hit by flying debris.

Using on-board impact recorders, Melvin and colleagues (#25) have investigated the impact protection provided by race cars of the Indianapolis type ('Indy cars'). These impact recorders were designed to record deceleration-

time histories and peak deceleration levels associated with Indy car crashes. Data from crash investigations have shown that serious head/neck injuries are uncommon in Indy cars. In the Abstract submitted to the Technical Programme Committee, Melvin indicated that simulated test-sled crashes, using instrumented dummies, have shown that the most significant body loads were placed on the head/neck region, in contradistinction to what is the case in real Indy crashes. The authors described some of the design features of Indy cars that might mitigate head/neck and other major injuries. Studies such as these lend themselves to new insights into human tolerance to impact loading as well as providing better impact protection in both passenger cars and aircraft.

5.9 Modelling Head Injury Countermeasures

Computer models of crash events in which both the human body and the safety system are simulated allow for the development of optimal protective systems to head and body motions. Wismans and colleagues (#26) developed a three-dimensional helmet computer model for effecting head injury protection in vehicular impacts. The model consisted of an outer shell, a protective padding liner, a chin strap and a comfort liner. Included in their presentation was a realistic simulation of impact responses using headform acceleration time histories for different helmet impact locations. The potential and limitations of current models as well as future developments were discussed.

Paper #27 was to have determined indirectly the degree to which protective head gear guards against diffuse axonal injury using the three-dimensional, translational and rotational kinematics of a Hybrid III head form to helmeted and unhelmeted head drops. The data obtained were to be applied to a three-dimensional, finite element model of the human head to assess the extent to which protective head gear modifies 'impact strain' throughout the brain. This paper was not given.

The use of validated computer models of human-systems interaction during different impact conditions together with standardized data bases of material properties that characterize the model will significantly enhance human safety issues in the provision of effective protective countermeasures. Models such as those of Wismans et al. (#26) and Alem et al. (#22) lend themselves to parametric analysis whereby many different human-systems interactions during impact can be studied quickly to develop optimal protective systems without resorting to costly test designs. Of course, such models are dependent on the imagination of the modeller and the availability and accuracy of the data that the models require.

6. CONCLUSIONS

The following conclusions may be drawn from this Specialists' Meeting and a knowledge of the relevant issues regarding impact head injury:

- Injuries to the head are prevalent in both aircraft and automotive impacts, accounting for up to 50% or more of cases.

- Brain injury is more associated with traumatic death than injury to any other specific body region in vehicular accidents.

- Appropriate and timely pre-hospital treatment of severe brain injury can significantly reduce preventable traumatic death.

- Diagnostic imaging techniques employing PET, fMR and other modalities are essential: They must be targeted at critical times in assessing acute brain injury and they should be incorporated in the Critical Care Unit.

- There are two stages that define brain damage following head injury - primary and secondary damage:

- Primary brain damage occurs at the moment of injury and is comprised primarily of contusions, lacerations, intracranial hemorrhage and diffuse axonal injury.
- Secondary brain injury is caused by ischemia and/or hypoxia, and as a consequence of biochemical cascades initiated by the mechanical trauma that affects cellular metabolism and causes microvascular damage leading to blood-brain barrier disruptions.

- Diffuse axonal injury, a major contributor to brain incapacitation, may involve a continuum of nerve (axon) damage resulting from subtle lesions caused by shear strain effects that manifests itself days later clinically, rather than as a consequence of an immediate axonal damage on impact.

- Some manifestations of secondary brain damage are: cerebral blood flow abnormalities, raised ICP, brain swelling, intracranial hematomas, hypoxia, shock and bacterial infection.

- Secondary brain damage is a poorly understood process that commences with an injury and, sometimes, continues on for months.

- The biochemical cascades initiated by trauma are part of the process of activation and release of inflammatory agents which lead to oxygen radical formation and lipid peroxidation that ultimately cause much of the nerve cell damage in secondary brain injury.

- Drug therapy aimed at neutralizing these biochemical cascades has been successful in animals, but has shown limited benefit in human clinical trials.

- Pathoanatomically, primary brain injuries can be classified as focal and diffuse injuries:

- Focal injuries, sometimes called coup and contrecoup injuries, are produced by both rotational and translational head motions and consist of contusions, lacerations and hemorrhages.
- Diffuse injuries result from rotational forces and are comprised of transient dysfunctions (e.g., unconsciousness and other concussion symptoms), brain swelling, multiple petechial hemorrhages and diffuse axonal injury.

- Advances in biomechanics, brain chemistry, brain imaging, physical models, and three-dimensional finite element analysis and other computational constructs are fundamentally changing and improving our perception of skull and brain injury mechanisms, treatment and countermeasures.

- Physical and computational (e.g., finite element) models employing biomechanical response data correlated to brain injury are essential for describing injury potential and establishing tolerance criteria; consequently, there is a continuing need to obtain good material and dynamic properties of skull and brain tissues under impact conditions to develop and validate such models.

- Physical or computational models will not mimic all brain injury conditions, nor will they replace or supplement all experimental animal or cadaver data or tissue studies in head injury fatalities.

- Criteria for determining head injury risk to airbags, helmets and other protective systems to both angular and translational accelerations not based on direct evidence of brain damage will continue to be controversial; however, these will have to be sufficient and used with caution until appropriately-validated tissue-level criteria are developed that have practical applications.

- Experimental protocols must be standardized, models must be validated, and mechanical input parameters such as acceleration and load must be quantifiable, graded and reproducible to correlate physical input to physiological strains and pathophysiological conditions in order to determine acceptable injury risk.

- Depending on the severity of the closed head injury, an aviator may return to flying status anywhere from 30 days due to a mild injury which indicates a lack of cognitive dysfunction or to more than 5 years for a severe injury involving a post-traumatic seizure risk.

- There is evidence that advanced brain imaging techniques, used in combination with standard neurological and novel neurobehavioural assessments, will more accurately predict the risk of seizure than current methods, and, therefore, will shorten the observation period for an aviator's return to flying after a closed head injury.

- The use of protective devices against impact, such as seat restraints, air bags, padding and improved helmets, have significantly reduced brain injury and death.

- The protective value of a helmet against head and neck injury is dependent on:
  - resistance to penetration,
  - absorption of linear impact forces,
  - reduction in angular impact forces,
  - control of mass and centre-of-mass location,
  - optimal rigidity and closeness of fit,
  - helmet retention, and
  - helmet aging.

- Perhaps it is significant that the large reduction in head injury risk in present US Army helicopter mishaps coincides with the recent introduction into service of an aircrew helmet, the SPH-4B, which has improved protective capability.

- New inflatable restraint systems for reducing the severity of head injury in cockpit aircrew look promising, but any safety concerns regarding air bag deployment should be resolved before these become operational.

- Suitable small, lightweight, self-contained, ruggedized, on-board impact recorders show promise for collecting good impact data to correlate deceleration exposure conditions to injury type and severity.

- Suitably-validated, three-dimensional computer models that mimic the interaction of the human, the protective system and/or the vehicle interior during impact can enhance or supplement other methods of systems design or accident reconstruction in a quick and cost effective manner.

- Systems designers in impact protection must take into account:
  - the effects of both translational and rotational head motion in inducing head injury,
  - the contributions of neck compressive forces on the basilar skull,
  - both contact and noncontact loading of the head, and
  - new developments in head injury criteria which more closely correlate with severity of injury.

7. RECOMMENDATIONS

This Specialists' Meeting was a venture between the AMP, the SCCCAC and the SAE. It marked the first time that these aviation and automotive interests have jointly addressed a topic of mutual concern; in this case, impact head injuries in vehicular accidents. All impact head injuries have common injury types and mechanisms, and novel crash protective measures for one vehicle may be applicable to other vehicle environments. Many of the papers delivered and the discussions that followed

during this meeting aptly demonstrated this fact.

Reaching out to the SAE and SCCCAC to address common issues is consistent with AGARD's goal of becoming more aware of the dual-use research and technology, and dual-concern activities of other organizations. The accomplishments achieved and benefits derived from this Meeting by AGARD and, in particular, by the AMP, is in accordance with goals that include:

- a recognition of Col Stapp's lifelong interests in and contributions to biodynamics and human protection to impact,
- a greater awareness of the important service rendered by the SCCCAC with its annual forum for disseminating crash protection information of direct relevance to the interests of the AMP,
- a better knowledge of the complementary role the SAE performs to that of AGARD as an engineering society furthering vehicle mobility technology worldwide,
- the potential for the exchange and sharing of scientific and technical information with new 'partners',
- new ideas and directions from the SAE, SCCCAC and others for addressing impact head injury,
- the potential for conducting joint programs for information exchange and collaborative ventures with these new partners,
- opportunities for AMP Members to form alliances and exploit technology commercially with newly-identified industries and others sharing common interests, and, importantly,
- the sharing of Meeting costs and resources with, and help in the organization and coordination of the Meeting programme by, these new partners.

The great success of this Specialists' Meeting in terms of benefits derived by all parties warrants further attempts by the AMP to seek joint opportunities in other areas of common interest.

8. ACKNOWLEDGEMENTS

A Tribute to John Paul Stapp

Henning E. VonGierke
Director Emeritus
Biodynamics and Biocommunications Division
Armstrong Laboratory, Wright-Patterson Air Force Base
2610 Seventh Street
Ohio 45433-7901, USA

Col Stapp
Ladies and Gentleman
Friends

Why do we have a picture of Col Stapp before one of his sled tests on the front page of our program? (Fig 1) I will try to explain this to you briefly without becoming too technical and without going into details. Since I discovered that Col Stapp himself will talk to us tomorrow about the pioneering early rocket sled experiments, it would be presumptuous to talk about facts and details which will be more authoritatively discussed by himself. Let me just set the stage for his talk and tell you from my perspective how I see the importance of his work.

I don't know the age distribution of this august audience, but I assume that for some of you this is old history and you are very familiar with it; but I hope that there are quite a few young ones among you, biodynamicists of a new generation, who might know and use the data of Dr. Stapp's sled tests, but are not necessarily aware of their historic significance and lasting importance.

I came to the aerospace medical and biodynamics community about the time of the first sled test runs at Edwards AFB or more correctly Muroc Army Air Base, California, where they were conducted. The rocket propelled sled facility, with the clasp-type mechanical deceleration brakes, had been build by Northrop for the joint Army Air Corps and Navy project on "Effects of Deceleration Forces of High Magnitude on Man." Capt Stapp from our Laboratory at Wright Field in Ohio was the project officer for this program to develop better, more realistic guidelines to industry for crashworthiness in human occupant spaces of aircraft, for seat and restraint design, and for open seat emergency escape. I saw the first movies and verbal reports, which Capt, and later, Maj Stapp brought back to the laboratory in 1947 to 49. I did not realize until 8 or 10 years later, when I wrote a comprehensive review on what was known and had been done since W.W. II on the effects of shock and vibration on people, how important these tests were, how this knowledge could be used for aircraft and automobile design, how these rocket sled human tolerance data had become the cornerstones of our knowledge: yes, the human body does not have to be the weakest part in an aircraft crash or automotive collision. We can design for the limits of human tolerance with optimum restraint in the backwards and forward facing position as established by Stapp (1). Examples of these limits, as summarized by Eiband (2) are shown in Figs 2 and 3. They stand, almost unchanged to this date, almost half a century later.

Whatever your disciplinary interest or training is, if you are physicians, engineers, accident specialists or designers, or if you are just travelers flying or driving to this conference: these data are of vital importance to all of us. They define the limits of human mechanical tolerance, they define the important boundaries for the field we now call biodynamics, or biomechanics, a multidisciplinary discipline, which hardly existed 50 years ago as a quantitative science.

At the 50th Anniversary of our Laboratory, a few years ago, Col Stapp gave a keynote address, which he entitled: "Biodynamics - The Key to Flight." (3) In this, he outlines the importance of the over 5000 sled tests in preserving human life in various adverse, mechanical environments from aircraft crashes to emergency escape, windblast, explosions and vibratory motions. He could have called the paper as well: Biodynamics - The Key to Safe Motion! The application of the seat belt and restraining techniques Col Stapp had developed in his early tests and the whole human sled test technology became of paramount importance to the increasing problem of automotive and highway safety.

When the automotive industry and the Society of Automotive Engineers (SAE) appointed a committee in the early 1950s to study early seatbelt proposals, Col Stapp invited them to the Aeromedical Field Laboratory, which he had organized and operated in the meantime at Holloman AFB, for a tour of the facilities and field demonstrations. This meeting of 26 individuals on 7 May 1955 became the first Stapp Car Crash Symposium. The rest is history. This meeting grew under Col Stapp's permanent chairmanship and with SAE assuming administrative sponsorship in 1966, to the worldwide annual event with hundreds of authors, thousands of participants and proceedings exceeding 1000 pages.

But this success and that we had this week the 40th Stapp Car Crash Symposium is only part of the story. The more important success to which Col Stapp significantly contributed, is: that we routinely wear seatbelts and upper torso restraints today, and that daily, the world over, hundreds of lives are saved. To show you how Col Stapp, the physician and biophysicist, contributed to all of this, let me quote from his introduction to the 25th Anniversary of the Stapp Car Crash Symposium (4) in his own words:

"In my one lifetime I have had the astounding experience of designing apparatus, having it fabricated, getting volunteer subjects to sustain exposure to the forces incurred in accidents, designing and testing protective equipment for them, participating in development of standards based on quantitative data from human experiments, advising legislators on laws to promulgate these standards, and in public promotion through every written and audio-visual communication media all over the world to advance the cause of automotive safety and crash protection."

It is this leadership, which gave us not only the new medical data, test methods and a whole generation of new investigators and restraint designers, but also convinced administrators, politicians, and the public that Col Stapp's dream of safer transportation and deliverance from accidental injury could be realized. He not only pointed the right way, but he fought for it, step by step, year after year - until we now all wear seat belts.

Concentrating on the strictly technical contributions, the biodynamics field has made great progress over the past half century (1): human volunteer tests combined with other advances allowed us to build and rely on models of the human body and its restraint systems which in turn give us the capability to calculate the body's response to various mechanical insults, from military aircraft escape forces to the windblast forces of supersonic escape in open ejection seats, and to predict the probability for safe survival in all kinds of automotive crashes and highway accidents. (5) (Fig 4) Instead of the sand-filled human dummies of the 1940s, we have today sophisticated anthropodynamic human analogues with realistic viscoelastic properties and joint dynamics, which indicate with their numerous sensors the resulting forces, motions, and pressures, and provide a means for assessing the injury potential of the aircraft ejection or crash loads on the crew member. These dummies, as well as the computer models we have today are calibrated against the live human data points we have. Volunteer human tests and animal tests become so less and less necessary, particularly if, as we hope all human test results from the early sled tests as well as subsequent tests in all laboratories all over the country, will be collected in one biodynamic data bank accessible to all users. (6)

Looking at the progress we made over these 50 years, you must admire the courage and foresight of Col Stapp when he planned and executed these early rocket sled tests, when he served 29 times as his own volunteer subject, when he withstood impacts exceeding 40 times gravity. (Fig 5) These tests, which are absolutely unique, will probably never be repeated. And we cannot but admire the tenacity, with which he promoted application of the results for aircraft, spacecraft and automotive safety. The steps of Dr. Stapp's career were further steps towards the realization of his dreams: safer transportation on earth, in the sky, and in space. He founded and led two AF laboratories at Edwards AFB and at Holloman AFB, he commanded the mother laboratory, the Aerospace Medical Laboratory at Wright Field, he became Chief Scientist of the Aerospace Medical Division and served as consultant to the Armed Forces Institute of Pathology. His final assignment was in 1967 at the newly established Department of Transportation, where, in the National Highway Safety Administration, he decisively influenced automobile safety and highway design.

I want to use the final few minutes to illustrate the rocket sled technology Col Stapp pioneered and to demonstrate the courageous human tests he and his volunteer subjects performed. I am sure in his talk tomorrow Col Stapp will show us better and more detailed movies and will describe himself what he planned, thought, felt, and had to overcome to conduct these tests. He might even correct some of my descriptions. I show these movies only to give those of you, who never saw these tests, a feel for what it took to establish the limits of tolerance, and to convince the world to design for seatbelts and to buckle up.

A short video shows the importance of Col Stapp's rocked sled tests in three sections:

1. An unrestrained parachute dummy is suddenly decelerated from a 100 miles per hour ride, flies through a plywood windshield, and hits the ground 170 ft down the track.

2. Human volunteer tests of increasing rates of deceleration (from 17 to 46 peak Gs at 500 and 1000 G/sec) are demonstrated with various restraint systems. The early tests on 14 subjects were safely conducted with no coincidence of injury.

3. Col Stapp's world speed record run of 639 miles/hr studying tolerance to windblast.

This is what it took to obtain the data points on human tolerance which I showed on my earlier slide. This is what it took to make progress in biodynamics - the key to safe motion. Col Stapp (Fig 6) we thank you for your accomplishments, for your ingenuity, persistence and the courage, with which you perceived and realized your ideas. We honor and salute you and wish you
  "Godspeed"   -   but safely restrained.

REFERENCES:

1. VonGierke, H.E. and Brammer, A.J., "Effects of Shock and Vibration on Humans," Shock and Vibration Handbook, 4th edition (C.M. Harris ed.), McGraw Hill NY, 1995.

2. Eiband, A.M., "Human Tolerance to Rapidly Applied Acceleration: A Summary of the Literature," NASA Memo 5-19 - 59E, National Aeromechanics and Space Administration, Washington DC, 1959.

3. Stapp, J.P., "Biodynamics - The Key to Flight," Aviation, Space, Environmental Medicine, Vol 57, pp. A32-A36, 1986.

4. Stapp, J.P., "Twenty-Five Years of Stapp Car Crash Conferences," Twenty-Five Years of Stapp Car Crash Conferences Society of Automotive Engineers, Warrendale PA, 1981.

5. Ma, D., Obergefell, L., and Rizer, A., "Development of the GEBOD Program," Proceedings of the 15th Southern Biomedical Engineering Conference, IEEE, Dayton OH, March 1996.

6. Committee on Hearing, Bioacoustics and Biomechanics (CHABA), "The Feasibility of a National Biomechanics Data Bank, "National Academy Press, Washington DC, 1981. (Also: Abrams, T.S., Maxwell, and Kaleps, I., "The AAMRL Biodynamics Data Bank," Wright-Patterson AFB OH AAMRL-TR-88-037, 1988).

Figure 1: Lt Col John Paul Stapp, USAF (MC) being prepared for a test run on Sonic Wind 1 at Holloman Air Development Center NM in the 1950's.

Tolerance to spineward acceleration as a function of magnitude and duration of impulse. (*Eiband.*[51])
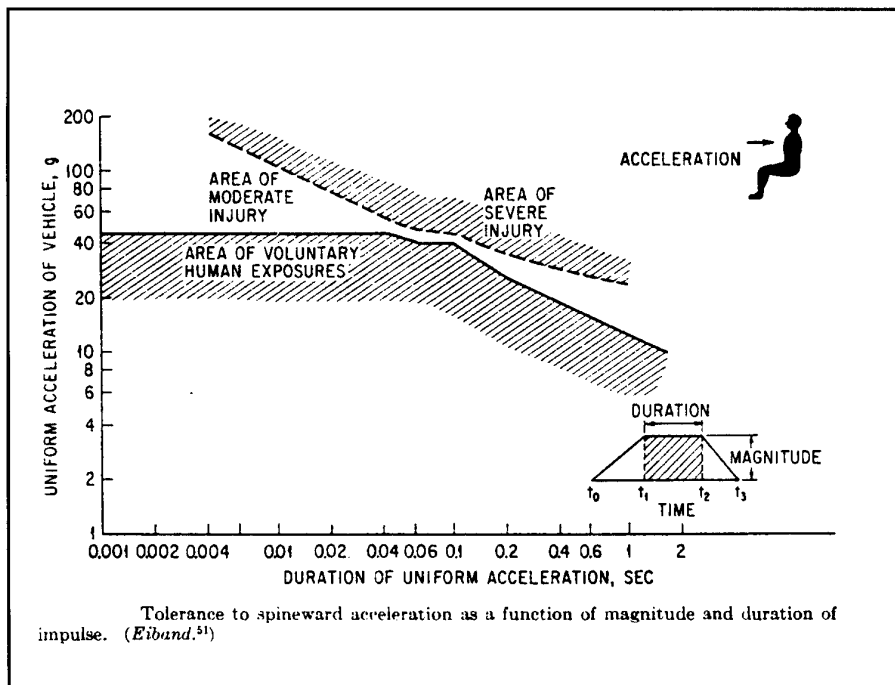
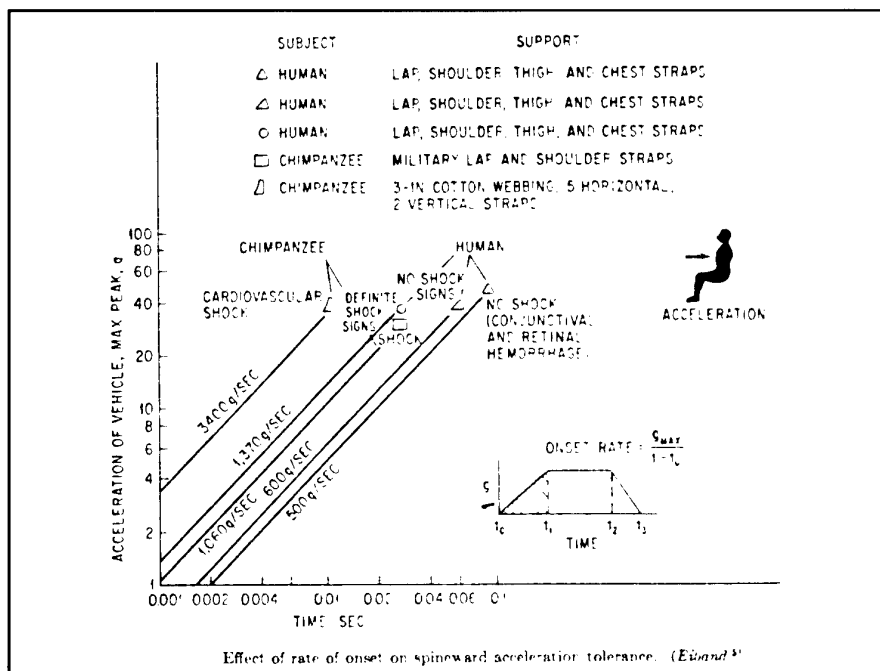Figure 2: Tolerance to spineward acceleration as a function of magnitude and duration of impulse.

Figure 3: Effect of rate of onset on spineward acceleration tolerance.
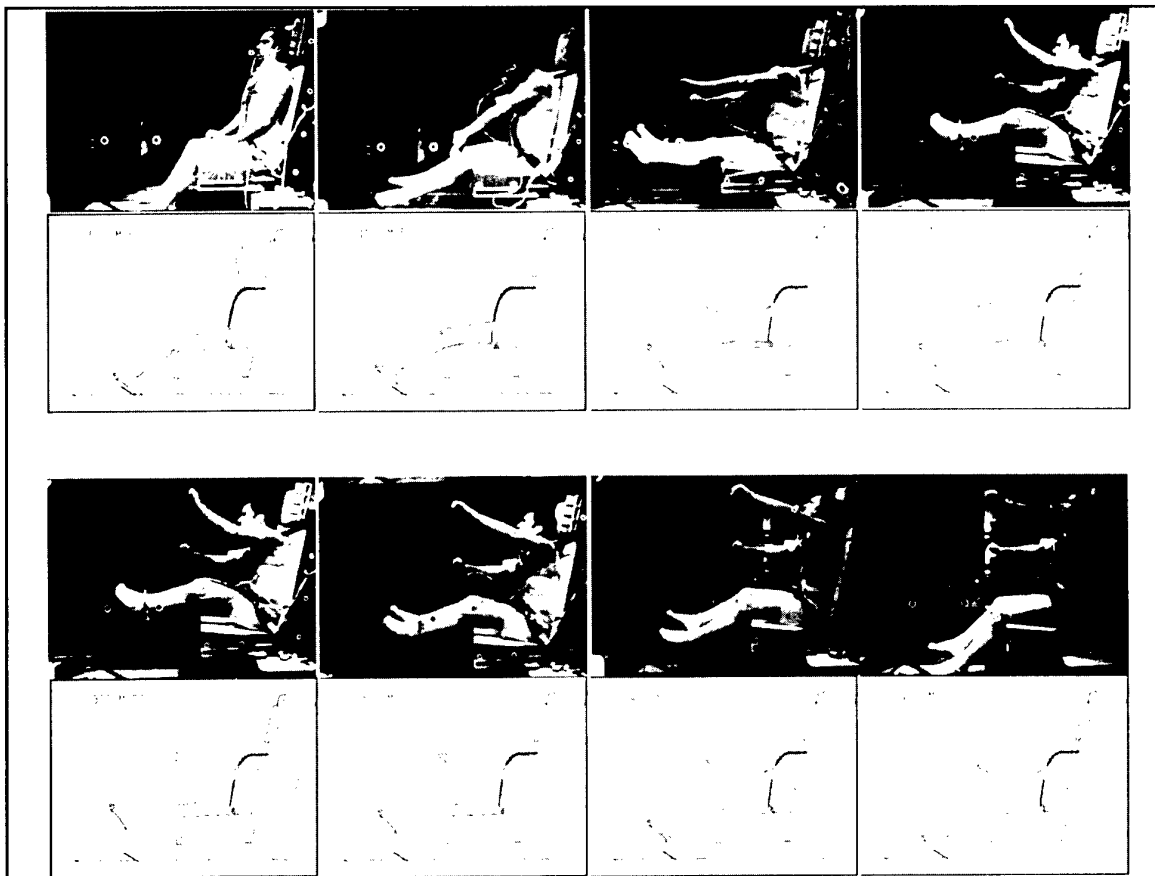

Figure 4: Comparison of computer simulated and human motion from -Gx whole-body impact.
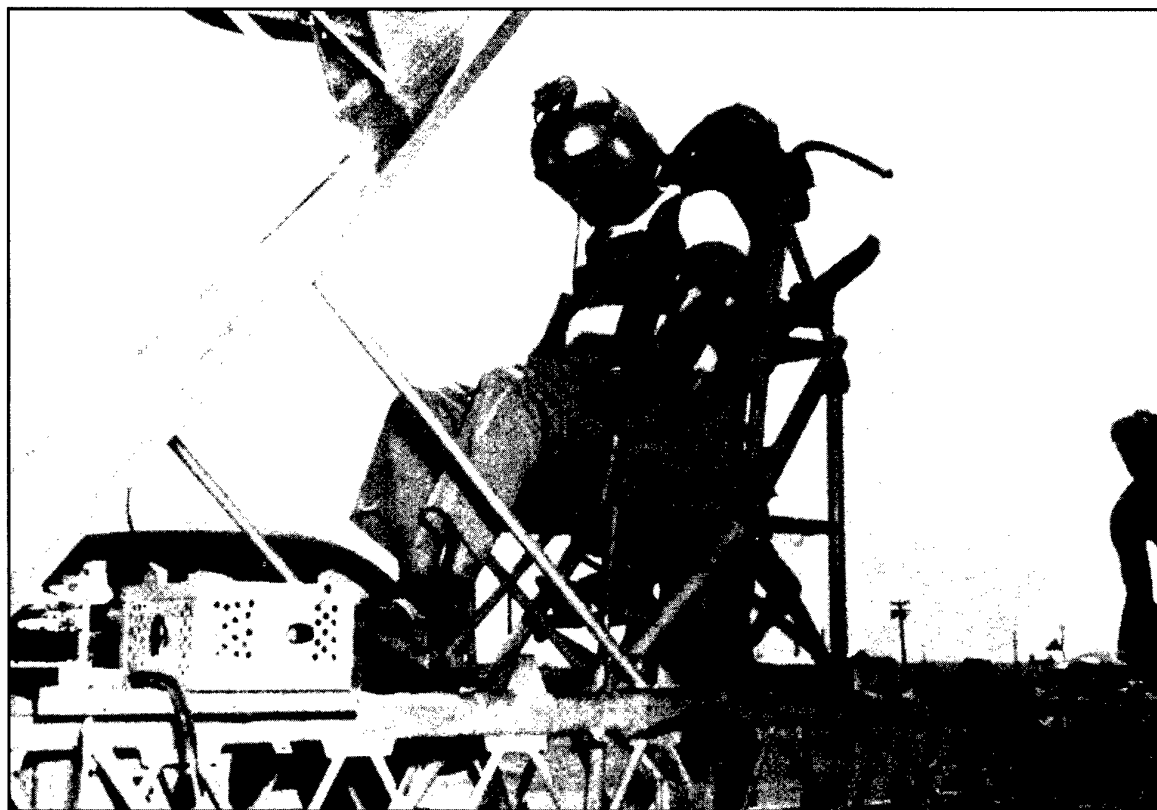
Figure 5: Major John Stapp on the second rocket sled built for human deceleration experiments at Holloman AFB.

Figure 6: Col John Paul Stapp, MD, PhD.

Some Observations to the Skull-Brain Trauma

Dimitrios Kallieris, Andreas Rizzetti, Rainer Mattern
University of Heidelberg, D-69115 Germany

Summary

Skull-brain injuries are caused through impact against rigid or padded obstacles.

Injury pattern and injury severity of skull-brain trauma from experimental head impacts and autopsy cases are reported.

The experimental part includes 10 head impacts (frontal, lateral or occipital and rigid or padded) with cadavers at a velocity of 20 km/h. A pneumatic impactor with a movable mass of 23 kg was used, the impact surface was a disc with 150 mm of diameter.

Accelerations at the top of the head and the epidural pressure at the contrecoup site were measured.

According to the acceleration measurements at the top of the head the evaluated acceleration at the head c.g. amounts between 85 g (padded) and 500 g (rigid); the rotational acceleration of the head around the rotation axis varies between 4700 rad/sec^2 (padded) and 19000 rad/sec^2 (rigid). Furthermore, the epidural pressure is between -20 kPa and -46 kPa.

The observed fracture pattern and the injury severity of the skull are well comparable between the experimental exposure and the head impact during a sudden fall on the road. Furthermore, the injury pattern of the brain is also comparable, however, not the injury severity; the haematoma is of higher intensity in the accident cases.

The brain injuries of the experiments include contrecoup subarachnoidal haematomas; furthermore skin lacerations were observed.

The results are critically discussed with those existing in the literature.

THE FREQUENCY of severe skull-brain trauma for all types of accidents amounts 70 %, 40 to 50 % are caused in car accidents (Parzhuber et al., 1996, Silver et al., 1993).
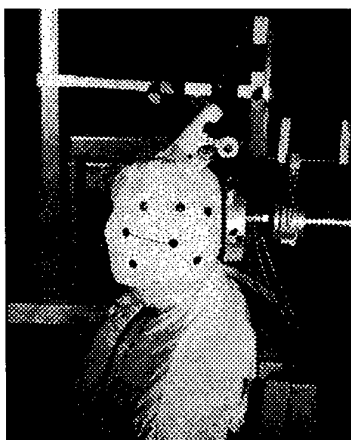

Fig. 1:
Pre-impact (occipital rigid impact) situation of the head with impact surface and marked Frankfort Plane.

The investigation of skull-brain trauma is relevant for safety aspects like a better protection of road users as well as for legal aspects.

A lot of work has been done in the last 30 years on injury mechanics and response of the skull-brain trauma; the most important papers are summarized in the SAE PT-43. Due to new equipments of protection devices for the car safety and the development of mathematical models, further work is needed.

The forensic pathologist is called to examine the victims of trauma because his or her scientific findings will often find their way into legal proceedings. His expertise lies in the interpretation of these scientific findings for the law with reference to the injury mechanics and mechanical response. The collection of data and careful description of injuries provide a basis for research of causes, treatment and prevention of accidents.

For the definition of protection criteria for the head, relationships between the mechanical response like force, pressure, linear and rotational acceleration and injuries are needed. Protection criteria include injuries of the AIS 3, which means serious, not live threatening injuries. Volunteers can not be exposed to this injury severity, therefore, cadaver testing is required. The current linear acceleration-time dependent head injury criterion (HIC) seems not to be a suitable criterion. Rotational acceleration or strains are additional injury related physical parameters to characterize the brain trauma; further experimental work is needed to define an optimal head injury criterion.

Regarding this aim, traumatomechanic research is done at the University of Heidelberg in cooperation with the Technical University of Berlin, which has to equip a FE model of the head.

Method

Test Subjects

10 tests were conducted with cadavers ranging from 26 to 86 years, the mean age was 58 years. Furthermore two accident cases were included, the age of the victims was 44 and 84 years.

Impactor

The tests were performed using a linear piston pneumatic impactor. The impact surface was a flat rigid aluminum plate, 15 cm of diameter. In some experiments a 40 mm thick polyurethane foam (density: 165 g/dm^3, standard dashboard padding material) was used to attenuate the head impact energy and distribute the impact forces. Frontal, lateral and occipital head impacts were performed. The axis of the impactor was aligned with the head center of gravity. Figure 1 shows the pre-impact situation of the test subject prepared for a rigid occipital impact. The impactor mass amounts 23 kg, the impact velocity ranged from 18 km/h to 20 km/h.

Two accident cases were investigated as autopsy cases, one was an occipital head impact through a tram with a speed of 20 km/h and the second was a forehead fall from 2 m height against a rigid surface.

Instrumentation

The instrumentation included a nine accelerometer module, as described by Padgaonkar et. al.(1976), which was screwed to the top of the skull. The accelerometers used were Endevco 2264-2000.

The location of the nine-accelerometer array to the head center of gravity (c.g.) and occipital condyles was measured in the lateral x-ray view (Fig. 2). Furthermore, the impact forces and in some tests also the epidural pressure at the contrecoup site were measured.

Data Analysis

The data were recorded in analog format. and digitized at 10,000 samples per second. The data of the 9-accelerometer array was processed further according to the Padgaonkar method. From these data the resultant head center of gravity (c.g.) linear acceleration. the angular velocities and accelerations were calculated. during this procedure a CFC 60 filter was used. For the evaluation of the head injury criterion (HIC) the signals were filtered with CFC 1000 as proposed by SAE J211a.
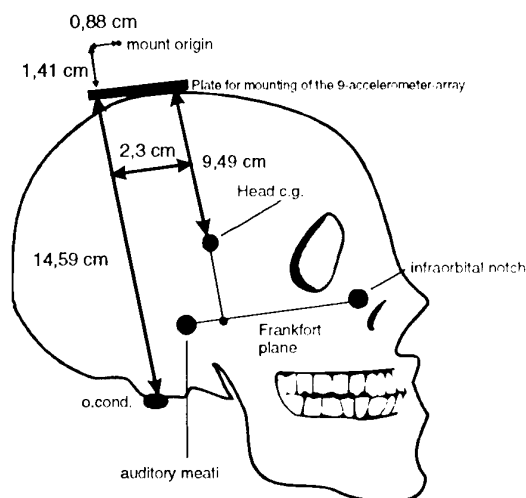
calculation, the signals of the 9-accelerometer were filtered alternatively according to the CFC 1000 and to the CFC 60. The nine-accelerometer processing is very sensitive for artefacts in the measured linear accelerations which will be pronounced visible in the calculated linear accelerations. Therefore the measured accelerations used for the 9-accelerometer processing have to be filtered at a lower Channel Filter Class than the CFC 1000 prescribed for measured head accelerations.

The illustrated curves show the calculated results from the filtered raw curves. e.g. the head acceleration curve with the corresponding CFC 60 does not follow from filtering the head acceleration curve with the corresponding CFC 1000. they are both derived independently from the filtered 9-accelerometer data.

The rigid impacts show maxima values of 200 to 500 g with peaks of short duration. The lower acceleration maxima were observed in frontal impacts because of the damping influence of the nose. The highest values were measured in occipital and lateral head impacts.

Fig. 2:
Example for distances between the nine-accelerometer array to the center of gravity and to the occipital condyles by marked Frankfort plane.
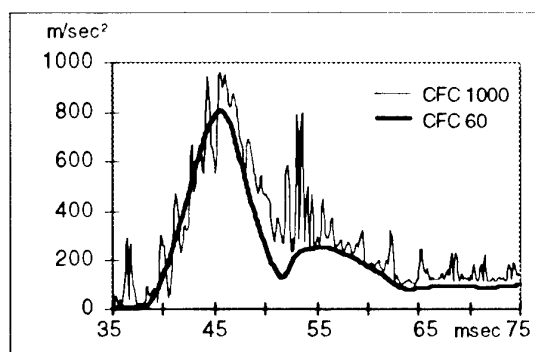
Fig. 3:
Resultant acceleration time-history at the head c.g. of a padded occipital head impact using CFC 1000 and CFC 60.

Results

Mechanical response

Impact forces
Impact forces between 3000 N to 4000 N for damped impacts and between 7000 N to 9500 N for rigid impacts were measured; the 3 ms peak of the rigid impact is close to the damped impact force value.

Linear acceleration / HIC
The evaluated maxima of the linear acceleration at the head c.g. amount for the damped impacts between 85 g to 100 g with corresponding HIC values of 250 to 350. An example of acceleration-time history of a damped occipital impact is shown in figure 3. For the

Rotational acceleration
The calculated rotational head accelerations are between 4700 rad/s² to 8200 rad/s² for the damped impacts; for the rigid impacts these values are between 11000 rad/s² and 19000 rad/s². An illustration of the rotational-time history for a padded occipital impact by using CFC 1000 and CFC 60 is shown in figure 4.

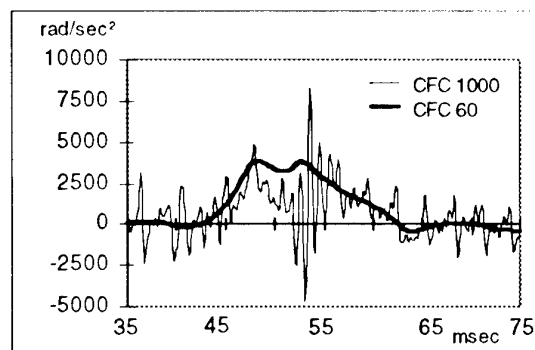Fig. 4:
Head rotational acceleration-time history around the y-axis of a padded occipital head impact using CFC 1000 and CFC 60.

Contrecoup pressure

In the frontal and lateral impacts the epidural pressure at the contrecoup site was measured. These values are between -20 kPa and -46 kPa. An example of pressure-time history of a rigid frontal impact is shown in figure 5; a negative pressure of 36 kPa was measured.
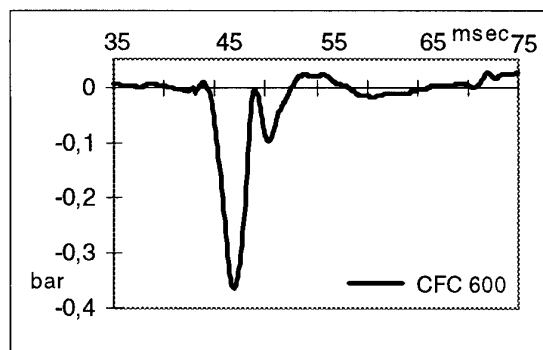

Fig. 5:
Epidural pressure-time history of a rigid frontal head impact using CFC 600.

Medical findings

In 50 % of the rigid impacts a laceration of the skin was observed. Except for one test, all the rigid impacts show skull fractures. These fractures are located at the impact area and also include the basis of the skull. The fractures of the face skull were more complex in frontal impacts. In all the cases the severity of the skull fractures were rated with AIS 3.

Schematical illustrations of accident and experimental skull fractures are shown in figure 6; the course of the fracture indicates the impact direction.
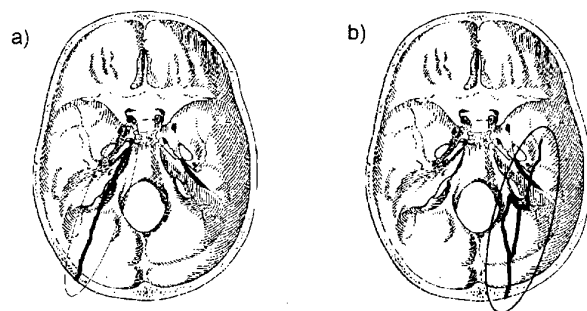

Fig. 6: Fracture patterns resulting from occipital head impact
a) Skull, hitted by a tram from occipital left (real accident)
b) Occipital impact with an impactor (test situation)

As brain injuries, subarachnoidal haematomas at the contrecoup site were found in 40 % of the impacts; this frequency includes the rigid as well as the padded impacts. Two examples of this type of injury are given in the figure 7 for realistic and experimental head impacts. In the real case, skull hitted by a tram from occipital left, contusions at the front and fronto-basal of the right hemisphere (contrecoup) of the brain were

found. In the experimental case, padded occipital impact, subarachnoidal haematomas fronto-basal on both sides were observed.
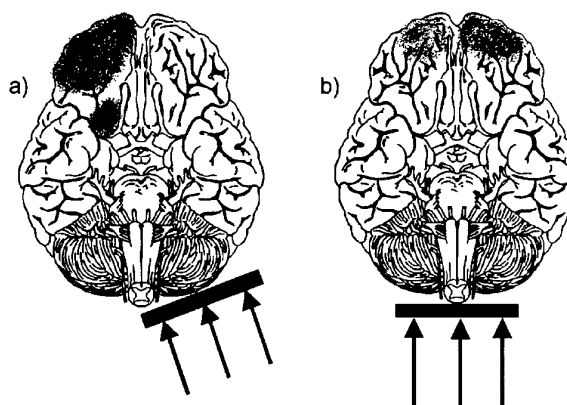

Fig. 7:
Contrecoup brain injuries suffered by a real accident and in an impactor test. (view of the brains: basis of the skull)
a) real accident   b) impactor test

Discussion

In the study, the blunt impact of the head by using human cadavers was investigated. Rigid impact conditions, with an impact veloctiy of 18 - 20 km/h and a movable impactor mass of 23 kg, are too severe; usually rigid impacts cause skull fractures of AIS 3, which can be connected with severe brain injuries. The impact forces, between 7000 N to 9500 N, and the calculated accelerations at the head c.g., between 200 g to 500 g, are extremely high, especially the duration of the spikes is very small and unrealistic. These response levels however, are in agreement with the results of Stalnaker et al. (1977), whose performed comparable head impacts with cadavers.

The accelerations evaluated in padded head impacts are at the same level as reported by Nusholtz et al. (1984) in 20 km/h padded (ensolite) head impacts. Also the range of the rotational accelerations of 4700 rad/sec^2 to 8200 rad/sec^2 is in agreement with the range of 6000 rad/sec^2 to 8000 rad/sec^2 of the Nusholtz et al. (1984) study. Further agreement exists also with the impact forces between the two studies.

At the contrecoup site, a negative epidural pressure of -20 kPa to -46kPa was measured which begins at about the same time as the head acceleration in impact direction. The measured values are lower than the ones observed by Stalnaker et al. (1975), who report that a negative pressure magnitude greater than 68 kPa can produce brain tissue damage.

According to the impact condition, the contrecoup theory explains the brain damage.
In 40% of the impacted heads subarachnoidal haematomas were found; this type of injury is the only one observed in cadaver testing. We don't think that this

is a problem due to the lack of blood pressure. Also Nusholtz et al. (1984) didn't find brain injuries in each impacted head of the repressurized vascular system in cadavers' head and Stalnaker et al. (1977) observed subarachnoidal haematomas without repressurization. Because of the overstressing of the superficial blood vessels, post-mortem lacerations occur of blood stained vessels and is evident in a small visible escape of blood. However an enlargement of the haematomas through blood flow by existing blood circulation is missing.

Possible mechanisms for causing of subarachnoidal haematomas are interactions between the skull-brain interface. It is assumed that the negative pressure, local movement of the skull with respect to the brain, leads to tension stresses and therefore to lacerations of the superficial blood vessels of the brain. (Nahum et al. 1980). Furthermore, rotational motion of the skull with respect to the brain may cause the subarachnoidal haematomas (Nusholtz et al., 1984). Fronto-basal subarachnoidal haematomas are explained with relative movements between the base of the skull and the brain.
The fracture pattern of the experimentally produced fractures is comparable with those investigated in autopsy cases in real accidents. Furthemore the experimentally observed brain injury mechanism is comparable with accident cases, but the intensity of the damage was different between the experiment and the real case. However, the impact severtity in the real cases was also higher than in the experimental cases. In the real cases, severe brain contusions through ruptures of the capillaries in the brain cortex were found. For the lack of this type of injuries in experimental work with cadavers, two reasons can be given: the first one, is the impact severity, the second one, the lack of filling of the capillaries of the brain cortex during the repressurization.

It is concluded that the tolerance limits of skull-brain trauma are exceeded under the impact severity investigated in this study. Padding prevents skull fractures, but not brain injuries.

Acknowledgment

References

Nahum A. Ward C, Raasch E. Adams S, Schneider D,(1980) Experimental Studies of Side Impact to the Human Head. Proc. 24 th Stapp Car Crash Conference, pp. 45-62

Nusholtz GS, Lux P, Kaiker P, Janicki MA. (1984) Head Impact Response-Skull Deformation and Angular Accelerations. Proc. 28 th Stapp Car Crash Conference, pp. 41-74

Padgaonkar AJ. Krieger KW, King AI. (1976) Measurement of Angular Acceleration of a Rigid Body Using Linear Accelerometers. J. of Applied Mechanics

Parzhuber A. Rucholtz S. Schweiberer L (1996) Das schwere Schaedel-Hirn-Trauma. Unfallchirurg 99:541-547, Springer

SAE-PT-43 (1993) Biomechanics of Impact Injury and Injury Tolerances of the Head-Neck Complex, ed. by SH Backaitis

Silver JM. Yudofsky SC, Hales RE, (1993) Neuropsychiatrische Aspekte traumatischer Gehirnverletzung. In: Hales RE, Yudofsky (Hrsg.): Handbuch der Neuropsychiatrie. Psychologie Verlags Union. Weinheim

Stalnaker RL. Benson JB, Melvin JW, (1975) Dynamic and Static Load Response of the Head. paper presented at the IRCOBI Conf. Sept. 9th to 11th, Birmingham, U.K.

Stalnaker RL. Melvin JW, Nusholtz GS, Alem NM, Benson JB,(1977) Head Impact Response. Proc. 21 th Stapp Car Crash Conference pp. 305-335

Impact Biodynamics of Human Skull Fracture

Anthony Sances, Jr., Ph.D., Narayan Yoganandan, Ph.D.
Frank A. Pintar, Ph.D. Srirangam Kumaresan, M.S.
Patrick R. Walsh, M.D., Ph.D.

Department of Neurosurgery, Medical College of Wisconsin
and the Department of Veterans Affairs Medical Center
9200 W. Wisconsin Avenue
Milwaukee, WI 53226, USA

Objective

The purpose of the present study was to determine the force-deflection biomechanics of the human cadaveric intact head under quasistatic and dynamic loading. Both nonfracture and fracture studies were conducted under known boundary conditions to delineate the stiffness, energy, and force-deflection characteristics for future use in finite element investigations and helmet protection studies.

Background

Previous skull fracture studies conducted by Gurdjian indicated that static human skull loading causes a skull to deflect with less force compared to dynamic loading [4]. An empty human skull fractured at an energy of 2.8 J; intact head with scalp required approximately 45 to 48 J for fracture [5]. Gurdjian also reported that, in human head studies with the scalp intact and dropped onto a heavy steel slab, fractures occurred at energies of approximately 70 J [4]. An acceleration-time tolerance curve for human linear skull fracture based

on a drop test demonstrated approximately 70 G to be a threshold for a 5 ms duration acceleration pulse, and approximately 50 G for a duration greater than or equal to 30 ms [4]. More recently, Nahum et al demonstrated depressed or comminuted fractures at the temporal parietal area at force levels of 2000 N, 4000 N at the frontal area, and 890 N at the zygoma, with a 645 mm^2 impactor [13]. Other studies indicated forces ranging from 980 to 1334 N to produce penetration of the parietal skull using an impactor of 200 to 297 mm^2 area [11, 12]. Studies have indicated that force is not a function of the area of the impactor, but of the circumference. Furthermore, soft tissues did not affect peak penetration force if the device had sufficient energy to penetrate. Fracture of the frontal region under static loading was produced at a force of 4727 N using a 10 mm x 100 mm x 10 mm plate [2, 3]. Hodgson and Thomas in 1971 indicated that plates produced linear fractures and the small impactors cause penetration fractures [6]. Melvin and Evans data indicated that large impactors produce comminuted depressed fractures [11]. Schneider

and Nahum recorded a force of 2113 N associated with the kinetic energy of 29 J at velocities of 5.2 m/s for temporal parietal fracture of severity of three [15]. For a skull 6.9 mm thick and 645 mm² area, the energy will be approximately 8.4 to 33.4 J [11]. Plate and shell theories have been used to predict skull fractures. Assuming that the modulus of elasticity of the skull is 1579 kg/mm², and a minimum strain energy of .22 kg/mm², shell theory predicts the fracture force at 3941 N for a 645 mm² impactor [11]. McElhaney et al provided static force-deflection properties from tests on the human head at the frontal and lateral sites [10]. Clinical follow-up of skull fracture studies have been given by Braakman, Walker, Unterharnscheidt, Stover, Jamieson, and others [1, 7-9, 16-18]. Recently, a review of skull fracture studies up to 1981 has been provided by Sances et al [14].

While the static and dynamic behaviors of the human skull have been evaluated, the force-deflection information required in finite element modeling in a suitable form is not currently available. These studies were therefore, undertaken to determine the local force-deflection characteristics of the human occipital, lateral, parietal and frontal areas of the intact head under known boundary conditions.

Materials and Methods

A total of 20 unembalmed human cadavers were used in the study. Details of the specimen data are given in table 1. The age, height and weight ranged from 50 to 85 years, 157 to 185 cm, and 56 to 102 kg, respectively. Subjects with severe degeneration or bone disease were excluded based on an evaluation of medical records and pre-radiography. All specimens were isolated at the base of the skull keeping the intracranial contents intact. Radiographs and computed tomography (CT) images were obtained prior to test. In addition, physical measurements were obtained for each specimen. These information are included in table 1.

Nondestructive quasistatic tests, failure quasistatic tests, and dynamic failure tests were conducted on a total of 20 specimens. For the nondestructive testing, the specimen was fixed in an adjustable device designed to locate both auditory meatii, and support the skull under the palate and the skull base. Polymethylmethacrylate was molded into the skull to provide additional strength at the supported regions. The fixture was mounted on a six-axis load cell fixed to the cross-frame of an electrohydraulic testing device (MTS Systems Corp., Minneapolis, MN). The load was applied to the occipital, vertex, lateral, temporal, and frontal regions of the head with a flat plate. Applied external force and the actuator displacement data, along with the six-axis load cell information placed at the distal end of the preparation, were recorded with a uniaxial force gauge, a linear variable differential transformer attached in series to the electrohydraulic piston, and a six-axis load cell placed underneath the specimen, respectively.

For the destructive quasistatic tests, the specimen was prepared in a similar manner as described above. Because of the destructive nature of the test, only one loading site was considered for each specimen. Following initial radiography, the specimens were aligned appropriately with the longitudinal axis of the electrohydraulic piston. They were loaded to failure at a loading rate of 0.002 m/sec. A Snell-type hemispherical anvil with a radius of 48 mm was used for loading. The anvil was rigidly attached to the electrohydraulic actuator. Failure was identified when an increase in the piston excursion resulted in a concomitant decrease of the external force. Following the test, the specimens were palpated and radiographs were obtained to evaluate the pathology. In addition, CT images were obtained following gross dissection, and then defleshing of the skull was done. Like the nondestructive quasistatic tests, the biomechanical data included the applied force and displacements from the electrohydraulic piston, and the distal output forces and moments in three anatomic directions.

Table 1: Specimen Data

Parameter	Units	Range	Mean
Age	years	50 - 85	70
Height	cm	157 - 185	171
Weight	kg	56 - 102	71
Lateral width	cm	13.3 - 16.2	15
AP width	cm	16.5 - 20.0	18.7
Nasion - occiput	cm	16.5 - 21.6	18.6
Inferior - superior	cm	13.5 - 17.6	15.5
Circumference	cm	49.5 - 61.0	55.6
Skin thickness	cm	0.30 - 1.00	0.65

AP: Antero-posterior

Using similar methods as described above for destructive quasistatic tests, in the dynamic series, loading was accomplished at rates ranging from 7.1 to 8.0 m/sec using the electrohydraulic testing device. The piston impacted the cranium at a constant velocity. After the test, the specimen was palpated, radiographs were taken, CT images were obtained, and the skulls were defleshed. Again, the biomechanical data included the applied forces, displacements, and the output generalized force histories. All data were sampled according to the Society of Automotive Engineers, SAE J221b specifications at a sampling rate of 8000 Hz using a modular digital data acquisition system.

Processing of the raw signals included a transformation of the force-time and displacement-time responses into a force-deflection behavior. Stiffness and energy absorbed by the specimen were obtained according to accepted techniques.

Results

For the nondestructive quasistatic series, the forces ranged from 1639 to 1702 N with deformations ranging from 1.9 to 7.2 mm. An evaluation of these force-deformation curves demonstrated no significant dips indicative of failure. Furthermore,

the specimen returned to the initial position suggesting the absence of pathological alterations. This was additionally confirmed by radiography, computed tomography, and gross dissection followed by defleshing of the skull.

For the destructive quasistatic failure tests, forces ranged from 4.5 to 11.9 kN (mean: 6.4 kN). The corresponding deflections at failure ranged from 7.8 to 16.6 mm (mean: 12.0 mm). The stiffness and energy absorption capacities of the structures ranged from 0.5 to 1.3 kN/mm (mean: 0.8), and 14.1 to 68.5 J (mean: 33.5 J), respectively.

For the dynamic failure tests, the forces ranged from 4.5 to 15.4 kN (mean: 10.5 kN), the deflections ranged from 3.4 to 11.5 mm (mean: 6.7 mm), stiffness ranged from 1.0 to 6.1 kN/mm (mean: 3.1 kN/mm), and energy ranged from 13.0 to 55.8 J (mean: 28.6 J). The forces and deflections of the stiffness were statistically significantly different between the quasistatic and dynamic loadings.

The pathology included linear and circular fractures, propagated unilateral and bilateral fractures, and multiple fractures due to external loading. Routinely, fractures identified on CT images were documented by the defleshed skull. Table 2 includes a summary of the biomechanical

Table 2: Summary of Biomechanical Parameters

Parameter	Units	Loading	Range	Mean
Force	kN	Static	4.5 - 11.9	6.4
		Dynamic	4.5 - 15.4	10.5
Deflection	mm	Static	7.8 - 16.6	12.0
		Dynamic	3.4 - 11.5	6.7
Stiffness	kN/mm	Static	0.5 - 1.3	0.8
		Dynamic	1.0 - 6.1	3.1
Energy	J	Static	14.1 - 68.5	33.5
		Dynamic	13.0 - 55.8	28.6

data obtained for both quasistatic and dynamic failure tests.

Discussion

The off-axis forces recorded by the distal load cell in the failure tests were significantly lower compared to the peak external input forces. The off-axis forces indicate the components of the force in two mutually orthogonal directions with the external loading applied in the vertical direction. These forces represent the unintended components sustained by the specimen during experimental loading. Since the magnitudes of these forces were small, the specimens can be considered to have sustained predominantly the intended external force vector.

An evaluation of the force-deflection responses for these tests indicated nonlinear characteristics typical of biological materials reported in literature. Unlike the force-deformation responses for the nondestructive tests, these force-deformation behaviors (for failure tests) indicated a significant amount of nonlinearity together with hysteresis.

The present series of tests revealed the fracture pattern to be complex and dependent upon the anatomical location of the external loading. Retrospective evaluations of the radiographs and CT images, without a prior knowledge of the external loading vector, produced no definite indications regarding the loading site during the experimentation. In fact, fracture widths were narrower at the loading site compared to the other regions where the specimen demonstrated wider separations of the fracture lines. Fractures generally continued to penetrate into the inner table with the loading applied superior to the outer table location.

Previous human facial tolerance studies have indicated the mineral content of skulls did not demonstrate any particular trend with respect to age of the specimen [19].

Results from the study delineated the biomechanics of the human skull under non-destructive quasistatic forces. The study has also provided the differences in static and dynamic loading responses. The forces, deformations, energies, and stiffnesses obtained in this study serve as fundamental data towards the understanding of the biomechanics of the structure. In addition, this information is crucial for the development and validation of mathematical models of the human head. For example, the three-dimensional bony geometry of the specimen can be obtained from the CT scans, the exact boundary and loading conditions used in the experiment can be accurately simulated, and the output experimental force-deflection

characteristics can be used for the validation of the finite element model. This procedure leads to the advancement of the experimentally validated three-dimensional finite element model of the human head which can be used to predict injury and develop anthropomorphic test devices.

References

1. Braakman R. Depressed skull fracture: data, treatment, and follow-up in 225 consecutive cases. *J Neurol Neurosurg Psychiatry* 35: 395, 1972.
2. Ehler VE, Eickhoff G, Pursian M. Zur Festigkeit und Elastizitat Druckbelasteter Menschlicher Weichteilbedeckter Kopfe. *Anat Anz* 140: S139, 1976.
3. Ehler VE, Weber J, Weber J, Steffin C. Der menschliche schadel unter dem einfluss vertikal im bereich der ossa parietalia eingeleiteter statischer drucklasten. *Anat Anz* 140 (S301), 1976.
4. Gurdjian ES. Impact Head Injury, Mechanistic, Clinical and Preventive Correlations. Springfield, IL: Thomas, C C, 1975.
5. Gurdjian ES, Lissner HR, Patrick LM. Protection of the head and neck in sports. *JAMA* 182 (5): 509, 1962.
6. Hodgson VR, Thomas LM. Breaking strength of the human skull vs. impact surface curvature. Springfield, VA: NTIS, U.S. Department of Transportation, 1971.
7. Jamieson KG. Surgical lesions in head injuries: their relative incidence, mortality rates and trends. *Aust. N.Z. J. Surg.* 44 (3): 241, 1974.
8. Jamieson KG, Kelly D. Traffic injuries in Brisbane hospitals over one decade. *Aust. N.Z. J. Surg.* 44 (2): 150, 1974.
9. Jamieson KG, Yelland JD. Depressed skull fractures in Australia. *J Neurosurg* 37: 150, 1972.
10. McElhaney JH, Stalnaker RL, Roberts VL. Biomechanical aspects of head injury. In: King WF, Mertz HJ, eds. Human Impact Tolerance. New York: Plenum Press, pp. 406, 1972.
11. Melvin JW, Evans FG. A strain energy approach to the mechanics of skull fracture. In: Proc 15th Stapp Car Crash Conf, Coronado, CA, 1971, 666.
12. Melvin JW, Fuller PM, Roberts VL. Frangible head form development Phase I: a six month study of the effects of localized impact on tissue. Ann Arbor, MI: Highway Safety Research Institute, 1969.
13. Nahum A, Gatts JD, Gadd CW, Danforth J. Impact tolerance of the skull and face. In: Proc 12th Stapp Car Crash Conf, Detroit, MI, 1968, 302.
14. Sances A, Jr , Myklebust JB, Larson SJ, Cusick JF, Weber RC, Walsh PR. Bioengineering analysis of head and spine injuries. *CRC Crit Rev Bioeng,* 2 (15): 1-79, 1981.
15. Schneider DC, Nahum AM. Impact studies of facial bones and skull. In: Proc 16th Stapp Car Crash Conf, Detroit, MI, 1972, 186.
16. Stover SL, Zeigler HE. Head injury in children and teenagers: functional recovery correlated with the duration of coma. *Arch Phys Med Rehabil* 57: 201, 1976.
17. Unterharnscheidt F, Higgins L. Traumatic lesions of brain and spinal cord due to nondeforming angular acceleration of the head. *Tex Rep Biol Med* 27 (1): 127, 1969.
18. Walker AE, Caveness WF, Critchley M. The Late Effects of Head Injury. Springfield, IL: Thomas, C C, 1969.
19. Yoganandan N, Pintar FA, Reinartz J, Sances A, Jr. Human facial tolerance to steering wheel impact: A biomechanical study. *J Safety Res* 24 (2): 77-85, 1993.

BASILAR SKULL FRACTURE RESULTING FROM COMPRESSION NECK LOADING

Barry S. Myers, M.D., Ph.D.
William J. Richardson, M.D.
Roger W. Nightingale, Ph.D.

Duke University
Department of Biomedical Engineering and
Division of Orthopaedic Surgery
Box 90281
Durham, NC
27708-0281
USA

SUMMARY

A cadaver head and neck impact model has been developed to produce a wide variety of clinically observed cervical spine injuries and basilar skull fractures. The impact model includes a drop track which allows impact of the head and neck with a simulated torso mass following into an obliquely oriented surface with varying amounts of surface padding. Twenty unembalmed ligamentous cadaver head-neck specimens have been dropped in an inverted posture with the head and neck in the anatomically neutral position. Multiaxis transduction recorded head impact forces, planar head accelerations, and neck reactions. In addition, the impact tests were imaged using a high speed imaging system at 1000 frames.

The head-neck-torso response was bimodal, including a head inertial loading mode followed by a neck-impact surface loading mode. A total of three basilar skull fractures were produced among 16 specimens suffering injuries, one in an impact to a rigid surface, and two in impacts to padded surfaces. Additionally, each of these injuries occurred in the neck-impact loading mode and were therefore unrelated to peak head impact force, or head acceleration. These data suggest that these injuries may occur with greater frequency than previously thought. They also suggest that some basilar skull fractures occur mechanistically like neck injuries and are not likely to be mitigated with the addition of impact surface padding.

1. INTRODUCTION

Skull fractures as a result of head impact have been documented in numerous studies over the last 35 years. The vast majority of these studies have been conducted in the absence of a cervical spine, or with horizonal impact velocities in which the neck acts primarily as a beam. Because of the low bending stiffness of the human neck as compared to its axial stiffness, the contributions of the neck to head injury in horizontal plane loading have often been assumed to be small. Following a similar line of thinking, most current standards for head impact protection (e.g. FMVSS 201, ANSI Z89.1, ANSI Z90.1, ASTM F717, Snell M85, and others) use either a free headform and measure headform center of gravity acceleration, or use a fixed headform and measure headform force as a result of a given impactor contact. In each case, either the inertial or the balanced neck-impact surface forces are not considered (Figure 1). For example, the components of the neck force which is balanced by the contact surface force does not influence the head center of gravity acceleration pulse. As a result, acceleration criteria for head injury (e.g. HIC, SI and others) are also not influenced by this component of the load. However, the presence of this additional neck force will increase skull loading, and may increase the risk for skull fracture. Unfortunately, little quantitative data are available to determine the significance of this neck-impact-surface force. Lissner et al. (1960) suggested that neck stiffness increased head injury risk in frontal impacts, however, this assertion was based on the study of embalmed cadavers in which the flexural stiffness of the neck is profoundly increased [1]. Clearly, understanding the role of neck loading in producing head injury remains a topic for further investigation.
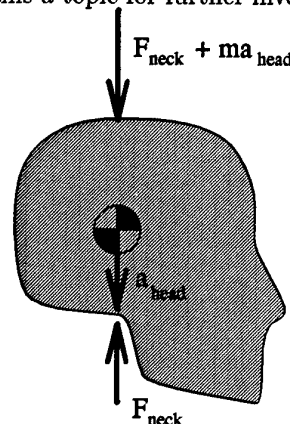

$$F_{neck} + ma_{head}$$

$$a_{head}$$

$$F_{neck}$$

Figure 1. Free body diagram showing forces applied to the head during head impact illustrating that the impact surface force is the sum of the D'Alembert and neck forces.

Basilar skull fractures (BSF) comprise a broad group of fractures involving the base of the skull. They include any fracture which propagates into the bones comprising the anterior, middle or posterior fossa of the skull. ring fractures of the skull base, and fractures of the occipital condyles. Vance (1927), as discussed by Huelke et al. (1988) observed that 471 of 507 fatalities with skull fractures had a component of fracture which included the skull base [2]. Restricting the definition to those fractures which are initiated in the skull base, the epidemiology of these injuries shows a number of important etiologies. Specifically, BSF occur most commonly as a result of motor vehicle accidents, and are most often fatal because of the resulting brain stem and vascular injuries which accompany these fractures [3]. Among patients presenting with BSF in Malaysia. 50% were motorcyclists, 22% were pedestrians struck by motor vehicles, and 20% were the victims of falls [4]. Pediatric data from the United States shows a similar distribution with pedestrian-vehicle collisions accounting for 42%, falls 27%, vehicle accidents 23%, and impact from a moving object 8% of BSF with survival [5]. Because of the high fatality rate associated with this injury, and its broad definition. estimates of the numbers of fatalities which result from BSF are not readily available. Miltner et al. (1990) reported occipital condylar fractures, in 25 of 600 traffic fatalities. suggesting that BSF fractures may be a common occurrence [6]. Similarly, Otte (1991) report BSF in 10.9% of motorcyclists with chin impact [7]. He also noted that 25% of head injuries involved chin impact.

Numerous mechanisms of BSF have been hypothesized including, cranial vault loading. facial loading, submental loading (tension-extension neck loading), and mandibular impact loading. Cranial vault loading resulting in fractures remote from the site of loading. including the skull base, are well documented as discussed by Huelke et al. (1988). Voigt and Skold (1974) and Huelke et al. (1988) also identified cases in which impact loads to the face resulted in BSF [2,3]. Tensile loading as a result of a judicial hanging in which the noose is placed laterally are perhaps the most well established mechanism of BSF [8]. Submental impact has been hypothesized by Cooter and David (1990) based on the examination of victims of motorcycle accidents [9]. This mechanism has recently been supported by cadaveric study of Hopper et al. (1994) [10]. In this study, mandibular impact tolerance as a result of isolated cadaver head impact into a fixed, rigid surface was found to be greater than basilar skull fracture tolerance in tensile loading of the skull base. Because these authors were unable to produce BSF as a result of mandibular loading in the isolated cadaver head, they asserted that inertial loading of the brain on the skull base was insufficient to produce BSF. They therefore concluded that

tensile loading from the ligamentous spine and neck musculature in conjunction with mandibular impact were required to produce this injury.

Compressive loading of the vertex of the head has also been postulated as a mechanism of BSF. LeCount and Hockzema (1934) attributed BSF to vertex impact [11]. Merignargues et al. (1975) suggest that small diameter BSF are the result of compression head loading. while larger diameter fractures were the result of extension [12]. Voigt and Skold (1974) reporting on 77 autopsy cases suggested that. ring fractures of the skull base could result from 'impression' [7]. Impression being the result of either a blow to the crown of the head or a fall on the buttocks.

Despite the apparent frequency of BSF in the population. few cadaveric studies of head and neck impact have produced these injuries. Pintar et al. (1995) used a hydraulic actuator to impact isolated cadaver head-neck preparations [13]. Among 20 specimens with injuries, none were reported to have BSF. Got et al.. dropped 42 obliquely oriented cadavers with and without helmets from 1.83 to 3.00 and observed skull fractures in only two tests [14]. It was not stated if these fractures involved the skull base. Culver et al. (1978) used a 10 kg impactor with velocities from 6.8 to 10.2 m/s to apply S-I impacts and produced cervical fractures without BSF in 11 specimens [15]. Nusholtz et al. (1981) using a 56 kg impactor with velocities from 4.6-5.6 m/s similarly did not observe BSF [16]. Yoganandan et al. (1986) reported five skull fractures following 12 whole cadaver drop tests in which drop height varied from 0.9 to 1.5 m [17]. Of these, one BSF was reported and two linear fractures propagated into the skull base. Interestingly, Nusholtz et al. (1983) did not report skull fractures following eight whole cadaver drop tests with drop heights between 1.0-3.7 m [18]. Alem et al. (1984) report on a total of 14 destructive S-I head impacts of whole cadavers using a 10 kg impactor. with varying amounts of impact surface ensolite padding [19]. One BSF was reported in which minimal padding. an impact velocity of 9 m/s, and large impactor forces, 17 kN. were measured. Another BSF was noted in a preliminary test though data were not reported. Based on these observations. the authors suggested that BSF occurred in large magnitude short duration head impacts and were either the result of skull deformation owing to head impact. or skull deformation owing to neck load. Unfortunately. these whole cadaver studies are unable to measure neck force-time histories. as a result. the mechanism of injury, the contribution of neck load to injury risk. and tolerance of the skull base remain largely unknown. As head loads can readily be mitigated by surface padding and neck loading is less readily decreased. determination of this injury mechanism may have a significant impact on injury

prevention device design. Therefore, the purpose of this research is to develop and analyze a realistic model of human head and neck impact. To allow for the quantification of injury, a fully instrumented human cadaver head and neck impact model is developed and presented.

2. MATERIALS AND METHODS

Experimental Apparatus

An experimental apparatus was designed to model head and cervical spine injury resulting from vertical head impact with a following torso (Figure 2). Two linear bearing sliders were used to mount a steel carriage to a drop track. The specimen preparations were mounted to the test frame in an inverted position with a torso mass of 16 kg. The initial orientations of the head and neck were established in the neutral position to preserve the resting lordosis of the cervical spine. This position was maintained using a suspension frame with breakaway sutures.
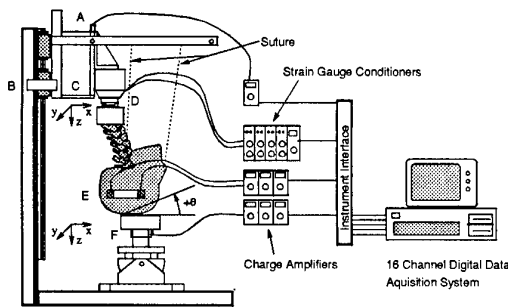

Figure 2. A diagram of the test apparatus showing the accelerometer on the torso mass (A), the optical velocity sensor (B), the carriage and torso mass (C), the six-axis load cell at T1 (D), the head accelerometers (E), and the impact surface and three-axis load cell (F).

A flat steel plate with a diameter of 15.25 cm and thickness of 4 cm served as an impact surface. Variation in impact angle about the y-axis (that axis normal to the sagittal plane) was achieved by mounting the impact plate on a locking clevis. The impact angle was varied between -15° (posterior head impact) and +30° (anterior head impact), according to the sign convention shown in Figure 2. The clevis was attached to a 42 kg steel plate using rail clamps which allowed for variation in positioning along the x-axis. The steel impact plate was mechanically isolated from the drop track. Its surface was covered with 3 mm of lubricated Teflon sheet in the rigid head impact tests to minimize friction. For the padded impacts, foams were attached to the steel plate

using duct tape. These included either an expanded polystyrene foam (EPS) (E =2096.1 kPa, σ_y =206.2 kPa, ρ =0.0284 g/cm^3) or an open cell polyurethane foam (OPU) (E =158.6 kPa, σ_y=7.0 kPa, ρ =0.0277 g/cm^3).

Multiaxis transduction was used to fully quantify the forces and moments acting on the head and neck during the impact event. Head impact forces were quantified using a Kistler 9067 three-axis piezoelectric load cell mounted under the impactor surface. A GSE Model 6607-00 six-axis load cell mounted to the specimen was used to measure forces and moments at T1. A PCB 302A02 uniaxial accelerometer measured torso deceleration. Sagittal plane kinematics were quantified using two PCB 306A06 accelerometers which were mounted to a fiber reinforced graphite composite beam which was then mounted on the head of the specimen. Impact velocity was recorded using an MTS optical sensor. The sixteen channels of transducer data were each sampled at 62.5 kHz using a PC-based digital acquisition system. Additionally, impact kinematics were imaged using two Kodak Ektapro EM-2 digital cameras, each operating at 1000 frames per second.

Specimen Preparation

Unembalmed human heads with intact spines were obtained shortly after death. The specimens were sprayed with calcium buffered isotonic saline, sealed in plastic bags, frozen, and stored at -20°. All donor medical records were examined to ensure that there were no pre-existing pathologies which could affect the structural responses of the specimens. Donor age ranged from 35 to 80 years. During specimen preparation all muscular tissues were removed, keeping all ligamentous structures intact, except for the ligamentum nuchae.

Each specimen was thawed and prepared for testing in a 100% relative humidity chamber. The specimens were transected at T3-T4 and the bottom two vertebrae were cleaned of musculature, defatted, and cast into aluminum cups with reinforced polyester resin. Care was taken to ensure that the most rostral uncast vertebra was free of resin and was allowed a full range of motion. Specimens were oriented to maintain the natural resting lordosis of the cervical spine with the Frankfort plane horizontal. Casting was performed with the specimen cup cooled in water to prevent possible specimen degradation due to the heat of polymerization. Photoabsorptive pins (4.0 mm diameter) were inserted into the anterior vertebral bodies, pars interarticularis, and spinous process of each vertebra for photogrammetric analysis of the impact event.

In addition, a strip of scalp was removed from the parietal bone, superior to the parieto-mastoid suture, and posterior to the coronal suture, to affix the accelerometer array. The exposed skull bone was defatted and dried, and the head was mounted in an alignment frame. A drill jig was used to make holes in the skull normal to the sagittal plane. The accelerometer array was attached to the head on a bed of dental acrylic using bone screws. The array position relative to the Frankfort plane was determined radiographically using lead pellets inserted into the acoustic meati and the infra-orbital foraminae.

Experimental Test Protocol

Cadaveric specimens were inverted and mounted to the carriage of the drop track system, in the anatomically neutral position. Break-away sutures were passed through the ear lobules and nasal septum and were tied to the suspension frame to establish the neutral orientation of the cervical spine. Each specimen was raised 0.53 m above the impact surface, and the cervical spine was mechanically stabilized by manual exercise through a flexion-extension range of motion of 60° for fifty cycles [20]. The specimens were released and allowed to fall onto the impact surface. Following impact, anteroposterior and lateral radiographs were obtained and the specimen was disarticulated at O-C1 and the head weighed. To document injuries, dissection, including craniotomy, was performed on both the heads and cervical spines following impact.

Data Analysis and Criterion for Failure

All transducer data were uploaded to a Sun SparcStation 2 for analysis. Digital filtration was performed in accordance with the Society of Automotive Engineers standard for head and neck impacts (SAE J211b Class 1000). In order to determine inertial head loading and evaluate the risk of head injury, linear acceleration of the center of gravity of the head was determined from the head mounted accelerometer array. The following criteria were used to define mechanical failure and relate mechanical failure to the occurrence of injury. Each decrease in force with increasing time was evaluated. The high speed images were coregistered to the load cell data and were analyzed to define the kinematics of each motion segment at the time of decreasing load. A decrease in load was related to a specific injury if the kinematics and injury mechanism were mutually consistent at the time of the decrease in load. Decreases in load as a result of slip at the head-impact surface were excluded by examination of image and head acceleration data. Decreases in load associated with increases in length of the neck were considered to be mechanical unloading and were similarly excluded. Any decrease in load with a concomitant increase in bending moment which also demonstrated a rapid transition from one mode of deformation to another mode of deformation on high speed images, and no evidence of injury at the site of the transition was defined as a stable buckle.

3. RESULTS

Using this test system, a total of 20 impact tests have been performed to date, producing basilar skull and cervical spine injuries in 16 cases (Table 1). Injuries were produced in five of the nine tests with a rigid impact surface. For the tests with a padded impact surface, injuries occurred in 11 of the 11 tests. Cervical spine injuries included anterior disc tears, anterior longitudinal ligament tears, Jefferson fractures, Hangman's fractures, odontoid fractures, burst fractures, facet dislocations, and posterior element fractures. Three basilar skull fractures were also produced.

The dynamics of the tests can be separated into a bimodal response as defined by local maxima in the head force histories (Figures 3, 4, and 5). For the rigid impacts, Mode 1 is attributed almost entirely to stopping the head and had a duration of 4.3±1.6 milliseconds. During the first half of this head inertial loading mode, the head impact force reached a maximum with no concomitant neck force (Figure 3). Neck loading at T1 was not observed until the latter half of Mode 1. For the padded impacts, the head contact times during Mode 1 were significantly increased (Figures 4 and 5). Therefore, the first mode contained loading by the torso in addition to the force required to stop the head. The inertia of the neck and torso mass represented 10 to 35% of the peak head force. Mode 1 durations for the padded impacts could not be calculated because the increased coupling of the head and cervical spine resulted in less separation between modes. For both impact surfaces, Mode 2 represents loading of the impactor surface by the head including inertial forces from the cervical spine and the effective torso mass. The duration of this neck-impact surface loading mode for the rigid impact was 27.3±14.3 msec. In all the tests there was a delay in the onset of measured neck load with respect to the head load. This lag in response at T1 was 1.6±0.3 msec for the rigid impacts which was significantly different than the 4.7±1.3 msec for the padded impacts (p<0.001; Figures 3, 4, and 5; Table 1). The lag is evidence that the head and cervical spine are not coupled during the first half of Mode 1.

Three basilar skull ring fractures were detected following craniotomy and removal of the cranial contents (N18, D40, and I11). No cranial vault fractures were detected. In each of the three

TABLE 1
SUBJECT DATA, TOLERANCE, AND INJURIES

Test	Age/Sex	Vel. (m/s)	Pad	Angle (deg.)	Head* (N)	HIC	Neck‡ (N)	Inj. Time‡ (msec)	Injury	Time lag* (msec)
N26	65M	2.43	no	0	-7638	-	-	-	None	1.4
N24	62M	3.20	no	0	-8566	1404	-1839	2.2	C1 2 part posterior ring fx. C2 Hangmans fx.	1.6
N22	71M	3.26	no	0	-8111	490	-1955	6.5	C1 3 part comminuted fx.	1.9
N11	55M	3.14	no	-15	-11621	543	-	-	None	2.0
N13	35F	3.28	no	-15	-5615	704	-	-	None	1.2
N18	-M	3.26	no	+15	-7498	1935	-1863	6.4	Basilar skull ring fx. C1 lateral mass fx. C2 Hangmans fx. C2-C3 disc, ALL C6-C7 bilateral facet dislocation	1.4
D41	69M	3.11	no	+15	-8604	1140	-	-	None	1.9
I32	78M	3.18	no	+15	-8234	1364	-2416	3.9	C5-C6 disc, ALL	1.2
N05	36M	3.23	no	+30	-8790	497	-1552	8.3	C3 burst fx. C3-C4 disc, ALL C4-C5 ALL	1.9
N039	75M	3.08	OPU	0	-5664	132	-3172	18.2	C4-C5 posterior left capsule C5-C6 disc C6-C7 bilateral facet dislocation	3.8
N029	75F	3.14	OPU	0	-3452	151	-715	14.7	C1 anterior ring fx. Type III Odontoid fx. Hangmans fx. C3-C4 disc, ALL left capsule C5, C6, C7 posterior fxs.	4.9
D40	53F	3.16	OPU	0	-4187	90	-1654	16.7	Basilar skull ring fx. C1 Jefferson fx. C2 Hangmans fx.	2.3
N19	42F	3.07	OPU	-15	-2604	175	-1011	18.8	C2-C3 disc, ALL, C2 chip C3-C4 disc, ALL, C3 chip	6.8
NA2	61M	3.16	OPU	-15	-4749	110	-1968	15.6	C3-C4 disc, ALL C5-C6 disc, ALL	3.8
I25	59F	3.07	OPU	-15	-5963	100	-2904	18.4	C1-C2 left capsular lig. C3-C4 disc, ALL, left capsule	3.5
I089	80M	3.15	OPU	+15	-5947	110	-2915	30.5	C2 Hangmans fx. C3-C4 disc, ALL, left capsule C4-C5 disc C5 burst fx.	5.4
D43	62M	-	OPU	+15	-4101	71	-1856	15.8	C1 Jefferson fx.	3.7
I11	63F	3.21	OPU	+15	-3115	119	-967	14.0	Incomplete basilar skull ring fx. Type III odonoid fx. C2-C3 right capsular lig., flaval lig. C4 laminar fx.	5.5
N21	61M	3.13	EPS	+30	-1759	50	-1632	14.8	C1 anterior ring fx. C4 spinous process fx. C5 spinous process fx. C5-C6 disc, left capsular lig., ALL	5.6
N23	46M	3.51	OPU	+30	-3857	197	-2240	18.7	C1 2 part right aspect fx. C3-C4 disc, ALL C4-C5 disc, ALL C5 sup. body chip	6.0

* Peak Resultant force applied by the impactor to the head.

‡ Magnitude of axial compressive neck force which produced the first detected injury and the time between impact and injury.

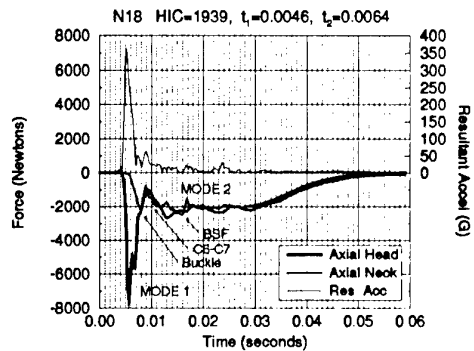* Time lag between onset of head load and onset of neck load.

N18 HIC=1939, t₁=0.0046, t₂=0.0064

Figure 3. Magnitude of the head and neck axial forces, and the head center of gravity acceleration for an impact into a rigid surface oriented at +15° (anterior). A bimodal response consisting of a head inertial deceleration mode (Mode 1), and a neck-impact surface loading mode (Mode 2) is shown. Analysis of the kinematic data revealed a stable buckle followed by a C6-C7 bilateral facet dislocation, and a BSF. The BSF occurred during the neck-impact surface loading mode (Mode 2).

D40 HIC=89.6, t₁=0.0191, t₂=0.0379

I11 HIC=118.5, t₁=0.0197, t₂=0.0404
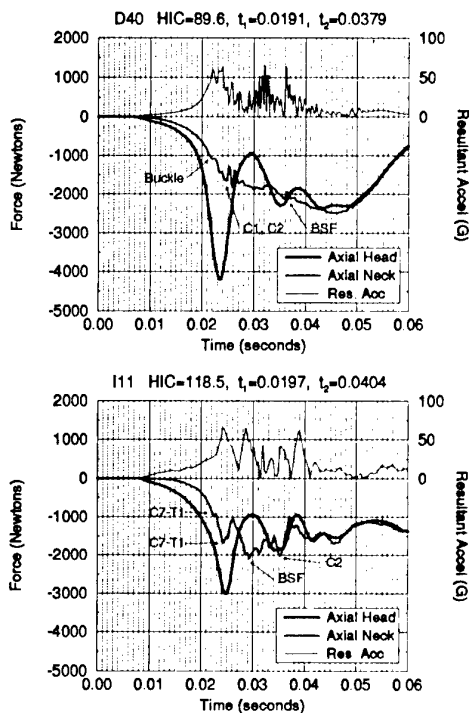
Figures 4 and 5. Magnitude of the head and neck axial forces, and the head center of gravity acceleration for a impacts into a padded surface oriented at +0° (D40) and +15° anterior (I11). Addition of padding significantly lowered the head accelerations and the Mode 1 head impact forces. The bimodal response of the head for the padded impacts is also shown. As a result of the increased contact time associated with a low stiffness padding, the head loading mode (Mode 1) and neck loading mode (Mode 2) overlap. The times, and injuries which occurred at that time are also shown. Despite the more closely phased modes, the BSF occurred in the neck loading mode.

cases, cervical injuries were also detected. Two cases (N18, and D40) involved contiguous fractures of C1, while the third (I11) had noncontiguous cervical injuries. Each basilar skull ring fracture originated in the dorsum sellae or the occipital clivus anteriorly. The fractures propagated bilaterally through the sphenoid bone, temporal bone, or adjoining sutures. The fractures then propagated posteriorly around, or into, the foramen magnum forming either complete (D40 and N18) or incomplete ring fractures (I11) (Figure 6). The rostral-most (anterior) portion of each fracture was displaced into the cranial vault by 3 to 5 mm. The caudal-most (posterior) portion of each fracture showed less displacement. Each fracture was mechanically stable to palpation as a result of soft tissue attachments, incomplete fractures, and interdigitation of the fracture fragments. With effort, the basilar skull fragment could be displaced into the vault. Because of the mechanical stability of the fracture and minimal displacement of the posterior portions of the fractures, the injuries were not readily apparent on external examination of the skull following craniocervical dislocation.
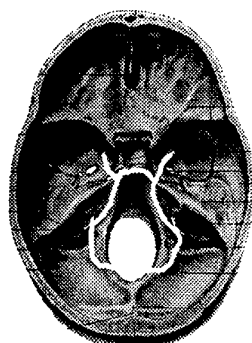
Each of the BSF occurred during the neck-loading mode (Mode 2) of the impact (Table 2; Figures 3, 4, and 5). Specifically, using the injury criterion and combining the kinematic and kinetic data sets, BSF occurred 15.4±3.2 msec following peak impactor force. At the time of the BSF, the impactor load was equal to, or less than the neck load, indicating the absence of head inertial forces, or a component of head rebound from the impact surface. Head Injury Criteria for the rigid and two padded BSF were 1935, 90, and 119, respectively. Time corridors (T1 and T2) selected to maximize the HIC calculation fell within the head inertial loading mode (Mode 1) for each of the three injuries. Thus, the time range used in the HIC calculation did not include the time at which the skull fractures occurred. The axial (spatially fixed, superior-inferior, z, direction) neck forces to produce the BSF were -2494, -2126, and -2085 N for the rigid and padded injuries (mean = -2235±225 N). The axial forces to produce BSF were larger than the forces required to produce each of the concurrent cervical injuries in each of the three cases (Table 2).

Peak resultant head force applied by the impact surface was significantly lower for the padded impacts, -4127±1375 N, than for the rigid impacts, -8297±1572 N (p=0.02). Similarly, the average HIC for the padded impacts, 136±32, was significantly lower than the average HIC for the rigid surface, 1010±534. Average axial neck force to produce the first neck injury was -1948±666 N and did not vary with impact surface.
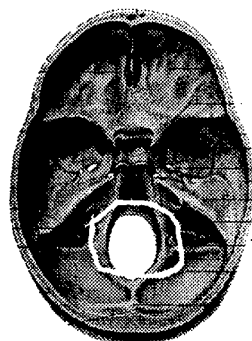
D40

N18

I11

Figure 6. Schematic drawing showing the fracture pattern in each of the three basilar skull fractures detected.

TABLE 2

BASILAR SKULL FRACTURE FORCES

Test Name	Time to Peak Head Force (msec)	Event	Neck Force (N)	Time (msec)
N18	1.4	Buckle	-2189	3.7
		C6-C7 fx.	-1863	6.4
		BSF, C1	-2494	11.8
D40	16.8	Buckle	-1085	14.2
		C1-C2 fx.	-1654	16.7
		BSF	-2126	27.9
I11	16.5	C7-T1 fx.	-967	14.0
		C7-T1 fx.	-1687	16.0
		BSF	-2085	20.9
		C2 fx.	-2016	26.8

4. DISCUSSION

Catastrophic head and neck injuries remain a significant societal problem. The purpose of this investigation is to understand these injury mechanisms, and provide insights into tolerance. This injury model produced a variety of clinically observed injuries, including Jefferson fractures, Hangman's fractures, burst fractures, posterior element fractures, bilateral facet dislocations, and BSF. The injuries in this study were produced in the absence of preflexion (i.e. the normal lordosis of the spine was preserved). Additionally, the distribution of injuries produced is consistent with the distribution of injuries reported in epidemiology studies [21].

The decoupling between the cervical spine and head observed in this study has been reported previously, and is a consequence of the low initial stiffness in the load deflection response of the spine [22, 23]. Liu et al. (1982) reported as much as 12 degrees of combined flexion and extension at O-C1 with less than 0.5 N-m of moment [24]. This laxity in the cervical spine and in the craniocervical articulation results in a bimodal characteristic for the head force which has been previously described by Nusholtz et al. (1981, 1983) [16, 18]. As a result of the bimodal response, two distinct loading intervals are present, a head inertial loading mode (Mode 1), and a neck-impact surface loading mode.

The primary limitation of this study is the inherent lack of muscle forces in the cadaver neck. During trauma, muscles undoubtedly play a role in stabilization and energy absorption. However, their importance is minimized during compressive loading. This was the rationale for limiting our tests to near vertex impacts with the head, neck and torso aligned in the anatomically neutral position. For vertical impacts,

the time for injury to occur is two to three times shorter than the cervical spine muscle reflex time, which further mitigates the role of musculature in these impact tests. For example, Foust et al. (1971) and Schneider et al. (1975) have reported cervical spine muscle reflex times ranging from 50 to 65 ms, which is longer than that required to produce injury in these vertical impacts [25, 26]. However, passive muscle forces will influence column bending stiffness and, therefore, cervical spine dynamics. Another limitation is the use a fixed weight for the torso mass regardless of the mass of the donor. As a result, the potential energy of the torso was the same for drops of equal height.

Basilar skull fractures clearly can be produced by near vertex head impact. In this study, three ring type BSF were observed among 16 specimens with injuries, an incidence of 18.7%. This suggests that BSF are a common consequence of near vertex head impact. In each case, BSF were accompanied with cervical injuries. Average neck force to BSF was -2,235 N which was slightly larger than the average required to produce neck injury (-1948 N). However, the force required to produce the neck injuries includes non-catastrophic, lower force to failure, injuries. Further, in each case, the BSF occurred at forces slightly larger (15.2%, Table 2) than those of required to produce the cervical injuries in the same specimens. Yoganandan et al. (1986) reported four skull fractures from head impacts [17]. Three of these had concurrent cervical injuries, including the one specimen with a true basilar skull fracture (i.e. without cranial vault injuries). Alem et al. (1984) reported a case of BSF as a result of head impact, and did not detect other cervical injuries in that specimen [19]. These results suggest that the skull base may have a slightly larger tolerance than the cervical spine, as a result, compression mediated BSF will more often than not be associated with cervical injury.

Several cadaveric studies involving higher energy impacts have produced neck injury without the reporting basilar skull fractures [14-16, 18, 22]. In contrast, in this study BSF occurred in 18.7% of those specimens sustaining injuries. In several of these earlier studies, however, the torso was stationary and the actuator was withdrawn or stopped by some mechanism other than the cervical spine. As a result, the neck-impact surface loading mode, in which this injury is produced, may have been attenuated or may not have occurred. Another reason for the absence of these injuries in other studies is the difficulty in detecting BSF. Specifically, our study shows that these fractures are stable to palpation, cannot be detected with conventional radiography, and are only revealed on dissection including craniotomy and removal of the cranial contents. External examination of the skull failed to detect this injury. Further, because

this injury occurs late in the dynamic event, decreases in force with increasing time may be neglected as simple ringing of the impact test frame. Additionally, in studies in which portions of the skull are used to apply forces to the cervical spine, injury to the skull base must be considered a failure at the end condition, and therefore not a meaningful injury. Combined these observations support the assertion that BSF is a common, severe consequence of near vertex head impact.

Because multibody impact force-time histories can produce decreases in load with increasing time, a stringent set of criterion were developed to determine the time and forces at injury. Specifically, our early experience has shown decreases in load with time as a result of non-injurious cervical spine buckling, slip of the head in the contact surface, decreases in the inertial loads on the torso mass (i.e. the end of the dynamic event), and mechanical failure of the specimen [21, 27]. By requiring a decrease in load with time to occur in conjunction with the observed motions of the specimen on high speed image data, and the demonstration of injury at a site in accordance with the mechanism suggested by the image data, a reliable set of forces and times to failure were determined.

Alem et al. (1984) was among the first to report BSF as a result of near vertex head impact [19]. Based on their observations, it remained unclear if BSF were the result of head impact acceleration or neck loading. By measuring neck and impact surface forces, our study demonstrates that BSF occur toward the end of the dynamic event in the neck-impact surface loading mode. At this time, the head is compressed between the cervical spine and the impact surface, and head inertia is small. In that regard, BSF as a result of near vertex head impact represent a quasi-static failure mechanism which is unrelated to the head acceleration. It is also, therefore, unrelated to head acceleration based injury criterion like the HIC. This study also suggests that basilar skull fracture tolerance is similar, or slightly higher, than that suggested for the cervical spine [28]. In the same context, this study suggests that BSF may be thought of mechanistically as a fracture of the cervical spine. Specifically, while head injuries are readily mitigated by the addition of surface padding (as measured by a decrease in HIC), neck injuries are insensitive to, and perhaps potentiated by the addition of surface padding [29, 30]. Thus, it is unlikely that addition of padding to an impact surface will prevent BSF as a result of near vertex head impact. Additionally, BSF can occur at drop heights of 0.53 m, a height at which skull fractures are uncommon, however, cervical injuries are common. It should be recognized that these fractures occur through other mechanisms however, and that these mechanisms may be governed by other tolerance criterion.

5. CONCLUSIONS

1. This experimental model is capable of producing clinically observed catastrophic basilar skull and ligamentous cervical spine injuries.

2. Head and neck impact loading is bimodal, including a head inertial mode and a neck-impact surface loading mode.

3. In near vertex compression head impact situations in which large neck loads contribute to head dynamics, BSF can frequently be produced.

4. Basilar skull fractures as a result of compression neck loading occur during the neck-impact surface loading mode (Mode 2). As a result, criterion for the prediction of skull fracture on the basis of head center of gravity acceleration (Mode 1), do not appear to be able to predict the risk for this injury. In contrast, compression neck injury force tolerance may be a suitable criterion for the prediction of BSF.

5. These fractures were produced at a drop height of 0.53 m, which is lower than the height typically required for skull fracture as a result of head inertial loading only.

6. While insufficient for meaningful statistical analysis, these data support the assertion that BSF compression force tolerance may be slightly larger, though not significantly different than that of the cervical spine.

7. Because the neck-impact surface mode is not significantly influenced by the addition of impact surface padding, it is unlikely that surface padding will decrease the frequency of BSF resulting from compression loading.

6. REFERENCES

1. Lissner, H.R., Lebow, M., and Evans, F.G., "Experimental studies of the relation between acceleration and intracranial pressure changes in man", Surg., Gyn., Obst., 3, 1960, 329-338.

2. Huelke, D.F., Smock, W.S., Fuller, P.M., and Nichols, G.R. II, "Basilar skull fractures produced by facial impacts - Case histories and a review of the literature. Proc. 32nd Stapp Car Crash Conference, 1988, 35-44.

3. Voigt, G.E., and Skold, G., "Ring fractures of the base of the skull", J. Trauma, 14, 1974, 494-505.

4. Chee, C.P., and Ali, A., "Basal skull fractures: A prospective study of 100 consecutive admissions", Aust. N. Z. J. Surg., 61, 1991, 597-602.

5. Liu-Shindo, M., and Hawkins, D.B., "Basilar skull fractures in children", Int. J. Pediatr. Otorhin., 17, 1989, 109-117.

6. Miltner, E., Kallieris, D., Schmidt, G., and Muller, M., "Injuries of the occipital condyles in traffic fatalities", Z. Rechtsmed., 103, 1990, 523-528.

7. Otte, D., "Technical demands on safety in the design of crash helmets for biomechanical analysis of real accident situations", Proc. 35th Stapp Car Crash Conference, 1991, SAE Paper #912911.

8. Wood-Jones, F., "The ideal lesion produced by judicial hanging", Lancet, 1, 1913, 53.

9. Cooter, R.D., and David, D.J., "Motorcyclist craniofacial injury patterns", Int. Motorcycle Safety Conf. Proc., I, 1990, 3.1-3.13.

10. Hopper, R.H., McElhaney, J.H., and Myers, B.S., Mandibular impact as a mechanism for basilar skull fracture", Proc. of the 38th Stapp Car Crash Conference, 1994, 123-131.

11. LeCount, E.R., and Hockzema, J., "Symmetrical traumatic fractures of the cranium: Symmetrical fragmentation – Comments on their mechanism", Arch. of Surgery, 29, 1934, 171-226.

12. Merignargues, G., Got, C., Tarriere, C., et al., "Les fractures circulaires de la base du crane au cours des accidents de la route. Nouvelle Press Med. 4, 1975, 2245-2248.

13. Pintar, F.A., Yoganandan, N., Voo,. L., Cusick, J.F., Maiman, D.J., Sances, A., Jr., "Dynamic characteristics of the human cervical spine", Proc. 39th Stapp Car Crash Conference, 1995, SAE Paper #95722.

14. Got, C., Patel, A., Fayon, A., Tarriere, C., and Walfisch, G., "Results of experimental head impacts on cadavers: The various data obtained and their relations to some measured physical parameters", Proc. 22nd

Stapp Car Crash Conference, 1978. SAE Paper #780887.

15. Culver, R.H., Bender, M., and Melvin, J.W., Mechanisms, tolerances, and responses obtained under dynamic superior-inferior head impact, UM-HSRI-78-21, 1978.

16. Nusholtz, G.S., Melvin, J.W., Huelke, D.F., Alem, N.M., and Blank, J.G., "Response of the cervical spine to superior-inferior head impact", Proc. 25th Stapp Car Crash Conference, 1981, SAE Paper # 811005.

17. Yoganandan, N., Sances, A. Jr., Maiman, D.J., Myklebust, J.B., Pech, P., and Larson, S.J., "Experimental spinal injuries with vertical impact", Spine, 1986: 11(9): 855-60.

18. Nusholtz, G.S., Huelke, D.E., Lux, P., Alem, N.M., and Montalvo, F., "Cervical spine injury mechanisms", Proc. 27th Stapp Car Crash Conference, 1983. SAE Paper #831616.

19. Alem, N.M., Nusholtz, G.S., and Melvin, J.W., "Head and neck response to axial impacts", Proc. 28th Stapp Car Crash Conference, 1984, SAE Paper #841667.

20. McElhaney, J.H., Paver, J.G., McCrackin, H.J., and Maxwell, G.M., "Cervical spine compression responses", Proc. 27th Stapp Car Crash Conference, 1983. SAE Paper #831615.

21. Nightingale, R.W., McElhaney, J.H., Richardson, W.J., Best, T.M., and Myers, B.S., "Experimental impact injury to the cervical spine: relating motion of the head and the mechanism of injury", J. Bone Joint Surgery, 78-A, 1996, 312-321.

22. Pintar, F.A., Sances, A. Jr., Yoganandan, N., Reinartz, J., Maiman, D.J., Suh, J.K., Unger, G., Cusick, J.F. and Larson, S.J., "Biodynamics of the total human cadaveric cervical spine. Proc. of the 34th Stapp Car Crash Conference. SAE Paper #902309, 1990, 55-72.

23. Oxland, T.R. and Panjabi, M.M., "The onset and progression of spinal injury: a demonstration of neutral zone sensitivity", J. Biomechanics, 25, 1992, 1165-1172.

24. Liu, Y.K., Krieger, K.W., Njus, G., Ueno, K., Connors, M.P., Wakano, K., and Thies, D., "Cervical spine stiffness and geometry of the young human male", Air Force Aerospace Medical Research Lab, 1982, AFAMRL-TR-80-138.

25. Foust, D.R., Chaffin, D.B., Snyder, R.G. and Baum, J.K., "Cervical range of motion and dynamic response and strength of cervical muscles", Proc. of the 17th Stapp Car Crash Conference. SAE Paper #730975, 1971, 285-308.

26. Schneider, L.W., Foust, D.R., Bowman, B.M., Snyder, R.G., Chaffin, D.B., Abdelnovr, T.A. and Baum, J.K., "Biomechanical properties of the human neck in lateral flexion", Proc. of the 19th Stapp Car Crash Conference. SAE Paper # 751156, 1975, 1037-1049.

27. Nightingale, R.W., McElhaney, J.H., Richardson, W.J., and Myers, B.S., "Dynamic responses of the head and cervical spine to axial impact loading", J. Biomechanics, 29, 1996, 307-318.

28. Myers, B.S., and Winkelstein, B.A., "Epidemiology, classification, mechanism, and tolerance of human cervical spine injuries", Critical Reviews in Bioengineering, 23, 1996, 1-102.

29. Nightingale, R.W., Richardson, W.J., DeMeyts D.D., and Myers, B.S., "The effects of padding on the risk for cervical spine injury", 23nd Meeting of the Cervical Spine Research Society, 1995, 61-62.

30. Myers, B.S., McElhaney, J.H., Richardson, W.J., Nightingale, R.W., and Doherty, B.J., "The influence of end condition on human cervical spine injury mechanisms", The Proc. of the 35th Stapp Car Crash Conference, 1991, 391-400.

7. ACKNOWLEDGMENTS

The Role of Kinetic Loading Parameters on the Severity of Diffuse Axonal Injury in Closed Head Injury

R. T. Miller,
D. H. Smith*,
X. Han*,
B. Xu*,
T. K. McIntosh*,
D. F. Meaney
Department of Bioengineering and *Division of Neurosurgery
University of Pennsylvania
3320 Smith Walk, 120 Hayden Hall
Philadelphia, PA 19104-6392, USA

Summary

In this report, we describe relationships between the kinetic loading parameters and the incidence of axonal injury in an experimental model of diffuse axonal injury used in our laboratory. Twenty animals (Hanford miniature pig, 13-20 kg, 3-4 months old) were injured using a coronal plane rotational acceleration of the head. Both the magnitude of angular acceleration and change in angular velocity were varied in these tests over a controlled range (56-260 krad/s^2; 174-472 rad/s). Seven days following injury, injured brains were examined using immunocytochemical markers for injury (NF200, SMI-31, and SMI-32) and maps of both the axonal injury distribution and severity were produced for selected coronal planes. Analysis of these injury maps revealed that the extent of injury in the mid-hippocampal plane was reasonably correlated to kinetic loading parameters (R=.66, .76), but that the correlations were less strong when focusing on specific intensities of axonal injury. Additionally, the severity of axonal injury in a given location, correlated to the loading parameters, but the changes were not statistically significant. Together, this study forms an important starting point for relating load parameters to injury within the brain, and can likely be improved with more advanced computational modeling capabilities.

Introduction

In the past several decades, investigators have developed a series of experimental models of brain injury in animals to study the many forms of brain injuries observed in humans (for review, see Lighthall 1988; Gennarelli 1994). Small animal species (i.e. cat, ferret, guinea pig, rat, mouse) are often used in these experimental models because of their low cost and wide availability. However, significant geometric and species constraints prevent these small animal models from mimicking the exact distribution and type of brain injuries observed in human closed head injury. As such, these small animal models are commonly used to develop better diagnostic procedures and to test new clinical treatment strategies; relatively few biomechanical studies on these models are conducted (see Meaney et al., 1993, 1994; Ueno et al., 1995).

In contrast, large animal models typically use a form of impact and impulsive acceleration to cause injury, and therefore provide a better correlate to the forces and motions that cause injury in humans. Stemming largely from animal studies conducted with non-human primates (Unterharnscheidt 1971; Ommaya et al., 1969; Gennarelli et al., 1982; Abel et al., 1978; Ono et al., 1980) and, more recently, miniature pig (Meaney et al., 1995), these large animal models offer a means to quantitatively relate the imposed forces and motions to intracranial injury patterns and, in turn, establish criterias for these injuries.

Although these large animal studies have provided important insight into the injury mechanisms involved during impact and impulsive head injury, several important issues remain unresolved. Perhaps most importantly, only a limited amount of injury criteria exists for specific brain injuries. In particular, one of the most prevalent and morbid forms of brain injury, diffuse brain injuries, remain an area of focus for several investigators.

Diffuse brain injury and its underlying pathology, diffuse axonal injury, is attributed to the widespread shearing of tissue at the moment of impact (Strich, 1956). Microscopic damage to the axons in the white matter appears within hours following impact, and may evolve over several weeks into areas of microglial clustering and scarring (Adams et al., 1981; Povlishock et al., 1994). At more severe levels of diffuse brain injury, tissue tears occur in the white matter immediately

following injury and are accompanied by a more extensive lesion pattern in the brain and brainstem. In all cases, the underlying axonal damage can produce immediate neurological impairment that, if persistent, can account for most forms of impairment in survivors of brain injury.

Albeit the significance and mechanisms of diffuse axonal damage are widely known, the exact conditions that create axonal damage within the brain are only beginning to be understood (Margulies et al., 1990). Recently, finite element models of the brain response to impact have emerged (Ruan et al., 1991; Bandak et al., 1995) and offer important computational tools to complement existing experimental studies of diffuse axonal injury. In particular, the parallel development of experimental models and computational simulations, exemplified in a recent study by Zhou et al., 1994, demonstrate the synergy such studies may have on understanding the incidence of this form of brain injury.

In light of these recent developments, we presented detailed data from an experimental model of diffuse axonal injury used in our laboratory to study the mechanisms and treatment of diffuse axonal injury. Specifically, we presented a method for quantitatively describing the microscopic lesions patterns within the porcine brain after acceleration injury, related the kinetic loading parameters to the quantitative measures of injury, and determined the thresholds of injury in this experimental model. With this analysis, we plan to pursue more rigorous studies to determine the exact *in vivo* conditions that cause injury, and to develop predictive capabilities for describing the onset of mild, moderate, and severe forms of this injury in humans.

Materials and methods

Pneumatic Injury apparatus - The device used to deliver an angular acceleration to the animal's head is based on previous designs (Gennarelli et al., 1982; Abel et al., 1978) and is centered on a six inch HYGE pneumatic actuator (Bendix Corp., Rochester, NY). The linear motion from the actuator is converted to an angular motion using a linkage assembly attached to the pneumatic device. Motion of the linkage is controlled through the linear stroke of the actuator, and was confined to either 94 or 104 degrees for this study.

Control of the angular acceleration and velocity profiles for the apparatus was adjusted through two primary mechanisms: (1) adjusting the hydraulic fluid level within the actuator, therefore changing the onset time of deceleration, and (2) controlling the pneumatic pressure supplied to the actuator, affecting changes in the magnitude and duration of the angular accelerations and angular decelerations. Although changes to the internal profiles of the deceleration and acceleration metering pins are possible with this device, these options were not exercised in the current study.

A schematic showing the cross sectional view of the pneumatic injury apparatus appears in Figure 1.
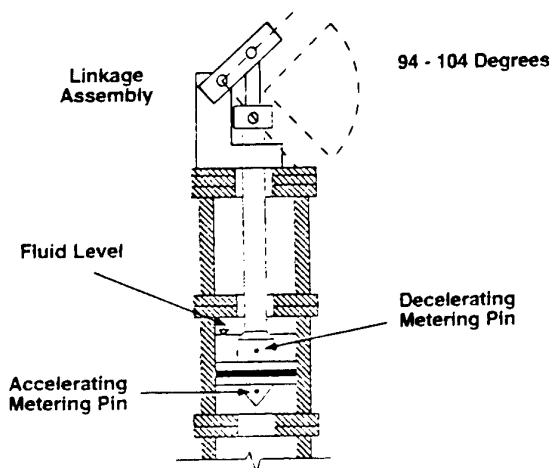

Figure 1 - Pneumatic injury apparatus (cross sectional view)

Experimental model of DAI - Young adult miniature pigs (3-4 months old, 13-20 kg, Hanford strain, Charles River, MD) were fasted for 12 hours prior to testing and water restricted for 2 hours prior to preparatory surgery. Prior to injury, the animal was premedicated by intramuscular injection of the benzodiazopine, midazolam (100- 500 mg/kg) and supplemented with atropine sulphate (0.05 mg/kg) to reduce endotracheal secretions. As soon as the desired depth of surgical anesthesia was attained, a venous catheter was inserted in the ear and the animal was intubated (endotracheally). After intubation, isoflourane anesthesia was maintained at 2% with a flow of 500-600 ml of oxygen per minute until a deep plane of surgical anesthesia was reached under sterile conditions.

Necessary surgical techniques were performed to allow arterial and intracranial pressure monitoring in a selected series of experiments, while noninvasive EKG and EEG electrodes were affixed to the scalp and chest. End tidal CO_2, respiration rate, and oxygen saturation were monitored continuously in all experiments. Additionally, blood samples were withdrawn to check blood gases periodically.

The animal's head was secured to the injury apparatus using a previously designed head holder apparatus (Meaney et al., 1993). The lower part of the clamp, a metal plate covered with a rubber bite plate, was inserted into the animal's mouth and the head was secured by tightening the padded spring steel bands which encircled the snout to the metal plate. All

procedures were approved by the University of Pennsylvania Institutional Animal Care and Use Committee.

This configuration, depicted in Figure 2, allows the animal's head to be subjected to a pure impulsive rotation in the coronal plane. Although considered a non-centroidal rotation, the alignment of the brain relative to the center of rotation (approximately 3 cm) minimized the translational acceleration effects in this model. A uniaxial accelerometer (Endevco Instruments, San Juan Capistrano, CA) mounted to the linkage's sidearm was used to calculate the rotational accelerations. We selected the coronal plane since this is the plane most likely to cause diffuse injury in non-human primates (Gennarelli et al., 1987).
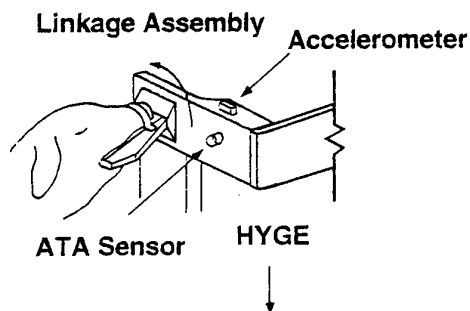
Figure 2 - Schematic of experimental model of diffuse axonal injury in the miniature pig. The animal's head is secured in a head holder apparatus and accelerated through an angle of either 94 or 104 degrees, depending upon the linkage design. Acceleration is restricted to the coronal plane since this is the plane often associated with DAI.

After each injury, the animal was allowed to stabilize and then transferred to an on site imaging facility for acute imaging studies. Once completed, the endotracheal tube was removed with all other monitoring equipment and all incisions were sutured closed. Upon awakening from anesthesia, all animals were administered Buprenorphine (0.1mg/kg, i.m.) for postoperative analgesia, supplemented every 12 hours until sacrifice. During the initial 6 hours of postoperative recovery, animals were continuously monitored. Once the animals righted themselves and began to eat and drink, they were returned to solo cages in the animal colony.

Recording and calculation of inertial loading parameters - A uniaxial accelerometer (Endevco, CA, Model # 2220D), with an amplitude response of less than ±5% between 1 and 10,000 Hz, was used to measure the tangential accelerations of the linkage. The signal was amplified and filtered with both a single-pole high pass filter and a two-pole active low-pass filter with a Butterworth-Thompson response with essentially a constant time delay. The bandwidth for the shock amplifier's

filters (Endevco, CA, Model #2740B) has a response of less than -5% at 4 and 2000 Hz. The signal was captured on a Smart IIa Data Acquisition Module (Endevco, CA, Model # 28956) with the following settings: 5000 Hz acquisition rate, 30% pretrigger, and triggering on the down slope of the signal.

After the experiment, both a hard copy and a digital output of the trace were acquired. This digital output was then read into a personal program and analyzed. Angular accelerations were calculated from the following formula:

$$\ddot{\theta} = \frac{a_t}{r} \quad [1]$$

Where a_t is the tangential acceleration, and r is the distance between the accelerometer and pivoting point on the linkage's sidearm.

Before additional kinetic parameters were calculated, the original signal's profile was fitted to a cubic spline and interpolated at a rate equal to two times the sampling rate. Then, a trapezoidal integration scheme was applied to calculate both the angular velocity and angular rotation profiles. The kinetic parameters of interest were as follows: peak angular acceleration/deceleration, peak change in angular velocity, acceleration/deceleration duration, rise time to peak deceleration, rise time to peak acceleration, total rotation, as well as the jerk in each phase of the acceleration phases.

An angular rate sensor (ATA Sensors, NM, Model ARS-01), with an operating response of less than -3 dB between .322 and 1.5 kHz, was used to verify both the recorded angular acceleration's peaks, as well as the general acceleration profiles that the HYGE can exhibit for different fluid levels. The ATA angular rate signal was again captured on the Smart IIa Data Acquisition Module. However, for these experiments the acquisition rate was increased to 10,000 Hz. After the experiment, the ATA signal was digitally filtered with a second order Butterworth low pass filter with a cut off frequency of 1000 Hz. Once again, the signal was fitted to a cubic spline and interpolated at twice its sampling rate. This signal was then differentiated with a five point differentiator based on the Taylor series to obtain the angular acceleration profile and integrated with a trapezoidal integration scheme to obtain the angular rotation.

Determining DAI injury patterns - One week following injury, comprehensive histological examination of the injured brains were used to document both the severity and extent of axonal damage. For these studies, the primary immunohistochemical markers used to identify damaged axons were NF-200, SMI-31, and SMI-32. NF-200 is a monoclonal antibody to the phosphorylated form of the heavy weight neurofilament protein (NF-H) in the triplet structure and is a

protein normally expressed in the CNS. SMI-31 is a mouse monoclonal antibody that labels a phosphorylated epitope shared by the Heavy (200kD, NF-H) and medium (160kD, NF-M) neurofilament proteins, while SMI-32 labels the non-phosphorylated epitopes of the NF-H and NF-M subset. We have used these antibodies extensively in rats, pigs, non-human primates, and human tissue and have found that it yields patterns of axonal labeling and swelling comparable to those produced using silver impregnation techniques.

Since the immunocytochemical markers used in the evaluation of the injured brains are normally expressed in the CNS, axons can be visualized in both a normal, uninjured state, as well as in an injured state. The distinguishing characteristics between normal and injured brains, however, is the caliber and appearance of injured axons. The neuropathologist (XH) evaluated injured brains for the appearance of hallmark axonal injury pathology (i.e. terminal clubbing or substantial swelling of axons), and verified these abnormalities by scanning several control, uninjured brains. Swellings well above the normal change in axonal caliber were considered injured. To ensure proper injury recording, the neuropathological recordings were verified independently by a second neuropathologist.

In each experiment, we scanned several coronal sections of brain tissue and marked the lesion patterns found under bright field microscopy. Seven coronal section maps outlining the gray and white matter regions for seven distinct coronal planes (Figure 3) were supplied to the neuropathologist (XH) and an injury criteria similar to grading human axonal injury patterns was used to evaluate the injury patterns. Injury scores were assigned to each box in the coronal map of the white matter, and a series of injury maps were recorded for each animal in the data set. If less than 1 bulb formations, or axonal swellings, were recorded in a microscopy (400x) field, then the neuropathologist assigned an injury severity of 0. Similarly, bulb formations of 1-5, 6-15, and >15 were assigned a grade of 1, 2, and 3, respectively. Color coded maps for the extent and severity of injury were recorded for each animal, and analysis of the injury pattern data was used to develop relationships with the inertial loading parameters.

Injury patterns were quantitatively described using three measures - the Total Injury Score (TIS), the Injury Severity Measure (ISM$_j$), and Total Axonal Injury (TAI) .

The TIS describes the extent of white matter damage. and is defined as follows:

$$TIS = \sum_{i=1}^{N} x_i \qquad [2]$$

where i represents an individual grid element, N is the total number of grid elements in a particular section, and x$_i$ is either

assigned a 0 or 1, indicating that there is no injury or injury, respectively. The maximum value of TIS is the total number of white matter elements within a specific section. A maximum value would indicate that the complete white matter in a coronal section is injured. Conversely, a TIS value of 0.0 denotes that none of the white matter was damaged.
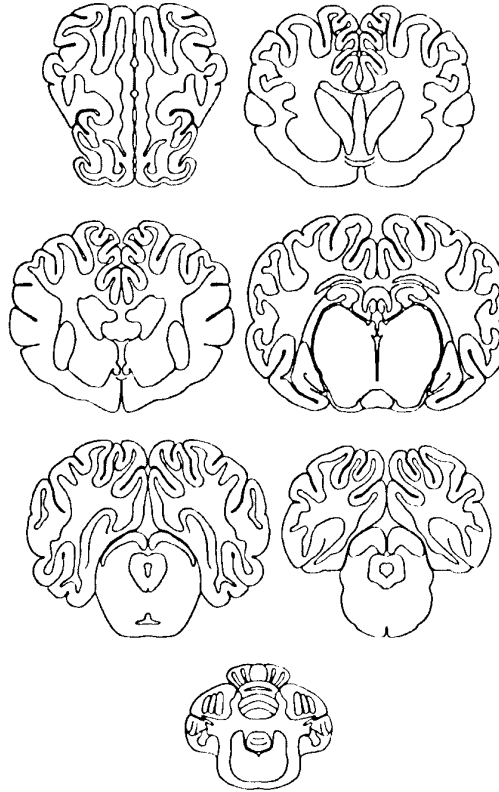

Figure 3 - Maps used to record injury patterns in the experimental model of DAI. See text for details.

The Injury Severity Measure (ISM$_j$) is constructed to denote the number of grid elements in a coronal plane map exhibiting injury of severity j:

$$ISM_j = \sum_{i=1}^{N} x_{i,j} \qquad [3]$$

where x$_{i,j}$ denotes injury (=1) of grade j in the ith element, and N is the total number of elements in a coronal plane diagram.

Finally, we used a measure of the total amount of axonal injury (TAI) to correlate load parameters with injury response data. TAI was calculated by multiplying the number of grid elements in a given injury region by the average number of bulb formations of swollen axons in this region (1+: 3 axons; 2+: 10 axons; 3+: 25 axons).

We used these measures to determine if correlations could be made between the extent of white matter damage and measurable load parameters, and if these correlations could be extended into the description of regional injury severity.

As a final quantitative measure, we focused on an anatomic region in a series of coronal plane images and recorded the severity of the injury (0, 1, 2, or 3) in this region as a function of the loading variables. We use this as an index of how inertial loading affects injury within a region, as well as the relationship between injury severities in a region.

Results

In this section, we described the performance of the experimental injury apparatus, the loading conditions used in the miniature pig experiments, the resulting injury patterns observed in the injured brains, and the correlations made between both the extent and severity of injury in this experimental model of diffuse axonal injury.

Since it is often desirable to examine the interrelationships between specific loading characteristics and resulting injury patterns, we first performed a series of experiments to determine the possible loading profiles with the pneumatic actuator injury apparatus. In these tests, we restricted the peak angular displacement of the head to be either 94 or 104 degrees, and changed the angular acceleration and angular velocity profiles by adjusting both the fluid level and pneumatic pressure inside the actuator.

Sixteen different operating conditions were examined, four at different hydraulic fluid levels (.9", 1.0", 1.1", 1.26") and four at different pneumatic pressures (75, 125, 175, and 250 psi). All of the tests were conducted under a fixed maximum rotation angle of 94 degrees. Acceleration and angular velocity were recorded at the time of testing; angular displacement was recorded by integrating the filtered angular velocity trace.

A typical angular acceleration/deceleration, angular velocity, and angular displacement trace for a test is shown in Figure 4. Clearly outlined in this figure is the biphasic nature of the angular acceleration loading condition, where an angular acceleration is followed by an angular deceleration of the linkage's side arm. In turn, the angular velocity reaches a maximum immediately prior to the deceleration phase of loading. Angular displacement, calculated from the angular

velocity signal, is within the physical limits of the machine's performance. Repeated tests under the same conditions yielded little variation in peak angular acceleration and peak angular deceleration values (<1%), as well as in peak angular velocity values (<1%).
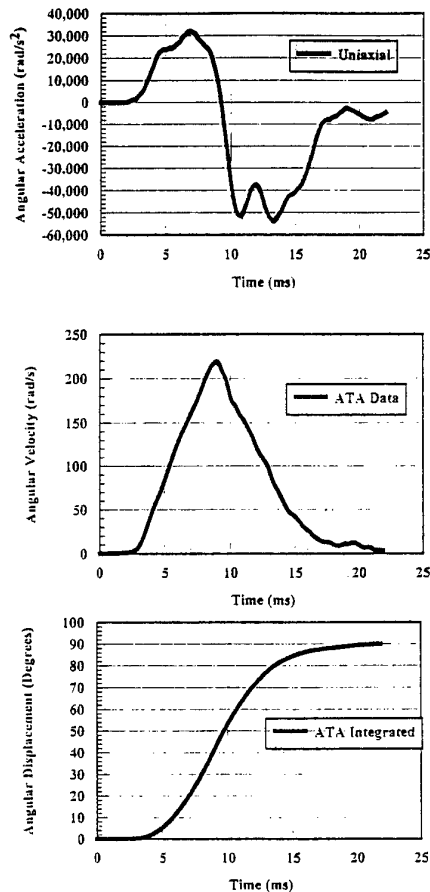
Figures 4(a), (b), and (c) represent rotational acceleration, ATA angular velocity, and integrated ATA angular rotation data for an experiment at 175 psi set pressure and 1.0 inch fluid level.

Altering the hydraulic fluid level in the pneumatic chamber altered both the maximum angular acceleration/deceleration ratios, and peak angular velocities (Figure 5). Shifts in peak angular decelerations were more apparent (50-111 krad/s^2), and likely due to the internal metering pin interacting with the fluid during the deceleration phase. Because the acceleration phase is not primarily dependent upon the hydraulic fluid, less change occurred in this aspect of the wave form (34-36 krad/s^2). Similarly, the angular velocity decreased with increasing fluid level, although the change was less

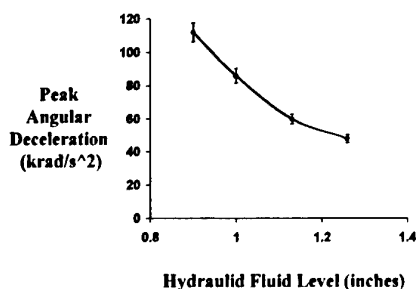pronounced (217-189 rad/s) in comparison to the deceleration phase.

Figure 5 - The pneumatic injury apparatus response depends on both hydraulic fluid level and pneumatic pressure. Change in the maximum deceleration over four fluid levels were quite pronounced (Shown). Change in the peak angular velocity and peak angular acceleration were less dependent upon fluid level, although each changed significantly (Not Shown).

In total, these testing profiles encompassed the range of settings used for the animal experiments, and form a basis for examining the brain injury patterns observed in the tests described in the next section.

Experimental model of DAI - In total, twenty animals were injured across a broad range of coronal plane rotational accelerations. Peak rotational accelerations were achieved in the deceleration phase of the biphasic acceleration pulse, and ranged between 56 and 260 krad/s^2. Peak change in angular velocity, calculated from the complete acceleration pulse, varied between 174 and 472 rad/s.

Most of the loading parameters were in the region predicted to cause injury within the brain according to a previous study (Meaney et al., 1995). Unlike the previous study, however, these data offer the opportunity to determine relationships between morphological signs of injury and the inertial loading parameters. Such information is valuable for properly predicting the extent of white matter damage from inertial loading parameters, and was the basis for a series of correlations between injury patterns and mechanical parameters describing the injury.

Determining DAI injury patterns - In general, injury patterns appeared as multi-focal areas of damage within a coronal plane section, with the most common areas of injury appearing along the periphery of the white matter (see example set in Figure 6). Axonal damage appeared throughout the cerebral hemispheres and brainstem, with areas of damage increasing with the inertial loading input.

Injury patterns were multi-focal in nature across coronal sections, with the spatial distribution changing as the studied coronal section was varied. Amount of fractional injured area was not consistent across sections within a given injured brain. These observations are similar to those observed in man and non-human primate, where injury patterns are in multi-focal sites throughout the brain.
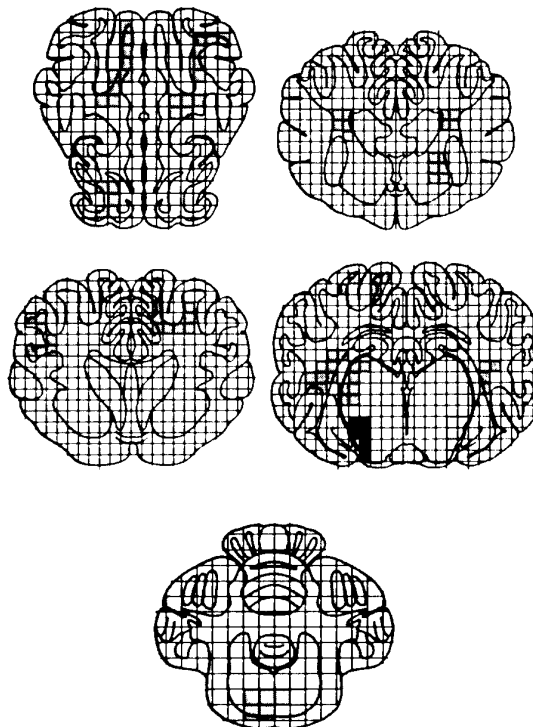

Figure 6 - Injury patterns in the miniature pig brain were in multi-focal regions throughout the white matter. Shown are the injured regions across five coronal sections in a miniature pig experiment (Scale: cross-hatch = 1-5 injured axons/field; gray = 6-15 injured axons/field; black = >15 injured axons/field).

Total Injury Score (NF200 staining) was linearly correlated (R=.659) to the peak angular deceleration used in each test, showing a reasonable predictive value for injury patterns in the mid-hippocampal plane. The intercept of this linear correlation, signifying the threshold at which injury appears in these planes, was calculated as 97 krad/s^2. Total Injury Score (NF200 staining) was also correlated to peak change in angular velocity (R=.676). The intercept of this linear correlation, indicating an angular velocity threshold required for injury was 325 rad/s.
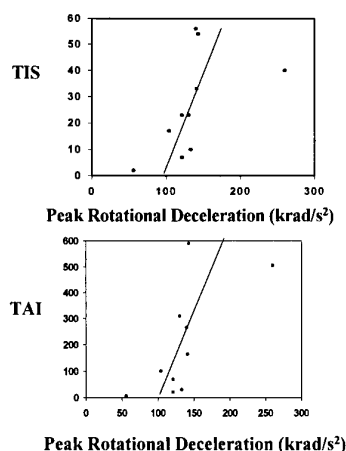
Figure 7 - Interrelationships between axonal injury and
inertial loading parameters.
TIS (R=.659) and TAI (R=.68)

Interestingly, total axonal injury score (TAI) correlated well
with angular deceleration (R=.68) and angular velocity
(R=.76) showing threshold values of 101 krad/s^2 and 338
rad/s, respectively. Note that these threshold values are very
similar to the TIS values.

Individual injury scores correlated less than total injury scores,
showing correlations that indicated either low or poor
statistical correlation (R < .3). Thresholds for injury that were
calculated from these regressions reflected the less favorable
correlations, with thresholds at different levels often
overlapping.

Finally, when a specific region (superior gyri) of the brain was
examined across all experiments, we determined that a dose-
dependent relationship existed between these injury patterns
(NF 200 staining) and the loading parameters. This difference
across severity levels was not significant, primarily due to the
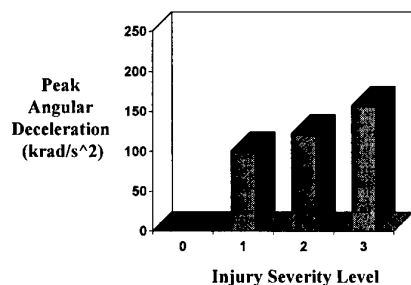small number of experiments conducted to date.

Figure 8 - Injury distribution across the superior gyri.

Discussion

In this report, we presented an analysis to understand the
relationship between the lesion patterns in an animal model of
diffuse axonal injury and the inertial loading conditions used
to produce these injury patterns within the porcine brain. Our
experimental technique, rotational acceleration/deceleration of
the porcine head, produced axonal injury throughout the
cerebral hemispheres and brainstem. We used
immunocytochemical data to reveal the extent and severity of
this axonal injury within selected coronal sections of the
injured porcine brain, and used a grid based scoring system to
quantify the lesion patterns in the porcine brain. By
correlating the inertial loading to the lesion pattern, we
developed injury onset thresholds in terms of the peak angular
deceleration and peak change in angular velocity.

This report is built upon previous investigations (Smith et al.,
1996; Ross et al., 1994), yet is the first study to quantitatively
determine the relationship between mechanical loading
parameters and injury incidences. Earlier studies with models
in the non-human primate developed general estimates of
inertial loading required to cause injury (Margulies et al.,
1990), as well as describing the functional consequences of
inertial loading in different planes (Gennarelli et al., 1982), but
did not examine relationships between injury patterns and
macroscopic head motion parameters. Still other groups used
animal experiments to determine thresholds for reversible
functional injuries, such as concussion (Ono et al., 1982;
Ommaya et al., 1968) but did not have the opportunity to
examine the microscopic damage to the white matter. In a
different vein, recent physical modeling studies (Meaney et al.,
1993) pointed towards the importance of matching
neuropathological lesions patterns with tissue deformation
parameters, but did not match these deformation response data
with inertial loading parameters.

From earlier studies, it has been proposed that either tissue
shear strain or stress is a possible predictor for axonal injury *in
vivo* (Ruan et al., 1994; Galbraith et al., 1994). The analysis
presented in this report is one step towards identifying a
rational mechanical criteria for the morphological damage,
since it provides relationships between loading parameters and
injury. Perhaps most importantly, it provides a foundation
upon which more rigorous computational models, such as
finite element models of the porcine brain (see Zhou et al.,
1994 for an example), can be used to quantitatively relate the
applied loading parameter to *in vivo* tissue states of material
stress and strain. Once developed and validated, these finite
element models can be exercised over a broad range of loading
conditions to identify material stress and strain during
acceleration/deceleration injury and to relate these parameters
to tissue injury. When complemented with other *in vivo*
models of white matter injury, these studies offer a practical
means to address both tissue injury criteria and, in a more
general sense, brain injury prediction.

References

Adams, J., Graham, D., Gennarelli, T., (1983), Head injury in man and experimental animals: neuropathology. Acta Neurochirurgica - Supplementum. 32:15-30, 1983.

Adams, J., et al., (1981), Diffuse axonal injury due to nonmissile head injury in humans: an analysis of 45 cases. Annals of Neurology 12: 557-563.

Abel, J., Segawa, Gennarelli, T., (1978), Incidence and severity of cerebral concussion following sagittal plane angular acceleration in the subhuman primate. Proc. of the 22nd Stapp Car Crash Conf., SAE.

Bandak, F., (1995), On the mechanics of neurotrauma: A review and critical synthesis, in Traumatic Brain Injury: Bioscience and Mechanisms, pp. 139-155, Mary Ann Liebert, Inc.

Blumbergs, P.C., G. Scott, et al., (1995), Topography of axonal injury as defined by amyloid precursor protein and the sector scoring method in mild and severe closed head injury. Journal of Neurotrauma, 12(4): 565-572.

Dixon, C., Clifton, G., et al., (1991), A controlled cortical impact model of traumatic brain injury in the rat. Journal of Neuroscience Methods 39: 253-262.

Galbraith, J., Thibault, L., et al., (1993), Mechanical and electrical responses of the squid giant axon to simple elongation. Journal of Biomechanical Engineering 115: 13-22.

Gennarelli, T., (1994), Animate models of human head injury [Review]. Journal of Neurotrauma 11(4): 357-68.

Gennarelli, T., (1983), Head injury in man and experimental animals: clinical aspects. Acta Neurochirurgica - Supplementum. 32:1-13.

Gennarelli, T., Thibault L., Adams J., Graham D., Thompson CJ., Marcincin RP., (1982), Diffuse axonal injury and traumatic coma in the primate. Annals of Neurology, 12(6):564-74, Dec.

Graham, D., Adams, J., et al., (1993), Quantification of primary and secondary lesions in severe head injury. Acta Neurochirurgica - Suppl. 57:41-8.

Graham, D., Adams, J., Gennarelli, T., (1988), Mechanisms of non-penetrating head injury. [Review] Progress in Clinical & Biological Research. 264:159-68, 1988.

Kanda, R., Nakamura, N., Sekino, H., Sakai, H., Masuzawa, H., Mii, K., Aoyagi, N., Aruga, T., Kono, H., Sugimori, T., Sugiura, M., Mori, N., Kikuchi, A., Ono, K., Kobayashi H., (1981), Experimental head injury in monkeys --concussion and its tolerance level--Neurologia Medico-Chirurgica. 21(7):645-56, Jul.

Lighthall, J., Dixon, C.E., Andersen, T.E., (1988), Experimental models of brain injury. Journal of Neurotrauma 6(2): 83-97.

Margulies, S., Thibault, L., Gennarelli, T., (1990), Physical model simulations of brain injury in the non-human primate. Journal of Biomechanics, 23: 823-36.

Meaney, D.F., D.H. Smith, D.I. Shreiber, A.C. Bain, R.T. Miller, D.T. Ross, T.A. Gennarelli, (1995), Biomechanical analysis of experimental diffuse axonal injury. Journal of Neurotrauma, 12(4):689-694.

Meaney, D. F., Thibault, L.E., Winkelstein, B.A., Brasko, J., Ross, D.T., Gennarelli T.A., (1994), Modification of the cortical impact brain injury model to produce axonal damage in the rat cerebral cortex. Journal of Neurotrauma. 12(4):320-329.

Meaney, D.F., Thibault, L.E., Brasko, J., Ross, D.T., Gennarelli, T.A. (1993), Significance of impact velocity in the production of axonal injury in the rat cerebral cortex using rigid indentation. Journal of Neurotrauma. 9(3):393.

Ommaya, A.K., Hirsch, A.E., Haris, E., (1967), Scaling of experimental data on cerebral concussion in subhuman primates to concessive thresholds for man. Proc. 11th Stapp Car Crash Conference. SAE, NY, pp. 47-52

Povlishock, J., Hayes, R., Michel, M., McIntosh, T., (1994), Workshop on animal models of traumatic brain injury. Journal of Neurotrauma. 11(6):723-32, Dec.

Povlishock, J., and Christman, C. Diffuse Axonal Injury, in The Axon. ed. S. Waxman. pp. 504-530, Oxford Press, NY

Ross, D., Meaney, D., Smith, D., Gennarelli, T., (1994), Experimental diffuse axonal injury in the miniature swine: histological characterization. Experimental Neurology 126: 291-299.

Ruan, J., Khalil, T., King, A., (1991), Human head dynamic response to side impact by finite element modeling. Journal of Biomechanical Engineering. 113:276-283.

Sekino, H., Nakamura, N., Kanda, R., Yasue, M., Masuzawa, H., Aoyagi, N., Mii, K., Kohno, H., Sugimori, T., Sugiura, M., Kikuchi, A., Ono, K., (1980), Experimental head injury in monkeys using rotational acceleration impact. Neurologia Medico-Chirurgica. 20(2):127-36, Feb.

Strich, S.J., (1956), Diffuse degeneration of the cerebral white matter in severe dementia following head injury. J Neurol Neurosurg Psychiat. 19:163-185.

Ueno, K., Melvin, J.W., Li, L., Lighthall, J., (1995) Development of tissue level brain injury criteria by finite element analysis. Journal of Neurotrauma. 12(4).

Unterharnscheidt, F.J., (1971), Translational versus rotational acceleration - animal experiments with measured input. in Biomechanics of impact injury and injury tolerances of the head-neck complex. ed. S.H. Backaitis, pp. 407-410. Society of Automotive Engineers, Inc.

Zhou, C., Khalil, T., King, A., (1994) Shear stress distribution in the porcine brain during rotational impact. Proc. 38th Stapp Car Crash Conference. SAE, Warrendale, PA

In Vivo Mechanical Thresholds for Traumatic Axonal Damage

Allison C. Bain[1]
Kris L. Billiar[2]
David I. Shreiber[1]
Tracy K. McIntosh[3]
David F. Meaney[1]

[1]University of Pennsylvania - Department of Bioengineering
120 Hayden Hall, 240 S. 33rd St., Philadelphia, PA 19104-6392
[2]University of Miami, Dept. of Bioengineering
[3]University of Pennsylvania, Div. of Neurosurgery

Abstract

A methodology to identify tissue level axonal stress and strain from macroscopic parameters is outlined. A non-linear, viscoelastic, structural relationship is proposed to describe the in vivo response of the guinea pig optic nerve to uniaxial elongation. The optic nerve is modeled as a bundle of parallely aligned axons undulated to varying degrees. When straightened, each axon displays non-linear, viscoelastic behavior that contributes to the overall behavior of the optic nerve. Optic nerves were examined microscopically to calculate the undulation of individual axons. Axonal undulation was found to follow a gamma distribution, with a mean undulation of 1.070 and a standard deviation of 0.053. A reduced relaxation function, consisting of two exponential terms, was approximated from in vivo, dynamic elongation of the guinea pig optic nerve. Results from the in vivo relaxation tests indicated that the relaxation behavior was independent of displacement, a requirement for linear, viscoelastic theory based on hereditary integrals. The instantaneous elastic function was expressed as an integral of the undulation distribution and a function of the stretch ratio. Initially, a linear stretch ratio function was assumed to analyze the effects of the undulation distribution on the instantaneous elastic response. These results were compared with those obtained by increasing the order of the stretch ratio function to a third order polynomial. The computed results of the proposed structural relationship compared well to the experimental data from in vivo optic nerve tests, indicating that this model could provide a framework for identifying axonal thresholds for traumatic injury.

Symbols list

$F_A(\lambda,t) =$ Force in an axon
$G_A(t) =$ Reduced relaxation function for an axon
$f(\lambda) =$ Stretch ratio function
$F_{ON}(\lambda,t) =$ Force in the optic nerve
$l_u =$ Undulated length
$l_A =$ Apparent length

$U = \dfrac{l_u}{l_A} =$ Undulation
$N =$ Number of axons
$P(\lambda) =$ Undulation distribution function
$K_0 - K_4 =$ Reduced relaxation function constants
$F^{(e)}(\lambda) =$ Elastic force function
$\alpha, \beta =$ Gamma distribution parameters
$A, B, C, D =$ Constants

Introduction

Injury is the leading cause of death among people under 45, and is the fourth leading cause of death in the general population[1]. Of the millions of injuries occurring every year, over 34% are traumatic brain injuries (TBI), and more than 50% are attributed to vehicular accidents[2]. Diffuse axonal injury (DAI) is a type of traumatic brain injury characterized by widespread, microscopic damage to axons throughout the brain, macroscopic hemorrhages, and overt tissue tears[3]. DAI is responsible for more than a third of all head injury deaths, and is now considered the cause of the majority of severe, long term disabilities observed in survivors of brain injury[2, 4]. Moreover, the conditions that cause DAI - severe levels of angular acceleration - most often occur during head impact in vehicular accidents[3].

Due to its clinical significance, many studies now focus on understanding the biomechanics and pathophysiology of DAI. Although significant strides have recently been made in describing how specific loading conditions create significant stress and strain levels in brain tissue, little is known about how stress and strain translate into the spectrum of morphological and functional axonal injury seen clinically[2]. Such information has become extremely important as finite element models of the human brain emerge as useful tools in studying human head injury[5-9]. Understanding the relationship between tissue stress and strain and the subsequent degree of microscopic injury is the basis for determining tolerance criteria for brain tissue. Stress- and strain-based – or tissue level – injury thresholds are unique because they are

independent of geometry and are appropriate to any type of loading condition. Thus, tissue based injury thresholds can be applied to analytical, physical, and computational models to predict the potential for axonal injury in any type of head injury[9].

Currently, development of tissue level thresholds is difficult because of the lack of a sufficient biomechanical understanding of axonal injury. Many researchers focus on experimental animal models to study the different aspects of axonal injury[10]. However, there are many factors which make current experimental models of TBI less than ideal for developing tissue level axonal injury thresholds. First, animal models of DAI generally necessitate the use of large animals because small animals lack sufficient white matter. This adds considerable cost to each experiment as well as increases the time required to grade the extent of injury. Also, the loading conditions are frequently severe and result in heterogeneous neuropathology which includes DAI. In these cases, difficulties can arise in attributing the pathophysiological consequences to primary axonal injury or to secondary mechanisms associated with other pathologies. Finally, the loading conditions and internal geometry of the brain are complex, making the determination of axonal orientation and the specific loading conditions imparted to an injured axon very difficult.

To simplify the injury parameters, several investigators have turned to isolated, in vitro, tissue studies to determine brain tissue characteristics, as well as tolerances for axonal injury[11-22]. Typically, the tolerance studies have focused on dynamic uniaxial stretch of central and peripheral nervous system nerves. In vitro models have led to a greater understanding of the pathophysiological consequences of stretch of nervous tissue, including the effects on electrophysiology and calcium ion flux. The mechanical response and strain thresholds of individual peripheral nervous system (PNS) axons have been characterized in vitro[20]. However, it is not known how the in vitro mechanical response compares to the in vivo response, nor how PNS axons compare to CNS axons. For example, in vitro axonal stretch experiments do not account for the in vivo undulation of axons.

Current methods of identifying thresholds for axonal injury involve simulating in vivo experimental models with analytical, physical, and computational models[5, 7-9, 23-27]. The results of these models are either compared with the neuropathological results from the experimental model to predict tissue deformation, or are combined with strain threshold criteria obtained from in vitro models to predict a severity of injury. The most widely used current models make use of the finite element method to predict the deformation field throughout the brain under specific loading conditions. These models require many simplifying assumptions concerning internal geometry, boundary conditions, and material properties. For example, the brain is typically considered to be a homogeneous, isotropic material with no constitutive differences between gray and white matter. Some models include a stiffer material description for white matter.

but do not account for the variation in axonal orientation in their final analysis[28]. Further, these models universally predict macroscopic strain fields that do not necessarily translate to the same magnitudes experienced by the individual axons because of the in vivo undulation of axons within white matter. For example, a model prediction of 25% strain in the corpus callosum does not imply that individual axons at that location are strained 25%. Subsequently, although these models have answered many questions regarding the response of brain tissue to a traumatic injury, no model permits direct quantification of the specific conditions causing axonal injury or of the level of tissue deformation.

Recently, a simpler model of axonal injury - dynamic, uniaxial elongation of the guinea pig optic nerve - has been developed by our laboratory as a means to better understand the biomechanics of in vivo axonal injury[29]. The guinea pig optic nerve is a bundle of parallely-aligned, myelinated, CNS axons which, when dynamically uniaxially elongated, exhibit an injury response that is morphologically identical to that seen in human DAI[30, 31]. This model is unique in that the loading condition required for injury (ie. elongation) is simple, easily controlled and quantified, and simulates the primary mechanism by which axons are damaged in human DAI. Also, because the direction of the axons and the direction of elongation are known, the tissue level deformation can easily be determined. Moreover, varying degrees of injury, indicated by the number of axons exhibiting injury, are easily achieved by controlling the level of elongation. Thus, this model is ideally suited to study deformation based axonal injury thresholds of in vivo central nervous system tissue.

The first step in determining the injury threshold for a single axon is the development of an appropriate relationship to describe the behavior of the optic nerve. The overall response of the optic nerve is strongly linked to its microscopic structure, namely the degree of waviness, or undulation, of the individual axons. Microscopic examination of optic nerve cross-sections clearly indicates that each axon has a characteristic undulation, defined as the ratio of the actual length to the apparent length, and that the undulations exhibit a unique distribution over a certain range.

When the optic nerve is initially elongated, the individual axons gradually straighten. It is believed that straightening axons takes very little force. Therefore, a negligible force is required to elongate the optic nerve to a small displacement. Eventually, the axons are stretched beyond their initial undulated length, and significant forces are required to further elongate the optic nerve. Consequently, the initial degree of waviness exhibited by individual axons, as well as the overall distribution of axonal undulations is very important in the overall behavior of the optic nerve. Thus, the proposed relationship is based on a structural model representation of the optic nerve, in which the optic nerve is modeled as a bundle of parallel axons, exhibiting a distribution of undulations. An advantage of using the undulation distribution approach is that it allows us to evaluate the overall behavior of in vivo CNS tissue as a whole, as well as the stress-strain behavior of the individual axons.

Similar procedures have been used to describe skin, aorta, muscle, the tympanic membrane, and many other biological materials[32-43]. Like the optic nerve, the behavior of these materials are highly dependent on the undulated nature of their constituents. A common feature to several models is the assumption that the fiber undulation follows a normal distribution[33, 42-44]. However, comparing axonal undulation to the normal distribution reveals several differences. The normal distribution is symmetric around a mean and stretches to infinity on both sides of the mean. Axonal undulation, by definition, is never less than one. Also, the mean axonal undulation falls close to one, forcing the distribution to be skewed. Although the normal distribution could be manipulated to be useful, it is clear that axonal undulation is better represented by a non-normal distribution. Therefore, it is necessary to characterize the microstructure of the optic nerve, and to determine an appropriate frequency distribution.

Although incorporating the undulated nature of the axons in the optic nerve allows us to characterize the elongation/strain behavior of the individual axons, the material response these strains produce in the axons and optic nerve as a whole remain unknown. To identify this, we must investigate the relationship between stress and strain during elongation. The optic nerve, like many biological tissues, exhibits non-linear viscoelastic behavior. A common technique to model this response is to apply the theory of quasi-linear viscoelasticity[14, 45-51]. This theory assumes that the mechanical behavior of a material is governed by two functions: a reduced relaxation function that is time dependent, and an instantaneous elastic force response that is strain dependent. Although this elastic force equation is often non-linear with respect to strain, principles of linear viscoelasticity and superposition still hold because the relationship between stress and the elastic force function is linear[52, 53]. By combining quasi-linear theory and an undulation distribution, we can develop a mathematical basis for transferring the structural response of the optic nerve into the stress and strain response of the individual axons in the optic nerve. Once completed, this analysis can be combined with information from computational, physical, and kinematic models to predict tissue level and axonal level thresholds for injury. Also, proper implementation of the model described in this report will enable us to quantitatively evaluate stress and strain as predictors for functional and morphological injury.

Materials and Methods

Using basic principles of quasi-linear viscoelasticity, we initially assume that the force in one axon, as a function of time, is proportional to the product of a function of the stretch ratio, $f(\lambda)$, and the reduced relaxation function, $G_A(t)$, of a single axon[53].

$$F_A(\lambda,t) = G_A(t)f(\lambda) \qquad [1]$$

If we assume that all axons are of the same caliber and that they behave identically, then the force in the optic nerve is simply the sum of the forces in all stretched axons.

$$F_{ON}(\lambda,t) = \Sigma G_A(t)f(\lambda) \qquad [2]$$

In vivo, each axon is undulated in appearance with an undulation parameter defined by,

$$U = \frac{l_u}{l_A} \qquad [3]$$

where l_u is the actual, undulated length of the axon, and l_A is the apparent length. For undulations greater than one, the axon does not bear any tensile force. Axons having an undulation equal to one contribute to the structural response of the nerve to elongation. Therefore, when the optic nerve is elongated, the only axons contributing to the overall force defined by Equation [2] are represented by the definite integral of the product of the stretch ratio function, the frequency distribution function, $P(\lambda)$, and the total number of axons in the optic nerve (N) from one to the current optic nerve elongation (Figure 1). Equation [2] then becomes

$$F_{ON}(\lambda, t) = G_A(t)\int_1^{\lambda(\tau)} f(\lambda(\tau))NP(\lambda)d\lambda \qquad [4]$$
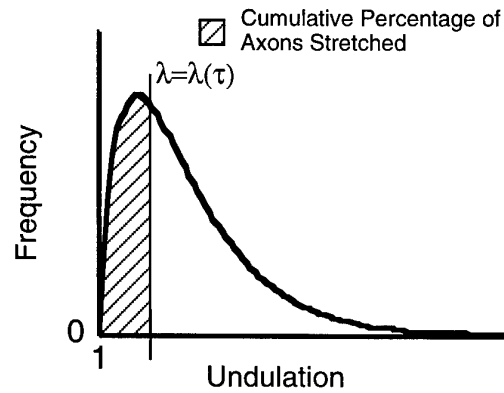

Figure 1: Schematic representing the percentage of total axons that contribute to the overall optic nerve force when the optic nerve is elongated to a stretch $\lambda(t)$. The percentage of axons is found by calculating the area under the undulation distribution curve. The area is determined by computing the integral from 1.0 to $\lambda(t)$.

The force (at time τ) generated by an infinitesimal increase in the stretch ratio is [42, 43]

$$dF_{ON}(\tau) = G_A(0)\int_1^{\lambda(\tau)} df(\lambda(\tau))NP(\lambda)d\lambda \qquad [5]$$

At time $\tau+t$, the force in the optic nerve is the existing force at time τ, slightly relaxed, superposed with the force generated by the newly stretched axons. The optic nerve force for all $t \geq \tau$, is then

$$F_{ON}(t) = \int_0^t G_A(t-\tau)\int_1^{\lambda(\tau)} \frac{df(\lambda(\tau))}{d\tau} NP(\lambda)d\lambda d\tau \quad [6]$$

Thus, implementation of this equation requires determination of the undulation distribution, $P(\lambda)$, the stretch ratio function, $f(\lambda(\tau))$, and the reduced relaxation function, $G_A(t)$.

Determination of Undulation Distribution

To characterize the axonal undulation distribution, uninjured guinea pig optic nerves were perfused and fixed, in vivo, and then removed and dissected from the globe and extraocular muscles. Optic nerves were cut on a freezing microtome into 20 μm thin longitudinal sections and immunohistochemically stained with the antibody SMI 31 (Sternberger Monoclonals, Inc), a monoclonal neurofilament antibody that recognized phosphorylated medium and heavy weight neurofilament proteins, which are commonly found in abundance in normal axons. Axons were visualized by reacting sections with diaminobenzidine (DAB). Stained sections were mounted on slides and prepared for light microscopic visualization. When magnified, many axons of varying undulation and diameter can be visualized.

Three evenly stained, uninjured nerves were chosen for analysis. For each nerve, one full longitudinal section was characterized. Undulations were calculated for several hundred (300-600) axons along the entire length of each optic nerve section.

Axonal undulations were determined using Neurolucida (MicroBrightField, Inc.), software specially designed to trace neuronal projections. Slides were placed on a motorized stage, so that the x,y,z coordinate of the cursor position could be recorded with respect to a reference point. The apparent length of a given axon was calculated as the distance between the two end points of the visualized axon. The undulated length was calculated as the sum of the distances between a series of closely placed points along the length of an axon (Figure 2). The undulation is then the ratio of the undulated length to the apparent length. The undulation of an axon must be greater than one, with an undulation of one being a perfectly straight axon.

To examine the characteristics of the distribution, the undulations for each group of axons were plotted as a frequency histogram, and the mean, variance, and standard deviation were calculated. These values were used to predict the parameters in the frequency distribution function. Goodness of fit tests, using the Chi-squared value (p>0.05), were used to compare the actual data with predicted distribution functions to select the best form of theoretical distribution[54].

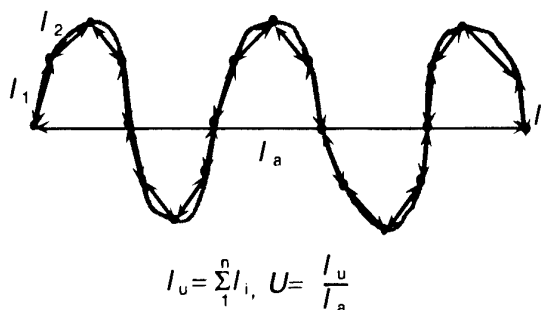$$I_u = \sum_1^n I_i, \quad U = \frac{I_u}{I_a}$$

Figure 2: Top: Example of in vivo undulation of guinea pig optic nerve axons. Bottom: Using Neurolucida (MicroBrightField, Inc.), an axon is approximated with lines connecting closely spaced points. The undulated length (I_u) is the sum of the lengths of all lines. The apparent length (I_A) is the length between the two endpoints. The undulation, U, is the ratio of undulated length to apparent length.

To determine an average distribution function that adequately represents the three separate distributions, the parameters calculated for each group were averaged. Goodness of fit tests were conducted for each actual-average distribution pair to ensure that the average predicted distribution function also represented the individual distributions (Chi-squared, p>0.05).

Determination of the Reduced Relaxation Function

The time dependent reduced relaxation function of the guinea pig optic nerve was determined using a custom designed device to dynamically elongate the in vivo optic nerve at very high strain rates. Adult, Hartley, albino, male, guinea pigs ($n=4$), weighing between 450-550 grams, were anesthetized with a mixture of ketamine (50 mg/kg) and xylazine (5 mg/kg). The right upper and lower eyelids were injected at the canthi with 2% lidocaine, and were retracted using suture. A small incision was made at each canthus of the right eye, to allow further retraction of the eyelids. Using iris scissors, a 360° opening was made in the conjunctiva, and the six extraocular muscle insertions were severed. A sling, constructed of sterile, surgical tape, was placed around the posterior side of the globe so that the optic nerve projected out the slit.

The animal was placed in a stereotaxic head holder angled at 30° to align the optic nerve in the direction of elongation. The free ends of the sling were then connected to the force

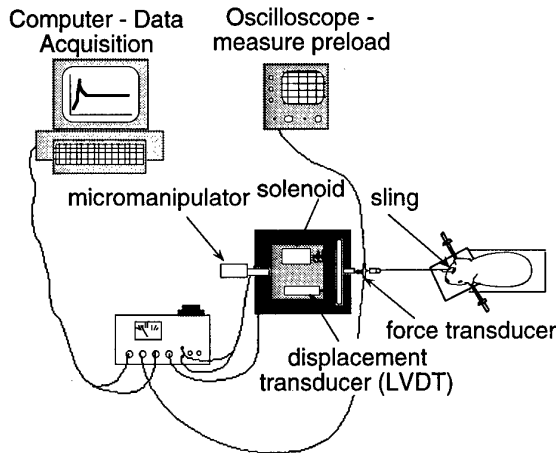transducer. To remove any slack, the nerve was preloaded until the force transducer registered a load.

Figure 3: Schematic of the experimental system used to find the reduced relaxation function. Guinea pig optic nerves were dynamically elongated, in vivo, to a set displacement. The force response of the optic nerve was recorded for 60 seconds.

A schematic of the optic nerve injury apparatus is shown in Figure 3. The apparatus delivers a reproducible, measurable uniaxial displacement (0-10 mm) with a very short rise time (5-10ms). The elongation is triggered by a solenoid and is measured by a linear variable differential transformer (LVDT) connected in parallel with the solenoid. The magnitude of the elongation is controlled by a micromanipulator that adjusts the distance traveled by the solenoid piston. The maximum displacement is held until the solenoid is manually switched off. When triggered by the electronic circuit, the solenoid displaces the optic nerve via the sling/suture attachment. The force experienced by the nerve is measured by a strain gauge force transducer (Entran) aligned in series with the optic nerve. A signal conditioner filters and amplifies the force transducer signal (gain = 10, cutoff freq. = 70kHz.). Both force and displacement are recorded, saved, and plotted by a Keithly-Metrabyte data acquisition board (DAS8).

For the current series of relaxation tests, each optic nerve ($n=4$) was tested three times at three levels of displacement: 2.0, 3.0, and 4.0 mm. For each experiment, data was recorded for sixty seconds, and each force signal was digitally filtered with a Chebyshev low-pass filter with a 250 Hz cutoff frequency. Each filtered set of data was normalized to unity by dividing by the peak filtered-force, and fit to a two-term exponential decay of the form

$$G_R(t) = K_0 + K_1 e^{-K_2 t} + K_3 e^{-K_4 t} \qquad [7]$$

Instantaneous Elastic Force Function

Quasi-linear theory stipulates that the elastic force function account for the strain dependence of a material. Thus, the elastic force function for the guinea pig optic nerve must include the undulation distribution, as well as a function of the stretch ratio. Initially, we chose to use a linear relationship between the force and stretch ratio to elucidate the non-linear effects of the undulation distribution on the overall structural response of the optic nerve model. Therefore, from Equation [5], the instantaneous elastic function is

$$F^{(e)}(\lambda) = G_A(0)\int_1^{\lambda(\tau)} A(\lambda - 1)NP(\lambda)d\lambda \qquad [8]$$

where $G_A(0)=1$, and A is a constant chosen to approximate the ramp phase of the experimental stress relaxation tests. The applicability of this choice was examined by comparing this form of the elastic force function with data from the experimental relaxation tests, using the goodness of fit methods (Chi-squared, p>0.05), and by comparing the overall responses of the theoretical and experimental results.

A similar analysis was performed using a third order polynomial of the form

$$f(\lambda) = A(\lambda - 1)^3 + B(\lambda - 1)^2 + C(\lambda - 1) \qquad [9]$$

as the stretch ratio function[39, 55].

The results using both stretch ratio functions were compared by determining the overall response of the model to elongation using Equation [6]. This information is compared with experimental data to asses the effect of combining the given stretch ratio function with the undulation distribution to describe an instantaneous elastic force function.

Results

Axonal Undulation Distribution

The mean undulation, variance and the standard deviation, calculated for each nerve, are shown in Table 1. As expected, all distributions were skewed towards the lower undulation limit. Based on the distribution characteristics, the gamma frequency distribution was chosen to represent axonal undulation[54]. The gamma distribution has a discrete lower limit of zero, an upper limit that stretches to infinity, and is skewed towards the lower limit. It is ideal for describing data, such as rainfall, that cannot be negative, but can at times be much larger than the mean. Therefore, it is assumed in the structural model, that axonal undulation can be adequately described by the gamma distribution, provided that all undulations (U) are offset to zero $(U - 1)$ to facilitate calculation of the distribution parameters. The equation for the gamma frequency distribution for $U - 1 > 0$ is

$$P(U - 1) = \frac{1}{\Gamma(\alpha)\beta^\alpha}(U - 1)^{\alpha - 1}e^{-\frac{(U-1)}{\beta}} \qquad [10]$$

where $\Gamma(\alpha) = (\alpha - 1)!$. The parameters, α and β, are calculated from the mean and variance of the distribution, using the following equations:

$$mean = \alpha\beta$$
$$var = \alpha\beta^2$$
[11]

These parameters determine a unique gamma distribution that describes the respective data. The parameters for each nerve are shown in Table 1. The average distribution was defined by the average values of α and β from the three separate distributions.

	Nerve 1	Nerve 2	Nerve 3	Average
mean	1.079	1.073	1.058	1.070
variance	0.0037	0.0027	0.0021	0.0028
standard deviation	0.061	0.052	0.046	0.053
alpha	1.67	1.95	1.55	1.726
beta	0.047	0.037	0.037	0.040

Table 1: Gamma distribution parameters are calculated from the mean and variance of the three nerve groups. The average values are determined by averaging the parameters from the three individual distributions.
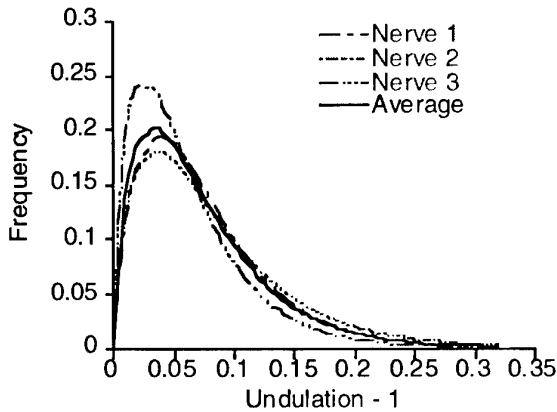
Figure 4: The representative gamma frequency distribution for each group is uniquely defined by the parameters, α and β. The average predicted distribution is described by the average of the parameters for the individual groups.

The gamma distribution approximated for each nerve, as well as the average distribution, are depicted in Figure 4. Goodness of fit tests, conducted for each nerve-gamma distribution pair and for each nerve-average distribution pair, were all significant ($p > 0.05$). A histogram, compiled using undulations from all

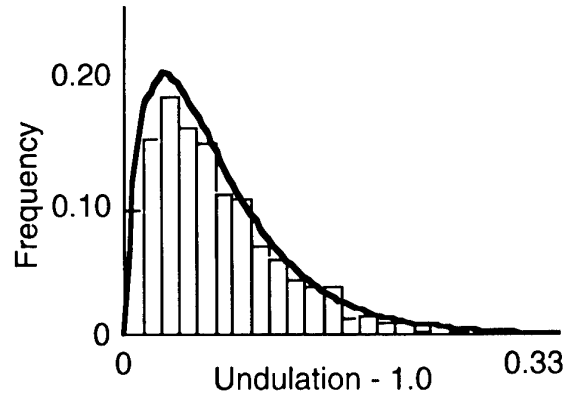nerves, and the average predicted distribution are shown in Figure 5.

Figure 5: The frequency histogram of all undulations calculated between the three nerves (total axons = 1306) closely follows the gamma distribution predicted by the averaged parameters.

Based on the average predicted distribution, the gamma frequency distribution used to describe axonal undulation in the guinea pig optic nerve is

$$P(U-1) = \frac{1}{(0.913)(0.04)^{1.723}}(U-1)^{0.723}e^{-\frac{(U-1)}{0.04}}$$
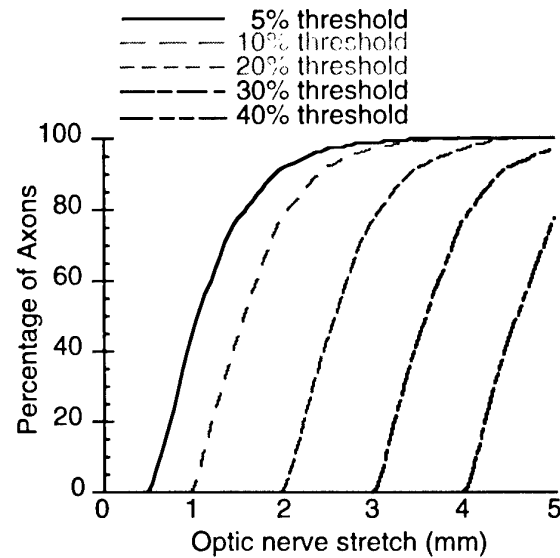[12]

Figure 6: The percent of total axons stretched above a certain threshold level for a given optic nerve elongation (mm) was calculated using the proposed gamma distribution.

Using this proposed distribution, the percentage of total axons stretched beyond a certain threshold level was calculated for varying degrees of optic nerve elongation (Figure 6). These values are a direct result of the microstructural characterization, and provide a means to compare morphological injury to mechanical response data.

Relaxation Function

Optic nerves were tested, in vivo, at three levels of elongation, 2mm, 3mm, and 4mm. Nerves were tested dynamically at rise times between 5-10 ms, corresponding to strain rates in excess of 20 sec^{-1}. Representative relaxation curves for the three different strain levels are shown in Figure 7.
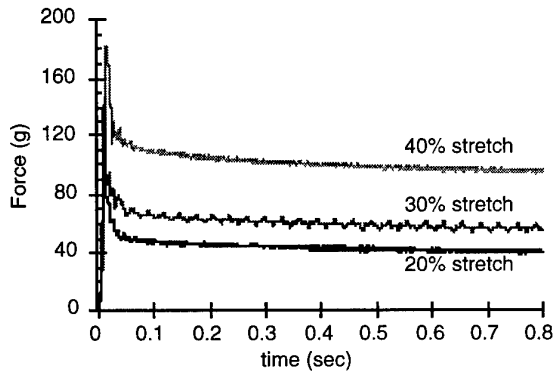
Figure 7: Relaxation data at three levels of stretch: 2mm, 3mm, 4mm. In agreement with quasi-linear theory, the relaxation behavior of the optic nerve appears to be independent of strain.

Each set of relaxation data was fit to a two-term exponential decay:

$$G_R(t) = K_0 + K_1 e^{-K_2 t} + K_3 e^{-K_4 t}$$

A representative relaxation curve and the exponential decay approximation are plotted in Figure 8.

	2mm	3mm	4mm	Average
K_0	0.480	0.563	0.624	0.556
K_1	0.095	0.098	0.099	0.097
K_2	19.646	19.070	10.570	16.429
K_3	0.514	0.395	0.315	0.408
K_4	516.38	437.45	310.46	421.430

Table 2: Coefficients for the two-term exponential equation that were determined from the stress relaxation data for different levels of elongation.
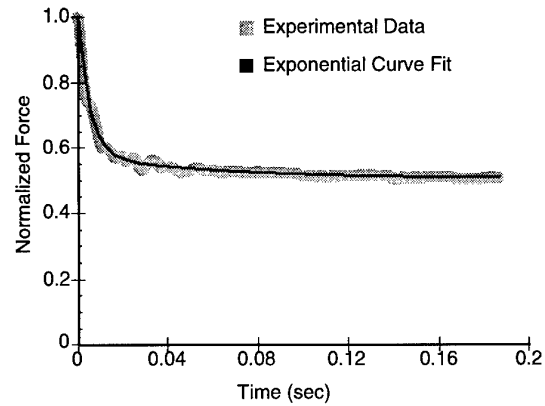

Figure 8: All experimental reduced relaxation data were approximated by a two-term exponential with correlation coefficients greater than 95%.

The average coefficient values for each level of strain are shown in Table 2. The final average coefficients were calculated using all strain levels.

Instantaneous Elastic Function

The computed instantaneous elastic function using a linear function of the stretch ratio, and an experimental trace from an equivalent relaxation test are shown in Figure 9. The Chi-squared value, indicating the goodness of fit, was calculated as 678.43. Acceptable levels ($p>0.10$) must be less than 140[56].
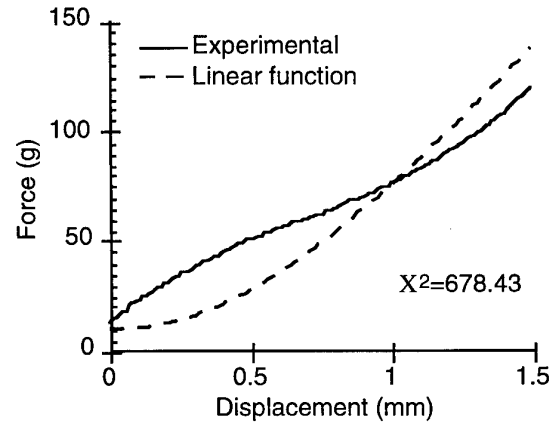

Figure 9: The computed elastic function containing a linear function of stretch ratio, and equivalent experimental data. The computed function is a quadratic shape due to the non-linear behavior of the undulation distribution. The experimental data resembles a higher order polynomial.

The computed instantaneous elastic function using a third order polynomial function of stretch ratio and experimental data are displayed in Figure 10.. The Chi-squared value for this fit, 111.37, was in the acceptable range of values ($p>0.1$).
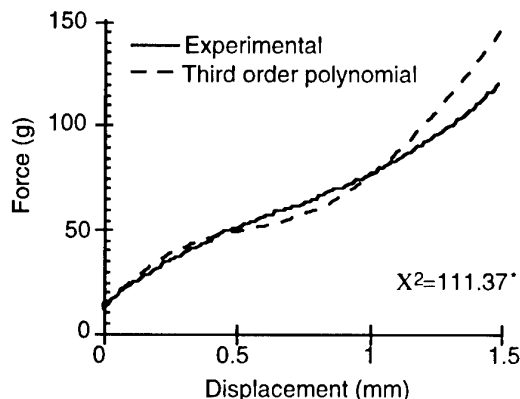

Figure 10: The computed elastic function containing a third order polynomial for the stretch ratio function, and equivalent experimental data. A third order polynomial more closely resembles the general shape of the experimental data, and has an acceptable Chi-squared value for goodness of fit ($p>0.1$).

Final Behavioral Relationship
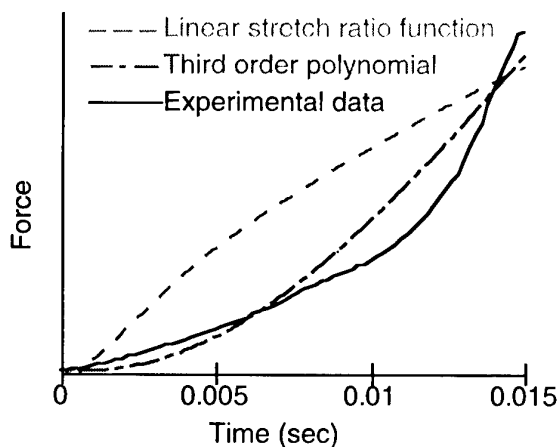
Figure 11: Model simulations of dynamic optic nerve elongation using a linear and a third-order polynomial elastic function along with experimental data. The third order polynomial model better predicted the experimental data.

Figure 11 demonstrates the ability of the model to predict the force in the optic nerve over time during dynamic elongation.

The model using a third order polynomial elastic function approximated the shape of the experimental data better that the model based on a linear elastic function.

Discussion

Undulation Distribution

Typically, in bioengineering circles, complex experimental models are simplified computationally to facilitate analysis of tissue level deformations. In contrast, we have chosen to use a relatively simplified experimental model of CNS injury - dynamic elongation of the guinea pig optic nerve - to achieve this task. The guinea pig optic nerve is ideally suited for the study of axonal injury. It consists of myelinated, CNS axons, aligned along a single axis, which are not complicated by gray matter or a substantial vascular system. Using this model, we can subject a discrete bundle of axons to a quantifiable elongation that allows a more precise determination of the deformation imparted to individual axons. This model is also capable of producing varying degrees of axonal injury. Furthermore, morphological injury in the optic nerve is easily identified using standard immunohistochemical techniques, and functional injury is easily assessed with visual evoked potentials. Thus, this experimental model is well suited to investigate thresholds for the spectrum of axonal injury seen clinically, and is the basis for the proposed mathematical model.

This analysis represents the first attempt to include the structural appearance and behavior of in vivo axons in a description of the tissue level response to deformations experienced during traumaticbrain injury. Material testing of brain tissue indicates that it is non-linear, anisotropic, and viscoelastic, with distinct differencesbetween gray and white matter[14, 55, 57, 58]. With few exceptions, most computational models simplify brain tissue behavior to be linear, isotropic, and homogeneous[28, 59]. None of these material or computational models includes a description of the microstructure in their characterization.

In vivo CNS axons, like constituents of other soft biological tissues, are undulated to a certain degree. The initial degree of waviness exhibited by individual axons, as well as the specific distribution of axonal undulations, are very important in the overall behavior of the optic nerve. Several material models of other soft tissues assume either a constant undulation or a normal undulation distribution, but most have neglected to explicitly determine the specific degree and characteristic distribution of undulations[33, 42-44]. Quantification of axonal undulations in the optic nerve reveals that axons exhibit a characteristic undulation distribution. Unlike other analyses, we found that axonal undulation in the guinea pig optic nerve closely resembled a gamma distribution. Characterization of three nerves produced amean undulation of 1.07, with a standarddeviation of 0.053. The distribution is skewed toward an undulation of one, with very few axons having an undulation greater than 1.20. A mean undulation of 1.07 implies that at 7% optic nerve stretch, 50% of the axons are completely straight. Interestingly, a previous study of the distribution of axonal diameter revealed that this particular

characteristic also followed a gamma distribution[29]. In the future, we may incorporate the distribution of axon caliber into the formulation.

By integrating the assumed gamma distribution we can determine the percentage of axons in an optic nerve that are stretched beyond a certain level at a given optic nerve elongation (Figure 6). For a typical 10mm optic nerve elongated only 3mm, over 97% of the axons are stretched beyond 20%. When the optic nerve is elongated 5mm (50%), nearly all the axons are stretched at least 30%. The significance of these results are primarily evident when compared to neuropathological results of the guinea pig optic nerve stretch model. Preliminary work indicates that very little morphological axonal injury is present when the optic nerve is elongated to levels as high as 40%. Further, we do not begin to see significant morphological or functional damage until optic nerve elongations as high as 60%, a level at which all axons are stretched at least 40%.

Although significant work is required before a strain threshold for axonal injury in CNS tissue is proposed, our preliminary results certainly indicate an injury threshold significantly higher than levels predicted by other investigators. In vitro work on the unmyelinated squid giant axon found mechanical failure to occur at strains of 25%[13]. Isolated studies of myelinated peripheral nerves indicated that PNS axons failed structurally at stretch ratios between 20-40%[20].

Thus, the undulation distribution information alone can be used to improve threshold predictions by computational models. For example, if the undulation distribution in the guinea pig optic nerve is at all similar to that of white matter tracts in human brain tissue, computational models which predict strain thresholds less than 15% imply an average axonal strain of less than 10% which, based on our preliminary studies and comparable in vitro work, may be too conservative.

In light of the differences in strain thresholds, it is important to discuss any systematic errors that may have affected the predicted distribution. As seen in Figure 2, undulations were determined by "digitizing" the length of the axon. Estimates of axonal length are increasingly more accurate as more points are placed along the length of the axon. Thus, it is possible that axonal lengths, as well as the mean undulation, were slightly underestimated. However, because undulation is a ratio between two lengths, the shape of the distribution should not be affected by uniformly underestimating axonal lengths. Also, as with any sample taken from a large population, it is possible that the group of axons traced for each nerve did not represent the total population. We attempted to minimize sampling errors by evenly characterizing the entire length of the nerve, and by choosing axons randomly. We hope to characterize several more nerves, possibly using different staining techniques, to confirm the choice of distribution. We also plan to confirm that the distribution is constant along the entire length of the optic nerve.

Applicability of Quasi-linear Viscoelasticity

Many biological materials are successfully modeled using quasi-linear viscoelasticity theory. The relative success of a model depends on how closely the assumptions of quasi-linear theory approximate the actual behavior of the material. Quasi-linear theory assumes that the behavior of a material can be separated into two functions: one that is time-independent; and one that is strain-independent. The validity of this assumption was tested for the optic nerve by conducting stress relaxation tests at different levels of elongation. Figure 7 depicts the similarity of the stress relaxation behavior of the optic nerve at three levels of elongation. To compare the behavior, the data was normalized to one by dividing by the peak force, and the reduced curves were then fit to a two-term exponential. Although there was some variation in the coefficients determined by the curve fit, the relaxation behavior appears to be independent of the peak elongation.

Based on the average coefficients calculated the two relaxation time constants were 2.4 msec and 61 msec. Although a wide range of relaxation time constants have been found experimentally for nerves and brain tissue, there are no reports of time constants as low as 2.4 msec[20, 55]. Frequently, materials are tested at ramp durations slow enough that it is possible that short relaxation time constants are missed. However, it is also plausible that the short time constant found for the optic nerve is due to material differences between gray and white matter. The presence of a small time constant indicates the necessity of using very short ramp times when testing materials. In fact, the reduced relaxation equation used in quasi-linear viscoelasticity inherently assumes an infinite ramp speed. Although our stress relaxation tests were conducted at ramp times as low as 5 msec, it is feasible that the material relaxed significantly in this short period of time. Several investigators have addressed this issue with some success by attempting to extrapolate the relaxation data back to the onset of the ramp[50, 55]. These methods are particularly useful for long ramp durations; we believe that the short ramp duration used in this study prevents severe underestimation of the peak force due to an infinite ramp. However, in the future we plan to investigate the need to extrapolate our data.

Unfortunately, quasi-linear theory alone provides little information about the microstructural response to tissue deformation. The present analysis is unique in that it combines the concepts of quasi-linear theory with a description of the microstructure of the material. However, this inclusion introduces computational difficulties in the model formulation. Quasi-linear theory makes use of an instantaneous elastic function that is easily determined by fitting the experimental data to an appropriate curve. This function is time independent, but includes the material's strain dependence. In the present analysis, this function was represented by an integral of the undulation distribution, as well as a function of the stretch ratio. For small strains, this combination could be easily fit to experimental data. However, the integral of the undulation distribution eventually reaches a maximum value of one, when all axons are completely straight (~30% optic nerve strain). As a result, it has less of an effect when the optic nerve is elongated to higher levels. Thus, a stretch ratio

function must be carefully chosen such that, when combined with the undulation distribution, it resembles the ramp portion of the stress relaxation data, as well as the experimental data at all levels of elongation.

The results of analyses using a linear stretch ratio function and a third order polynomial function indicate that experimental data is better approximated by a third order polynomial. Figures 9 and 10 represent both forms of the stretch ratio function and the experimental curve from the stress relaxation tests. Goodness of fit tests found the experimental data to be significantly different from the theoretical results using a linear stretch ratio function, but that the experimental data could be represented by using a third order polynomial. Also, by comparing Figure 11 and Figure 6, we note that the undulation distribution dominated the model results when we assumed a linear stretch ratio function. The shape of the theoretical curve is very similar to that obtained by integrating the undulation distribution. In contrast, when using a third order polynomial, the theoretical curve was similar in shape to the experimental data. Ultimately, the feasibility of using quasi-linear theory in conjunction with an undulation distribution will have to be tested by comparing the model results to experimental data for many varying levels of elongation.

The accuracy of the model results hinges upon the validity of the assumptions made during the formulation. One inherent assumption is that the strain field throughout the optic nerve during uniaxial elongation is uniform. At any instant in time, all regions within the nerve experience the same deformation. Before we can reliably use this model to predict axonal injury thresholds, it is necessary to confirm this assumption.

Also, the applicability of small animal results to human head injury is frequently questioned, especially when the results are based on material properties and/or geometry. Tissue level injury thresholds determined in the optic nerve model are useful only if some assumption is made about the similarities between human and guinea pig white matter. The validity of this assumption is questionable due to the variability in the undulation of axons within different white matter tracts in different species. Although it is unlikely that the guinea pig optic nerve behaves exactly like white matter tracts in human brain tissue, it is believed that myelinated axons similar in size behave identically regardless of the species. Thus, deformation based thresholds for individual axons determined in the guinea pig optic nerve could be applicable to a human brain computational model. It is likely that tissue level injury criteria for the human brain will be regionally specific. For example, the undulation and orientation of axons in the corpus callosum may be significantly different than that of the internal capsule. To implement this methodology, researchers must concentrate on characterizing the specific undulation distribution and orientation of axons in regions susceptible to traumatic injury.

Conclusion
We have developed a structural model of the guinea pig optic nerve that can approximate individual, in vivo axonal strain based on a characteristic undulation distribution. By

combining the structural model results with morphological injury patterns seen in the guinea pig optic nerve, we can determine deformation based thresholds for CNS injury at both the tissue level and the individual axon level. Axonal thresholds determined by this model are immediately applicable to human head injury, and the methodology could be implemented, after proper characterization of the microstructure of particular regions of the brain, to develop tissue level criteria.

References
1.Pope, A. and A. Tailor, *Disability in America: Toward a National Agenda for Prevention.* 1991, Washington, D.C.: National Academy Press.

2.Gennarelli, T., L. Thibault, J. Adams, D. Graham, C. Thompson, and R. Marcincin. *Diffuse axonal injury and traumatic coma in the primate.* Annals of Neurology, 1982. **12**: p. 564-574.

3.Adams, J., D. Graham, L. Murray, and G. Scott, *Diffuse axonal injury due to nonmissile head injury in humans: an analysis of 45 cases.* Annals of Neurology, 1981. **12**: p. 557-563.

4.Gennarelli, T., G. Spielman, et al., *Influence of the type of intracranial lesion on outcome from severe head injury.* Journal of Neurosurgery, 1982. **56**: p. 26-32.

5.Bandak, F. and R. Eppinger. *A three-dimensional finite element analysis of the human brain under combined rotational and translational accelerations.* in *38th Stapp Car Crash Conference.* 1994. SAE.

6.Chu, C., M. Lin, H. Huang, and M. Lee, *Finite element analysis of cerebral contusion.* Journal of Biomechanics, 1993. **27**(2): p. 187-194.

7.Ruan, J., T. Khalil, and A. King, *Human head dynamic response to side impact by finite element modeling.* Journal of Biomechanical Engineering, 1991. **113**: p. 276-283.

8.Ruan, J., T. Khalil, and A. King, *Dynamic response of the human head to impact by three-dimensional finite element analysis.* Journal of Biomechanical Engineering, 1994. **116**: p. 44-50.

9.Ueno, K., J. Melvin, L. Li, and J. Lighthall, *Development of Tissue Level Brain Injury Criteria by Finite Element Analysis.* Journal of Neurotrauma, 1995. **12**(4): p. 695-706.

10.Gennarelli, T., *Animate models of human head injury [Review].* Journal of Neurotrauma, 1994. **11**(4): p. 357-68.

11.Beel, J., L. Stodieck, and e. al., *Structural properties of spinal nerve roots: biomechanics.* Experimental Neurology, 1986. **91**: p. 30-40.

12.Easton, D., *Some tensile properties of nerve.* Journal of Cellular and Computational Physics, 1956. **48**: p. 87-94.

13.Galbraith, J., L. Thibault, and e. al., *Mechanical and electrical responses of the squid giant axon to simple elongation.* Journal of Biomechanics, 1993. **3**: p. 211-221.

14.Galford, J. and J. McElhaney, *A viscoelastic study of scalp, brain, and dura.* Journal of Biomechanics, 1970. **3**: p. 211-221.

15.Gray, J. and J. Ritchie, *Effects of stretch on single myelinated nerve fibers.* Journal of Physiology, 1954. **124**: p. 84-99.

16.Haftek, J., *Stretch injury of peripheral nerve.* Journal of Bone and Joint Surgery, 1970. **52B**(2): p. 354-365.

17.Koike, H., *The extensibility of aplysia nerve and the determination of true axon length.* Journal of Physiology, 1987. **390**: p. 469-487.

18.Liu, Y., *Biomechanics and Biophysics of Central Nervous System Trauma,* in *Central Nervous System Research Status Report,* P.H.S. NIN, Editor. 1979, p. 36-52.

19.Rydevik, B., M. Kwan, and e. al., *An in vitro mechanical and histological study of acute stretching on rabbit tibial nerve.* 1990. **8**: p. 694-701.

20.Saatman, K., *An isolated single myelinated nerve fiber model for the biomechanics of axonal injury.* 1993, University of Pennsylvania:

21.Thibault, L., J. Galbraith, and e. al., ed. *The effects of high strain rate uniaxial extension on the electrophysiology of isolated neural tissue.* Advances in Bioengineering, ed.ASME. 1981, New York. 211-214.

22.Thibault, L., T. Gennarelli, S. Margulies, J. Marcus, and R. Eppinger. *The strain dependent pathophysiological consequences of inertial loading on central nervous system tissue.* in *International Conference on the Biokinetics of Impact.* 1990. Lyon, FR:

23.Holbourn, A., *Mechanics of head injuries.* The Lancet, 1943. p. 438-441.

24.Margulies, S., *Biomechanics of traumatic coma in the primate.* 1987, University of Pennsylvania:

25.Margulies, S. and L. Thibault, *A proposed tolerance criterion for diffuse axonal injury in man.* Journal of Biomechanics, 1992. **25**(8): p. 917-923.

26.Meaney, D., *The Biomechanics of Acute Subdural Hematoma in the Subhuman Primate and Man.* 1991, University of Pennsylvania:

27.Ward, C., P. Nikravesh, and R. Thompson, *Biodynamic finite element models used in brain injury research.* Journal of Aviation, Space, and Environmental Medicine, 1978. : p. 136-142.

28.Zhou, C., T. Khalil, and A. King. *A new model comparing impact responses of the homogeneous and inhomogeneous human brain.* in *39th Stapp Car Crash Conference.* 1995. Coronado, CA: SAE.

29.Gennarelli, T., *et al., Axonal injury in the optic nerve: a model simulating diffuse injury n the brain.* Journal of Neurosurgery, 1989. **71**: p. 244-253.

30.Adams, J., D. Graham, and e. al., *Contemporary Neuropathogical Considerations Regarding Brain Damage in Head Injury,* in *Central Nervous System jTrauma Status Report,* N. NINCDS, Editor. 1985, p. 65-77.

31.Erb, D. and J. Povlishock, *Axonal damage in severe traumatic brain injury: an experimental study in the cat.* Acta Neuropathologica, 1988. **76**: p. 347-358.

32.Egan, J., *A constitutive model for the mechanical behaviour of soft connective tissues.* Journal of Biomechanics, 1987. **20**(7): p. 681-92.

33.Kastelic, J., I. Palley, and E. Baer, *A structural mechanical model for tendon crimping.* Journal of Biomechanics, 1980. **13**: p. 887-893.

34.Kwan, M. and S. Woo, *A structural model to describe the nonlinear stress-strain behavior for parallel-fibered collagenous tissues.* Journal of Biomechanical Engineering, 1989. **111**: p. 361-363.

35.Lanir, Y., *Constitutive equations for fibrous connective tissues.* Journal of Biomechanics, 1983. **16**(1): p. 1-12.

36.Frisen, M., M. Magi, L. Sonnerup, and A. Viidik, *Rheological analysis of soft collagenous tissue.* Journal of Biomechanics, 1969. **2**: p. 13-20.

37.Comninou, M. and I. Yannas, *Dependence of stress-strain nonlinearity of connective tissues on the geometry of collagen tissues.* Journal of Biomechanics, 1976. **9**: p. 427-33.

38.Viidik, A., *A rheological model for uncalcified parallel-fibered collagenous tissue.* Journal of Biomechanics, 1968. **1**: p. 3-11.

39.Woo, S., G. Johnson, and B. Smith, *Mathematical modeling of ligaments and tendons.* Journal of Biomechanical Engineering, 1993. **115**: p. 468-473.

40.Jenkins, R. and R. Little, *A constitutive equation for parallel-fiberedelastic tissue.* Journal of Biomechanics, 1974. **7**: p. 397-402.

41.Haut, R. and R. Little, *A constitutive equation for collagen fibers.* Journal of Biomechanics, 1972. **5**: p. 423-430.

42.Decraemer, W., M. Maes, and V. Vanhuyse. *An elastic stress-strain relation for soft biological tissues based on a structural model.* Journal of Biomechanics, 1980. **13**: p. 463-468.

43.Decraemer, W., M. Maes, V. Vanhuyse, and P. Vanpeperstraete, *A non-linear viscoelastic constitutive equation for soft biological tissues, based upon a structural model.* Journal of Biomechanics, 1980. **13**: p. 559-564.

44.Lanir, Y., *A structural theory for the homogeneous biaxial stress-strain relationships in flat collagenous tissues.* Journal of Biomechanics, 1979. **12**: p. 423-436.

45.Best, T., J. McElhaney, W. Garrett, and B. Myers, *Characterization of the passive responses of live skeletal muscle using the quasi-linear theory of viscoelasticity.* Journal of Biomechanics, 1994. **27**(4): p. 413-419.

46.Dehoff, P., *On the nonlinear viscoelastic behavior of soft biological tissues.* Journal of Biomechanics, 1978. **11**: p. 35-40.

47.Fung, Y., *Stress-strain-history relations of soft tissues in simple elongation.* Biomechanics: Its Foundations and Objectives, ed. Y.C. Fung, Perrone, N., and Anliker, M. 1972, Englewood Cliffs: Prentice-Hall, Inc.

48.Fung, Y., *Biorheology of soft tissues.* Biorheology, 1973. **10**: p. 139-155.

49.Markenscoff, X. and Y. IV, *On the stress-strain relation for skin.* Journal of Biomechanics, 1979. **12**: p. 127-129.

50.Myers, B., J. McElhaney, and B. Doherty, *The viscoelastic responses of the human cervical spine in torsion: experimental limitations of quasi-lineartheory, and a method for reducing these effects.* Journal of Biomechanics, 1991. **24**(9): p. 811-817.

51.Simon, B., R. Coats, and S. Woo, *Relaxation and creep quasilinearviscoelastic models for normal articular cartilage.* Journal of Biomechanical Engineering, 1984. **106**: p. 159-164.

52.Fung, Y., *A first course in continuum Mechanics.* Second ed. 1977, Englewoods Cliffs, New Jersey: Prentice-Hall, Inc. 340.

53.Flügge, W., *Viscoelasticity.* 1975, New York: Springer-Verlag.

54.Scheaffer, R. and J. McClave, *Probability and statistics for engineers.* Second ed. 1986, Boston: Duxbury Press. 648.

55.Arbogast, K., D. Meaney, and L. Thibault. *Biomechanical characterization of the constitutive relationship for the brainstem.* in *39th Stapp Car Crash Conference.* 1995. San Diego, CA: Society of Automotive Engineers, Inc.

56.Sokal, B. and F. Rohlf, *Biometry.* Second ed. 1981, New York: W.H. Freeman and Company. 859.

57.Pamidi, M., *Constitutive properties of brain tissue.* 1976, West Virginia University: Morgantown.

58.Shuck, L. and S. Advani, *Rheological response of human brain tissue in shear.* Journal of Basic Engineering, 1972. : p. 905-911.

59.Mendis, K., R. Stalnaker, and S. Advani, *A constitutive relationship for large deformation finite element modeling of brain tissue.* Journal of Biomechanical Engineering, 1995. **117**: p. 279-283.

Modeling Cavitation during Head Impact

Guy Nusholtz *   Lee G. Glascoe †   E. Benjamin Wylie †

Chryslter Motor Corporation, CIMS 483-05-10

800 Chrysler Drive East, Auburn Hills, MI 48326-2757, USA

Abstract

The effects of stress in brain material was investigated with experimental and computational idealizations of the head. A water-filled cylinder impacted by a free traveling mass serves to give insight into what could happen to the brain during impact; particularly the effect of the state of stress on possible physical changes in the brain material. When the cylinder is struck by a free-flying mass of sufficient velocity, cavitation is initiated at the boundary opposite impact. Significant vaporous regions may develop at the boundary, while only limited vaporization occurs internally. The vaporization that does occur internally consists of diffuse micro-voids. Higher accelerations, or an additional loading of the domain by a constant acceleration perpendicular to impact, adds to the likelihood and to the increased severity of internal cavitation, increasing the size, number and density of micro-voids. As a result, the micro-voids that form may not only produce injuries in the typically perceived cavitation damage response, i.e., violent cavity collapse, but also by producing local large strains as a result of cavity formation. In addition, when a local section of brain is significantly populated with micro-voids, the bulk and shear properties can change. Therefore, cavitation-caused cellular damage, including a non-violent collapse mechanism resulting from stress in the brain material might be more common than previously thought. Cavitation occurred in these experiments at accelerations greater than 150 g's.

Introduction

The effect of stress in the brain as a mechanism of injury is rarely considered in head impacts, even though there have been some experimental studies indicating fluid vaporization (cavitation) through pressure limiting effects. These effects have been observed in impact tests using repressurized human cadavers and live anesthetized primates, where negative gage pressures of less than one atmosphere have not been observed unless skull fracture occurred [1, 2, 3]. Despite the possible fluid vaporization and no observed injury, the authors

---

*Chrysler Corporation, Auburn Hills, MI
†University of Michigan, Ann Arbor, MI

hypothesized that fluid vaporization limited the gage pressure to a negative one atmosphere. The theory was that the cavitation occurred either in the cerebral spinal fluid or between the dura and the skull, and was not significant enough to cause injury as geometric attenuation effectively reduces the force of cavity collapse.

To study this hypothesis, an experimental and numerical analysis of a simple model of the human head under impact was used [4, 5]. A water filled 14-cm diameter cylinder was struck by a 10-kg free-flying mass. Rigid-body acceleration-time-histories and the pressure at the fluid-cylinder interface were monitored during impact. Comparisons between the experimental results and the results of a two-dimensional computational model were made.

As a result of this work, the following view of head impact was developed: when the head receives a blow and a positive pressure develops under the point of impact, a small cavity, opposite the impact, can form between the skull and the dura. Vaporization limits the maximum pressure drop in the head to vapor pressure. Since the brain is nearly incompressible, the small amount of volume needed to create the cavity is accomplished by either pushing a very small amount of material down the foramen magnum or by skull deformation.

This leads to the following possibility for a negative gage pressure-limiting impact phenomena that could occur at the skull-dura interface. During severe impact to the human head, a greater tension would develop between the cerebral spinal fluid and the dura, than between the dura and the skull. The dura would then move with the brain cerebral spinal fluid. As the dura moves away from the skull, a small cavity (of thickness less than 10^{-5}m) could form representing a slight stretching between the skull and the dura of the periosteum. Although it may be possible that enough surface tension could develop between the skull and dura for a cavity to form on either side of the dura, this does not seem as likely as the above suggested mechanism. Therefore, it is this motion of the dura as coupled with the small fluid flow through the foramen magnum that can have a significant effect on the pressure response of the brain during impact. If the impact is severe enough, it may be possible to produce fluid vaporization and the associated violent cavity collapse. This violent cav-
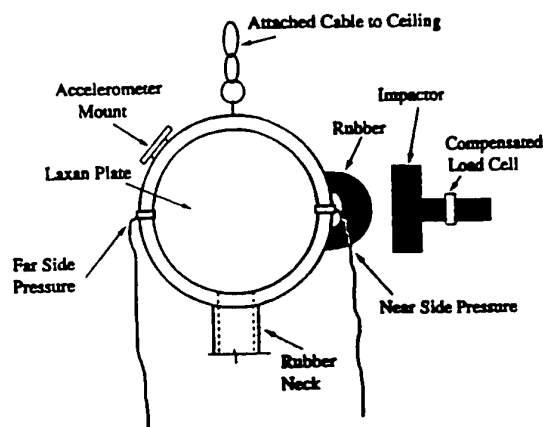
Figure 1: Experimental setup.

ity collapse, which could be a mechanism of injury, is strongly modified by the dura motion minimizing the amount of damage that could occur.

Recently, a follow up study indicated that under complex loading conditions, cavitation could occur in the brain material – not just at the boundary [6]. It was found that if the head underwent pre-impact acceleration immediately before the head strike, a vaporous region could form in the brain material and internal cavitation was likely. As a result, it was postulated that, in a vehicle environment, head impact could generate internal cavitation. Seeking further understanding, the same simplistic physical model of the head is used in this current study. In addition to cavities forming at the skull-dura boundary cavities in the brain material are addressed, with implications of potential cellular tissue damage. No attempt is made to model the anatomical structures of the head, the skull-dura boundary, the complex geometry of the head, head impact response, skull deformation, head angular motion, or brain shear. Instead, a simple physical model is used to generate test data. These data are modeled by a numerical simulator to gain insight into cavitation and into the general effect of pre-stressing, such as neck loading, on pressures in the brain material.

Physical Model

The physical model used is briefly outlined herein; it has been discussed in more detail in earlier papers [3, 4, 5. 6]. The simplified mechanical head form consisted of two parts: an internally polished aluminum cylinder and a rubber neck attached to the base of the cylinder, Figure 1. The cylinder was closed at each end with flat plates of 1.3 cm thick plexiglass, and for most of the tests, the plexiglass was reinforced with aluminum channel. To complete the head form the cylinder was connected by a rigid joint to a flexible viscoelastic rubber neck structure; fluid flow between the cylinder and the neck was through a two-centimeter diameter hole at the head neck interface. A nine-accelerometer array, used to measure three-dimensional motion (six degrees of freedom), was rigidly affixed to the aluminum cylinder and pressure transducers monitored the interface of the fluid and the cylinder.

The fluid tap water used to fill the system was boiled for several hours and allowed to return to room temperature. Before filling the cylinder with the fluid the air in the cylinder was evacuated and a partial vacuum was maintained. The vacuum was used to draw the fluid through a valve into the neck, then through the hole in the base of the cylinder. A vacuum was maintained until the cylinder was filled and no visible cavities or vacant spaces could be observed. Before each test series the mechanical head form was impacted several times and inspected to ensure that no air or cavities were visible in the cylinder.

The impact was delivered through the center of mass of the cylinder by a 10 kg free-traveling mass fitted with an inertial-compensated load cell assembly. The impacting surface consisted of a flat rigid 5-cm diameter disk [1, 2, 3]. To bring the contact force time-history closer to that of a head impact, a neoprene rubber hemisphere was fixed to the cylinder so that loading impact to the cylinder came through the neoprene hemisphere. The impact mass velocity was measured by timing the pulses from a magnetic probe which sensed the motion of targets in the mass.

Computational Models

Two finite difference models were used to simulate the impact response of the fluid-filled cylinder, a continuum model and a discontinuous or discrete model. For both models it was assumed that boiling the tap water removed the free gas. Therefore, even though tap water had a significant number of nucleation sites to allow for fluid vaporization in the impacted cylinder and plastic neck, there was no free gas in the water. It was also assumed that even though there was no visible air in the physical model, it was impossible to remove all of the air at the boundaries of the water and the cylinder walls. The air at these boundaries was modeled as a continuous thin layer less than 10^{-6}m thick. Finally, it was assumed that the flow velocities through the neck were proportional to the force acting on the fluid in the neck.
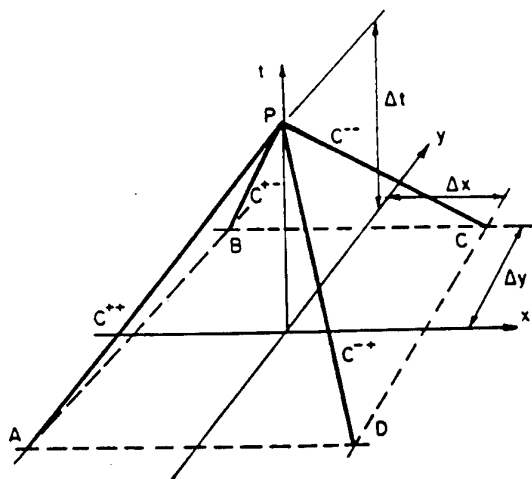
Figure 2: Staggered grid for continuum model.

Continuum model

The continuum model is based upon the two-dimensional unsteady equations of motion and continuity in a compressible fluid continuum. The procedure is based upon Henke's method [7] that was applied to fluids by Wylie [8, 9]. The linearized version of the more general compressible flow equations that describe pressure waves in a two-dimensional continuum provide the most simple case to develop the method. A combination of equations for the conservation of mass and momentum in the longitudinal and lateral directions are linearized into a set of four characteristic-like equations. The numerical procedure is developed by integrating these equations along paths in space and time, Figure 2. In this linearized model with constant isentropic wavespeed, $\Delta x = \Delta y$ in the computational grid.

The following set of equations result:

$$\frac{p_P}{\rho c} + u_P + v_P - q_P \Delta x = e_1 \qquad (1)$$

$$\frac{p_P}{\rho c} + u_P - v_P + q_P \Delta x = e_2 \qquad (2)$$

$$\frac{p_P}{\rho c} - u_P - v_P - q_P \Delta x = e_3 \qquad (3)$$

$$\frac{p_P}{\rho c} - u_P + v_P + q_P \Delta x = e_4 \qquad (4)$$

in which

$$e_1 = \frac{p_A}{\rho c} + u_A + v_A + q_A \Delta x \qquad (5)$$

$$e_2 = \frac{p_B}{\rho c} + u_B - v_B - q_B \Delta x \qquad (6)$$

$$e_3 = \frac{p_C}{\rho c} - u_C - v_C + q_C \Delta x \qquad (7)$$

$$e_4 = \frac{p_D}{\rho c} - u_D + v_D - q_D \Delta x \qquad (8)$$

where for point P, p_P is the absolute pressure, u_P is the x-direction velocity, v_P is the y-direction velocity, and $q_P = (\frac{\partial u}{\partial y} + \frac{\partial v}{\partial x})/2$. Equations 1 through 4 are applied along lines C^{++}, C^{+-}, C^{-+}, and C^{--}, respectively, Figure 2. This two-dimensional spatial grid in the $x-y$ plane with time represented in the third dimension was used to simulate the plexiglass cylinder. Handling of the vaporization-free gas at the water-cylinder (or skull-dura) interface requires special consideration.

At the cylinder's perimeter the pressure drop is limited to vapor pressure as pressures below this are not physically possible. Under these conditions, in the absence of free gas, the fluid is assumed to vaporize, the pressure is fixed to vapor pressure, and a cavity is permitted to develop. The cavity grows while the liquid moves away form the boundary, and collapses as the liquid moves back to the boundary. In the model a small amount of air is assumed to exist at the wall and isothermal expansion and compression of the gas layer is assumed. The ideal gas law is used to relate the cavity volume to pressure. The gas law may be written as

$$V_{air} = \frac{C_4}{p_p - p_v} \qquad (9)$$

where V_{air} is the volume of free gas at any boundary node; p_p is the absolute pressure at that node; p_v is the vapor pressure of water; and C_4 is the product of the gas constant, absolute temperature, and the mass of free gas at the node. The volume of air per unit depth at each boundary node is equal to the air thickness multiplied by two distance intervals.

A boundary condition is used at the neck node to model the effect of the rubber neck on the dynamic response of the cylinder. With a relatively low wave speed in the rubber neck, it was assumed that the neck was long enough so that the far end condition did not influence the dynamic response at the cylinder-neck connection. This meant that the neck acted like an infinitely long tube. The additional equation necessary to interact with the C^{-+} and C^{--} equations was provided by the following one-dimensional compatibility equation for the neck

$$p_P = p_i - \rho c_i (v_P - v_i) \qquad (10)$$

In equation 10 $p_i = 1$ atmosphere (absolute), $v_i = 0$, and c_i is the wave speed in the rubber neck. The variable q_P was set to zero, enabling a solution for the variables p_P, u_P, and v_P at each computational time step.

Discontinuous Model

Because the first method of modeling requires a continuum it can be used to estimate cavitation only at the boundaries but not inside the fluid. This is a result of the discontinuity caused by the cavities formed inside the fluid media. To address this problem a second method is used. A description of this method and its equivalence to the first method are found in [9, 10]. A brief description of this approach as it relates to the cylinder follows.

The numerical procedure to analyze two-dimensional transients is essentially the same as in one-dimensional problems. At internal nodes, or line element intersection points, a common pressure is assumed at each instant and the mass conservation law must be satisfied. A scaling relationship is needed between the acoustic wavespeed, a, in the line element and the acoustic velocity, c, in the two-dimensional domain [9].

$$a = \sqrt{2}c \qquad (11)$$

Figure 3 illustrates a square grid of latticework elements. The compatibility equations used in the method of characteristics, without friction produce the following equations for point P in Figure 3.

$$p_P = p_A - a\rho(u_2 - u_1) \qquad (12)$$

$$p_P = p_B - a\rho(v_2 - v_1) \qquad (13)$$

$$p_P = p_C + a\rho(u_3 - u_4) \qquad (14)$$

$$p_P = p_D + a\rho(v_3 - v_4) \qquad (15)$$

where g is gravity, p_P is the pressure at point P, u_1 is the horizontal velocity just to the right of point A, v_2 is the vertical velocity just below point P, etc. Conservation of mass at any instant provides the fifth equation to solve for the five variables $(p_P, u_2, u_3, v_2, v_3)$.

With the second model, when low pressures develop in a region of the domain, one of two procedures is used depending on whether computation is at a boundary or an interior point. At an interior point, the minimum allowable pressure is vapor pressure, and the liquid vaporizes to form a vapor cavity which grows and collapses in response to the fluid dynamics. When the transient would have the pressure drop below vapor pressure, the pressure is set to vapor pressure, and the four velocities at the node, Figure 3, are computed. A time-dependent cavity volume per unit depth, V_V is then calculated from continuity

$$\frac{dV_V}{dt} = (v_{out} - v_{in})\Delta x \qquad (16)$$

in which v_{in} is the net velocity to the left or below the volume, and v_{out} is the net velocity to the right or
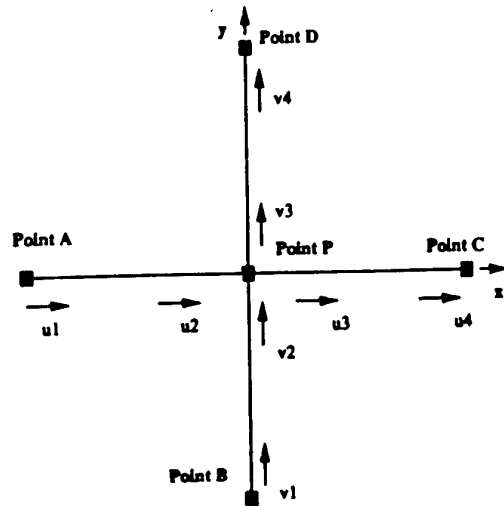

Figure 3: Latticework elements and velocities for discrete model.

above the cavity. The size of the cavity at each point grows and collapses in response to the dynamic behavior. At the boundary, the procedure is the same as at the boundary in the first method, that is, isothermal expansion and compression of the gas layer is assumed.

Results from Experimental and Continuum Models

The parameters used in the model were those of water under standard conditions. The density of water, ρ, was 1000 kg/m^3, the Bulk Modulus was 2.05 GPa; the wave speed, c, was 1435 m/s; the step distance interval, Δx, was 0.00318 m; and the time step, Δt, was $2.22(10^{-6})$ sec. Vapor pressure was set at 4550 Pa (absolute). The acceleration recorded from the physical model was input to the computer model to generate pressure-time histories at various points in the cylinder. As mentioned before, determined efforts were made to remove all of the air from the physical model, however, it is likely that a microscopic layer existed at the fluid/cylinder boundary. Therefore, on the perimeter an initial thickness of air of 10^{-6}m was used to model this effect.

The initial conditions for the model were set such that there was no velocity in the cylinder and the pressure everywhere was atmospheric. The right and left boundaries were then accelerated according to a digitized acceleration from a specific experimental run. Two runs are evaluated here, a low acceleration (5 m/s impact velocity) and a high acceleration (8 m/s impact
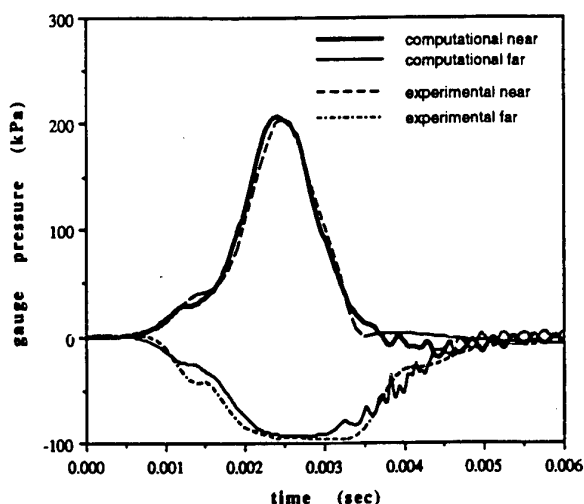
Figure 4: Low acceleration pressure response.

Figure 5: High acceleration pressure response.

velocity). Both are analyzed in the model with vaporization at the boundary. The points presented for comparison are the near side and the far side pressure-time histories of the extreme left and extreme right boundaries.

Low acceleration (5 m/s impact velocity). An impact test was considered appropriate for this study if: 1) the impact velocity was within 0.1 m/s of 5 m/s; 2) no visible air could be seen in the cylinder before and after impact; and 3) the peak angular accelerations during impact were less than 100 rad/s². In the set of impact tests that met the above requirements the angular and linear accelerations and velocities were similar and reasonably close to that of a rigid body. Peak linear accelerations were within 5 percent of 190 g's and there was less than 0.01 rad of rotation. Therefore, for this set of tests it was assumed that: the motion of the cylinder was one-dimensional, the acceleration of each point on the aluminum cylinder was equal to the tangential acceleration obtained from the nine accelerometer array, and that each impact represented a repeatable event. In simulating this set of tests rotation did not need to be considered in the mathematical model. The near side and far side pressures from these tests also represented repeatable phenomena. As can be seen from Figure 4 the computational results compare very well with the experimental results. Both the experimental and computational results show the effect of the vaporization/free gas boundary though the experimental results show a slightly sharper drop to vapor pressure.

High acceleration (8 m/s impact velocity). The re-

quirements for the 8 m/s tests differ from the 5 m/s tests only in impact velocity, that is, the impact velocity had to be within 0.1 m/s of 8 m/s. The motion of these tests was also one-dimensional without rotation. Although these tests were repeatable in terms of acceleration and near side pressures, the far side pressures were not. The differences occur at a time near the end of impact as the negative pressure starts to rise. Additionally, the magnitude of the pressure overshoot varies from test to test.

As is the case for the 5 m/s run, the minimum pressure on the far side for the 8 m/s run is limited to vapor pressure, Figure 5. In the model, low pressure lasted longer implying a larger vapor cavity, and the subsequent pressure rise is due to the vapor cavity's violent collapse. The near side pressure peak of the computational model is somewhat higher (by about 15 percent) than the experimental results. The computational results also show a more narrow peak. For the most part, however, the experimental results and the computational results for the near side compare reasonably well. The far side experimental data show a smaller vapor cavity growth than the computational results as the pressure is at vapor pressure for about 0.4 ms less in duration. However, the experimental runs gave some variations as to the exact time of vapor cavity collapse (6). Some of this variation may be experimental in nature as the sampling rate may be low enough (10,000 Hz) that the exact magnitude of the instantaneous pressure spike after cavity collapse cannot be obtained.
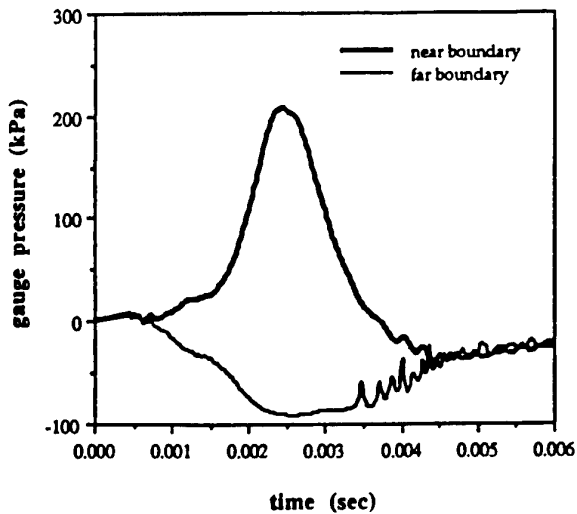
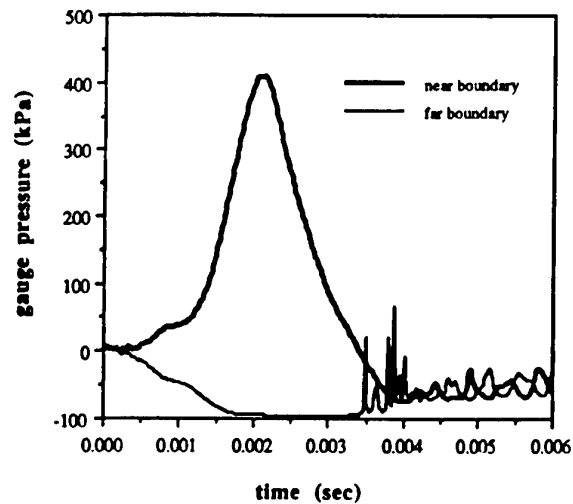**Figure 6:** Low acceleration pressure response with 20-g neck acceleration.

Figure 7: High acceleration pressure response with 20-g neck acceleration.

Discrete Model Results

If it is assumed that the numerical model reliably reflects the response of the physical model at the measured points, then it is reasonable to use the model to estimate the response at points where measurements cannot be made. In addition, it is also reasonable to evaluate impact conditions in the numerical model that were not tested in the physical model. In this study the physical model was struck by a free traveling mass and the pressure response at the cylinder fluid boundary was measured. All cavitation occurred at the fluid cylinder boundary. To build on these results we used the computer model to estimate the cavitation response inside the fluid as a result of an impact similar to that of the test, and also a hypothesized neck loading.

The impacts of the physical model and simulation of these impacts by the computational models represent a stationary-test subject struck by a moving mass. However, in most automobile crashes the occupant is moving and strikes a moving object. The motion normally subjects the occupant to a force through the neck. This force can produce an acceleration perpendicular to the impact load and is typically of longer duration and lower magnitude. Therefore, the following results represent impacts similar to those above with the addition of a constant acceleration from the neck, in this case the acceleration is about 20 g's. Figures 6 and 7 show the near and far side boundary pressure histories

of the low and high acceleration impacts, respectively, with a 20-g upward acceleration at the neck. When comparing Figures 6 and 7 with Figures 4 and 5, respectively, it can be seen that the additional stress incurred by the 20 g's results in a more violent cavity collapse. Greater internal cavitation is predicted by the model under the 20-g neck acceleration. The second model is able to predict an internal vaporous zone with small cavities (on the order of 10^{-6} m in diameter) at a number of internal nodes. Figure 10 shows the internal response of the fluid when the 20-g neck acceleration is added to the acceleration from the impact event. The figure shows the extent of the vaporous zone (the white region) in the cylinder at a time of 3.1 ms. The computational model demonstrates that the higher the acceleration from impact the greater the chance of cavitation in the fluid material. However, as illustrated by Figure 10, even at the low velocity the potential for internal cavitation exists when additional loading is included. By providing a constant vertical acceleration, in addition to the time-varying horizontal acceleration, the vector addition results in a larger resultant acceleration on the container. During peak acceleration the change is small. However, during low horizontal acceleration periods the prestressed vertical loading changes the magnitude and direction of the resultant significantly. This change in the resultant acceleration biases the vaporous zone towards the top of the cylinder. This is particularly evident for this case since the onset of

vaporization is well before the time of peak horizontal acceleration, and the largest cavity size is beyond the time of peak horizontal acceleration. The numerical model also shows that the vertical acceleration on the head produces a higher net mass outflow at the neck, Figure 8 (less than 1 mm of fluid displacement), thus contributing to lower overall internal pressure and corresponding vaporization. Therefore, the amount of vaporization associated with this acceleration profile is greater than the amount of vaporization if the same resultant acceleration was entirely in the horizontal direction.

Scaling

In addition to the effect of different levels of acceleration, pre-existing stress, and flow through the foramen magnum, it was possible to investigate the effect of cylinder size on cavitation response. In the computational model, the size of the cylinder was reduced by scaling all relevant dimensions (diameter, thickness, neck size, etc.) by a scaling factor. For separate simulations the cylinder size was reduced by a factor of 2, 5, and 10. Although the time histories are somewhat different, in each case the peak pressure on the near side was reduced by an amount similar to the scaling factor. For example, Figure 9 contains the pressure time history as a result of the high acceleration when the cylinder size was reduced by a factor of 5. The peak pressure is 55 compared to 440 for the full size model. Important to note is that the negative pressure also reduces, in this case cavitation effects have been eliminated. Conversely, to maintain the same pressure-time history magnitudes and the same level of cavitation, it was necessary to increase the input acceleration time history at each point by approximately the scaling factor amount. In an impact environment, that would be similar to increasing the impact velocity by approximately the scaling factor. These results have relevance for comparing the impact response on primates to that of the impact response humans. It would be expected from these results that to produce cavitation in primates significantly greater acceleration would be required.

Discussion

Complex loading conditions are common in an automobile crash. In most automobile crashes the occupant is moving with the vehicle before it crashes. As the vehicle slows down the occupant keeps moving. Normally the head and torso will move differentially and a load will develop through the neck, resulting in angular as
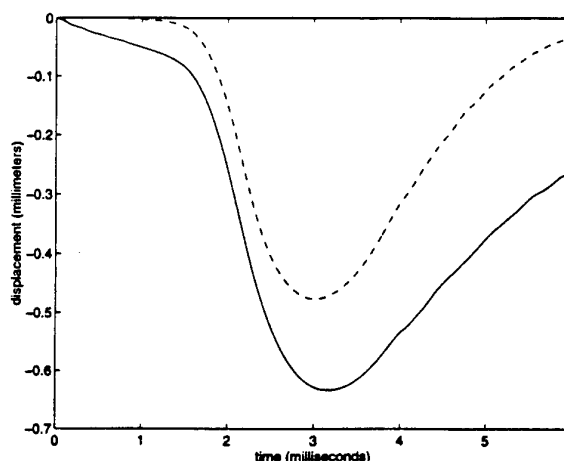

Figure 8: Fluid displacement with time for the continuum model (no internal vaporization, dashed line) and for the discrete model (with internal vaporization and neck loading, solid line) at the high acceleration.
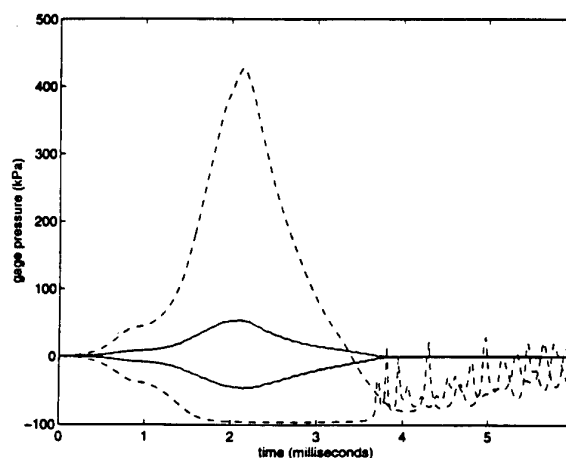

Figure 9: Pressure-time history for high acceleration when cylinder is reduced by a factor of five (solid line) and compared to standard size response (dashed line).

well as linear motion. If the head makes contact with a hard object during impact, the neck force produces an acceleration perpendicular to the impact load, creating a complex loading, that can affect the cavitation response. The influence is similar to what has been observed in low pressure transients in pipes, i.e., gravity may have a profound effect on cavitation during water-hammer events [9]. By changing the angle of the pipe with respect to the earth the cavitation response can be enhanced or eliminated. Therefore, the pre-stressing of the fluid by gravity before a water-hammer event affects the cavitation response.

A discussion of the pressure distribution in a closed container during acceleration may help in visualizing internal cavitation. For a constant horizontal acceleration the pressure pattern is:

$$p = p_0 + \rho k g x \qquad (17)$$

where x is measured from the front of the container, p_0 is the reference pressure at the front, k is the number of g's of acceleration, and p is the absolute pressure. Low pressures causing vaporization are always initiated at the boundary. If the low pressure pulse is visualized to be initiated at the far side boundary ($x = D$), the magnitude of the pressure pulse causing vaporization is:

$$\Delta p = -p_v + p_0 + \rho k g D \qquad (18)$$

where p_v is absolute vapor pressure and D is the container diameter. The pressure at the wave front is

$$p - \Delta p = p_v - \rho k g (D - x) \qquad (19)$$

That is, for any x the pressure is trying to reach a value less than vapor pressure, a necessary condition for internal cavitation. It is the combination of the sloped initial gradient and the limitation in the pressure excursion to not less than vapor pressure that creates internal cavitation. Invariably, the largest cavities develop at the boundary. However, distributed internal vaporization can occur and will be more severe for high acceleration.

Vertical accelerations on the head may be more severe since the additional acceleration may create a high pressure in the vicinity of the neck, which would force material down the foramen magnum thus increasing the likelihood of internal cavitation. Even a small net out-flow reduces the overall pressure, which amplifies the opportunity for cavitation. A time-varying acceleration, such as experienced in an accident, complicates a transient pressure pattern, but the above discussion provides the fluid dynamic basis for internal cavitation.

Both the physical and computational model used in this study are over-simplified versions of the human head. However, the same mechanism that influences pressure and cavitation in the cylinder under impact may influence pressure cavitation in the human head under impact. When the head or the cylinder is abruptly accelerated a positive pressure develops under the point of impact and negative pressure develops opposite the impact. When there is enough acceleration then a small cavity from fluid vaporization forms opposite the impact. At low accelerations the model does not compute significant cavitation away from the boundary. The dominant vapor cavity is always located at the skull/fluid boundary. However, if there are large accelerations, if a pre-existing stress is added to the load, or if there are complex loading conditions, then cavitation is possible inside of the fluid.

Therefore, it is reasonable to assume that when testing human surrogates an impact to a stationary head is unlikely to produce cavitation in the brain material. However, it is possible for cavitation to occur opposite impact at the skull-dura boundary, in the brain material near the skull-dura boundary, as well as elsewhere in the brain if there is pre-existing stress or a complex load path. Such conditions would exist in a vehicle crash as the occupant moves with respect to the vehicle before head impact. To attempt to understand what might happen in a vehicle crash, the model was pre-stressed according to estimated neck loadings. In addition, it is possible to generate pre-existing stress from other sources such as previous accelerations, angular acceleration, or angular velocity.

The numerical model predicts a cavitation zone on the boundary opposite impact with more cavitation occurring in the upper far side quadrant than in the lower far side quadrant. There is a variable void fraction throughout the zone at any instant. A more sizable cavity develops at the boundary. The cavitation zone grows spatially during the early stages of the low pressure, then reduces the size and disappears just before the collapse of the boundary cavity. Small amplitude pressure spikes are associated with the condensation of the internal vaporous zone. The largest pressure spike occurs at the instant of boundary cavity collapse. This type of behavior is entirely in keeping with low-pressure transients in liquid pipelines [9]. In this setting, high frequency pressure oscillations are common during the collapse of a vaporous zone, followed by larger amplitude pulses, normally associated with isolated cavity collapse at boundaries, or at high points in the pipeline.

Cavitation has been proposed as a mechanism of counter-coup lesions, which are found in the area of the head opposite impact [11, 12]. This hypothesis states that during impact an area of pressure low enough to cause a cavity exists at the counter-coup site. However, the exact mechanism by which cavitation may cause injury is unknown. Cavitation erosion is a well-known damage mechanism in fluid mechanisms [13]. However, the conditions of occurrence are quite dif-

ferent from those that occur herein and in head impacts in that it normally appears under high velocity flow near an imperfect surface. Small vapor bubbles form, grow and collapse all within 1 to 3 ms. The violent collapse occurs at a time scale of micro seconds, during which time high intensity pressure spikes may do localized physical damage to a solid surface if the phenomena is repeated over a sufficiently large number of cycles. Pressure intensities of the order of a gigapascal may be possible, and temperatures as high as 5,000°C [13]. Because most of the published data addresses damage in metals, cavity creation does not play a significant role; instead, the damage done by cavitation is the result of violent cavity collapse. However, there may be additional mechanisms of damage in brain tissue. When a vaporous region is formed in the brain, large local strains in the tissues that have contact with each micro-void develop. The micro-voids are generally small enough so that geometric attenuation limit the magnitude of the effect. Nonetheless, if this occurs near a sensitive cellar structure, then it is possible that significant disruption of cellular neurofilament, microtubular structure, or axioplasmic transport might occur. Therefore, the size of the cavity and the forces generated during expansion or collapse do not have to be as large as in metals to cause damage in brain tissue. They could be as much as several orders of magnitude smaller.

Therefore, cavitation damage in brain tissue may be more common and have a greater variety of modes than previously thought. Injury attributed to other mechanism may be the result of cavitation. Cavitation damage/cell-disruption mechanism could be a cause of some of the diffuse axonal injuries (DAI) seen in head injuries from vehicle accidents. It is possible that the cellular disruption causes local damage that does not cause immediate cell death, but instead disrupts the cell activity to the degree that visible injury occurs later [14, 15, 16, 17]. The mechanism of numerous micro-voids forming a large vaporous region, by its nature, would produce damage that could be non-local and defuse throughout the brain. Cavitation requires the high accelerations generally driven by head strikes which are considered the sole or dominant cause of head injuries in the automobile environment (DAI inclusive) [18].

Although the complexity of head injury with apparent multiple injury modes created by many possible injury mechanisms appears to preclude one mechanism, cavitation is consistent with many of the observed biomechanics. For example, the 150-g acceleration for the initiation of vaporous regions to form in the head as an injury mechanism is consistent with the results previously observed [19]. It is also consistent with the logic behind HIC, both acceleration magnitude and duration are important. Short duration accelerations need higher accelerations to produce equivalent cavitation strain or accompanied violent collapse in the brain.

In addition, the smaller the brain cavity the greater the acceleration needed to produce cavitation and the associated damage. This is consistent with observations that it requires greater acceleration to cause damage in the smaller brain sizes [20, 21]. The acceleration necessary to cause damage in a primate is greater than that in a human. This acceleration could be either linear or angular or a combination of both. Angular acceleration adds significant complication for predicting where cavitation will occur in both primates and humans. For example, if the head is spun about its center of mass without linear acceleration (difficult to do if the head is attached to the neck) then cavitation will occur internally without any surface events. If both the linear and angular accelerations are complex such as occurs in a head impact in the automobile environment, then cavitation could occur at multiple locations in the brain.

For both large and small brains it is important to have a pressure gradient (caused by linear or angular acceleration) of sufficient duration to cause cavitation damage. This damage could be produced by impact or inertial load. However, the accelerations needed to produce cavitation are unlikely to occur by inertial loads in an automobile environment. Instead, impacts of the head would be the only way to produce cavitation type damage. This is consistent with previous results [18] in which no injury to the brain material occurred without impact in the automobile environment. Coupled with the acceleration response, impacts produce additional complexity in that the pressure gradients are also influenced by the skull deformation.

Implication for Biologic Soft Tissue Modeling

The results presented here have implication for modeling of biologic material. As a result of cavitation, it is reasonable to expect that soft tissue will have a material model that is a function of the state of stress, both the yield surface and elastic response. For example, shear response is considered important in brain injury mechanisms. As discussed above, when the head acceleration exceeds 150 g's then some form of voids in the brain can occur. How these voids affect the response of the brain in terms of shear, local brain material properties, volumetric and shape changes, energy management and damage properties is unknown. When the head acceleration exceeds 200 g's cavitation response can be violent and there is the chance that the temperature of

the collapsing cavity can exceed 5,000°C [22, 23, 24]. In addition, brain material also has weak Van der Walls bonding forces and may behave like organic polymers with both tension/compression and shear response a function of hydrostatic forces. It may turn out that a brain material model, or any soft tissue model, may have to be developed that takes into account the state of stress including the effects of cavitation and micro voids. Furthermore, it has been reported [25, 26] that the Casimir effect can be significant in biological materials. This may also affect how voids form in brain tissue and influence their effect on response and injury.

In the experiments and in the computational model no deformation occurred. Deformation in the human skull can cause both magnitude and phase differences in the pressures as well as contaminate the acceleration response [2]. However, it would seem reasonable to assume that an impact which increases the skull volume, front to back or back to front, would cause greater cavity formation and conversely, an impact that decreased volume would decrease cavity formation.

Conclusions

This paper presents a limited experimental and computational study of the impact response of the head with regard to cavitation. The main consideration involved in this study is the effect of pre-existing stress in the brain material on the resulting cavitation. This additional stress was evaluated by inducing a long duration low acceleration on the head form before impact. However, this pre-existing stress could also be induced by angular rotation or acceleration. The numerical model predicts a zone of cavitation tending towards the upper far side of the cylinder when this pre-existing stress is incorporated. Because of the complex nature of the cavitation phenomenon during an impact event more work is necessary before the results can be generalized. However, the following conclusions can be made for non-skull fracture cases:
1. The potential for cavitation during impact is influenced by pre-existing stress.
2. Vertical loading on the head by the neck before impact can affect the potential for cavitation in the brain material. This is particularly true if the preloading causes a higher pressure at the base of the head, leading to an outflow of material through the foramen magnum. This outflow reduces the overall brain pressure level and increases the potential for vaporization.
3. In the computational model it was not possible to produce significant cavitation inside the brain material at low accelerations without a pre-existing stress or a complex load path. This may have an

implication for human head impacts. Impacts to a stationary-test subject may produce results different from a test in which a moving subject strikes a hard object.
4. Computational models of the head, addressing severe head impacts, should include some form of fluid vaporization at the skull-brain boundary and in the brain material.
5. Cavitation in the form of micro-voids inside the brain material may cause local cellular damage that does not produce immediate cell death. It may be one of the causes of DAI.
6. Cavitation may be more common than previously thought because there may be more than one damage mechanism.
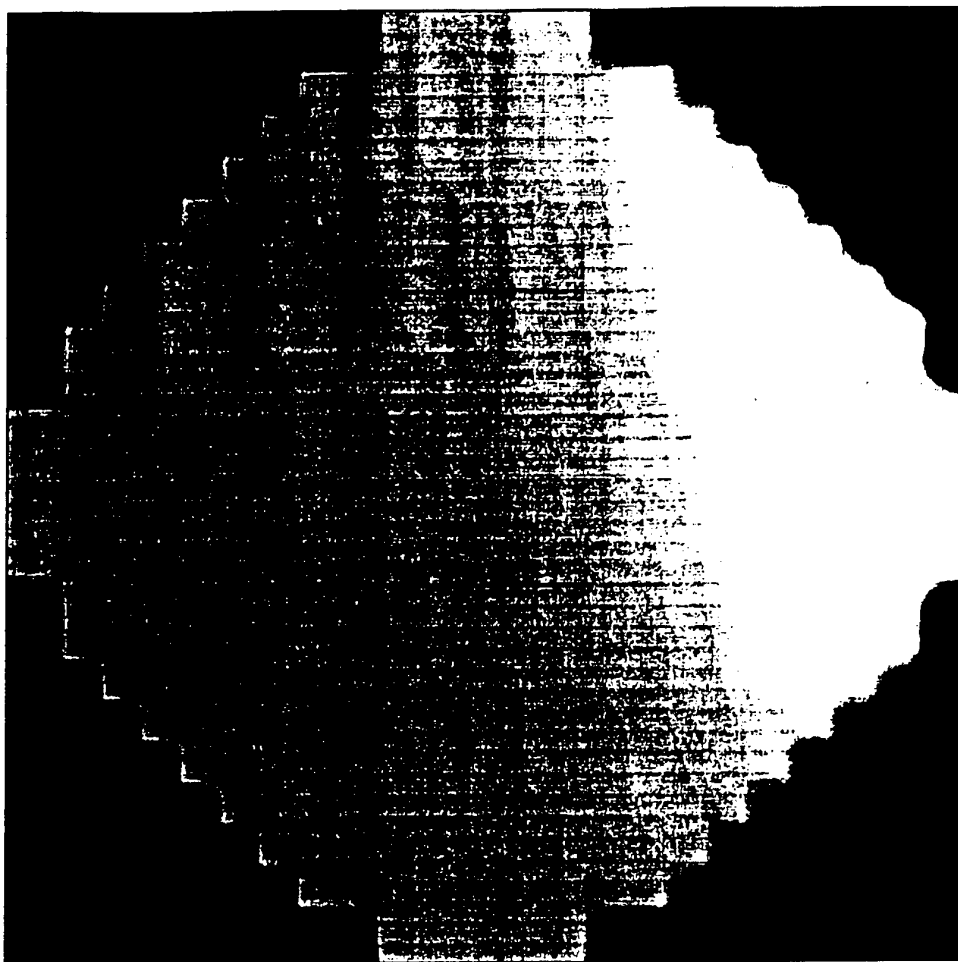
Figure 10: Vaporous region of head model for low acceleration, t = 3.1 ms. Note the vaporous region is in white while the rest of the head model domain is in gray.

References

[1] NUSHOLTZ, G. S., LUX, P., KAIKER, P. S., and JANICKI, M. A. (1984). Head impact response-skull deformation and angular acceleration. Proc. 28th Stapp Crash Conf. 841657, pps. 41-74.

[2] NUSHOLTZ, G. S., KAIKER, P. S., and LEHMAN, R. J. (1986). Critical limitations on significant factors in head injury research. Proc. 30th Stapp Car Crash Conf. 861890, pps. 237-68.

[3] NUSHOLTZ, G. S. and WARD, C. C. (1987). Comparison of epidural pressure in live anesthetized and postmortem primates. Aviat. Space Environ. Med. 88:9-17.

[4] NUSHOLTZ, G. S., KAIKER, P. S., WYLIE, E. B., and GLASCOE, L. G. (1994). The effects of the skull/dura interface and foramen magnum on the pressure response during head impact. 14th ESV Conference, Munich, paper 94 S1 0 26.

[5] NUSHOLTZ, G. S., WYLIE, E. B., and GLASCOE, L. G. (1995). Cavitation/Boundary Effects in a Simple Head Impact Model. Aviat. Space Environ. Med., 66(7):661-667.

[6] NUSHOLTZ, G. S. and WYLIE, E. B., and GLASCOE, L. G. (1995). Internal Cavitation in Simple Head Impact Model. Journal of Neurotrauma, 12(4):707-714.

[7] HENKE, R. (1980). Numerical procedure for predicting the torsional response of solid media. Ph.D. dissertation, The University of Michigan

[8] WYLIE, E. B. (1984). Linearized two-dimensional fluid transients. J. of Fluids Engineering, ASME 106, 227-232.

[9] WYLIE, E. B. and STREETER, V. L. (1993). Fluid transients in systems. Prentice Hall, New Jersey.

[10] WYLIE, E. B. and STREETER, V. L. (1980). Multi-dimensional fluid transients by latticework. J. of Fluids Engineering, ASME 102:203-210.

[11] BENEDICT, J. V., HARRIS, E. H., and VAN-ROSENBERG, D. V. (1970). An analytical investigation of the cavitation hypothesis of brain damage. Biomechanics and Human Factors Conf. ASME 70-BHF-3.

[12] LUBACK, P. and GOLDSMITH, W. (1988). Experimental cavitation studies in a model head-neck system. J. Biomech. 13:1041-1052.

[13] KNAPP, R. T., DAILY, J. W., and HAMMETT, F. G. (1970). Cavitation. New York; McGraw Hill.

[14] POVLISHOCK, J.T., BECKER, D.P., CHENG, C.L.Y., and VAUGHAN, G.W. (1983). Axonal change in minor head trauma. J. Neuropathol. Exp. Neurol. 42:225-242.

[15] CHENG, C.L.Y., and POVLISHOCK, J.T. (1988). The effect of traumatic brain injury on the visual system: A morphologic characterization of reactive axonal change. J. Neurotrauma 5:47-60.

[16] ERB, D.E., and POVLISHOCK, J.T. (1988). Axonal damage in severe traumatic brain injury: An experimental study in cat. Acta Neuropathol. 76:347-358.

[17] TOMEI, G., SPAGNOLI, D., DUCATI, A., et al. (1990). Morphology and neurophysiology of focal axonal injury experimentally induced in the guinea pig optic nerve. Acta Neuropathol. 80:506-513.

[18] McLEAN, J.A. (1996). Brain Injury Without Head Impact Traumatic Brain Injury Bioscience and Mechanics edited by Bandak, F.A., Eppinger, R.H., and Ommaya, A.K.

[19] MERTZ, H.J., PRASAD, P. and NUSHOLTZ, G.S. (1996). Head Injury Risk Assessment for Forehead Impacts SAE 960099.

[20] GENNARELLI, T.A. (1994). Animate models of human head injury. J. Neurotrauma, 11:357-368.

[21] GENNARELLI, T.A., THIBAULT, L.E., ADAMS, J.H., GRAHAM, D.I., THOMPSON, C.J., and MARCINCIN, R.P. (1982). Diffuse axonal injury and traumatic coma in the primate. Ann. Neurol. 12:564-574.

[22] KNIGHT, P. (1996). Sound, Light and the Vacuum, Nature Vol. 381(6):27.

[23] EBERIEIN, C. (1996). Phys. Rev. Lett 76 3842.

[24] POOL, R. (1994). Science Vol. 286:1804.

[25] SPRUCH, L., Long-range Casimir Interactions, Science, Vol. 272.

[26] NIR, S. (1976). Prog. Surf. Sci. Vol. 8.

HEAD INJURY ASSESSMENT OF A REAL WORLD CRASH BY FINITE ELEMENT MODELING

Chun Zhou, Tawfik B. Khalil, and Albert I. King

Bioengineering Center
Wayne State University
818, West Hancock
Detroit, Michigan 48201, USA

Ljubisa J. Dragovic

Chief Medical Examiner
Oakland County, Michigan, USA

SUMMARY

This paper demonstrates the potential of the WSU Brain Injury Model in predicting brain injuries sustained in a real motor vehicle crash. The particular case simulated here was a side impact in which the victim succumbed to multiple injuries, including a severe brain injury. The first step in the process was to use the EDSMAC code to obtain gross vehicular kinematics. The output of the EDSMAC run was used as input to a MADYMO simulation of the occupant kinematics and interaction with the vehicular structures of both the struck and striking vehicles. The computed head acceleration was then applied to the new three-dimensional finite element model of the head to determine the response of the brain to this crash loading. The injury severity was assessed by identifying areas of high shear strain and comparing them with autopsy data that showed locations of petechial hemorrhage where diffuse axonal injury (DAI) presumably occurred.

The crash reconstruction revealed a possible head contact with the hood of the striking vehicle, even though no signs of contact were seen on the head at autopsy. The estimated resultant linear acceleration was about 220 g's. The estimated lateral angular acceleration was about 20,000 rad/s^2. The estimated sagittal angular acceleration was about 11,000 rad/s^2. Better estimation could have been made if more information were available. The shear strain distribution within the brain exhibited some degree of correspondence with the sites of DAI. It is very promising that the shear stress contours can be used to make predictions of DAI.

INTRODUCTION

Head injury is a leading cause of death and disability among people involved in motor vehicle crashes. One way to investigate the injury mechanisms is to take field accident data and to reconstruct the accident, which needs tremendous efforts accompanied by many approximations and assumptions. This paper demonstrates the use of techniques in computer reconstruction of crashes and in occupant simulation to obtain input data for use in the WSU Brain Injury Model. The finite element model was then used to assess brain injury severity by identifying areas of high shear strain in the brain. The results were compare with autopsy data which identified locations of petechial hemorrhage where diffuse axonal injury (DAI) presumably occurred. The particular case simulated was a side impact in which the driver of the struck vehicle succumbed to multiple injuries, including a severe closed head injury featuring DAI consistent with sudden acceleration/deceleration injury pattern. The simulation results will be presented in the sequence of vehicle kinematics events predicted by EDSMAC, occupant kinematics calculated by MADYMO and brain response as determined by the WSU Brain Injury Model.

VEHICLE KINEMATICS DURING COLLISION BY THE EDSMAC

Crash Conditions

The striking car, Vehicle #1, was a 1992 Chevrolet Caprice 4-door sedan, heading west at a speed of no less than 40 miles per hour. The struck car, Vehicle #2, was a 1986 Plymouth Caravelle SE 4-door sedan, going south at a speed of less than 25 miles per hour. Vehicle #1 hit the left side of Vehicle #2, crashed into a light pole, a bus stop shelter and then into the plate glass window of a store. Damage to Vehicle #1 included the front bumper, grille, leading edge of the front fender, hood, right front door, and the right rear door, according to the police report. Damage to Vehicle #2 was to the left front fender, left front tire and wheel assembly, left front door, left rear door, left rear quarter panel, left rocker panel, the "A" pillar, and the "B" pillar.

Simulation Results

The EDSMAC program was used to obtain the collision course shown in Figure 1. The impact started at 0.06 second and ended at 0.19 second, so the whole impact duration was 0.13 second. Changes in velocity due to impact were:

ΔU_1 = -7.91 m/s, ΔV_1 = -1.39 m/s, ΔW_1 = -115.6 deg/s.

ΔU_2 = -4.38 m/s, ΔV_2 = 12.25 m/s, ΔW_2 = 43.8 deg/s.

Where,

U - velocity in the longitudinal direction of the vehicle.

V - velocity in the lateral direction of the vehicle.

W - yaw velocity.

Vehicle rotation during impact was 9.2 deg for Vehicle #1 and 3.5 deg for Vehicle #2. The vehicle velocities are shown in Figure 2 and the vehicle accelerations in Figure 3. Vehicle #2 reached its longitudinal peak deceleration of 235 ft/s² (71.86 m/s²) at 0.13 second, and its peak lateral acceleration was 643 ft/s² (196.24 m/s²) at 0.14 second. The damage profiles are shown in Figure 4. The estimated damage depth on the left side of Vehicle #2 was about 22.3 inches (566 mm) which can be used as an approximation of intrusion.

OCCUPANT DYNAMICS BY MADYMO MODELING

Model Description

The victim was a 23-year old, male, 5'11" (1.80 m) tall, weighing 150 lb (68 kg). The dimensions, mass, moment of inertia and center of gravity of all body segments of the occupant model were generated by GEBOD based on the height and weight of the human subject to be simulated. The occupant model contained 15 body segments and 14 joints. The front of Vehicle #1 was modeled as two plates of the front bumper and hood to simulate intrusion during collision. The slope of the hood was chosen to be 22.83 deg to account for deformation of the hood and potential contact-impact between the head and the hood. Vehicle #2 was modeled as consisting of a seat, seat belt system, foot rest, steering wheel, left door, left side "A" pillar and "B" pillar, rail, windshield, and roof. Figure 5 shows the side impact configuration of the entire MADYMO model. The +X-direction was in the direction of travel of Vehicle #2, the +Y-direction to its left side and the +Z-direction was upward.

Most of the joint characteristics were taken from the 572 dummy model. The joint stiffness for the head-neck joint and neck-upper torso joint was based on Wismans et al (1986). A flexural stiffness of 3 Nm/deg and a torsion stiffness of 0.4 Nm/deg were used for the neck joints in the model. The contact stiffness of the head was taken from Ishikawa et al (1993). It was assumed to be 9 kN at 10 mm. The contact stiffnesses for the chest, abdomen and pelvis were based on Viano (1989). The contact stiffnesses for other body segments were taken from the 572 dummy model. The contact stiffness of the left side of Vehicle #2 was assumed to be 100 kN/m for door deflections less than 10 mm, 200 kN/m for additional door deformation. The contact stiffness for the hood of Vehicle #1 was chosen as 60 kN/m based on Ishikawa et al (1993).

The vehicle models were defined as null systems with prescribed motions taken from the output of the EDSMAC analysis. The motion data of Vehicle #1 could not be directly applied to the MADYMO model, because the motion of the front end was different from that of its CG, due to compression. At the beginning of contact, the distance in the Y-direction (lateral to Vehicle #2) between the CG of the two vehicles was d_o = 10.5 ft. During impact, the distance in the Y-direction between the CG of the two vehicles was $d_i = Y_1 - Y_2$ ft. The total compression of the two vehicles was $\Delta = d_o - d_i$. The compression of each vehicle was assumed to be inversely proportional to its contact stiffness. So the compression could be calculated by:

$$\Delta_1 = \Delta \frac{K_2}{K_1 + K_2} \qquad (6.3.1)$$

$$\Delta_2 = \Delta \frac{K_1}{K_1 + K_2} \qquad (6.3.2)$$

where K1, K2 are the contact stiffnesses of Vehicle #1 and Vehicle #2, respectively.

The displacement in Y-direction of the front of the Vehicle #1 was approximated by:

$$Y_i = Y_1 - \Delta_1 \qquad (6.3.3)$$

The maximum intrusion thus calculated was about 18.93" (480 mm).

Simulation Results

Shown in Figure 5 are the impact events describing how Vehicle #1 intruded into Vehicle #2 and how it impacted the left side of the occupant, and how the head hit the hood. Without head-to-hood contact, the acceleration of the head was about the same as that of the vehicle. But when the head impacted the hood, a peak head acceleration of 220 G's occurred. The linear accelerations of the head are shown in Figure 6. The highest acceleration occurred in the vertical direction (Z-direction). The acceleration in the lateral direction (Y-direction) was also high. But the acceleration in the X-direction was negligible when compared to those in the other directions. The angular accelerations of the head are shown in Figure 7. The lateral angular acceleration (X-component) of the head was high. The peak lateral angular acceleration was about 20,000 rad/s² and the peak lateral angular deceleration was about 10,000 rad/s². The sagittal plane angular acceleration (Y-component) of the head was at a level of 11,000 rad/s². The horizontal angular acceleration (Z-component) was only about 7,000 rad/s².

IMPACT RESPONSE OF THE BRAIN BY FINITE ELEMENT ANALYSIS

Model Description and Method

The WSU Brain Injury Model, shown in Figure 8, consisted of the scalp, skull, dura, falx, tentorium, pia, CSF, venous sinuses, ventricles, cerebrum (gray and white matter), cerebellum, brain stem and bridging veins. The geometry of the head model was based on an atlas by McGrath and Mills (1984), and on brain sections prepared in our laboratory. The locations of the bridging veins were based on Oka et al (1985).

The overall geometry of the model represented a 50th percentile male human head. The head consisted of 17656 nodes and 22995 elements. Its total mass was 4.37 kg with the brain being 1.41 kg. Details of the model can be found in Zhou (1995).

One of the distinctive features of the model was the differentiation of the gray and white matter. The irregular boundaries between the gray and white matter were simulated in the model, but were greatly simplified. Different material properties were used for the gray and white matter. The inhomogeneous nature of the brain could be better simulated with these geometrical and constitutive descriptions.

Another new feature was the inclusion of the ventricles in the model. The corners of the ventricles are common sites of DAI. Without ventricular representation in the model, stress concentrations around ventricles could not be produced in our previous study (Zhou et al, 1994).

Figure 9 shows a third new feature - the modeling of ten pairs of parasagittal bridging veins with string elements. It was the first attempt to simulate bridging veins in a human head finite element model. With these bridging veins, their impact response could be analyzed and the mechanism of subdural hematomas could be studied by computer modeling.

Material properties for the model were reported in Zhou et al (1995). In this study, viscoelastic material properties were used for the brain, based on data by Shuck and Advani (1972),

$G_0 = 41$ kPa, $G_\infty = 7.6$ kPa, $\beta = 700$ s^{-1} for white matter,

$G_0 = 34$ kPa, $G_\infty = 6.3$ kPa, $\beta = 700$ s^{-1} for gray matter.

where G_0 is the short term shear modulus, G_∞ is the long term shear modulus and β is decay factor. The shear relaxation behavior is described by:

$$G(t) = G_\infty + (G_0 - G_\infty) e^{-\beta t}$$

We assumed that the white and gray matter had the same decay factor but the shear modulus of the white matter was higher than that of the gray matter. The only justification for this assumption is that white matter should be stronger and tougher because it is composed of axonal fibers and gray matter is composed of nerve cell bodies. A bulk modulus (K) of 2.19 GPa was used for both tissues.

The velocity time histories of the head from the MADYMO model were taken as the input for the human head finite element model. But only those at the interval between 40 ms and 130 ms were simulated. Shown in Figures 10 and 11 are the input linear velocities and angular velocities, in which time = 0 corresponded time = 40 ms in the MADYMO simulation. By defining the outer surface of the skull as a rigid body and assuming the CG of the rigid body to be coincident with the CG of the head, the velocity boundary conditions of the CG of the head were prescribed.

Results and Discussion

Figure 12 shows pressure time histories at four representative points in the brain. They are the frontal pole (Element No. 9,231), occipital pole (Element 9,195), genu of the corpus callosum (Element No. 6,560), and brain stem (Element No. 10,868). The pressure level at the four points varied from -87 kPa to 139 kPa. The pressure time histories exhibited a somewhat complicated pattern due to the combination of the six components of the head acceleration. The frontal pole and genu were mostly under compression. The occipital pole experienced cyclic compression and tension. The brain stem was mostly under tension. The genu and brain stem experienced the highest tensile stress (87 kPa) at 73 ms and 42 ms, respectively.

The genu sustained the highest shear stress (8.5 kPa) and shear stain (32.4%), as shown in Figure 13. Note that the stress time history is not of the same shape as of that for strain because of viscoelasticity. The shear strain sustained by the brain stem was about half of that for the genu. The shear stress at the genu was so high that an injury at this site would be inevitable. This was confirmed by the tearing of the corpus callosum at various levels found at autopsy. Shear stress level at the brain stem also predicted an injury in the brain stem, which was consistent with the partial lacerations of the brain stem white matter found at autopsy.

The pressure contours of the cortical surface at 46 ms are shown in Figure 14. At this moment, the left side was under compression and the right side was under tension. Note that there was an abrupt change in the pressure distribution at the longitudinal fissure, and that the medial surface of the right hemisphere was under compression because of the constraint applied by the falx cerebri.

The shear stress contours of the cortical surface at 46 ms are shown Figure 15 (top view) and Figure 16 (bottom view). The high shear stress areas predicted possible injury medial aspects of both right and left temporal lobes.

The shear stress contours in a coronal section approximately at the level of the optic chasm at 46 ms, when the peak shear stresses at the genu occurred, are shown in Figure 17. The brain injury sites are shown in Figure 18 for comparison. The left and right sides in these figures correspond to the left and right hemispheres. The high shear stresses at the corpus callosum shown in Figure 17 correspond

well with the tearing of the corpus callosum shown in Figure 18. The high shear stresses at the left lower corner matched the DAI site in the left temporal lobe while those at the right upper corner correspond with DAI in the right upper corner. The prediction of DAI locations by the model was not as good as expected, but the model did partially demonstrate that shear stress/strain could be used as a predictor of DAI.

CONCLUSIONS

1. A side impact accident was simulated. It is estimated that the victim might have contacted the hood of the impacting vehicle, even though no contact area was identified on the head. The estimated resultant linear acceleration was about 220 g's. The estimated lateral angular acceleration was about 20,000 rad/s^2. The estimated sagittal angular acceleration was about 11,000 rad/s^2. These estimates are approximate in view of the many assumptions in the models that must be introduced due to lack of precise information about the crash event reconstruction.

2. The performance of the WSU Brain Injury Model in simulating a real crash situation was tested. Simulation results of the human head model showed that shear stress/strain exhibited some degree of correspondence with the DAI sites. High shear regions in the shear stress contours of the brain were consistent with observed DAI locations. Although the predictions were not perfect, they provided a promising technique to understand the process and mechanisms involved in a real world closed head injury.

ACKNOWLEDGMENTS

REFERENCES

Ishikawa, H., Kajzer, J. and Schroeder G. (1993). Computer simulation of impact response of the human body in car-pedestrian accident. Proc. 37th Stapp Car Crash Conference. SAE Paper No. 933129.

McGrath, P. and Mills, P. (1984). Atlas of sectional anatomy: head, neck and trunk. Krage, Basel, Switzland; New York.

Oka, K. et al (1985). Microsurgical anatomy of the superficial veins of the cerebrum. Neurosurg., 17:711-748

Shuck, L. Z. and Advani, S. H. (1972). Rheological response of human brain tissue in shear. J Basic Eng., pp 905-911.

Wismans, J., Oorschot, H. and Woltring, H. J. (1986). Omni-directional human head-neck response Proc. 30th Stapp Car Crash Conference, SAE Paper No. 861893.

Zhou, C., Khalil, T. B., and King, A. I. (1994). Shear stress distribution in the porcine brain due to rotational impact. Proc. 38th Stapp Car Crash Conference. SAE Paper No. 942214.

Zhou, C., Khalil, T. B., and King, A. I. (1995). A new model comparing impact responses of the homogeneous and inhomogeneous human brain Proc. 39th Stapp Car Crash Conference. SAE Paper No. 952714.

Zhou, C. (1995). Finite element modeling of impact response of an inhomogeneous brain Ph.D. Dissertation, Wayne State University.
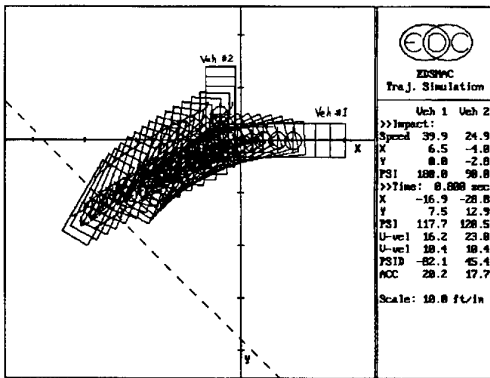
Figure 1 Vehicle collision course by EDSMAC.
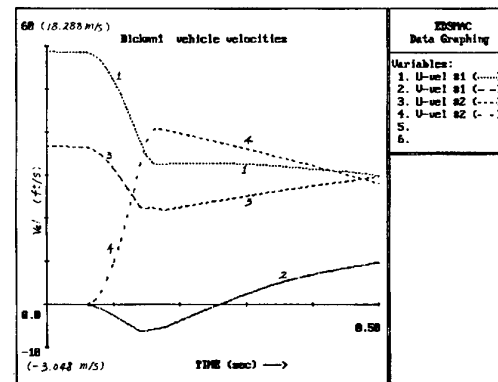
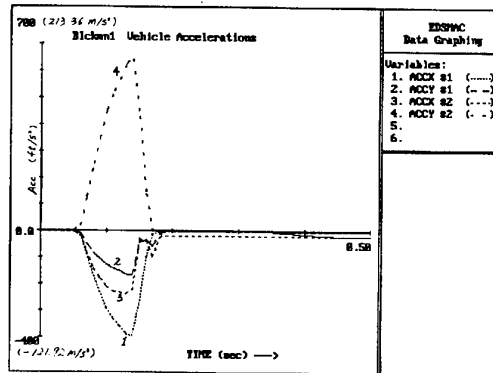
Figure 2 Vehicle velocities during collision.

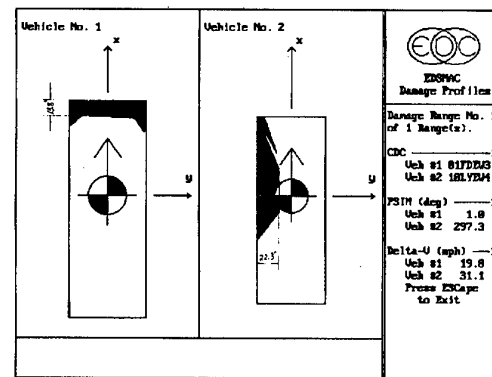Figure 3 Vehicle accelerations during collision.

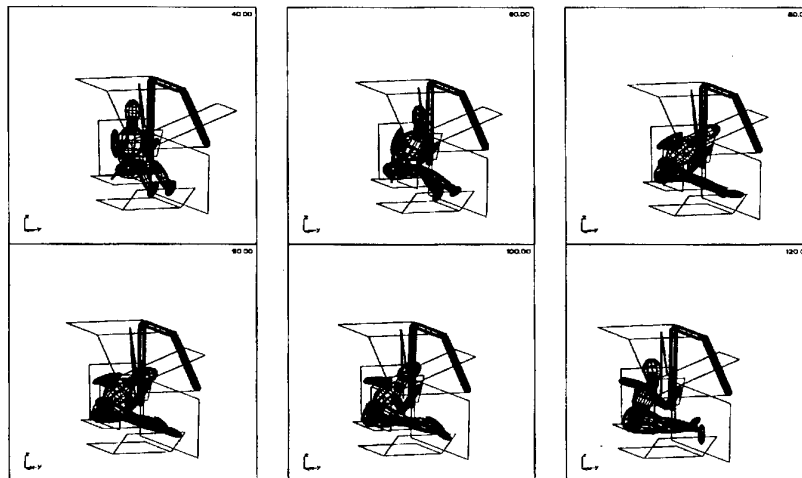Figure 4 Vehicle damage profile by EDSMAC.

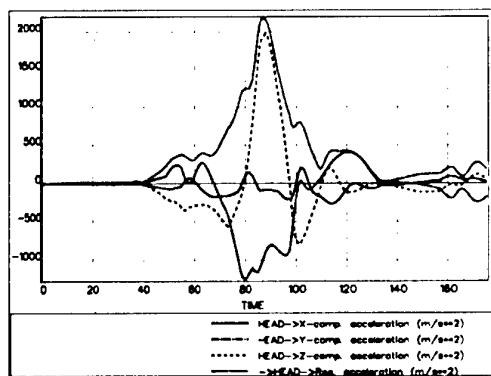Figure 5 Occupant dynamics by MADYMO modeling.
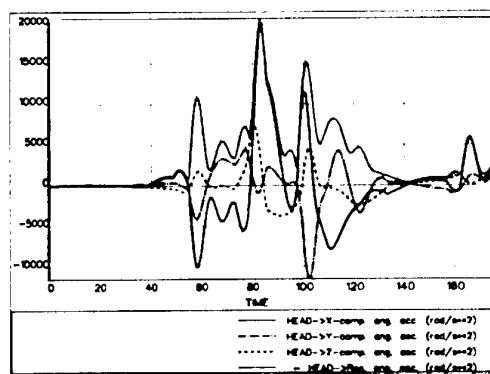
Figure 6 Linear accelerations of the head.

Figure 7 Angular accelerations of the head.

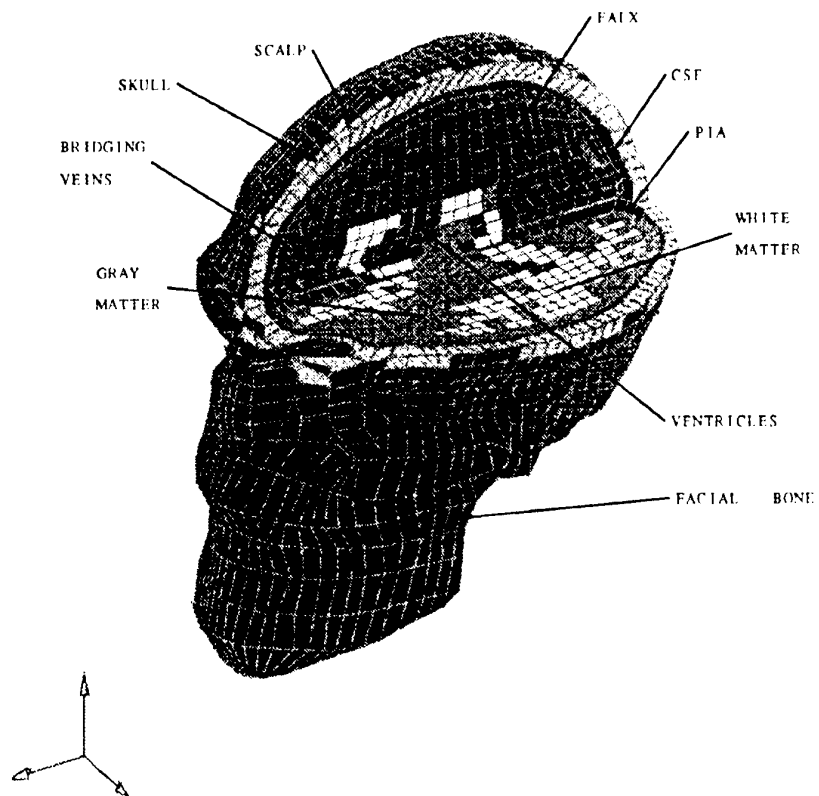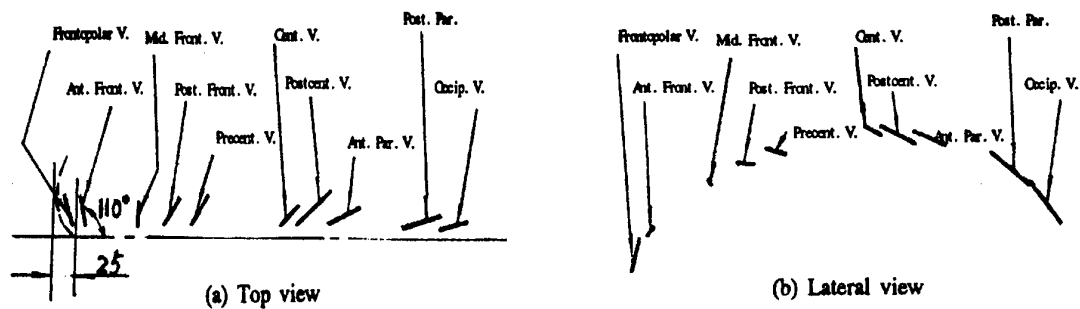Figure 8 Overview of the WSU Brain Injury Model.

(a) Top view

(b) Lateral view

Figure 9 Finite element representation of the bridging veins.

A= V-X   B= V-Y   C= V-Z
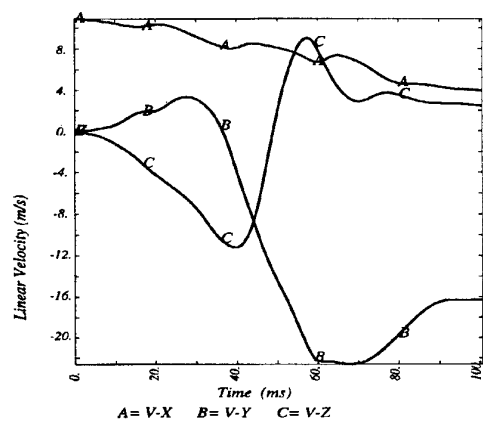
Figure 10 Input linear velocities to the head model.

A= W-X   B= W-Y   C= W-Z
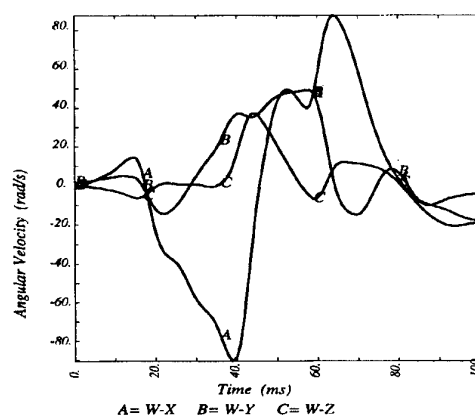
Figure 11 Input angular accelerations to the head model.

A= Frnt. Pole B= Occi. pole   C= Genu   D= Brainstem
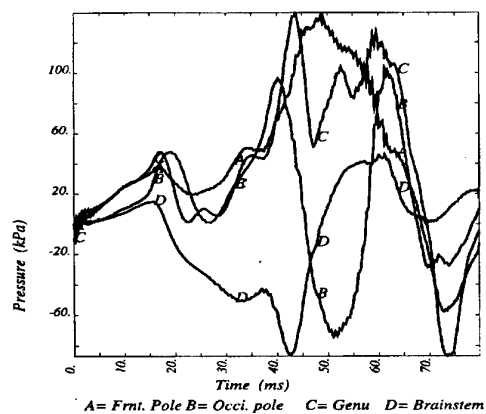
Figure 12 Pressure time histories at four representative points.

A= STRESS   B= STRAIN
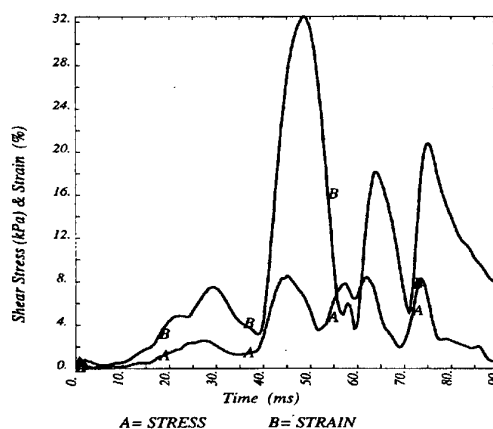
Figure 13 Shear stress and strain time histories of the genu.

Time = 46 ms
Pressure (kPa)

Figure 14 Pressure contours of the brain at 46 ms.

Time = 46 ms
Max Shear Stress (kPa)
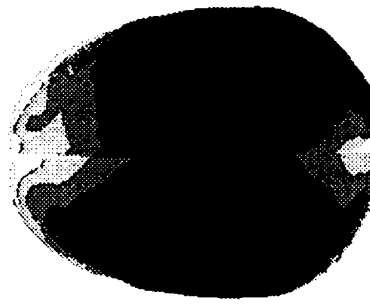
Figure 15 Shear stress contours - top view.

Time = 46 ms
Max Shear Stress (kPa)
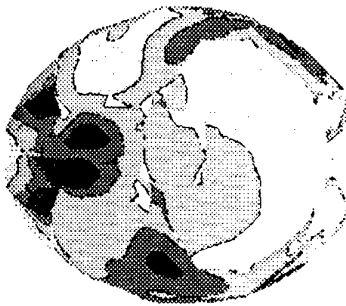
Figure 16 Shear stress contours - bottom view.
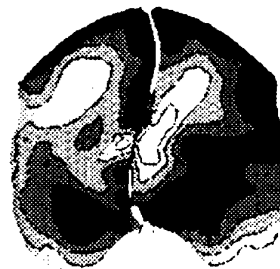
Time = 46 ms
Max Shear Stress (kPa)

Figure 17 Shear stress contours in a coronal section.

Figure 18 Injury sites in the coronal section.

Tissue Level Injury Criteria using Brain Finite Element Analysis, Bilateral Impact Model

Kazunari Ueno
John W. Melvin
Safety Research Department, R & D Center
General Motors, 30500 Mound Road, Box 9055
Warren, MI 48090-9055, USA

Purpose

A finite element model of a bilateral cortical impact was built and executed in three different general purpose finite element programs. The models were exercised as a part of method validation in establishing tissue level injury criteria of the human head.

Abstract

A finite element model of a cortical impact experiment following double craniotomy was built and exercised independently with three different finite element programs, i.e., Dyna3d, Pamcrash and Abaqus as a partial validation of the protocol in establishing tissue level injury criteria for the head/brain subjected to an impact load. A typical experimental impactor motion (4 mm displacement in 1.5 ms, 5 m/s initial velocity) was successfully simulated in all programs and the results were favorably compared to each other in terms of overall stress values, time histories and distributions. The peak Von-Mises stress (120 kPa) was observed in the depth of the brain while the pressure peak (160 kPa) was observed at the surface of the brain. Both pressure and Von-Mises stress wave propagations were in accord with the theoretical wave speeds. The explicit programs (Dyna3d and Pamcrash) have a 600 fold CPU advantage and a smoother stress response compared to the implicit program (Abaqus).

Introduction

Dynamic finite element models are very effective to determine the stress and strain in the human brain during a head impact. Before the stress and strain data can be used as a basis for tissue level injury criteria, however, anatomical injury data from experiments must be correlated with the computed stress and strain.

In our previous studies [6, 9, 11], a protocol for establishing tissue level injury criteria using a cortical impact experiment and a corresponding finite element model were proposed. In this protocol, the experiment yields threshold impact loadings that result in particular brain injuries. The finite element model executed under the same loading conditions yields threshold values of stress and strain that relate to the injuries at particular locations. Tissue level injury criteria determined from the threshold can, in turn, be applied to a human head/brain dynamic finite element model of a head impact in order to assess the risk of human head injury. This extrapolation to human head injury is possible with the assumption that the brains of different species have similar material properties.

The previous single craniotomy cortical impact experiments [5] involved a series of laborious microscopic examinations of multiple frontal cross sections of the brain specimens. If our goal is to look only for correlation of impact thresholds and resultant injuries, however, a different experiment can be devised to produce an injury concentration more effectively near the impact site where post-mortem examinations can be targeted.

A double craniotomy cortical impact experiment was designed so that a concentration of axonal injuries would occur near the impact site. The brain mass which was hit by the impactor at the left craniotomy site would move toward the right craniotomy site rather than toward the foramen magnum. This creates a situation where more injuries would occur near the impact site rather than the remote site. Double craniotomy cortical impact experiments were conducted during 1990 and 1991. A finite element model counterpart was also built to investigate brain response in terms of stress and strain under the same loading as in these experiments. No subsequent experiments were performed for this study. Although the model geometry was based on the previous single craniotomy model [9], there are twice as many elements due to an asymmetric loading condition that requires a whole model. The element mesh is also uniformly smoother than the previous model. At the skull-brain and the impactor-brain interfaces, initial gaps were created to facilitate more effective contact algorithm executions.

In the theory of finite element analysis [3, 12], the analysis is accurate assuming the errors induced from the finite size of elements, the numerical round-off, and the numerical approximation are secondary. Practically speaking, using multiple programs for solving some specific problems is an advantage because users can utilize more effective techniques in each program and gain insights into the problems. Since the multiple programs use the same input data, the similarities and differences among the results from various programs can serve as validation of the program applications. For this reason, three

finite element programs, Dyna3d, Pamcrash (both explicit codes) and Abaqus (implicit code), were used independently to model the double craniotomy cortical impact experiments. The differences among the programs are discussed in terms of methods, results, and cost efficiency.

Methods

Double (Bilateral) Craniotomy Brain Model
The geometry of bilateral craniotomy model was based on the mid-sagittally symmetric single craniotomy model [Figure 1] studied previously [9]. The element mesh was improved to yield more evenly spaced and less skewed elements. The overall surface contour was modified to be smoother by eliminating sharp corners. Part of the spinal cord extension of the previous model was truncated because of its relatively unimportant role in the current double craniotomy study.

Figure 2 shows the bilateral craniotomy model. The model consists of the brain, the skull and the impactor. The brain is composed of 5616 eight-node brick elements. The skull is composed of 2946 triangular shell elements. The impactor is composed of 282 quadrilateral shell elements. The left craniotomy was created by boring the skull with a cylinder of radius 6.5 mm in the direction of the impactor motion. The right craniotomy was created by mirroring the left craniotomy at the midsagittal plane. The impactor of 9 mm diameter with an edge radius of 2 mm was initially placed 0.8 mm off the brain surface. The skull was separated 0.4 mm, 2.4 % of the brain depth (16.4 mm), off the brain surface in the element's normal direction.

The skull nodes are fixed in space to represent an immobile rigid skull. The entire brain is encased in the skull with contact surface elements between them. There are no skull elements at both craniotomy and spinal cord cut ending sites. These free boundary conditions at the exposed brain surface create zero pressure.

Finite Elements Codes
Three commercially available nonlinear finite element codes, Dyna3D [4], Pamcrash [7] and Abaqus [1], were used with a HP9000-J200 workstation and a Cray YMP supercomputer. Dyna3d and Pamcrash are based on the explicit code (central difference method) for solving dynamic equilibrium equations while Abaqus is based on the implicit code (Newton's method). The time step in the explicit codes is automatically calculated during the analysis based on the smallest size of the elements and material properties to ensure the numerical stability. As the implicit code is unconditionally stable, a user can choose the time step according to the program economy and the rate of loading/deformation. The initial time step chosen for the Abaqus analysis was 0.1 ms.

To compare results fairly among the three programs, material properties were chosen as simple as possible at this stage of our study. The linear elastic brain material as used before [11, 9]

was used in each program. Table 1 lists the types of elements and materials used for the brain.

The use of contact elements is a key to success of this nonlinear dynamic analysis. Various contact elements were tried during the course of this study in search of the best performer in each program in terms of failure in contact (element penetration) and deformed element shape at contact surfaces. Among the contact elements tried are automatic-nodes-surface and automatic-surface-to-surface of Dyna3d, simple segment to segment contact and simple node to segment contact of Pamcrash, and inter4 (gap element) in Abaqus. The contact elements finally chosen are listed in Table 2.

The Input Loading and the Boundary Conditions
The impactor displacement time history obtained from a direct measurement of a typical bilateral cortical impact experiment was used to drive the impactor by either velocity or acceleration. Figure 4 shows the time history plots of the acceleration, velocity and displacement of the impactor. The velocity (an input loading for Dyna3d and Pamcrash) and acceleration (an input loading for Abaqus) were calculated from the displacement by differentiation.

The impactor hits the brain obliquely at approximately 27 degrees from the mid-sagittal plane and directs its tip toward the bottom of the brain. The input of the impactor motion (velocity or acceleration) for the model was resolved into its components in the head coordinate system. The initial position of the model impactor tip was 0.8 mm off the brain surface. Because the maximum stroke of the impactor was about 4.8 mm, the maximum brain displacement was about 4 mm (about 24 % of the brain depth). The initial velocity of the impactor was about 5 m/sec.

Parameters to Be Analyzed
The pressure and the Von-Mises stress are stress invariants and were therefore chosen to be compared. The displacement of the impactor node was monitored to ensure that it matched the experimental motion.

One representative frontal section at the impact site was chosen to display stress fringe patterns as well as time histories of stresses. Figure 3 shows this particular cross section of the brain model indicating the selected elements and nodes for the post-processing. As shown, the elements, 1722, 1721, 1720, 1782, 1787, 1792, and 3585 as well as the nodes, 10011 (the impactor rigid node), 3982, 4107, 4074, 4089, and 4086 are chosen for the time history plots.

The resultant stress history and contour plots were displayed by Taurus for Dyna3d, Pamview for Pamcrash and Abaqus/Post for Abaqus.

Results

The results from Dyna3d are reported first to provide a basis for comparison with the other two programs. The results from Pamcrash and Abaqus are presented later.

The Impactor Motion and the Brain Displacement
Figure 5 shows the resultant displacements of the impactor and the selected brain nodes. The impactor motion was successfully enforced by the given input velocity as shown as the curve A. The impactor reached the maximum stroke of 4.8 mm at 1.5 ms. The brain surface node (3982, the curve B) follows the impactor after the contact at 0.16 ms, reaching the maximum displacement of 4.0 mm (24 % of the brain depth). The peak displacement of the surface node at the right craniotomy was 1 mm at 1.5 ms. The node at the spinal cut ending, node 6354, displaced 0.3 mm. Figure 6 shows the contour plot of resultant displacement of the brain section at about 1.5 ms. The largest displacement is seen at the impact site.

Resultant Stresses
Figure 7 shows the history plots of Von-Mises stresses for the selected elements. The history patterns are smooth and the peak stresses occur at different times for different locations indicating shear stress wave propagations from the surface to the deep region of the brain. The peak stress for the brain surface (element 1722) was 85 kPa and occurred at 0.7 ms. Overall maximum stress of 120 kPa at 0.9 ms was observed at element 1720, which is located at the third layer from the surface. Figure 8 shows the fringe pattern of the Von-Mises stress at the time of 0.96 ms. Again the maximum stress was seen at the depth of the third finite element layer from the impact surface.

Figure 9 shows the history plots of the pressure for the same selected elements. The onset pressure peaks occurred at 0.4 ms, much earlier than the peak Von-Mises stress. The time of peak pressure for each element shifted slightly but consistently, suggesting a pressure wave propagation. The overall peak pressure was observed at surface element 1722 which reached 160 kPa at 0.25 ms. The pressure at the impact surface elements was consistently higher than that of remote elements throughout the analysis. The general patterns of pressure history plots were more oscillatory than those of Von-Mises stress. Figure 10 shows the fringe pattern of pressure at 1.4 ms.

Results and Comparison Among the Three Programs
The surface deformation at the brain impact site is less smooth in Abaqus(Figure 13) as compared to Dyna3d(Figure 11) and Pamcrash(Figure 12). In Abaqus, there is skewed or possible "hour-glass mode" deformation at the impact site.

The Von-Mises stress history plots from Pamcrash for the selected elements are shown in Figure 14. Overall patterns are similar to those from Dyna3d shown in Figure 7. The peak stress for element 1720 is 123 kPa at 0.95 ms in Pamcrash.

The pressure history plots from Pamcrash are shown in Figure 15. Unlike Dyna3d shown in Figure 9, the peak pressure does not occur at onset of impact. The patterns are similar to those of Dyna3d, but the initial peak of the element 1722 (125 kPa) is lower and the pressure increases after the initial peak.

The Von-Mises history plots from Abaqus are shown in Figure 16. Overall patterns are similar to those from Dyna3d (Figure 7) and Pamcrash (Figure 14). For element 1720 (the third finite element layer from the impact surface), there are two peaks in the Abaqus model while there is a single peak in both Dyna3d and Pamcrash models. The first peak (145 kPa at 0.8 ms) is less than the second peak (180 kPa at 1.3 ms).

The pressure history plots from Abaqus are shown in Figure 17. The peak pressure occurs early in the time history, as in Dyna3d. However, the maximum pressure for the surface elements occurs at a later time.

Discussion

Displacement in the Brain
While displacement itself may not be a parameter related to brain injury, it is a parameter to be used toward a verification of the finite element model against the physical model where a high speed camera captured the displacement of an embedded marker.

The displacement (4 mm) of the brain was localized near the impact site as shown in Figure 6. At the center section of the brain and at the region of right craniotomy site, the displacement was less than 1 mm. The displacement at the foramen magnum was only 0.3 mm. The 0.4 mm gap between the skull and the brain and the large right craniotomy may be why brain movement was quickly distributed to all directions.

Stresses in the Brain
Unlike the previous single craniotomy model [9], the double craniotomy model has zero stress boundary at the right craniotomy site. This stress condition produced localized stresses near the impact site. The ring pattern shear stress observed at the impact surface of the brain in the previous single craniotomy model was not observed in the double craniotomy model. However, the maximum Von-Mises stress appears in the third element layer from the surface, not at the direct contact surface layer. The mechanisms of the impactor induced stresses in a solid media and the role of pressure/shear stress for particular brain injuries should be carefully studied in the future.

The peak Von-Mises stress appeared early in the time history (0.9 ms), before the peak acceleration of the impactor (1.2 ms). Therefore, the brain response has a different time history (Figure 7) from the input impactor time history (Figure 4). The pressure history (Figure 9) also indicates that the initial pressure peak at the onset of the impact has nothing to do with the pattern of the input impactor motion (Figure 4). It is a typical response of a solid exposed to high speed contact. This difference in the analyses between responses(output) and input

motions such as accelerations as in the case of HIC is one of the most important aspects of head impact study using a finite element model.

The stress wave speed can be calculated based on the equations for linear elastic solid media [2]. According to these equations (see Table 3), the dilatational (longitudinal) wave speed is 64 m/s and the distortional (shear) wave speed is 9 m/s. On the other hand, we can estimate the resultant stress wave speed from the model using the history plots of stresses by taking the time of peak stress for each element and the distance between the elements. We identified both pressure and shear wave propagations in the brain model with the calculations listed on Table 3. The dynamic finite element analysis can be verified in this respect as well.

Contact Surfaces and Initial Gap

There are many types of contact algorithms available in the programs used here. The contact elements listed in Table 2 were used after several trials of different contact elements in this study. They may not be the ultimate choices for the finite element model of a head injury since new contact algorithms are constantly being updated.

The existing contact algorithm can cause problems with contact interactions to dynamic equations. Typically, when a contact is detected, efforts to reject penetrating nodes cause large deformation on contacting elements. The contacting surfaces where nodes must recognize contact may not be smooth enough because of the size of the elements involved. This may be solved by creating finer mesh on contact surfaces. The stress history also reveals more oscillatory results if the contact fails or is unstable.

The trials and errors in searching for a good contact element may be time consuming but, often, the element best suited for an application can be found in other unrelated fields. In the case of Pamcrash, for example, the contact element type 36 is not meant to be used for the contact between two bodies but for the self contact of one body. However, it behaved the best compared to the other contact types.

The original single craniotomy model has no gap between the skull and the brain surface, i.e., the nodal coordinates are duplicated for opposing contact surfaces. This did not create a problem for the Abaqus contact elements but the contacting nodes penetrated too easily in both Dyna3d and Pamcrash. With an initial gap between the impactor tip and the brain, both Dyna3d and Pamcrash were able to detect an approaching contact surface and therefore prevent penetration. The magnitude of the gap (0.8 mm between the impactor and the brain, 0.4 mm between the skull and the brain) was chosen to avoid contact problems in Dyna3d and Pamcrash. It does not reflect a realistic or anatomical gap.

In biomechanics, contact elements in conjunction with a fluid type interface element may be very useful for modeling many bone joints and interfaces between different body parts. In the brain-skull interface, contact surface elements may be more appropriate than the continuous solid element interface used in some head injury models [8, 10].

For human head/brain models exposed to the impact loading, the separation of brain from the skull and the corresponding stress field remains one of the major interests in the study of head injury. The brain separation from the skull and its association with negative pressure at the contrecoup injury site can be studied with models that incorporate contact surfaces.

Justification of Using Three Programs

It is commonly observed that different finite element programs yield different results, even with the same input data. From a theoretical point of view, finite element programs, if properly used, should strive for accurate results regardless of individual differences in methodology. In this study, justification of using multiple programs with the same input data is based on a hypothesis that if all programs yield the same result, the result must be, at least, close to the true solution for the specific boundary, loading and modeling conditions used. Comparison among the different programs may lead not only to further insights in the problems at hand, but also to a form of validation of the method itself especially when the other means of validation such as the experimental data are scarce.

To compare the results from the three finite element programs, each input data has to be absolutely equivalent. Even if the geometry, material properties, loading and boundary conditions are the same, each program is coded differently for its own efficiency and economy. The choice of element types for a particular solid or shell, material types and material properties definition, convergence criteria (if the program is implicit), the time step (if the program is explicit), and the method of contact algorithm are user and program dependent. Therefore, opportunities in program choices should be taken as a means to explore the possibility for better modeling of the problem addressed.

Comparison Among the Three Programs

Regardless of different techniques used in each program, Von-Mises stresses are similar to each other as shown in Figure 7, Figure 14, and Figure 16. The pressures shown in Figure 9, Figure 15 and Figure 17 are somewhat different in terms of oscillatory patterns of pressure time history. However, both Von-Mises stress and pressure from all programs demonstrated the proper wave propagations.

Figure 18 and Figure 19 show the comparison of the Von-Mises stress history and pressure history of the impact surface element (element 1722) among the three programs. The results from Dyna3d and Pamcrash are similar but the result from Abaqus is markedly different in its pressure history pattern. Contact elements themselves seem to be a significant factor on the stresses at the impact surface since the impact surface elements show major differences.

Figure 20 and Figure 21 show the comparison of the history plots of Von-Mises stress and pressure of the deep brain element (element 1787) from the three programs. The Von-Mises stresses are very similar to each other at this site of the brain. The approximate peak Von-Mises stresses of the element 1787 are listed in Table 4. The pressure history pattern from Abaqus is also markedly different from Dyna3d and Pamcrash. Since the pressure time history has distinct peaks at the onset of the impact, the peak onset pressures are given in Table 5.

After their initial peaks, the pressure time histories differ significantly. This should be studied further since the model will be validated, in part, by comparing the models' pressures to those measured experimentally.

An explicit program is very attractive because of its 600 fold economy in CPU time as listed in Table 6. Also, the behavior of the contact surface elements is superior to that of implicit code as compared in Figure 11, Figure 12 and Figure 13.

Reduced Integration
In constructing an element matrix (stiffness matrix), it is essential to integrate its approximation function over the entire element. To accurately integrate numerically, the number of points where the function is evaluated must be as great as the order of the function itself. Often, because of the desire for cost reduction, it is possible to use fewer integration points without much loss of accuracy (reduced integration).

For nearly incompressible materials, reduced integration is beneficial because it imposes numerical singularity on the stiffness matrix [12, 3]. This counteracts an imbalance that results from very large bulk modulus and high Poisson's ratio. On the other hand, a disadvantage of using reduced integration is the possibility of generating hour-glass modes (zero energy modes) where an affected element can be deformed without any strain. However, there are many hour-glass control methods used in today's programs and the use of reduced integration is very common in explicit codes such as Dyna3d and Pamcrash.

For Abaqus, reduced eight node elements (C3D8R and C3D8RH) did not behave well with over-deformed (element splash appearance at the impact site) elements and the corresponding erratic stresses at the impact site. The high Poisson's ratio (0.49) may have induced the errors in Abaqus since the element used does not use the reduced integration for the nearly incompressible materials. For this reason, the fully integrated element (C3D8) was used in Abaqus.

To investigate the effect of reduced integration, the model using fully integrated elements was executed in Dyna3d. The resultant plot of the Von-Mises stress and pressure are shown in Figure 22 and Figure 23, respectively. With fully integrated

elements, the results, especially the pressure plot, were more oscillatory. This may indicate the errors generated by the fully integrated elements of a nearly incompressible material. For this reason, in Dyna3d or Pamcrash, the use of reduced integration for the brain elements is recommended.

Implicit and Explicit Methods
One of the major distinctions in nonlinear transient dynamic finite element programs is a type of method to solve a dynamic equilibrium equation. A program can be categorized under either the explicit time integration method (e.g., the central difference method) or the implicit time integration method (e.g., the Newmark method) [3].
In the explicit method, a current time solution is obtained solely from the states of the past time. Therefore, the solution is easily obtained without any iteration and, in some cases, without triangulation of system matrix (when the mass matrix is diagonal, for example). For this reason, the explicit method is very economical in numerical procedures. However, because the solution of the current time step is based on the information of the previous time step, the accuracy of the solution depends on the time step size. To avoid unstable and erroneous calculations, the time step must be less than the critical time step size calculated from material properties and the smallest element size. For this reason, the explicit method is said to be conditionally stable. Most codes available today, including Dyna3d and Pamcrash, automatically calculate the time step size and apply it to the dynamic analysis.

The implicit method, on the other hand, uses the solution based on both the current and the past time step conditions. Therefore, numerically, the solution has to be obtained through an iteration. Since this method makes sure the equilibrium of the dynamic equations is satisfied in the current time step, the solution is more accurate compared to the explicit method and it is unconditionally stable. However, convergence in the iterative solution procedure is time consuming and costly. The time step in the implicit method can be much larger than that of the explicit method, reducing the total number of time steps.

Table 6 shows the comparison of CPU times for models executed on the CRAY and HP9000. It is more practical to use explicit codes in general nonlinear impact analysis. However, the accuracy of the results has to be examined carefully. In our study, the results from Abaqus were comparable to those of Dyna3d and Pamcrash.

Summary and Conclusions

A finite element model of a bilateral cortical impact was built and transformed to be executed in explicit codes with reduced-integrated elements (Dyna3d and Pamcrash), and in implicit code with fully integrated-elements (Abaqus).

The input impactor motion was taken from a typical double craniotomy cortical impact experiment and was used to drive the impactor by acceleration (Abaqus) or velocity (Dyna3d and Pamcrash).

The results were obtained from the three finite element analysis programs and post processed to be compared in terms of the displacement and stresses in the brain. The following conclusions were based on these results:

1. For this model, the stresses were localized at the immediate region under the impact site. The deformations of the brain at the contra-lateral craniotomy site and at the spinal opening were minimal.

2. Dyna3d gave the smoothest deformation at the contact surfaces and stable patterns of the stress time histories. Pamcrash results were similar to Dyna3d with slightly less smooth deformed surfaces and stress history patterns. In Abaqus, the impact surface of the brain was excessively warped and skewed, although the stress history was smooth and stable.

3. The pressure and shear wave velocities produced in Dyna3d matched those theoretically calculated for the dilatational and distortional waves.

4. For the particular impact loading used in this study, which produced diffuse axonal injuries in the experiment (5m/s initial impactor velocity, 4 mm maximum impactor stroke to the brain at 1.5 ms), the maximum Von-Mises stress was observed about 3 mm deep under the impact site at 0.9 ms, while the maximum pressure was observed very early (0.3 ms) at the contacted brain surface element and the high pressure was observed at the surface rather than sites away from the impact site.

5. For the area where the majority of injury data are expected, i.e., upper middle section of the brain, the differences in the stresses among the three programs were minimal. For the same loading condition, the Von-Mises stress of about 90 kPa and the pressure of 25 kPa were seen as the peak values.

6. For efficiency and economy, the explicit codes (both Dyna3d and Pamcrash) performed much better than the implicit code (Abaqus) with the CPU time ratio of 1 (explicit code) to 600 (implicit code).

Table 1. The Element Types and Material Types for the Brain		
	Element Types	Material Types
Dyna3d	element-solid	mat_elastic [4], E=0.24MPa ν=0.49
Pamcrash	8-node solid	Type 1; elastic plastic [7], E=0.24Mpa ν=0.49
Abaqus	C3D8RH	elastic [1], E=0.24Mpa ν=0.49

Table 2. The Contact Elements Used for Each FE Program	
Program	Contact Site: 1 = between the skull and the brain 2 = between the impactor and the brain
Dyna3d	type 3 (surface to surface) for both site 1 & 2 [4]
Pamcrash	type 36 (self-impacting contact with edge treatment [3D bucket search]) for both site 1 & 2 [7]
Abaqus	IRS4 (Rigid surface element for use with solid elements which have 4 nodes on the element face that interfaces with the rigid surface) for site 1. IRS13 (Three dimensional rigid surface element for contact between a single node of a three-dimensional mesh and a rigid body) for site 2 [1]

Table 3. Wave Velocities in the Brain Model [2]		
name of wave	definition	brain model
Longitudinal Wave (dilatational wave)	$$C_L = \sqrt{\frac{E(1-v)}{\rho(1+v)(1-2v)}}$$	64 m/s
Shear Wave (distortional wave)	$$c_s = \sqrt{\frac{G}{\rho}}$$	9 m/s

Brain Material Properties Used in the Model
E = Young's modulus = 0.24 MPa = 0.24 N/(mm)^2
G = shear modulus = E/ = 0.0805 N/(mm)^2
ν = Poisson's ratio = 0.49
ρ = density = 1 × 10^{-9} Ns^2/(mm)^4

Table 4. Comparison of Von-Mises Stress peak of element 1787		
Program	Peak Values	Time
Dyna3d	90 kPa	1.2 ms
Pamcrash	91 kPa	1.2 ms
Abaqus	90 kPa	1.2 ms

Table 5. Comparison of Pressure peak of element 1787 at onset of the impact.		
Program	Peak Value	Time
Dyna3d	27 kPa	0.3 ms
Pamcrash	24 kPa	0.3 ms
Abaqus	19 kPa	0.35 ms

Table 6. Comparison of CPU time for this particular data set		
Program	CPU time	computer used
Dyna3d	140sec (2min 20sec)	CRAY
	209sec (3min 29sec)	HP9000 J200
Pamcrash	N.A.	CRAY
	550sec (9 min 10sec)	HP9000 J200
Abaqus	172800sec (48 hours)	CRAY
	N.A.	HP9000 j200
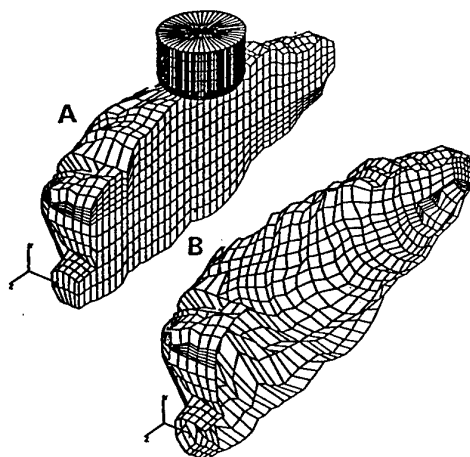
Figure 1 The original mid-sagittally symmetric brain model. The model consists of the skull, the brain and the impactor. The skull and the brain surface share the same nodes in this model, creating no initial gap at the contact surfaces. The bilateral craniotomy model was based on this geometry.

Figure 3 The frontal section of the brain where the impactor hits. The elements 1722, 1721, 1720, 1782, 1787, 1792, and 3585 of this section are used to monitor the stress result history. The nodes 10011 (impactor), 3982, 4017, 4074, 4089, 4086 and 4125 are used to monitor the displacement result history.

Figure 2 Bilateral craniotomy model. The model consists of the skull, the brain and the impactor. The skull has two craniotomies, but the impactor hit the brain only through the left craniotomy. There is a 0.4 mm initial gap between the skull and the brain.
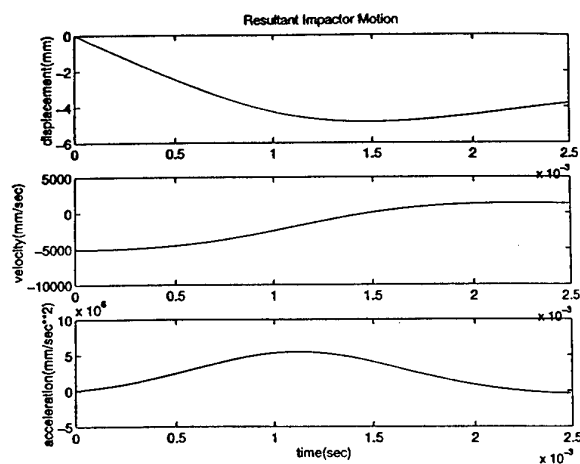
Figure 4 A: The time history of experimental impactor displacement measured by a Linear Variable Differential Transformer. B: The velocity time history used to drive the Pamcrash and Dyna3D models was derived by differentiating the displacement time history. C: The acceleration time history used for drive the Abaqus model was derived by doubly differentiating the displacement time history.
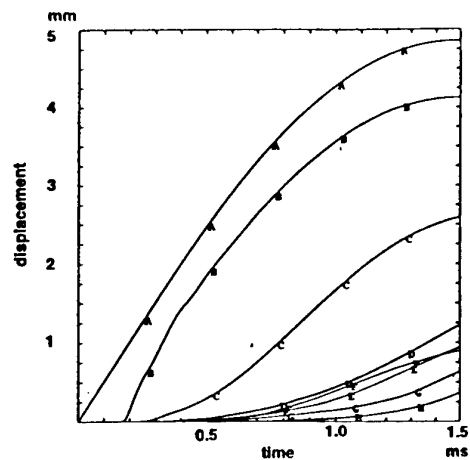
Figure 5 The results from Dyna3d: The resultant total displacement history of the selected nodes, 10011 (A, impactor), 3982(B, brain impact surface), 4017(C), 4074(D), 4089(E), 4086(F, contra-lateral brain site), 4125(G, brain bottom surface) and 6354(H, spinal cut ending) are shown. There is a gap (0.8 mm) between the impactor tip and the brain impact surface.
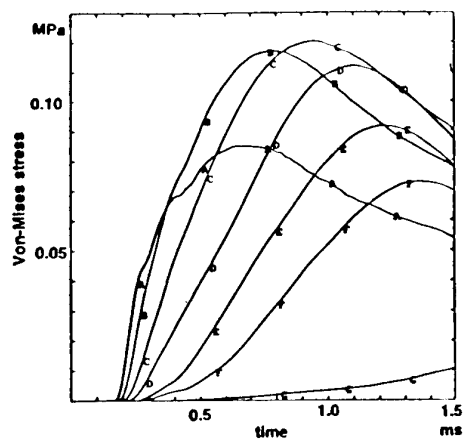

Figure 7 The results from Dyna3d: Von-Mises stress time history of the selected elements which are located in the cross section of the brain where the impactor hits. The elements are labeled in sequence as (A)1722-the impact surface, (B)1721, (C)1720, (D)1782, (E)1787, (F)1792, and (G)3585-the deep center of the brain. Stress is in MPa and time is in seconds.
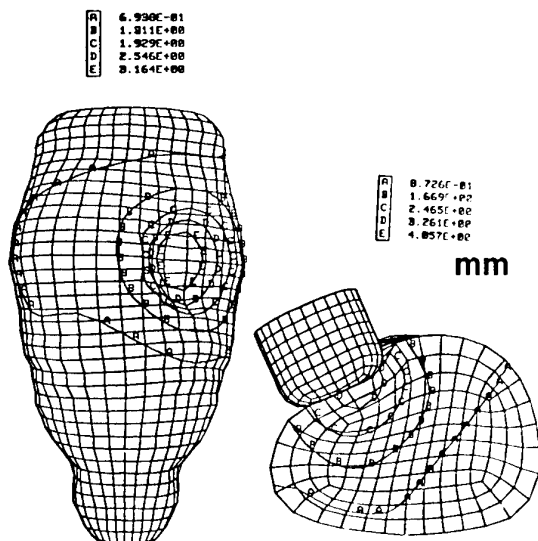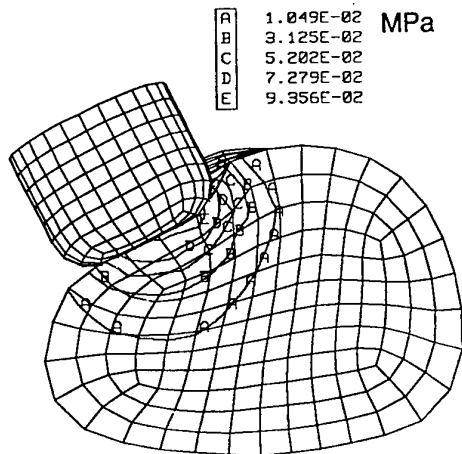

Figure 6 The results from Dyna3d: The contour plot of brain displacement at t=1.5 ms. A: Top view of the brain. B: Frontal cross sectional view at impact site.
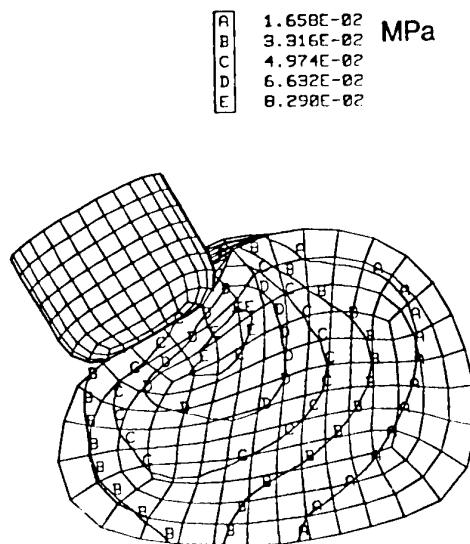
Figure 8 The results from Dyna3d: Von-Mises stress fringe plot of the frontal section of the brain at impact site. (time = 1.5 ms)
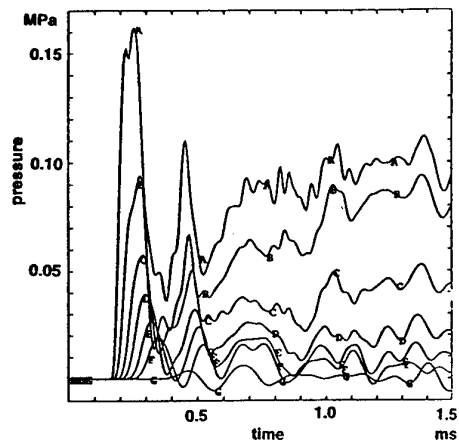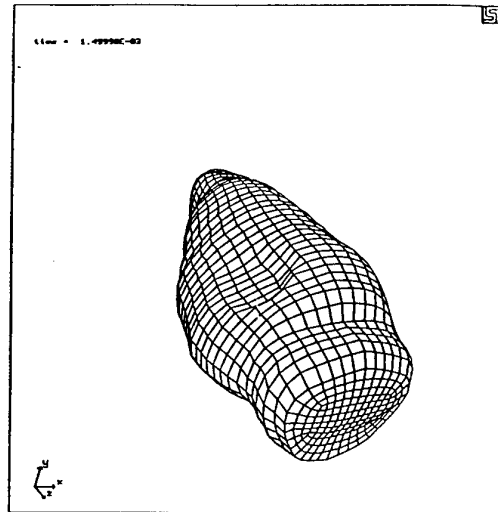
Figure 9 The results from Dyna3d: Pressure time history of the selected elements which are located in the cross section of the brain where the impactor hits. The elements are labeled in sequence as (A)1722-the impact surface, (B)1721, (C)1720, (D)1782, (E)1787, (F)1792, and (G)3585-the deep center of the brain. Pressure is in MPa and time is in seconds.

Figure 11 The results from Dyna3d: The deformed surface of the impact site of the brain at 1.5 ms.

		MPa
A	1.049E-02	
B	3.125E-02	
C	5.202E-02	
D	7.279E-02	
E	9.356E-02	

Figure 10 The results from Dyna3d: Pressure fringe plot of the frontal section of the brain at impact site. (time = 1.5 ms)
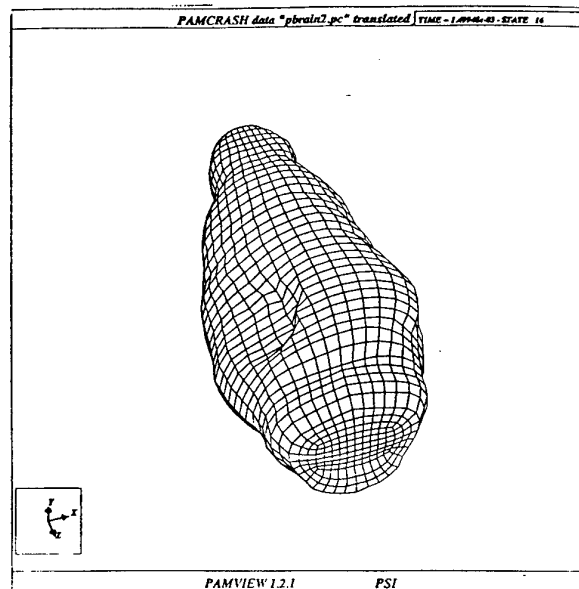
Figure 12 The results from Pamcrash: The deformed surface of the impact site of the brain at 1.5 ms.
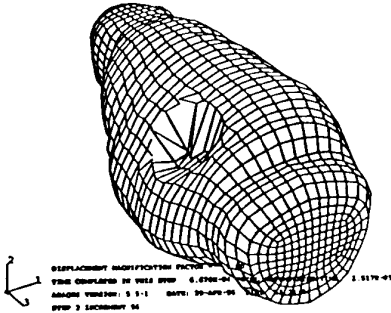
ABAQUS

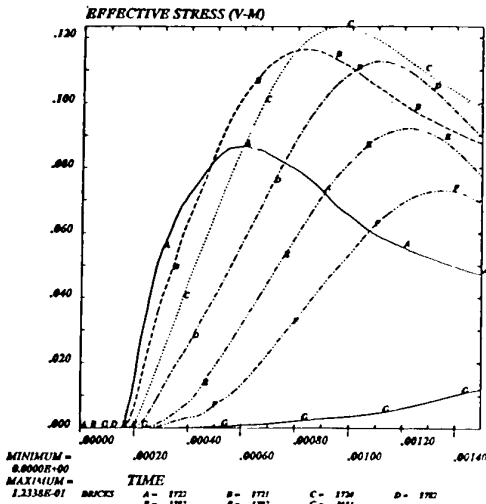**Figure 13** The results from Abaqus: The deformed surface of the impact site of the brain at 1.5 ms.
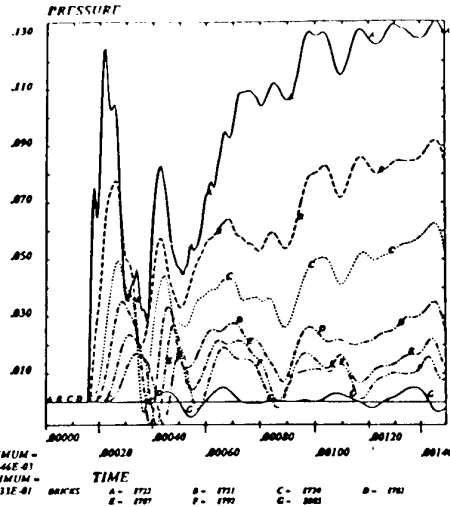

Figure 15 The results from Pamcrash: Pressure time history of the selected elements which are located in the cross section of the brain where the impactor hits. The elements are labeled in sequence as (A)1722-the impact surface, (B)1721, (C)1720, (D)1782, (E,1787, (F)1792, and (G)3585-the deep center of the brain. Pressure is in MPa and time is in seconds.

ABAQUS

Figure 14 The results from Pamcrash: Von-Mises stress time history of the selected elements which are located in the cross section of the brain where the impactor hits. The elements are labeled in sequence as (A)1722-the impact surface, (B)1721, (C)1720, (D)1782, (E)1787, (F)1792, and (G)3585-the deep center of the brain. Stress is in MPa and time is in seconds.
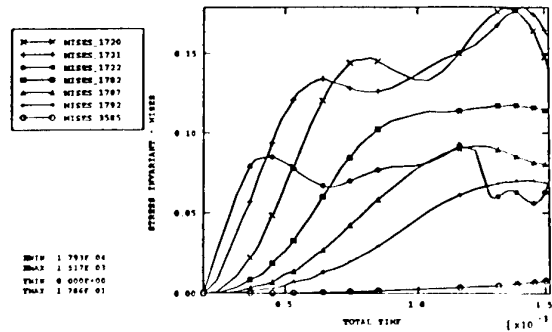
Figure 16 The results from Abaqus: Von-Mises stress history of the selected elements which are located in the cross section of the brain where the impactor hits. The elements are labeled in sequence as (A)1722-the impact surface, (B)1721, (C)1720, (D)1782, (E)1787, (F)1792, and (G)3585-the deep center of the brain. Stress is in MPa and time is in seconds.
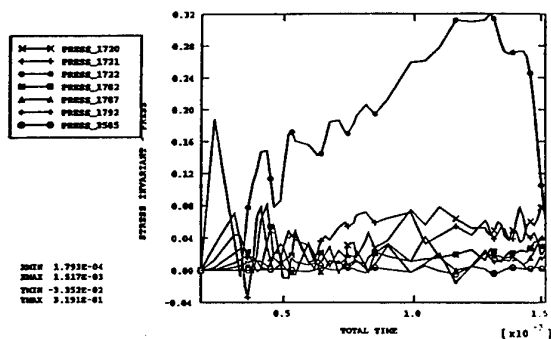
Figure 17 The results from Abaqus: Pressure time history of the selected elements which are located in the cross section of the brain where the impactor hits. The elements are labeled in sequence as (A)1722-the impact surface, (B)1721, (C)1720, (D)1782, (E)1787, (F)1792, and (G)3585-the deep center of the brain. Pressure is in MPa and time is in seconds.
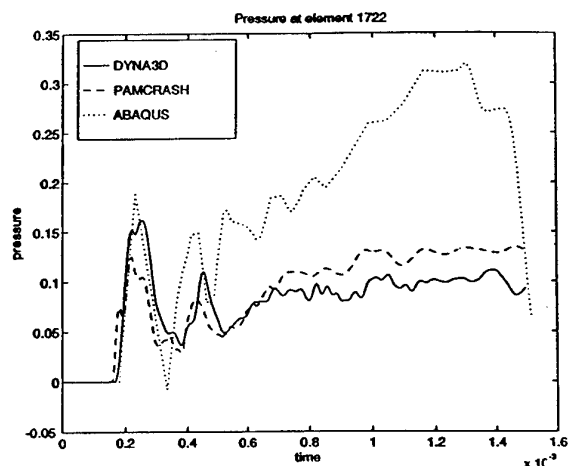

Figure 19 Comparison of pressure at element 1722 (impact surface) from Dyna3d, Pamcrash and Abaqus. Pressure is in MPa and time is in seconds.
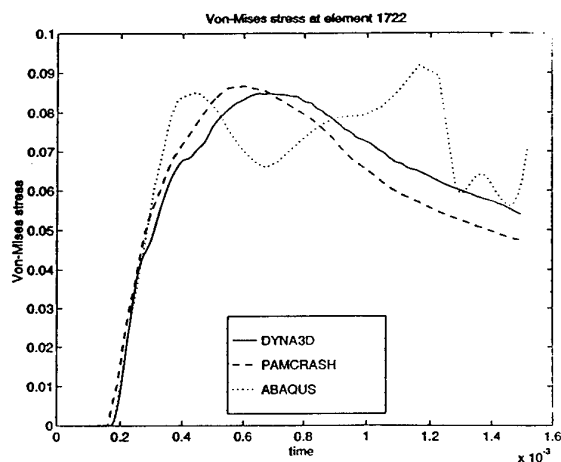

Figure 18 Comparison of Von-Mises stress at element 1722 (impact surface) from Dyna3d, Pamcrash and Abaqus. Stress is in MPa and time is in seconds.
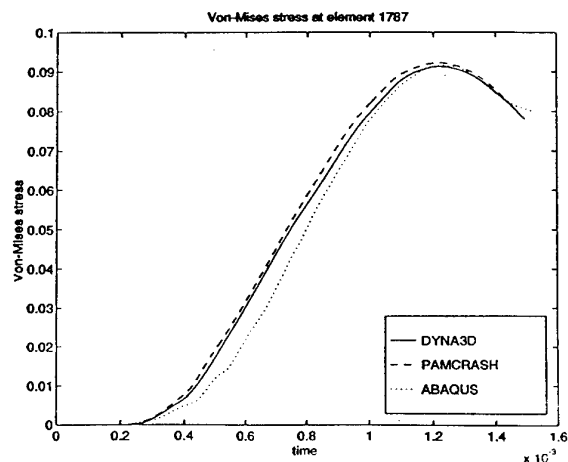

Figure 20 Comparison of Von-Mises stress at element 1787 (deep brain) from Dyna3d, Pamcrash and Abaqus. Stress is in MPa and time is in seconds.
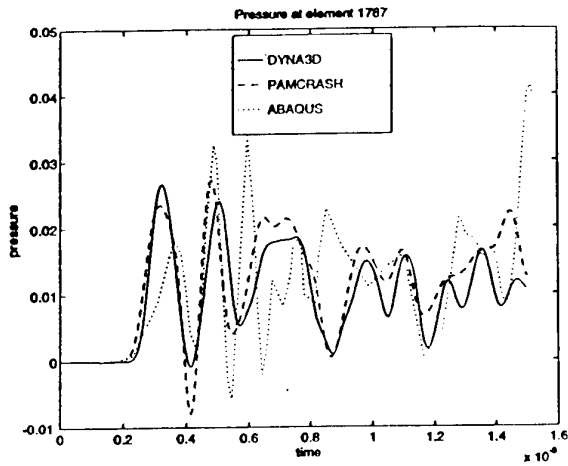
Figure 21 Comparison of pressure at element 1787 (deep brain) among from Dyna3d, Pamcrash and Abaqus. Stress is in MPa and time is in seconds.
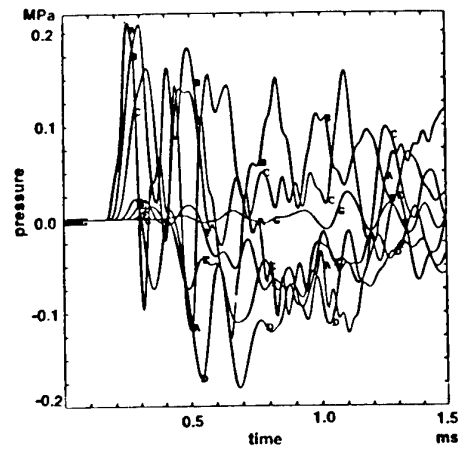

Figure 23 The results from Dyna3d with fully integrated elements: Pressure time histories of the selected elements which are located in the cross section of the brain where the impactor hits. The elements are labeled in sequence as (A)1722-the impact surface, (B)1721, (C)1720, (D)1782, (E)1787, (F)1792, and (G)3585-the deep center of the brain. Pressure is in MPa and time is in seconds.

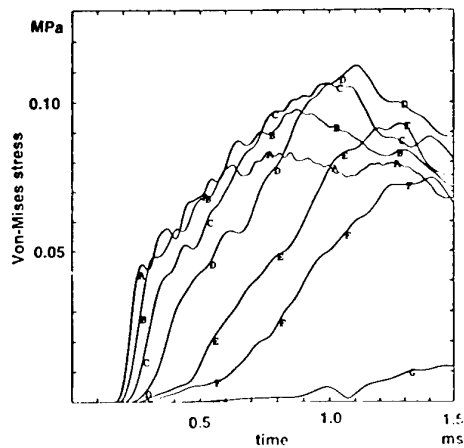**Figure 22** The results from Dyna3d with fully integrated elements: Von-Mises stress time histories of the selected elements which are located in the cross section of the brain where the impactor hits. The elements are labeled in sequence as (A)1722-the impact surface, (B)1721, (C)1720, (D)1782, (E)1787, (F)1792, and (G)3585-the deep center of the brain. Stress is in MPa and time is in seconds.

References

1. "Abaqus/Standard, User's manuals", Vol 1 & 2, Version 5.5, Hibbitt, Karlsson & Sorensen, Inc. , 1995.

2. Achenbach, J. D.: Wave Propagation in Elastic Solids, American Elsevier, New York, 1973.

3. Bathe, K. J.: Finite Element Procedures in Engineering Analysis, Prentice- Hall, Inc., 1982.

4. Hallquist, J. H., Stillman, D. W. and Lin, T-L.: "LS-Dyna3d User's Manual, Nonlinear Dynamic Analysis of Structures in Three Dimensions", version 930, Livermore Software Technology Corporation, April 1994.

5. Lighthall, J. W., Goshgarian, H. G. and Pinderski, C. R.: "Characterization of Axonal Injury Produced by Controlled Cortical Impact", Journal of Neurotrauma, Vol. 7, No. 2, 1990, pp65-76.

6. Lighthall, J. W., Melvin, J. W. and Ueno, K: "Toward a Biomechanical Criterion for Functional Brain Injury", 12th ESV Conf. US DOT 1989.

7. Pam System International, :"Pam-Crash, Pam-Safe User's Manual", Version 1996, ESI Group Software Product Company, February 1996.

8. Ruan, J. S., Khalil, T. and King, A. I.: "Human Head Dynamic Response to Side Impact by Finite Element Modeling", Journal of Biomechanical Engineering, Vol. 113, 1991, pp276-283.

9. Ueno, K., Melvin, J. W., Li, L. and Lighthall, J. W.: "Development of Tissue Level Brain Injury Criteria by Finite Element Analysis", Journal of Neurotrauma, Vol. 12, No. 4, 1995, pp695-706.

10. Ueno, K. and Melvin, J. W.: "Finite Element Model Study of Head Impact Based on Hybrid III Head Acceleration: The Effects of Rotational and Translational Acceleration", Journal of Biomechanical Engineering, Vol. 117, 1995, pp319-328.

11. Ueno, K., Melvin, J. W., Rouhana, M. E. and Lighthall, J. W.: "Two-dimensional Finite Element Model of the Cortical Impact Method for Mechanical Brain Injury", Crashworthiness and Occupant Protection in Transportation System, Proceedings 112th ASME Winter Annual Meeting, AMD-Vol. 126/BED-Vol. 19, 1991, pp121-154.

12. Zienkiewicz, O. C.: The Finite Element Method, McGraw-Hill Book Company (UK) Limited, 1977.

Use of Finite Element Analysis and Dummy Test Measurements in the Assessment of Crash Impact Traumatic Brain Injury

F. A. Bandak[1,2], R. E. Tannous[2], A. X. Zhang[3],
R. H. Eppinger[1], T. Toridis[2], and F. DiMasi[4]

[1]National Highway Traffic Safety Administration
U. S. Department of Transportation
400 Seventh Street, SW
Washington, DC 20590, USA

[2]School of Engineering and Applied Science
The George Washington University
Washington, DC

[3]Conrad Technologies Inc.
Washington, DC

[4]Volpe National Transportation Research Center
U. S. Department of Transportation
Cambridge, Mass.

SUMMARY

Three computational models were used to interpret experimental data as a first step in developing a process to predict traumatic brain injury (TBI) potential in motor vehicle crashes. The process and the prevailing conditions limiting its current viability are discussed. The first model, a two dimensional model of the miniature pig brain, was gauged against existing experimental data using a previously introduced *Cumulative Strain Damage Measure* (CSDM). Results from this model were utilized in the analysis of output from two simple three dimensional models of the human brain, one representing and adult and the other scaled in a crude attempt to simulate the six year old child brain.

The miniature pig computer model was subjected to loads identical to those used in existing brain injury experiments. The human models were loaded using measured kinematic response data from actual crash dummy tests. The dummy test data was converted to model loadings using a previously reported method and a new experimental technique for measuring the spatio-temporal distribution of pressure resulting from head impact is also introduced.

Twelve cases were analyzed using the two human finite element models. Six involved the Hybrid III dummy and six involved the six year child version of the dummy. The crash test results were evaluated on the basis of several proposed finite element based brain damage measures as well as the values of the Head Injury Criterion. Preliminary results indicate that the proposed procedure is feasible for the assessment of head injury potential pending the availability of material data and consistent load measurement processes.

1. CATEGORIZATION OF CLOSED-HEAD TBI

Injury to the head can mean damage to the scalp, skull, and/or the intracranial contents. Closed-head injury can be defined as injury where the dural membrane remains intact. Serious head injuries, as defined by their relative threat to life, are those generally associated with the brain. Injuries to the brain have, in recent times, been referred to as traumatic brain injuries distinguishing them from the designation as head injuries. A particular class of TBI consists of any type of traumatic damage affecting brain function and resulting from non-penetrating contact or non-contact mechanical head loading. Closed head TBI resulting from non-penetrating head impacts can be categorized, on a mechanical basis, as *diffuse* or *focal*. The first refers to bulk mechanical effects associated with axonal, neural, micro-vascular, and dendritic injuries. The second is of the type of injuries that occur in localized regions of the brain subjected to tensile (rupturing) or compressive (contusive) stresses. A sub-category of focal injuries resulting from bulk mechanical loading is primarily dependent on gross movements of the brain surface relative to the cranial cavity. These include subdural hematomas and brainstem injuries. A brief description of a proposed mechanical categorization of impact brain injuries will be described below.

Diffuse Brain Injury

Diffuse brain injury involves damage to the neuronal, axonal, micro-vascular, and dendritic structures. This class of injuries is usually a consequence of distributed head loading conditions that generally induce relatively low-energy damage affecting

substantial volumes as opposed to high energy damage affecting small, localized, volumes of the brain A frequently occurring result of blunt head impact is an injury to the axonal structure referred to as Diffuse Axonal Injury (DAI) [1] [2] [3]. DAI is a distribution of focal lesions in the axonal components of the neural structure and thus the term diffuse Holbourn [4] and then Ommaya and co-workers [5] [6] [7] investigated brain injury with the hypothesis that isochoric brain deformations resulting from combined rotational and translational accelerations of the head producing DAI

Although the delicate axonal structure is more vulnerable to diffuse mechanical damage than the vascular structure, there is evidence of microvascular injury also consisting of a distribution of microlesions. Maxwell and co-workers [8] showed evidence of microvascular lesions in mechanically traumatized specimens used for the study of DAI. They observed morphological changes in the microvascular structure up to several hours after the DAI inducing accelerations were applied. It is not clear whether these morphological changes are a direct result of the mechanical forces or are a physiological consequence of other resulting damage in the brain such as alteration of the endothelial membrane as has been hypothesized [8] Maxwell and co-workers suggested that the microvascular response to brain insults occurs in two ways. A relatively rapid and localized swelling disrupting the blood-brain barrier and a more diffuse disruption of the endothelial structure occurring later in the injury cycle. Blumbergs [9] indicated that diffuse microvascular ruptures can occur in the corpus callosum without the presence of axonal injury

Focal Brain Injury

Focal brain injuries result from relatively localized responses of the brain to loading. These include cranial and extracranial injuries affecting the bone and soft tissue components of the non-brain portion of the head. For instance a direct impact to the head can cause tissue damage to the scalp along with fracture damage to the skull. The type of loading determines whether the scalp-skull-dura laminate will experience 1) a depressed-type, localized shear-dominated fracture. 2) a linear-type, bending-dominated fracture, or 3) comminuted-type, large rapid stretch and shear dominated fracture Cranial vault fractures can be differentiated from fractures of the base of the skull by the types of brain injury that can result with each. In general the location and type of fracture is important mostly for its injurious effects on the brain For instance basilar skull fracture can cause direct brain stem damage and temporal skull fracture crossing the meningeal groove can cause dural vessel ruptures resulting in extradural bleeding affecting the brain in a less direct mechanical way

Bleeding that occurs between the inner surface of the skull and the outer surface of the dura mater (extradural) is referred to as epidural hematoma This injury occurs as the primary lesion in about 6% of patients with severe closed head injuries

[10] Although it is commonly associated with skull fracture, it can result from other common focal damage such as torn dural arteries or, in some cases torn venous sinuses The effect of this injury on the brain can be compared by the degree of resulting unconsciousness Unlike subdural hematoma which is almost always accompanied by immediate unconsciousness, only about one third patients with epidural hematomas experience unconsciousness, with one third experiencing no unconsciousness, and the last third mixed [11] Approximately 91% of epidural hematoma in adults and 75% in children is associated with a skull fracture [12].

Another mode of brain damage that is also related to skull deformation with or without concomitant skull fracture or hemorrhage is focal brain contusion Certain contusions result from the forces associated with direct contact between the brain and the solid and fluid material surrounding it. This injury is usually in the form of cortical bleeding reaching some depth into the brain Contusions resulting from any impact direction but lateral have been observed to occur mostly in the frontal and temporal regions of the brain [13]. They have been postulated to be a consequence of the anatomical characteristics associated with the sphenoidal region affecting the frontotemporal region of the brain Lowenhielm [14] hypothesized that coronal accelerations can cause a type of lesion termed by Lindenberg and Freytag [15] as gliding contusions They observed these lesions to be associated with subcortical traumatic hemorrhages in the upper region of the brain near the parasagittal sinus Lowenhielm [14] reported that this type of lesion occurs in 25% of motor vehicle crash fatalities

Relative Motion Brain Injury

A class of focal brain injuries results from somewhat tangential motion of the brain surface relative to the interior surface of the cranium This motion can produce some of the focal contusions discussed above or can result in blood vessel rupture A common vascular rupture injury is associated with the parasagittal bridging veins These are a prominent set of vessels that cross the subdural region somewhat radially at several points on either side of the parasagittal sinus. Along with the CSF layer and the trabecula connecting the arachnoid with the dura, the bridging veins affect brain movement They experience a tethering force when the brain moves tangentially relative to the dura along a direction vector in the mid-sagittal plane This motion has been postulated to be mechanically sufficient to cause bridging vein ruptures [14] that result in subdural hematoma Subdural is the most frequent type of hematoma occurring as the primary lesion in approximately 24% of patients with severe closed head injuries [10]. Intracerebral hematomas typically located in the frontal and temporal lobes can also occur as a result of brain motion and are primary lesion in 10% of the severe closed head injuries [10]

2. HEAD INJURY CRITERION

The term injury criterion is commonly used to refer to a quantity that relates injury potential with an associated mechanical action. Usually, such criteria are statistically based because of their intended range of application and the great variability in biological systems. The current criterion for the assessment of potential for motor vehicle head injury is the Head Injury Criterion (HIC) as specified in US Federal Motor Vehicle Safety Standard 208. This criterion has a historical basis in the work of Gadd [16] who used the Wayne State Tolerance Curve (WSTC) to develop what eventually became known as the Gadd severity index GSI [17]. The WSTC is based on the resultant translational head acceleration. It evolved from the early work of Gurdjian and co-workers [18] who used the clinically observed prevalence of concomitant concussions in skull fracture cases (80% of all concussion cases also had linear skull fractures [19] to relate cadaver impacts to brain injury. Gurdjian and co-workers concluded that by measuring the tolerance of the skull to fracture loads one is effectively inferring the tolerance to brain injury. Lissner and co-workers [20] later developed a relationship between the magnitude of the translational anterior-posterior acceleration and the load duration that became known as the WSTC. The current HIC is based on the amplitude and duration characteristics of the resultant translational head accelerations.

3. PROPOSED MECHANICAL MEASURES OF TBI

Cumulative Strain Damage Measure

A finite element based mechanical measure to evaluate strain-related brain damage has been proposed [22] as a tool for the evaluation of a class of deformation-related brain injuries resulting from head impacts. It is postulated that DAI is associated with the cumulative volume of the brain matter experiencing tensile strains over a critical level sometime during the impact. The severity of strain related injury may be associated with the magnitude, and its extent with the volume of strain exceeding a particular level. The proposed measure, referred to as the *Cumulative Strain Damage Measure* (CSDM), monitors the accumulation of strain damage by calculating the volume fractions in a model of the brain experiencing strain levels greater than various specified levels under dynamic loading. The measure, as implemented in finite element routines, is based on the maximum principal strain calculated from a strain tensor obtained by integration of the rate of deformation tensor effectively giving the natural strain. At each time increment the volume of all the elements that have experienced a strain above prescribed threshold values is calculated based on the measure described above. The affected volume monotonically increases in time during conditions where regions of the brain are undergoing tensile stretching deformations. It remains constant (does not decrease) for all other deformation conditions such as those occurring during compression or unloading. The cumulative nature of this measure means that the end state of a calculation represents the strain damage that may be related to DAI associated with a particular loading regime up to that point in time. The final state CSDM can be related to DAI strain damage occurring during the whole event. The spatial distribution of affected volumes of brain matter exceeding various levels of strain can also be examined. The spatial distributions can be viewed sequentially, versus time, to evaluate nucleation and growth of damage sites aiding in the determination of the regions of the brain that may be more vulnerable than others under particular loading conditions. Additionally, the time history evolution of damage in the brain as a whole can be monitored for various choices of strain levels. The CSDM has been evaluated using an approximate finite element model of the human brain model and a model of the miniature pig devised to simulate DAI experiments. Results from these applications will be discussed in a later section.

Dilatation Damage Measure

A second measure in preliminary development is proposed for the evaluation of brain injury that is postulated to occur as a result of dilatational stress states. It is referred to as the *Dilatation Damage Brain Measure* (DDM). It involves localized regions where stress states in the brain result in mechanical pressures exceeding negative values large enough to produce tissue damage. The measure calculates the volume fraction of the brain material reaching prescribed threshold pressure values. Dilatational stress modes are proposed to be involved in the damage processes in the biphasic brain with fluid (cerebrospinal, blood, and water) permeating nearly all of its solid soft tissue. Although no direct observational evidence has been reported on the relationship between pressure mechanisms and the production of diffuse axonal, vascular, dendritic, or other soft tissue injury, we propose that, on a mechanics basis, there are significant indications that such mechanisms can cause these injuries

Relative Motion Damage Measure

This measure is proposed for the assessment of injury related to brain movements relative to the interior surface of the cranium. It is referred to as the *Relative Motion Brain Measure* (RMDM). The focus of this measure is the assessment of the tangential movement of the brain surface resulting from combined rotational and translational accelerations of the head. This motion results in subdural hematomas associated with ruptures of the parasagittal bridging veins. The measure involves the calculation and interpretation of tangential brain movement without the explicit modelling of the vascular structure tethered to the interior of the cranium. It has been suggested that the mechanisms responsible for subdural hematoma involve large stretch ruptures of the bridging veins. The measure accounts for this mode of rupture while leaving open the possibility of

other micro or macro rupture modes associated with more complex vascular tethering states.

4. MEASUREMENT OF HEAD LOADING

In this section we will discuss two techniques for measuring motor vehicle crash head loading. One of these is an established technique that measures head accelerations and is used currently in crash test dummies. The second is a new, still experimental, technique for measuring the spatio-temporal pressure distribution occurring under contact head impact. The next two sections describe those two techniques and their uses for measuring head impact loading relevant to the assessment of brain injury.

Acceleration Measurements

A technique to process 9 accelerometer dummy head data was developed by Padgaonkar et al. [23]. It provides both the 3 translational and 3 rotational body fixed accelerations that define the three dimensional rigid body motion of the dummy head. The accelerometers are arranged in a 3-2-2-2 configuration where three accelerometers are at the head CG aligned along each principal body axis, and two on each principal arm, with sense axes oriented normal to the arm (FIG. 1). DiMasi [24] developed a procedure that allows these measured head accelerations to be transformed into kinematic loading inputs for finite element models. This is done by computing the generalized six degree-of-freedom angular and translational velocities, relative to inertial coordinates, occurring at the center of gravity of the rigid dummy headpart instrumented with a 3-2-2-2 accelerometer arrangement. In a non-rotating system, a simple direction cosine matrix is used to transform vector quantities from body to fixed coordinates. The transformation of vector quantities from the rotating, decelerating (non-inertial) dummy headpart requires considering changes due to both the rotating body coordinate system as well as time dependent vector variations within the body coordinate system. The transformation to fixed coordinates can be expressed as the summed transformation of the vector time-rate of change in the body coordinate system plus the cross product of the body angular velocity vector and the vector quantity in the body coordinate system. If changes in orientation between body and fixed coordinates are limited to very small incremental angular displacements (e.g., 1 milliradian or less), then both components may be related to the fixed coordinate system using a common transformation matrix. The orientation of the body coordinate system is computed and continually updated relative to fixed coordinates based on incremental changes in the body angular velocity vector. At the end of each time step, a new transformation matrix is computed based on the previous position, along with small incremental changes in body coordinate system orientation. This data is subsequently used to update the position of the new body coordinate system and re-compute the direction cosine matrix for transforming of vector quantities

from body to fixed coordinates. A compensation algorithm, that corrects for cross products of angular velocity and centripetal accelerations, resulting from the non-centroidal locations of accelerometers at the CG and on each arm, is also implemented. Typical NHTSA crash test head acceleration data is digitized at 8,000-10,000 samples/sec assuring small incremental headpart angular displacements making this updated coordinate tracking algorithm suitable for this data. In the event the 1 milliradian limit on angular displacements is exceeded in a particular increment, the time step is sub-divided to assure a 1 milliradian maximum (vector) coordinate system angular displacement. The technique has been validated against data from several crash tests and results have been successfully compared [25] with corresponding film data. Additional data files containing related kinematic quantities in body vs fixed coordinates are also produced, and a single output file containing the three translational and three angular velocities at the headpart CG is also generated for direct use in finite element analysis. The resulting generalized six-degree-of-freedom inertial loadings reflect all dummy headpart
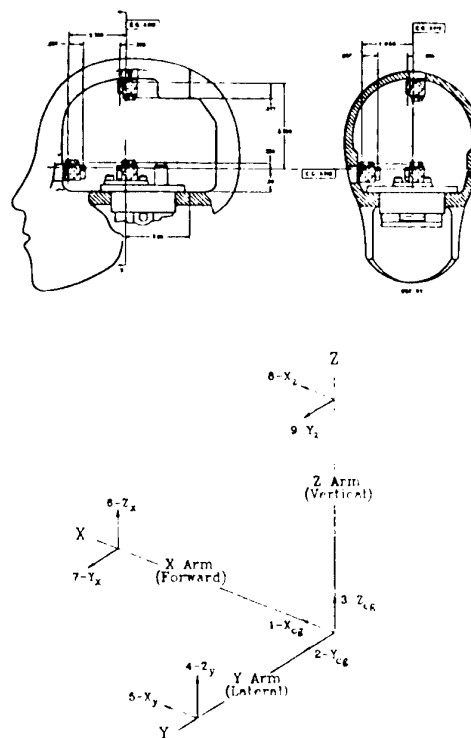

Figure 1: (a) Accelerometer Locations in Dummy Headpart 3-2-2-2 Arrangement (b) Ideal 3-2-2-2 Configuration

impacts as well as dummy neck reaction forces during the event.

Contact Pressure Measurement

The spatio-temporal distribution of the pressure resulting from head impact provides measurable parameters, essential in the assessment of experimental head impact results, as well as providing accurate loading information in computational analysis. These measurements are useful in the analysis of skull fracture but more importantly in the accurate evaluation of the local input energy affecting the brain. Several methods, using MetNet or Fuji film for example, have been used in the past to measure the contact pressure distribution resulting on the head from impact.

We investigated the spatio-temporal distribution of contact pressure using a commercially available pressure measuring device developed by TekScan, Incorporated [26]. The TekScan sensor is a thin, flexible, plastic sheet imprinted with pressure sensitive ink grid arranged in a rectangular array. The sensor is connected to an interface board in an Intel-based computer. Each pressure sensitive location is sampled in sequence by the hardware and stored for later display. While the individual pressure sensors can respond in a few microseconds, that system can only sample through the array once every 10 milliseconds. This sampling rate is inadequate for the impact duration times associated with motor vehicle crash head impacts. We developed performance specifications for a new system that can be used in the evaluation of head impacts. The new TekScan system can sample an array of pressure sensors on a 0.005 in flexible printed circuit every millisecond. The system can continuously sample up to 1000 frames per second and can measure pressures up to 1200 psi. Each sensor has a 14 by 14 grid of 0.2 in by 0.2 in sensing elements with each 14 by 14 data array constituting a data frame. Figure 2 shows the handle, the connecting cable, and the grid patterns on the two sides of the TekScan sensor.

The new TekScan system was used as part of a test apparatus for measuring the dynamic loading under the vertical drop of a sphere onto various impact partners. In addition to the spatio-temporal pressure measurement by the sensor, the force time history was measured with force ring transducer sandwiched between two 1/2 inch aluminum plates. The bottom plate was firmly fixed to prevent movement during impact and the top plate was overlaid with a neoprene sheet (with three thickness values of 0.25 in, 1.0 in, and 2.0 in) and used as the impact target. The TekScan sensor was evaluated under three different test configurations. In the first configuration, the sensor was placed directly against a rigid surface and covered with a 60 durometer neoprene sheet; in the second it is placed on top of a neoprene sheet. For these arrangements the load was delivered either by the free fall impact of a weighted sphere or through the compression of the spherical cap by the compression tester. In the third configuration the load was transferred from the compression

tester through powder in a cylinder to the sensor. The powder provides a means to more uniformly distribute the pressure over the covered area. The setup for the static and drop impact test is shown in Figure 3.

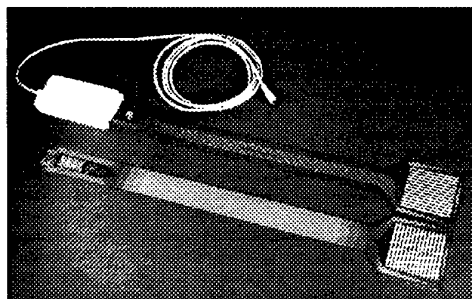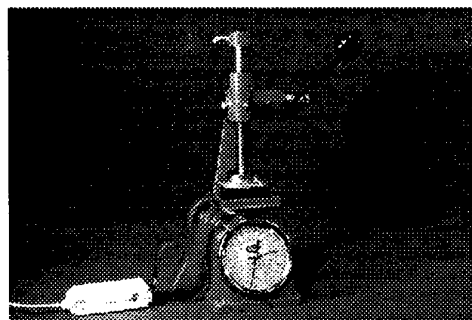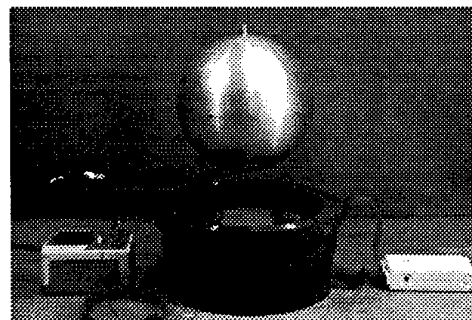Static and dynamic loading tests were conducted to assess

Figure 2: TekScan 9500 sensor: Front and back view, handle and cable

(a)

(b)

Figure 3: Apparatus for testing the modified TekScan device (a) static test (b) dynamic test

the performance of the device. The TekScan sensor had to be statically loaded several times (up to 10) before it produces a repeatable output thereafter, the total load can be reproduced within ±5%. The sensor is quite durable provided that it is not stretched beyond its material strength. If the sensor receives too much lateral stress, it will wrinkle and the individual pressure sensors will fail. Such stretching can occur when the material is placed on a highly compliant surface or when it is covered with a compliant material that is undergoing large lateral stretching. Static and dynamic calibrations differ, perhaps because of a rate dependence of the sensor material. Once calibrated for a particular dynamic condition, there is little variation between sensors and impact strength. The total loading variation with time found by integrating the individual sensors agrees well with the force transducer output, as long as the impact has a duration of several milliseconds. If the impact is over a shorter period of time, the finite sampling rate of the device cannot produce a correct instantaneous distribution of pressure. When calibrated dynamically and corrected for finite sampling rates, the TekScan instrument can be used to measure the load distribution under limited impact conditions including some nonspherical impact partners.

We have been able to use the TekScan system, modified to be suitable for head impact applications, in experimental head impact studies to support finite element model development

5. FINITE ELEMENT ANALYSIS

The application of finite element brain models to the assessment of injury under measured crash test loadings requires a relationship between calculated strain levels and the occurrence of observed injuries. This can be accomplished through the use of the proposed mechanical measures
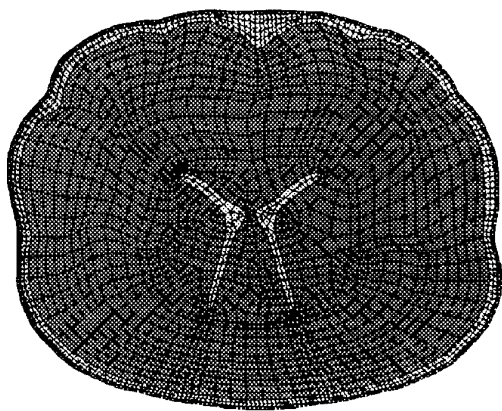

Figure 4: Two dimensional finite element model of the mid-coronal slice of the miniature pig brain

A two dimensional finite element model of the midcoronal plane of the miniature pig was developed and calibrated to existing experimental data. Figure 4 shows the model including the dura, arachnoidal membrane, subarachnoidal cerebrospinal fluid, the ventricles, and the sulcal surfaces separating the cortical gyri. The model does not include explicit modelling of the white versus gray matter in the brain. The skull was taken to be rigid since it has been reported to experience nearly no deformations during purely rotational
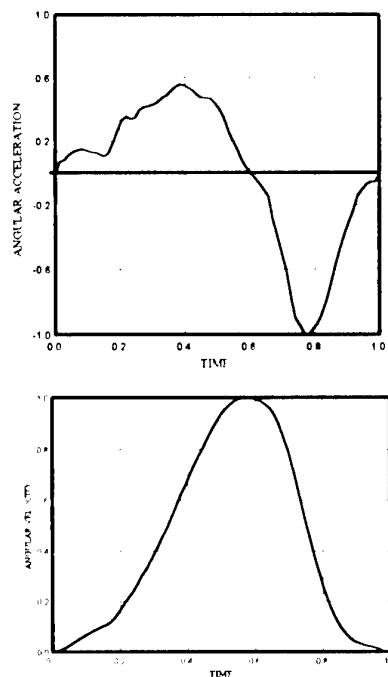

Figure 5: Typical shapes for rotational a) acceleration and b) velocity waveforms replicating experiment.

motion. The model loading was derived from measured angular acceleration pulses applied in the experiments. These acceleration-time histories were applied to the model rigid skull in the form of rotational velocity-time history. Typical acceleration and velocity pulses are shown in figure 5. The CSDM was calculated for each experimental condition calibrating it against that set experimental injury data. This empirically derived relationship between the CSDM and injury data is then used in simulations using finite element models [27] of the human brain

Relation of Cumulative Strain Damage Measure to Experimental DAI Data

Data from experiments conducted at the University of Pennsylvania [28] were used to relate CSDM strain levels to observed occurrence of DAI. These experiments were conducted using an acceleration device that utilizes a six-inch diameter Bendix HYGE actuator designed with linkage specialized to the miniature pig head configuration. This mechanical linkage enabled the application of centroidal rotations with varying amplitudes and stroke angles. The maximum rotational acceleration, $d^2\theta_m / dt^2 = a_m / r$,and

maximum velocity, $\Delta d\theta_m / dt = (d^2\theta_m / dt^2)t_m / 2$, from experiment, were computed according to the above equations from tangential accelerations measured on the instrumented linkage. In these equations a_m is the tangential component of the acceleration vector, t_m is the duration of the rotational deceleration portion of the pulse, and r is the distance from the center of rotation to the acceleration measurement point on the linkage. The data gives approximations to the location and severity (FIG. 6) of DAI for each test case along with peaks of rotational velocity and acceleration magnitudes for a given pulse shape (FIG 5). Values for maximum rotational velocity
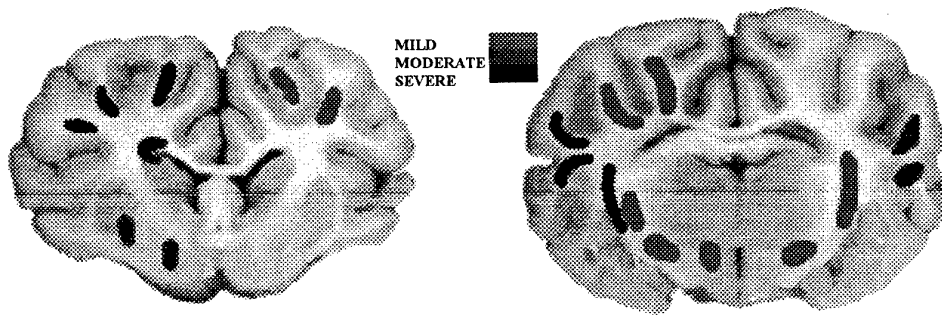

Figure 6: Schematic of typical locations of experimentally observed Diffuse Axonal Injury in the mid-coronal plane of the miniature pig brain.
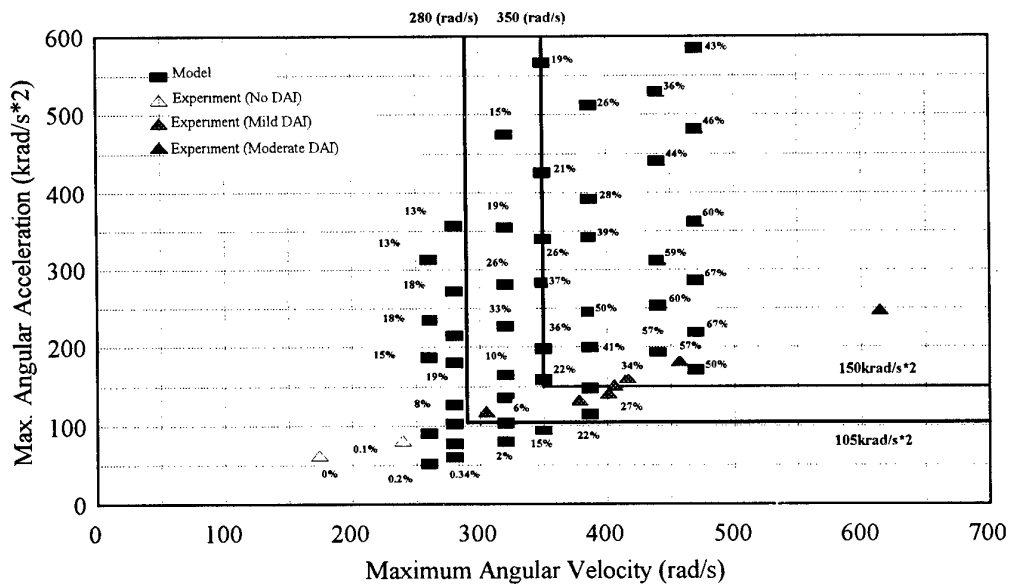

Figure 7: CSDM comparison with. maximum rotational acceleration vs. velocity threshold values from experiment.
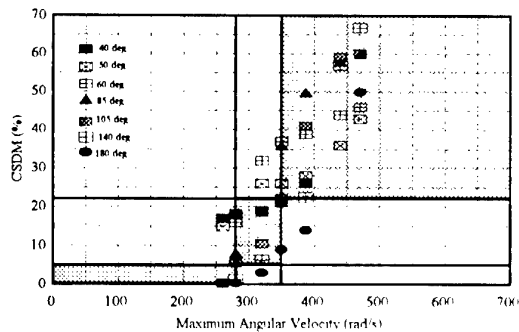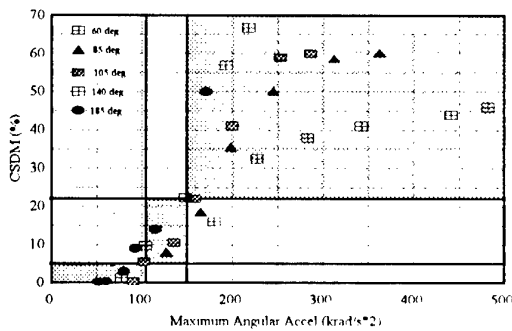
Figure 8: CSDM vs. Maximum Angular Velocity

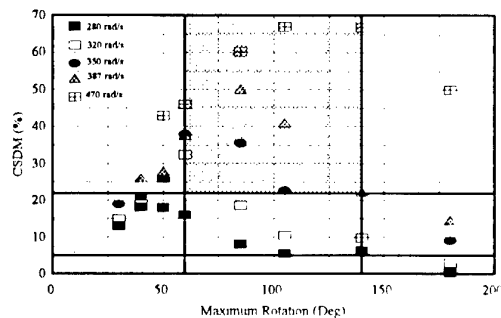*Figure 9: CSDM vs. Maximum Angular Acceleration*

Figure 10: CSDM vs. Maximum Rotational Angle

and acceleration defined for mild and moderate levels of DAI are shown in figure 7. The triangle symbols indicate some of the experimental tests that were used to define the threshold limits indicated by the solid L-shaped lines [29]. The maximum rotational velocity values shown in the figure were calculated by integrating the acceleration data and not approximated by the equation given above. The square

symbols indicate results of model calculations using the 2-D model of the midcoronal slice of the miniature pig head. These symbols, along with the associated labels, indicate the maximum rotational velocity and acceleration as well as the resulting CSDM value for the 0.15 strain threshold value. In other words, the percent values next to each square symbol indicate the volume fraction of the brain that has experienced at least 0.15 strain value. Figure 7 shows that a CSDM value of 5.5% can be chosen for this model to correspond to the threshold for mild injury giving a CSDM range of 5.5% to 22.7% with the latter value being the threshold for moderate DAI. Several checks were conducted to determine the consistency of these CSDM threshold values with the maximum velocity and acceleration levels. Figure 8 shows the CSDM vs maximum angular velocity plotted with the threshold values (dark lines) for each of those variables. The figure also shows that for the broad range of stroke angles and maximum velocities, the CSDM threshold levels are consistent with the maximum velocity thresholds. Similarly in figure 9, the CSDM threshold levels are consistent with the maximum rotational acceleration thresholds.

The implications of this consistency with observed DAI under the prescribed maximum rotational velocity and acceleration thresholds are several. The first is that once the CSDM relation to observed values is firmly established, a brain model of any shape (corresponding to a particular species) can be used to correlate with DAI for that shape. In other words shape scaling is not needed to assess the occurrence of DAI across species. Second, mass scaling is also not required enabling the CSDM to be used for any size brain including the various human sizes for females, children, etc. Third, cross-species data can, with some limitations, be utilized by using the associated material properties. Forth, the CSDM can be used to design further experiments by narrowing the kinematic range as shown in figure 10 for the case of the miniature pig. The figure shows the CSDM vs. maximum stroke angle plotted with the physiological limits of 60° to 140° for the miniature pig. Note that for the particular pulse shape used, the maximum CSDM occurs at 60° for the maximum rotational velocity of 320 rad/sec, 70° for 350 rad/sec, 85° for 387 rad/sec and 105° for 470 rad/sec.

ADULT AND CHILD HEAD MODEL LOADING FROM CRASH DUMMY DATA

Several crash tests from the National Highway Traffic Safety data base were used in this study. The cases spanned a variety of crash conditions with a range of HIC values (shown in Table 1). Six cases involved 50th percentile Hybrid III male dummy head accelerations and six involved the head accelerations on a six year old child Hybrid III dummy subjected to out of position airbag loadings in the baseline and downloaded conditions. Each case was compared with film data to obtain qualitative verification of the head kinematics.

TABLE 1

(a)

Test Data and HIC Values for Adult HIII Dummy Tests (1-6) and Six Year Old Child Dummy Tests (P1-x and P2-x)

Test Number	Crash Direction	Δv (mph)	HIC	t₁	t₂	Max. Rotational Acceleration (Krad/s^2)	Max. Rotational Velocity (rad/s)
1	45°	26	2268	60.75	64.38	23700	64.0
2	0°	20.5	545	56.38	65.00	9980	54.5
3	270°	15	170	62.25	70.63	5470	34.2
4	0°	42	1206	69.50	105.50	6090	57.9
5	30°	70	618	59.88	87.84	2860	34.0
6	180°	51	569	72.00	90.08	7050	46.3
P1-B			1051	10.48	53.44	22.6	61.3
P1-30			245	13.75	44.15	10.5	38.1
P1-60			24	19.1	35.7	4.8	20.5
P2-B			2331	7.6	56.45	29.3	45.0
P2-30			301	11.3	21.25	7.0	50.8
P2-60			65	15.75	27.05	3.4	34.1

P1 - Air Bag Position 1, P2 - Air Bag Position 2, B - Baseline Airbag, 30 - 30% De-Powered Airbag, 60 - 60 % De-Powered Air Bag

This procedure cannot be used for complete validation since the photographic setup was not designed for this purpose.

Description of Crash Tests Involving Adult Dummies

The cross section of crash tests selected includes a wide range of impact and occupant restraint conditions and provides a representative sample of fleet-wide accident conditions. Impact conditions include side, rear, full frontal and frontal oblique impacts, with initial velocity conditions ranging from zero (standing) to high speed vehicle to vehicle impacts. Data is included from full scale vehicle, vehicle to moving deformable barrier and laboratory sled tests. Restraint conditions range from unrestrained to airbag with 3 point belt for anthropometric dummies located at either the driver or passenger location. The range of HIC values resulting from the six tests are given in Table 1 below. Data preparation for selected tests included assessing the quality of each data channel, adjusting for signal bias and/or polarity if required, time shifting the data to the beginning of the impact event, and truncating the data after peak accelerations and major kinematic motions had subsided. The data was also filtered at 500 Hz. The kinematics from analysis were entirely consistent with all aspects of the test scenario and compared very well with available film data. A brief summary of each test follows:

Test 1 Oblique Impact with Roof Header. A 1981 Chevrolet Citation body mounted to a sled at a 45° angle to produce contact between the A-pillar and the left side of the dummy head. The sled is accelerated into the dummy producing a velocity change of 40.7 K/H (26 mph). The objective of the test was to compare full dummy response with component test data. An unrestrained 50th percentile male Hybrid III dummy is located in the driver position.

Test 2 Frontal Impact with top of Roof Header. Sled test using a 1984 Ford Tempo sedan body, with the objective of comparing head impact responses using production trim vs. special foam padding. An unrestrained 50th percentile Hybrid III dummy is positioned in the right front passenger seat and the sled buck is accelerated into the dummy causing the headpart to contact the roof header and windshield. Impact speed or this test is 33 K/H (about 20.5 mph), producing principal angular kinematics about the lateral axis.

Test 3 Side Impact, Vehicle Standing. A sled test using a 1984 Ford Tempo sedan body for the purpose of evaluating head impact with the roof side header, and to compare head impact responses using production trim vs special foam padding. An unrestrained 50th percentile Hybrid III dummy is positioned in the right front passenger seat and the sled buck is accelerated into the dummy causing the headpart to contact the roof side header. The impact velocity for this test is 24.4 K/H (about 15 mph) and produces principal angular kinematics about the headpart forward (x) axis.

Test 4 Frontal impact - (Vehicle Standing). Sled test using a 1985 Ford Tempo body, with the objective of developing component test procedures for head to instrument panel impact. A 50th percentile Hybrid III dummy restrained with a 3 point belt system is located in the passenger seat and the sled buck is accelerated rearward causing the headpart to rotate down toward the instrument panel. (head contact cannot be verified for this test since there is no film data. The test report. however, indicates that no head contact occurred. consistent with resulting NAP kinematics.) Closing speed for this test was 68.24 KPH (approx 42 mph). This test results in principal angular kinematics about the lateral axis.

Test 5 Standing Vehicle to Moving Barrier Oblique Impact. Oblique impact of a standing 1995 Ford Taurus with a moving deformable barrier (MDB) at an angle of 30° where the target vehicle is struck in the left front quarter. The target vehicle is standing and the closing speed of the bullet vehicle is 113 K/H (70 mph). A 50th percentile male Hybrid III dummy, located in the driver position in the standing Taurus, is restrained with a 3 point belt and airbag which deployed properly, cushioning the impact.

Test 6 Standing Rear Impact - by Moving Barrier. A standing 1996 Suzuki Sidekick is rear-impacted by a moving deformable barrier with approximately 70% overlap between bumpers at the impact location, at a closing speed of 81.6 K/H (51 mph). A 50th percentile male Hybrid III dummy, located in the driver position in the Suzuki Sidekick, is restrained with a 3 point belt system. Although film data was unavailable for this test, the kinematic response is consistent with the above test description. Resulting angular velocities occur primarily about the headpart lateral (Y) axis.

Description of Crash Tests Involving Child Dummies

Two types of out of position test conducted by NHTSA were used in this study. The first, position 1, involves the deployment of an air bag into the thoracic region of

a six year old child dummy. The test was designed to evaluate what is taken as a worst case out of position condition where a child has voluntarily or involuntarily (i.e. due to pre-impact braking and/or impact) moved against a vehicle's frontal interior structure. The dummy is placed such that the chest is in contact with the leading edge of the dashboard/airbag structure with the rib/chest plate aligned with the center of the center of the air bag cover. Head acceleration and neck loading were measured in this test position

The second, position 2, also involves a six year old child dummy placed such that a deploying air bag makes direct contact with the head. This test was also designed to represent a worst case condition where a child slides forward is sitting forward in the seat while the upper torso jack-knifes downward into the dashboard. One major difference between the two positions is that position 1 has the spine aligned vertically while in position 2 the spine is not vertical

Six tests involving baseline, 30% downloaded, and 60% downloaded airbags for each of two positions were evaluated The tests were conducted statically using top-mounted airbags where the dummies were positioned according to the requirements of each of positions 1 and 2. Four accelerometers, mounted on the head, were used to measure planar accelerations. The coordinate system for this accelerometer array had an origin at the center of gravity of the head with the x direction horizontal and pointing anterior the y direction horizontal and pointed left, and the z direction pointing upwards. Acceleration data was filtered at 1650Hz cutoff frequency.

6. ASSESSMENT OF TBI POTENTIAL FROM CRASH DUMMY DATA

The acceleration response from the six adult and six child dummy tests described above were used as input to the finite element models to assess TBI using the proposed measures Figure 11 plots values of HIC, and CSDM in the commonly used injury space of maximum

Table 2

Injury Assessment According the Various Measures as Related to Experimental Thresholds of Figure 11.

	Adult Cases						Child Cases					
	1	2	3	4	5	6	P1-B	P1-30	P1-60	P2-B	P2-30	P2-60
HIC	+	0	0	+	0	0	+	0	0	+	0	0
CSDM	+	0	0	0	0	0	0	0	0	0	0	0
RMDM	+	0	0	0	0	0	+	0	0	+	+	0
PEAK ROT ACCEL/VEL	0	0	0	0	0	0	0	0	0	0	0	0

+ injury, 0 no injury.

P1 - Air Bag Position 1, P2 - Air Bag Position 2, B - Baseline Airbag, 30 - 30% De-Powered Airbag, 60 - 60 % De-Powered Air Bag

rotational acceleration vs. maximum rotational velocity. The injury thresholds demonstrated by the large and small quadrants (dark shaded in the figure) were obtained from Margulies et al. [30] for the 1400 gram and the 500 gram brains respectively. Table 2 summarizes the potential injury according to the various measures. HIC≥1000 is used as an indication of injury for both the adult and child cases. DAI injury threshold chosen for the CSDM from the pig model is 5.5%
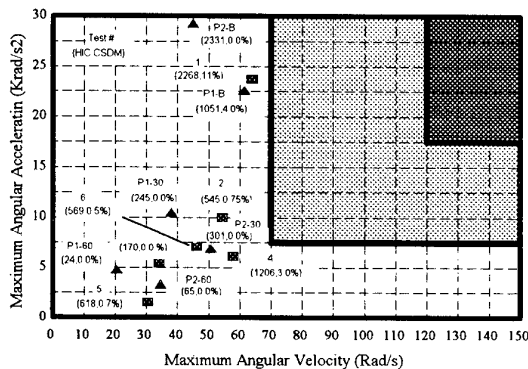

Figure 11: Assessment of TBI Potential for 6 Adult and 6 Child Hybrid III Dummy Test Cases Based on Experimental Thresholds for the Adult Brain (large quadrant) and the 6 Year Old Child Brain(Dark Shaded section of the large quadrant).

CSDM at 15% strain level for injury. Relative motion of 0.2 in. between the brain and skull is used as a threshold of bridging vein rupture injury. A maximum rotational acceleration and velocity value of 7500 rad/s² and 70 rad/s is used as an indication of injury for an adult brain whereas a value of 17500 rad/s² and 120 rad/s is used for a child brain [30]. HIC shows that four cases (case 1, 4, P1-B, and P2-B) indicated injury. The CSDM, related to DAI, also implies injury for adult case 1. This is the only case where the CSDM (value of 11%) indicated injury. The RMDM shows possible injury in adult case 1 and child cases P1-B, P2-B, and P2-30, based on a relative displacement exceeding the chosen 0.2 inch threshold. The peak rotational acceleration and velocity criteria indicate no injury in all the cases. In addition, a comparison between HIC, and RMDM suggests that the relative injury severity for the child dummy cases decreases with air bag depowering.

The Dilatation Damage Measure (DDM), discussed earlier, is related to regions of large negative pressures experienced by the brain during impulsive loadings.

Theoretical models [31, 32] have demonstrated that areas of significant underpressure are present adjacent to both coup and contre-coup zones, with the maximum severity of underpressure near the contre-coup area. Negative pressure has also been observed in transient pressure changes which occur during impact [33]. From theoretical point of view, negative pressure in the brain can cause soft tissue ruptures provided that localized volume redistribution occurs. The DDM measures the percentage of volume in the brain experiencing negative pressure -14.7psi (the boiling pressure of water). Higher volume fraction would indicate that a larger volume in the brain might experience cavitation and thus has higher possibility of lesions. This measure is still in the developmental stage, more simulations along with experiments are needed to explore its validity.

Preliminary results on the feasibility of the concept of computationally-based assessment of TBI is encouraging, even though the current process utilizes simple models of the brain. The critical injury thresholds for each measure can be further refined as more experimental data becomes available. Complex loading conditions in conjunction with well defined threshold can be used as input to FE models in the assessment of head impact injury.

8 . REFERENCES

1. Gennarelli, T.A., Thibault, L.E., Adams. J.H., Graham, D.I., Thompson, C.J., and Marcincin, R.P., *Diffuse Axonal Injury and Traumatic Coma in the Primate.* Annals of Neurology, 1982. **12**(6): p. 564-574.

2. Gennarelli, T.A., Thibault, L.E., Tomei, G., Wiser, R., Graham, D.I., and Adams, J.H., *Directional Dependence of Axonal Brain Injury due to Centroidal and Non-Centroidal Acceleration,* in *Biomechanics of Impact Injury and Tolerances of the Head-Neck Complex,* S.H. Backaitis, Editor. 1987, Society of Automotive Engineers, Inc. p. 595-599.

3. Ross, D.T., Meaney, D.F., Sabol, M.K., Smith, D.H., and Gennarelli, T.A., *Distribution of Forebrain Diffuse Axonal Injury Following Inertial Closed Head Injury in Miniature Swine.* Experimental Neurology, 1994. **126**(2): p. 291-9.

4. Holbourn, A.S., *Mechanics of Head Injuries.* Lancet, 1943. **2**: p. 438-441.

5. Ommaya, A.K., Hirsch, A.E., Flamm, E.S., and Mahone, R.H., *Cerebral concussion in the monkey: an experimental model.* Science, 1966. **153**(732): p. 211-2.

6. Ommaya, A.K., F. Faas, and P. Yarnell, *Whiplash injury and brain damage: an experimental study.* Jama, 1968. 204(4): p. 285-9.

7. Ommaya, A.K. and P. Corrao, *Pathologic Biomechanics of Central Nervous System Injury in Head impact and Whiplash Trauma,* in *Accident Pathology,* K.M. Brinkhous, Editor 1969, US Government Printing Office.

8. Maxwell, W.L., Irvine, A., Adams, J.H., Graham, D.I., and Gennarelli, T.A., *Response of cerebral microvasculature to brain injury* Journal of Pathology, 1988. 155(4): p. 327-35.

9. Blumbergs, P.C., Scott, G., Manavis, J., Wainwright H., Simpson, D.A., and McLean, A.J., *Topography of Axonal Injury by Amyloid Precursor Protein and the Sector Scoring Method in Mild and Severe Closed Head Injury,* in *Traumatic Brain Injury: Bioscience and Mechanics,* F.A. Bandak, R.H. Eppinger, and A.K. Ommaya, Editors. 1996, Mary Ann Liebert, Inc. p. 61-68.

10. Foulkes, M., H.M. Eisenberg, and J.A. Jane, *The Traumatic Coma Databank: Design Methods, and Baseline Characteristics.* Journal of Neurosurgery, 1991. 75(Suppl.): p. s8-s13.

11. Jamieson, K.G. and J.D.N. Yelland, *Extradural Hematoma: Report of 167 Cases.* Journal of Neurosurgery, 1968. 29: p. 13-23.

12. Jennett, B., G. Teasdale, and S. Galbraith. *Severe Head Injuries in Three Countries.* J. Neurol. Neurosurg. Psych., 1977. 40: p. 291-298.

13. Ommaya, A.K., *Head Injury Mechanisms and Concept of Preventive Management: A Review and Critical Synthesis,* in *Traumatic Brain Injury Bioscience and Mechanics,* F.A. Bandak, R.H. Eppinger, and A.K. Ommaya, Editors. 1996, Mary Ann Liebert, Inc.: Larchmont, NY. p. 19-38.

14. Lowenhielm, P., *Dynamic Properties of the Parasagittal Veins.* Zeischr. Rechtsmedizin. 1974. 74: p. 55-62.

15. Lindenberg, R., and Freytag, E., *A mechanism of Cerebral Contusions: A Pathalogical-Anatomic Study.* Arch. Pathology, (1960). 69: p. 440-469.

16. Gadd, C.W., *Criteria for Injury Potential,* in *Impact Acceleration Stress Symposium.* 1961, National Academy of Sciences.

17. Gadd, C.W. *Use of Weighted Impulse Criterion for Estimating Injury Hazard.* in *10th Stapp Car Crash Conference.* 1966.

18. Gurdjian, E.S., J.E. Webster, and H.R. Lissner *Observations on the Mechanism of Brain Concussion, Contusion, and Laceration.* Surg., Gynec., & Obstet., 1955. 101: p. 680-690

19. Melvin, J.W., J.W. Lighthall, and K. Ueno, *Brain Injury Biomechanics,* in *Accidental Injury: Biomechanics and Prevention,* A.M. Nahum and J.W. Melvin, Editors. 1993, Springer-Verlag: New York. p. 268-291.

20. Lissner, H.R., Lebow, M. Evans, F. G., *Experimental Studies on the Relation Between Acceleration and Intracranial Pressure Changes in Man.* Surg. Gynecol Obstet., 1960 111: p. pp 329-338.

21. Stalnaker, R.L., T.C. Low, and A.C. Lin. *Translational Injury Criteria and Its Correlation with Head Injury in the Sub-Human Primate.* in *International Conf. on Biomechanics of Impact.* 1987. Birmingham.

22. Bandak, F.A. and R.H. Eppinger *A Three-Dimensional Finite Element Analysis of the Human Brain Under Combined Rotational and Translational Accelerations.* in *38th Stapp Car Crash Conference.* 1994.

23. Padgaonkar, A.J., K.W. Kreiger, and A.I. King, *Measurement of Angular Acceleration of a Rigid Body Using Linear Accelerometers.* Journal of Applied Mechanics, 1975: p. 1-5.

24. DiMasi, F.P., *Transformation of Nine-Accelerometer Package (NAP) Data for Replicating Headpart Kinematics and Dynamic Loading,* 1995, US/DOT/Volpe Center.

25. DiMasi, F.P., R.H. Eppinger, and F.A. Bandak. *Computational Analysis of Head Impact Response under Car Crash Loadings.* in *39th Stapp Car Crash Conference* 1995: Society of Automotive Engineers, Inc

26. Bandak, F.A. *Biomechanics of Impact Traumatic Brain Injury* in *NATO Advanced Study Institute on Crashworthiness of Transportation Systems: Structural Impact and Occupant Protection.* 1997. Troia, Portugal: Kluwer.

27. Bandak, F.A., *On the Mechanics of Impact Neurotrauma: A Review and Critical Synthesis.* Journal of Neurotrauma, 1995 12(4): p. 635-649.

28. Meaney, D.F., Smith, D.H., Ross, D.T., and Gennarelli, T.A., *Diffuse Axonal Injury in the Miniature Pig: Biomechanical Development and Injury Threshold.* in *Crashworthiness and Occupant Protection in Transportation Systems, ASME.* 1993.

29. Meaney, D.F., et al., *Experimental Investigation of the Relationship between Head Kinematics and Intracranial Tissue Deformation.* ASME SAM, 1993. 24: p. 8-11.

30. Margulies, S.S. and Thibault, L.E., "*A Proposed Tolerance Criterion for Diffuse Axonal Injury in Man*", J. Biomech., **25**(8), 1992, p. 917-23.

31. Benedict, J.V., Harris, E.H., and Rosengerg, D.U., "*An Analytical Investigation of the Cavitation Hypothesis of Brain Damage*", J. Basic Engrg., (September), 1970, p. 597-603.

32. Engin, A.E. and Liu, Y.K., "*Axisymmetric Response of a Fluid-Filled Spherical Shell in Free Vibrations*", J. Biomech., **3**(1), 1970, p. 11-12.

33. Tsubokawa, T., Nakamura, S., Hayashi, N., Miyagami, M., Taguma, N., Yamada, J., Kurisaka, M., Sugawara, T., Shinozaki, H., Goto, T., Takeuchi, T., and Moriyasu, N., "*Experimental Primary Fatal Head Injury Caused by Linear Acceleration - Biomechanics and Pathogenesis*", Neurol. Med. Chir., **15**, 1975, p. 57-65.

HEAD INJURY RISK ASSESSMENTS
BASED ON 15 MS HIC AND PEAK HEAD ACCELERATION CRITERIA

H. J. Mertz, General Motors Corporation
Safety Center, MC480-111-S29
30200 Mound Rd.
Warren, MI 48090-9010 U.S.A

P. Prasad, Ford Motor Company
G. Nusholtz, Chrysler Corporation

SUMMARY

A review is given of the development of the Head Injury Risk Curve (HIRC) which is based on 15 ms HIC, and the Skull Fracture Risk Curves (SFRC) which are based on the 15 ms HIC and the Peak Head Acceleration criteria respectively. Each of the risk curves was developed by analyzing the relevant cadaver head impact data using the Mertz/Weber Method which is a simplified form of the Median Rank technique. The Mertz/Weber Method was used to estimate the injury risk to the adult driving population because the test samples of cadavers were biased with specimens having poorer bone conditioning factors than the driving population. The Mertz/Weber Method is not affected by this type of bias since the form of the distribution curve is assumed apriori.

The efficacy of the Head Injury Risk curve is demonstrated by noting that the predicted reduction in head injuries due to certification of American football helmets based on the HIRC was 78 percent compared to the actual reduction in head injury risk of 74 percent. The efficacy of the Skull Fracture Risk Curve based on 15 ms HIC is demonstrated using a finite element model of the head. There was no agreement between model results and the SFRC based on peak head acceleration since the time-dependency associated with bone failure is not addressed by the Peak Head Acceleration criterion. This limitation of the Peak Head Acceleration criterion is demonstrated by analyzing Transport Canada's 30 mph rigid barrier vehicle test results. Assuming a 5 percent risk of skull fracture as a design limit, then 20 tests would fail to meet this limit based on the 15 ms HIC criterion, but only 10 tests would fail based on the Peak Head Acceleration criterion. Further, it is noted that the proposed 80 G limit for Peak Head Acceleration is very design-restrictive since it represents a 0.1 percent risk of skull fracture. The corresponing 15 ms HIC value for this level of skull fracture risk is 100.

HEAD INJURY RISK CURVE (HIRC)

In 1985, Prasad and Mertz (1) analyzed the available biomechanical data for frontal bone impacts to heads of cadavers where values for the Head Injury Criterion, HIC, were given (2-9). They noted that no HIC value corresponded to the minimum (threshold) value required to just produce skull fracture or brain damage for the corresponding cadaver. For impacts where skull fracture or brain damage did occur, the corresponding HIC value for a given specimen, exceeded its threshold value by some unknown amounts (left censored). For impacts that did not produce damage, the corresponding HIC values were less than the specimens' threshold values by some unknown amounts (right censored). Prasad and Mertz chose to analyze the cadaver data using the Mertz/Weber method (10) which is a simplification of the Median Rank method (11-12). An important feature of the Mertz/Weber method is that the form of the threshold distribution function is assumed apriori. Further, it is assumed that the lowest HIC associated with damage (weakest known specimen) and the highest HIC associated with no damage (strongest known specimen) are good approximations for the damage thresholds of those two specimens. Consequently, only estimates of the median ranks of the weakest and strongest specimens are needed to quantify the threshold function. This method eliminates the need for the tested specimens and the adult driving population to have the same threshold distribution. Figure 1 is the Head Injury Risk Curve (HIRC) for the adult driving population proposed by Prasad and Mertz (1). This curve is also identical to their Skull Fracture Risk Curve (SFRC).

LIMITATION ON HIC DURATION

Figure 2 is a graph of the HIC durations and the corresponding average accelerations for these durations for the specimens used by Prasad and Mertz in their analysis. Also shown are lines of constant risk of head injury (constant HIC levels) obtained from Figure 1. Prasad and Mertz noted that no specimen experienced a skull fracture and/or brain damage for HIC durations greater than 13 ms, and that most of the cadavers that were damaged had HIC durations less than 10 ms. These observations are consistent with Hodgson's (13) conclusion that in order to produce skull fracture or concussion the duration of the effective part of the impact must be less than 15 ms. Based on these

observations, Prasad and Mertz concluded that the search for the maximum HIC level should be restricted to HIC durations of 15 ms or less. They pointed out that this restriction on the search for the maximum HIC value is necessary for assessing the head injury potential for lap/shoulder belted occupants who have no head contact with the vehicle interior, but have long duration, low-level head acceleration as the head whips forward. Such occupants have a low risk of brain damage and no risk of a skull fracture. However, without restricting the HIC duration, the HIC value and, consequently, the assessed risk of head injury would be unrealistically high due to the long HIC duration level. Restricting the HIC duration to 15 ms or less gives a lower HIC value and a more realistic risk estimate of head injury for this condition.

Mertz et al (14) noted that the assessment of the risk of head injury for occupants restrained by air bags also requires the HIC duration to be limited to 15 ms or less. HIC values were obtained from human volunteers who were restrained by air bags without *any* injuries. These results are depicted by the triangles within the dashed circle shown in Figure 2. The estimated risks of head injury for these volunteers (12 to 16 percent) are too high and inconsistent with the test observations of no head injury. However, if the HIC duration is limited to 15 ms or less, then lower HIC values are obtained which are associated with more realistic risk estimates of head injury (2 to 3 percent) as indicated by the solid triangles shown in Figure 2. Note if the HIC duration is limited to 10 ms or less, then the HIC values for human volunteer tests would be associated with a risk of brain injury of less than 1 percent.

Obviously, to obtain realistic estimates of the risk of head injury from the curve of Figure 1, the search for the maximum HIC value must be restricted. While Hodgson (13), Mertz and Prasad (1) and Mertz et al (14) have suggested a 15 ms search limit, based on the data given on Figure 2, a 10 ms search limit may be even more appropriate. Unfortunately, the Federal Motor Vehicle Safety Standard 208 limits the search for maximum HIC values to 36 ms or less. This results in overestimating the risk of head injury for compliance and NCAP tests of vehicles equipped with air bags.

ADDITIONAL SKULL FRACTURE DATA

Mertz et al (14) noted that a number of the cadavers in the Prasad/Mertz data set were subjected to increasing severity impacts until skull fracture occurred. These non-fracture HIC values provide additional information concerning the strength of these cadavers for higher HIC values. Also, the cadaver forehead impact data of Ono (15) and the additional tests reported by Tarriere (16) were added to the Prasad/Mertz data base. Risks of skull fracture for various HIC levels were calculated by Mertz et al (14) and the resulting normal distribution curve is shown in Figure 3.

Figure 4 shows Cartesian plots of the SFRC curves for the original data set of Prasad and Mertz (1) and the expanded data set of Mertz et al (14). The addition of non-fracture HIC levels for stronger cadavers has increased the HIC levels associated with higher risks of fracture while having a minimal effect on the fracture risks associated with low HIC values. Note that for the HIC levels less than 1200, there is no appreciable difference between the SFRC proposed by Prasad and Mertz and the revised SFRC of Mertz et al. The HIRC of Figure 1 is not changed by the analysis since no additional brain damage data were analyzed.

SKULL FRACTURE RISK CURVE BASED ON PEAK HEAD ACCELERATION

Welbourne (17) has proposed to limit peak resultant head acceleration to 80 G as a way of regulating the severity of head impacts for the Canadian Motor Vehicle Safety Standard 208 (CMVSS 208). To assess the risk of skull fracture associated with the proposed 80 G limit, Mertz et al (14) analyzed the peak resultant head acceleration data of the cadavers in their expanded data set as well as the cadaver data of Stalnaker et al (18) and Nusholtz et al (19). The resulting SFRC is shown in Figure 5. Note that the risk of skull fracture associated with the proposed 80 G limit is less than 0.1 percent.

COMPARISON OF 15 ms HIC AND PEAK HEAD ACCELERATION PREDICTIONS

Figure 6 gives comparisons of the maximum 15 ms HIC values and corresponding peak resultant head acceleration values for frontal, rigid barrier vehicle tests conducted by Transport Canada at 30 mph (17, 20). The tests involved Hybrid III dummies seated in either the driver's or right front passenger's position and restrained by either a lap/shoulder belt (122 occupants) or a lap/shoulder belt with air bag and knee restraint (13 occupants). Also plotted on the graph are dotted lines representing 5 percent risk of skull fracture based on the SFRC curves of Figure 3 (15 ms HIC = 710) and Figure 5 (peak resultant head acceleration = 180 G). Note that 20 tests failed to meet the 15 ms HIC limit of 710 while only 10 tests failed to meet the peak head acceleration limit of 180 G. On the basis of equal risk of skull fracture, the 15 ms HIC criterion is more stringent than the Peak Head Acceleration criterion because the effect of time on fracture is included in the 15 ms HIC criterion and is not included in the Peak Head Acceleration criterion. Further, it should be cautioned that the proposed 80 G limit for peak head acceleration is very design-restrictive since it represents a 0.1 percent risk of skull fracture. The corresponding 15 ms HIC value for this risk level is 100.
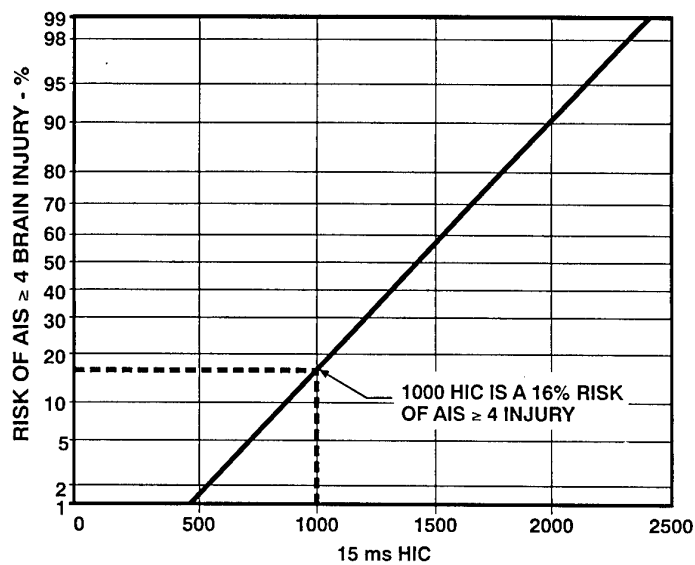
IMPORTANCE OF TIME IN PREDICTING SKULL FRACTURE

Figure 1 - Head Injury Risk Curve (HIRC) for the adult driving population as a function of 15 ms HIC developed in 1985 by Prasad and Mertz (1). This curve is identical to their skull fracture risk curve (SRFC).
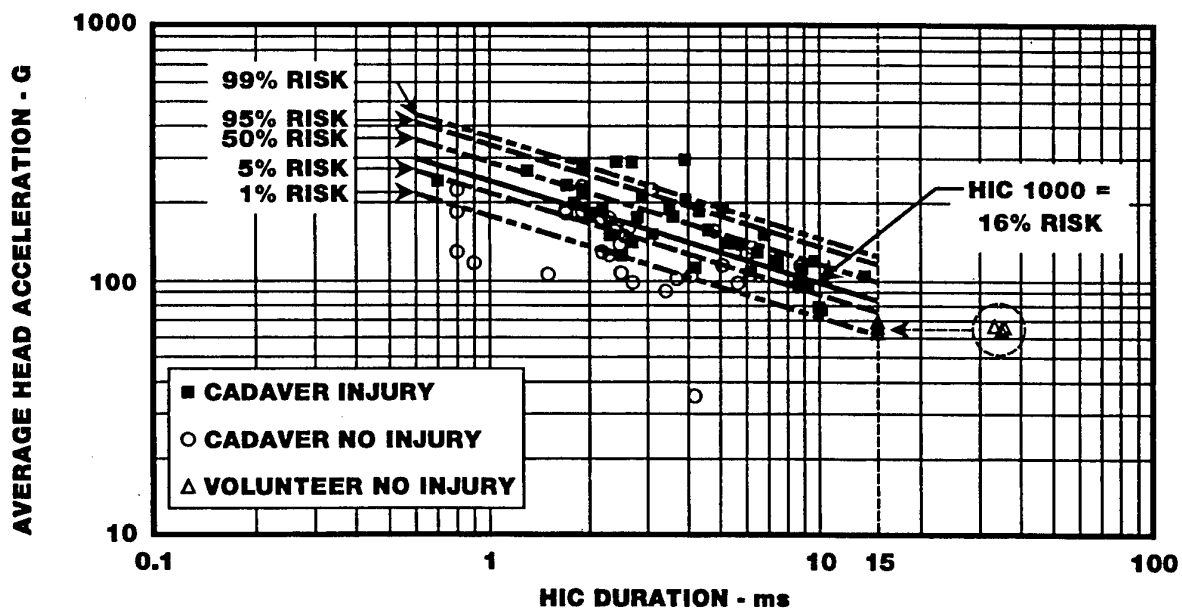

Figure 2 - Average HIC acceleration levels versus corresponding HIC durations for cadavers used by Prasad and Mertz in their 1985 analysis. Also shown are lines of constant risk of head injury obtained from Figure 1. Triangles represent data from airbag restrained human volunteers. Dashed triangulars = no restriction on HIC duration. Solid triangulars = HIC duration constrained to 15 ms or less.
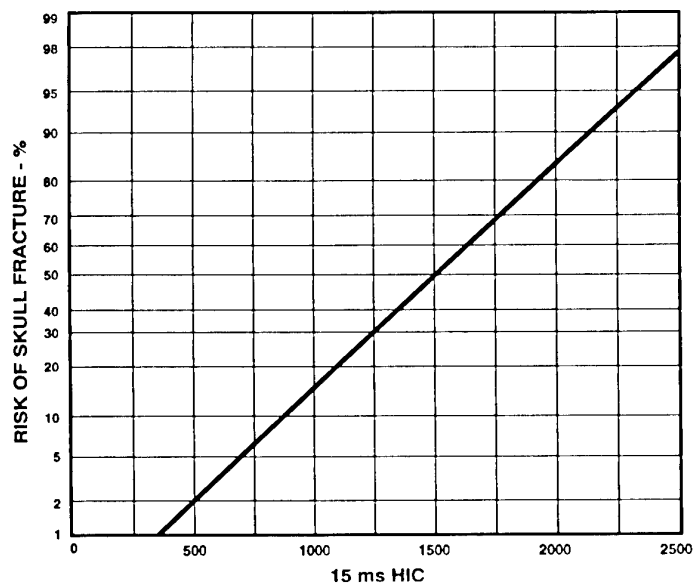
Figure 3 - Skull Fracture Risk Curve (SFRC) based on the expanded cadaver skull fracture data set of Mertz et al (14). Curve plotted on normal probability grid.
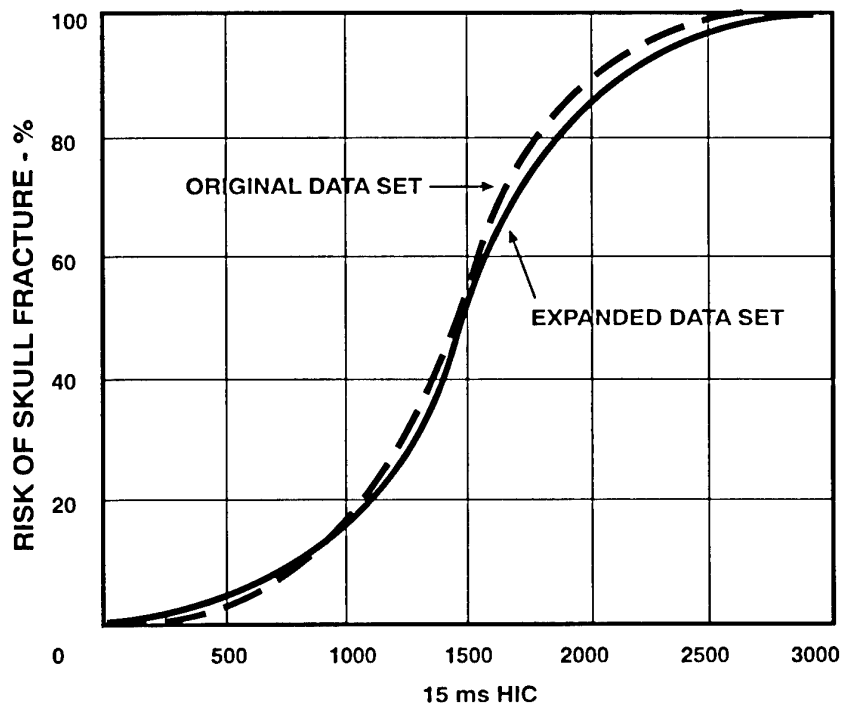

Figure 4 - Comparison of the SFRC of Prasad and Mertz (1) and the SFRC of Mertz et al (14) which is based on the expanded data set. Curves plotted on Cartesian grid.

A finite element model of the head developed by Ruan et al (21) was used to assess the effect of time dependency on skull fracture. Average values for material properties were used. Skull fracture was associated with a tensile stress of 97 MPa in the skull. The model was subjected to half sine pulses of various peaks and durations. Figure 7 is a plot of the average accelerations and corresponding pulse durations that produced 97 MPa tensile stress in the skull. This graph demonstrates the time dependency between peak head acceleration and pulse duration. Clearly, the Peak Head Acceleration criterion does not comprehend this important skull failure characteristic.

The model was further exercised using the head acceleration data from three tests conducted by Transport Canada, where hard surface head impact occurred. Table 1 summarizes the peak G levels, 15 ms HIC levels and associated risks of skull fracture, and maximum tensile stress of the skull. The maximum tensile stress range from 8.5 to 30 MPa. These values are much lower than the 97 MPa average failure stress for skull bone. They are also much less than 48 MPa which is the lowest known failure stress for skull bone, showing low probability of skull fracture. These model results are consistent with the low risk of skull fracture predicted by the SFRC of Figure 3 for the 15 ms HIC values for these tests. Note that all three impacts would be rejected by Transport Canada's 80 G limit as having an unacceptable risk of skull fracture which is totally inconsistent with the low skull stress levels. For two of the three peak head accelerations, the risks of skull fracture based on the SFRC curve of Figure 5 are low. However, the risk of skull fracture for Test No. 3 is a bit high (7.5 percent). This is because the effect of time duration of skull fracture, shown in Figure 7, is not included in the Peak Head Accleration risk curve of Figure 5.

EFFICACY OF HIRC

The efficacy of the Head Injury Risk Curve (HIRC) of Prasad and Mertz shown in Figure 1 was demonstrated by Mertz et al (14) by comparing predictions made for head injury reductions due to the introduction of air bags and due to improvements in American football helmets to reductions that actually occurred.

AUTOMOTIVE RESTRAINT SYSTEMS—Mertz and Irwin (22) analyzed the brain injury risk associated with frontal crash tests conducted by Transport Canada and the National Highway Traffic Safety Administration. Table 2 is a summary of the results for both the driver and right front passenger for the 30 mph full frontal compliance tests and for the 35 mph NCAP tests. Most of the tests were conducted with the occupant wearing a 3-point belt system without air bags. Consequently, the risk of head injury is quite low for both the driver and passenger for the compliance test at 30 mph. However, the risk is substantially greater in the 35 mph NCAP test since head impacts to the steering wheel and/or header and/or instrument panel are more severe due to the increase in collision severity. Twenty-seven percent of the drivers and twenty-one percent of the right front passengers had 15 ms HIC values that exceeded 1000, which corresponds to a head injury risk of 16 percent or greater. For comparison, there were 22 occupants restrained by a 3-point belt plus an air bag. The 15 ms HIC values for these occupants were all less than 710, which corresponds to a head injury risk of less than 5 percent. While the reduction of significant head injury due to the introduction of the air bag has not yet been quantified, qualitatively there has been a substantial reduction which is consistent with the prediction from these test results.

HELMET PROTECTION IN FOOTBALL—The National Operating Committee on Standards for Athletic Equipment (NOCSAE) standard was published in 1973, and by 1977 a significant downward trend in fatal head injuries was observed. Analysis of field data has been reported by Hodgson in 1980 (23) and 1985 (24). Before voluntary adoption of NOCSAE standards by helmet manufacturers, fatal head injuries in junior and high school football averaged 1.51 per 100,000 players. Between 1981 to 1985 the fatal head injury rates averaged approximately 0.3 per 100,000, showing a reduction of nearly 74 percent from the pre-NOCSAE period. Although tackling rule changes were also adopted in the same time frame, it is hypothesized that the head injury reductions were mainly due to changes in helmet design and improved reconditioning practices and not due to reduction in head impacts. This hypothesis is supported by the data (23) that indicate that the incidence of neck injuries increased by 26 percent, showing continued involvement of the head despite rule changes.

The performance of 849 helmets in the NOCSAE tests before reconditioning to the standard has been reported by Hodgson in 1985 (24). The data show that 84 percent of the helmets tested exceeded the 1450 Severity Index (SI) limit in the NOCSAE test. Hodgson further reported that the 15 ms HIC values in the NOCSAE tests are approximately 85 percent of the recorded SI values. For the purpose of Head Injury Risk analysis, Mertz et al (14), converted the SI values to 15 ms HIC values and determined the head injury risk for each helmet using the HIRC curve of Figure (1). They estimated the risk of head injury to the total population wearing non-certified helmets to be 55.2 percent for the impact level of the NOCSAE test (1525 mm drop height).

For certified helmets (average 15 ms HIC of 902), they estimated the risk to the population to be 12 percent. Hence, the *predicted reduction* in head injuries after certification is (1-12/55.2) 100 = 78 percent. The *actual reduction* in head injury risk due to helmet certification was 74 percent. The expected results when compared to the real-world experience are quite close, 78 percent
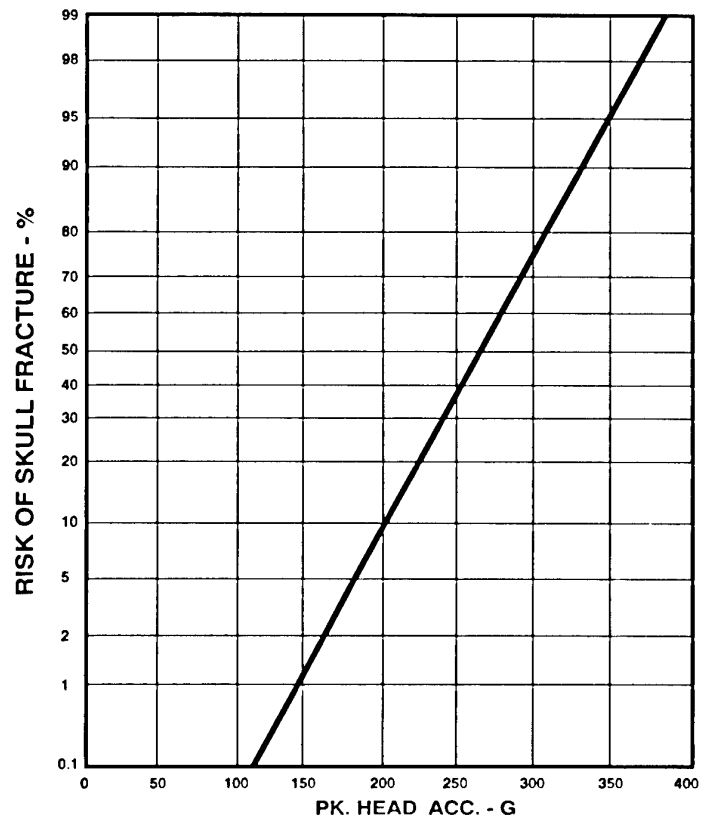
Figure 5 - Skull fracture risk curve (SFRC) for Peak Head Acceleration criterion (14). Curve plotted on normal probability grid.
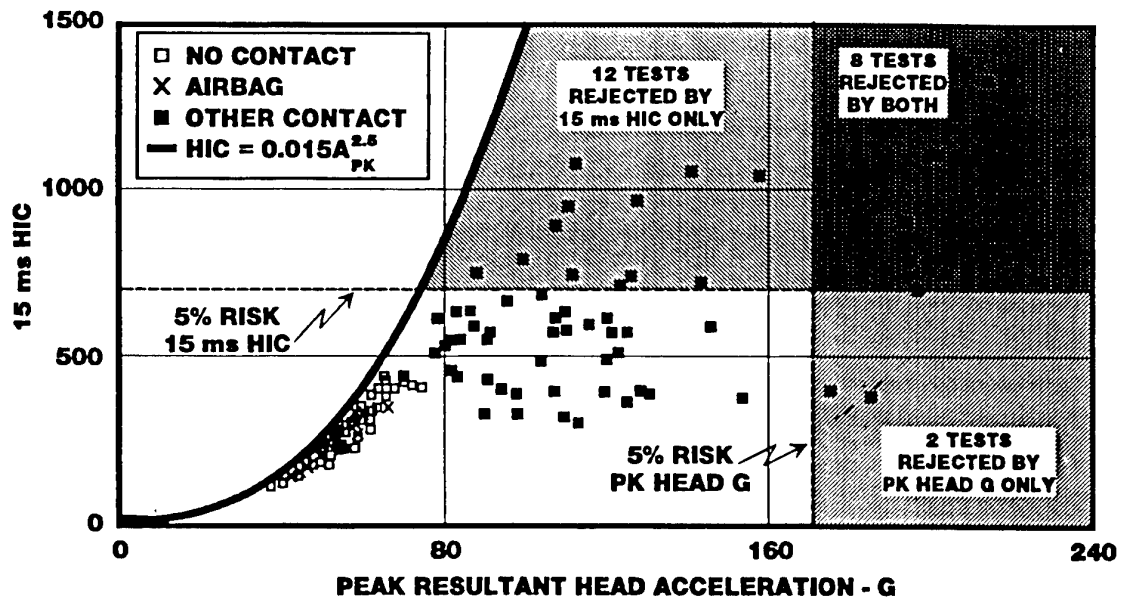

Figure 6 - Transport Canada's test results for 30 mph, full-frontal, rigid barrier vehicle impacts assessed relative to 5% risk of skull fracture based on 15 ms HIC and Peak Head Acceleration criteria.

Table 1- Summary of peak head accelerations, 15 ms HIC, maximum skull tensile stress and risk of accelerations skull fracture obtained from Ruan (21) head model subjected to head contact from Transport Canada tests.

Test	Skull Tensile	Peak Head Acc.		15 ms HIC	
No.	Stress MPa	Acc. (G)	Frac. Risk (%)	HIC	Frac. Risk (%)
1	9.5	133	0.3	411	1.2
2	8.5	153	1.1	384	1.1
3	30	194	7.5	396	1.2

Table 2 - Summary of life-threatening brain injury risks for 30 and 35 mph full-frontal, rigid barrier tests (22).

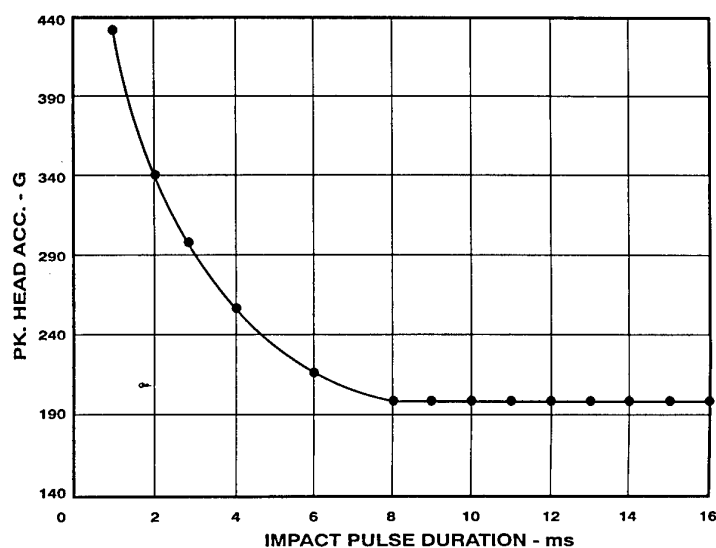| Test Condition	DRIVER		PASSENGER	
	Percent With Risk < 5% (15 ms HIC < 710)	Percent With Risk > 16% (15 ms HIC > 1000)	Percent With Risk < 5% (15 ms HIC < 710)	Percent With Risk > 16% (15 ms HIC > 1000)
30 mph	(95/97 =) 98%	(2/97 =) 2%	(96/98 =) 98%	(2/98 =) 2%
35 mph	(172/301 =) 57%	(80/301 =) 27%	(200/296 =) 68%	(61/296 =) 21%

Figure 7 - Peak head acceleration vs. pulse duration for half sine wave shaped impacts that produced 97 MPa stress in FE head model.

compared to 74 percent, showing the efficacy of the HIRC of Figure 1 to predict head injury reduction.

CONCLUSIONS

No change was made to the Head Injury Risk Curve (HIRC) proposed by Prasad and Mertz (1) because no additional brain damage data from cadaver impacts were analyzed. However, the efficacy of the HIRC was demonstrated by comparing its predictions to head injury risk reduction due to installation of air bags and due to reconditioning of football helmets.

The cadaver skull fracture data of Prasad and Mertz were expanded by including non-fracture 15 ms HIC values for cadavers that were exposed to repeated impacts until failure occurred. Cadaver test results of Ono and Tarriere were also included. These data increased the information about the strength of the stronger cadavers and substantially reduced the skewness of the data set. A revised SFRC was developed and is shown in Figure 3. The additional data for the stronger cadavers has increased the 15 ms HIC levels for higher risks while having minimal effect on risks for low 15 ms HIC values, Figure 4.

The efficacy of the revised SFRC based on 15 ms HIC (Figure 3) was demonstrated by using a finite model of the head (Table 1). This head model also demonstrated the need to include time-dependency in the skull fracture criterion, Figure 7.

The peak head acceleration cadaver data of Stalnaker (18) and Nusholtz (19) were added to the expanded cadaver skull fracture data. These were analyzed to determine the relationship between peak resultant head acceleration and the risk of skull fracture, Figure 5. The inability to predict maximum skull stress based on peak head acceleration was demonstrated using a finite model of the head, Figure 7.

On the basis of equal skull fracture risk, the 15 ms HIC criterion is more discerning than the Peak Head Accleration criterion since it is time dependent. For example, a 5 percent risk of skull fracture corresponds to a 15 ms HIC of 710 and a peak resultant head acceleration of 180 G. If these levels are assumed to be design limits, then according to the results of Figure 6 twenty of the Transport Canada 30 mph rigid barrier vehicle tests would be above the 15 ms HIC limit of 710 while only ten tests would be above the peak head acceleration limit of 180 G. Further, it should be cautioned that the proposed 80 G limit for peak head acceleration is very design-restrictive since it represents a 0.1 percent risk of skull fracture. The corresponding 15 ms HIC value for this risk level is 100.

REFERENCES

1. Prasad, P. and Mertz, H. J., "The Position of the United States Delegates to the ISO Working Group 6 on the Use of HIC in the Automotive Environment", SAE 85 1246, 1985.

2. SAE Information Report, "Human Tolerance to Impact Conditions as Related to Motor Vehicle Design", SAE J885, July 1986, Society of Automotive Engineers, Warrendale, Pennsylvania, July 1986.

3. Hodgson, V. R. and Thomas, L. M., "Breaking Strength of the Human Skull Versus Impact Surface Curvature", DOT-HS-146-2-230, Wayne State University, 1977.

4. Hodgson, V. R., Thomas, L. M. and Brinn, J., "Concussion Levels Determined by HPR Windshield Impacts", SAE 730970, 17th Stapp Car Crash Conference, 1973.

5. Got, C., Patel, A., Fayan, A., Tarriere, C. and Walfisch, G., "Results of Experimental Head Impacts on Cadavers: The Various Data Obtained and Their Relations to Some Measured Physical Parameters", SAE 780887, 22nd Stapp Car Crash Conference, 1978.

6. Tarriere, C., Walfisch, G., Fayon, A., Got, C., Guillon, F., Fatel, A. and Hureau, J., "Acceleration, Jerk and Neck Flexion Angle: Their Respective Influences on the Occurrence of Brain Injury", ISO/TC22/SC12/WG6 Document N 118, 1982.

7. Got, C., Guillon, F., Patel, A., Mack, P., Brun-Cassan, F., Fayon, A., Tarriere, C. and Hureau, J., "Morphological and Biomechanical Study of 146 Human Skulls Used in Experimental Impacts in Relation With the Observed Injuries", SAE 831619, 27th Stapp Car Crash Conference, 1983.

8. Nahum, A. M. and Smith, R. W., "An Experimental Model for Closed Head Impact Injury", SAE 760825, 20th Stapp Car Crash Conference, 1976.

9. Nahum, A. M., Smith, R. W. and Ward, C. C., "Intracranial Pressure Dynamics During Head Impact", SAE 770922, 21st Stapp Car Crash Conference, 1977.

10. Mertz, H. J. and Weber, D. A., "Interpretations of the Impact Responses of a 3-Year Old Child Dummy Relative to Child Injury Potential", SAE 826048, SP-736 Automatic Occupant Protection Systems, February 1988.

11. Johnson, L. G., "The Median Ranks of Sample Value in Their Population With Application to Certain Fatigue Studies", Ind. Math., Volume 2, 1951.

12. Gibson, C. and Sheth, N. J., *"Statistical Design and Analysis of Engineering Experiments"*, McGraw-Hill, 1973.

13. Hodgson, V. R. and Thomas, L. M., "Effect of Long-Duration Impact on Head", SAE 720956, 16th Stapp Car Crash Conference, November 1972.

14. Mertz, H. J., Prasad, P. and Nusholtz, G., "Head Injury Risk Assessment for Forehead Impacts", SAE 960099, February 1996.

15. Ono's Data Reference, Personal Communication, from Mr. Stan Backaitis, NHTSA.

16. Tarriere, C., "Relationship Between Experimental Measuring Techniques and Real World Injuries in Head Injury Mechanisms", Symposium Report, September 30, 1987, New Orleans, Louisiana, USA, sponsored by AAAM and Volvo Car Corporation.

17. Welbourne, E. R., "Use of the Head Injury Criterion as a Measure of Vehicle Occupant Protection Performance", *Proceedings of 1994 Joint Conference of AAAM and IRCOBI*, September 1994.

18. Stalnaker, R. L., Melvin, J. W., Nusholtz, G. S., Alem, N. K. and Benson, J. B., "Head Impact Response", 21st Stapp Car Crash Conference, SAE 770921, October 1977.

19. Nusholtz, G. S., Lux, P., Kalker, P. and Janicki, K. A., "Head Impact Response—Skull Deformation and Angular Accelerations", 28th Stapp Car Crash Conference, SAE 841657, November 1984.

20. Gardner, B. and St. Laurant, A., "Proposed Requirement for Protection of Front Seat Occupants in Frontal Impact", Transport Canada, October 21, 1992.

21. Ruan, J. S., Khalil, T. B. and King, A. I., "Finite Element Modeling of Direct Head Impact", SAE 933114, 37th Stapp Car Crash Conference, 1993.

22. Mertz, H. J. and Irwin, A. L., "Brain Injury Risk Assessment of Frontal Crash Test Results", SAE 941056, SP-1045 Occupant Containment and Methods of Assessing Occupant Protection in the Crash Environment, March 1994.

23. Hodgson, V. R., "Reducing Serious Injury in Sports", *Intrascholastic Athletic Association*, Volume 7, No. 2, 1980.

24. Hodgson, V. R. and Thomas, L. M., "Utility of Head Injury Criteria in Injury Reduction in Head Injury Prevention: Past and Present Research", Wayne State University, Department of Neurosurgery, December 1985.

Complementary role of Functional Brain Imaging and Multi-Modality Bedside Monitoring for Acute Brain Injury - Pathophysiology and Surrogate End Points.

John D. Pickard [1,2] Peter J. Kirkpatrick [1,2] Marek Czosnyka [1,2] David Menon [1,3]
Parvan Minhas [1,2] Peter Smielewski [1,2] John Clark [1] Nick Herrod [1] Adrian Carpenter [1]
Stephen Downey [1] Iona Kendall [1]
Wolfson Brain Imaging Centre, [1] Academic Neurosurgical Unit, [2] Academic Department of Anaesthesia, [3]
University of Cambridge, Box 167, Addenbrooke's Hospital, Cambridge,
CB2 2QQ, UK. Telephone : 01223 336946. Fax : 01223 216926.
E-Mail : jj229@medschl.cam.ac.uk

Summary

This paper reviews the advances in management of non missile head injury over the past 30 years, and the factors known to affect outcome. It has proven difficult to exploit recent advances in the development of novel neuroprotective agents in patients with head injury and the reasons are explored together with the emerging role of multi-modality bedside monitoring and functional brain imaging (Positron Emission Tomography and Magnetic Resonance) in defining more homogeneous sub-groups of patients for more focussed trials of such novel agents.

Glutamate (NMDA) receptor antagonists and calcium antagonists such as Nimodipine reduce the size of a standard cerebral infarct in various species. However, large scale (Phase III) clinical trials of such novel neuroprotective agents have proven disappointing in head injury in contrast to the more straightforward homogeneous condition of aneurysmal subarachnoid haemorrhage. The search is on for surrogate end points which can be used to define more homogeneous sub-groups of patients with common therapeutic targets to give an early indication of efficacy and side effects before embarking on more expensive Phase III studies and to assist with dose setting and the introduction of drug cocktails.

Introduction.

Until relatively recently, the management of head injury met with therapeutic nihilism except for the straightforward evacuation of extra-cerebral clots. Over the past twenty five years, this attitude has changed through advances, both clinical and experimental, in our understanding. Neuropathology has revealed different patterns of injury with different temporal patterns of development including diffuse axonal injury, contusion and cerebral ischaemia. Development of the Glasgow Coma scale, the CT scanner, monitoring of intracranial pressure and delineation of avoidable factors (hypoxia, hypotension, hyperpyrexia etc) has defined those factors that affect final outcome. Outcome measures have become more refined to include not only the Glasgow outcome scale but also more detailed neuropsychology.

Development of robust experimental preparations has revealed cascades of secondary events leading to cerebral ischaemia/infarction and hence potential therapeutic targets that include glutamate receptors and excess intracellular calcium entry.

Global assessment of cerebral blood flow, oxygenation and haemodynamic reserve - multi-modality bedside monitoring.

The outcome of acute brain injury depends both upon the primary insult and the series of poorly understood secondary events that start immediately and continue for months. The final common pathway for much of the secondary damage after head injury is cerebral ischaemia/infarction, focal and diffuse, found in the majority of patients at post mortem. The fundamental concept is that there is mis-match between the brain's haemodynamic reserve - the ability to maintain an adequate blood supply to the whole brain and lesions within it - and the stresses that may precipitate ischaemia. Such stresses include arterial hypotension, hypoxia, hyperpyrexia, hypercapnia, raised intracranial pressure, local hypermetabolism and mediators of secondary injury including excitotoxic amino acids, free radicals etc. Such mechanisms of secondary cell injury frequently last only for a few minutes and their detection requires sophisticated real time monitoring and computation.

Multi-modality bedside monitoring is fundamental to defining the evolving problems in these critically ill patients that is not without difficulty. Uni-modality monitors assessing brain health have evolved in a largely independent fashion over the past twenty years and include measurement of intracranial pressure, cerebral perfusion pressure, peripheral arterial oxygen saturation, jugular venous oxygen and metabolite content, middle cerebral artery flow velocity, cortical microcirculatory perfusion with laser Doppler flowmetry, parenchymal oxygenation using non-invasive near infrared spectrometry, and brain temperature. All these methods are susceptible to practical problems when attempting long-term clinical monitoring, and when used alone represent difficulties in identifying artefacts. However, when employed in combination, the information gathered from several modalities facilitates a more informed interpretation of any signal change.

Common artefacts are individual to each measured parameter, hence signal changes that occur in several measured parameters at the same time are unlikely to represent artefact. Computer analysis of respective signal changes may also provide immediate diagnostic information (eg. resolving raised intracranial pressure secondary to hyperemia verus cerebral oligaemia) which promotes a rapid and more appropriate clinical response (Fig 11)

Following brain trauma, the complex controlled system for cerebrovascular circulation loses significant feed-back information. One aim of intensive care monitoring is to replace this missing data and help to restore the disruptive control loop by appropriate intervention. An ideal monitoring system should not only detect the secondary events, but also identify grades of cerebral dysfunction that render the brain susceptible to such insults. Therefore, testing of cerebral pressure autoregulation and cerebrovascular reactivity has received considerable attention in neurointensive care. Most techniques are based on the responses of cerebral blood flow to changes in arterial blood pressure. Each can be repeated only periodically. However more recently several methods have been described that provide for the continuous assessment of autoregulatory reserve and are based upon the endogenous variations in cerebral perfusion pressure. In particular, the response of intracranial pressure and transcranial doppler flow velocity to slow spontaneous changes in arterial blood pressure and of transcranial doppler flow velocity to transient carotid compression have been exploited and shown to relate to the development of refractory intracranial hypertension and final outcome.

Examples of different types of ICP waveform detected using multimodality monitoring methods. From Kirkpatrick et al.[11] Left: NIRS signals register a fall in HbO₂ (arrowed) and rise in Hb indicating cerebral oxygen desaturation confirmed by the fall in SjO₂. The CPP, FV and LDF also fall indicating primary intracerebral hypertension with a secondary fall in cerebral blood flow. Right: In this event (arrowed) increases in tHb, FV, and LDF all indicate that the rise in ICP was due to cerebral hyperaemia. ICP = intracranial pressure (mm Hg); CPP = cerebral perfusion pressure (mm Hg), FV = right middle cerebral artery flow velocity (cm/s); LDF = laser Doppler flux from the right frontal region (AU). NIRS = near infrared spectroscopy (recording from the right frontal region); HbO₂ = oxy-haemoglobin (μmol/l); Hb = deoxy haemoglobin (μmol/l), tHb = total haemoglobin (μmol/l), (SjO₂ = right jugular venous oxygen saturation (%). SaO₂ = peripheral oxygen saturation (%).
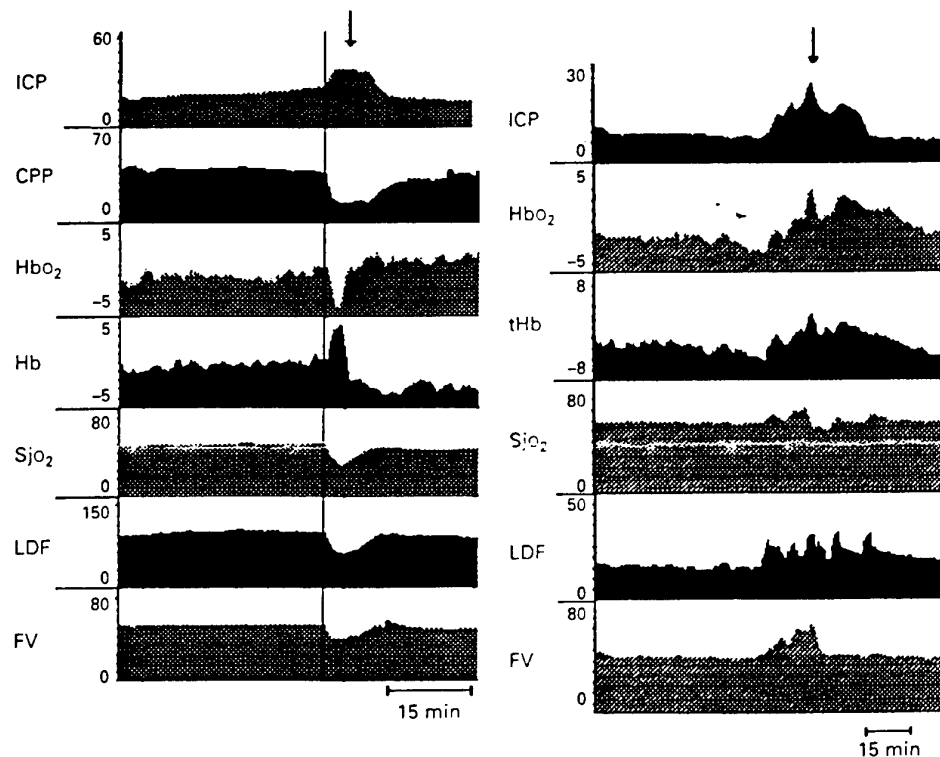
It is particularly important to monitor haemodynamic reserve in the first 48 hours after head injury to identify those patients who may be especially vulnerable to secondary insults and in whom an aggressive autoregulation - orientated therapy ought to be introduced. It is proving possible to model mathematically such changes in intracranial dynamics as an aid to the interpretation of multi-modality monitoring.

Functional Brain Imaging.

Although multi-modality bedside monitoring provides a necessary continuous physiological background and gratifyingly relates to outcome, such techniques do not reveal regional variations in tissue viability, blood brain barrier permeability, drug penetration and binding, metabolic stress or mechanisms of local brain swelling. X-Ray computer tomography and MRI (Magnetic Resonance Imaging) are able to define anatomical changes. Positron Emission Tomography will provide single time point quantification and regional cerebral blood flow, oxidative and glucose metabolism, ligand binding and tissue viability.

Functional Magnetic Resonance Imaging (Diffusion weighted, T1 and T2) and spectroscopy are able to dissect the consequence of ischaemia. T1 imaging is related to brain water content. T2/DWI will define whether cellular swelling or extracellular oedema (vasogenic) are present. Phosphorus and proton spectroscopy will detect changes in high energy phosphates, lactate production and N-acetyl aspartate, a marker of neuronal integrity.

However patients with acute brain injury have not been investigated in any great detail with the techniques of Functional Brain Imaging simply because of the logistical problems involved in taking critically ill patients on ventilators to the scanner. That process of transfer may increase the risk of secondary deterioration. The Wolfson Brain Imaging Centre in Cambridge has resolved the problem by incorporating both PET and Magnetic Resonance Scanners within the Neurosciences Critical Care Unit. Early studies have confirmed the regional heterogeneity of cerebrovascular and metabolic changes following head injury and the potentially deleterious effects of conventional therapy such as hyperventilation. Enhanced glucose metabolism around some brain contusions has been confirmed.

References

1. Pickard J D, Czosnyka M.
Management of raised intracranial pressure. Journal of Neurology, Neurosurgery and Psychiatry 1993:Vol 56: 845 - 858.
2. Kirkpatrick P J, Czosnyka M, Pickard J D
Multi-Modality Monitoring in Neurointensive Care. Journal of Neurology, Neurosurgery and Psychiatry 1996:Vol 61: 131-139.
3. Czosnyka M, Kirkpatrick P J, Pickard J D
Multi-modal monitoring of assessment of cerebral haemodynamic reserve in severe head injury in cerbrovascular and brain metabolism reviews. Vol 8 : 273 - 295 1996.

CLOSED HEAD INJURY AND THE MILITARY AVIATOR: ASSESSING COGNITIVE DYSFUNCTION AND SEIZURE RISK

William E. Drew, Lt Col, USAF, MC, SFS
John C. Patterson, PhD
Neuropsychiatry Branch
Clinical Sciences Division
Armstrong Laboratory, 2507 Kennedy Circle
Brooks AFB, Texas, USA 78235-5301

ACRONYMS
ACS = Aeromedical Consult Service
CHI = closed-head-injured
CT = computerized tomography
MRI = magnetic resonance imaging
PET = positron emission tomography
MEG = magnetoencephalogram
EEG = electroencephalography

INTRODUCTION
Over the last several years, two concerns have become evident with respect to the aeromedical disposition of aviators following closed head injuries. The first problem is that aviators, even with mild closed head injuries, often have subtle cognitive impairment. This impairment is often not apparent on clinical examination or cursory mental health evaluation such as the Folstein Mini-Mental State Examination. The second problem is the risk of post-traumatic seizures primarily in aviators with moderate or severe closed head injuries.

Both of these conditions clearly are problematic for the flying population in terms of information processing and sudden incapacitation. As task saturation poses a problem for individuals with the highest levels of cognitive functioning and psychomotor skills, i.e., "Top Guns", any cognitive impairment, to include cognitive slowing, poses a risk for flying safety. Clearly, sudden incapacitation, such as those resulting from post-traumatic seizure are incompatible with flying safety as well.

The current USAF practice of formally evaluating only moderate and severe closed head injuries for cognitive impairment is felt to be inadequate. Recently, two cases have been seen at the ACS at Brooks AFB that had significant cognitive impairment following only mild closed head injuries.

The current practice of waiting a number of years prior to returning an aviator to flying status following a moderate or severe closed head injury is similarly problematic. Modern diagnostic procedures may enable earlier assessment of an individual's seizure risk and identify individuals who can return to flying status earlier, thereby preserving military aviator assets.

An important aspect of closed head injury in occupational and aerospace medicine is the classification. USAF current policy defines mild closed head injury as one in which there was an episode of loss of consciousness of less than 30 minutes and/or an episode of anterograde anmesia or confusion of less than one hour. Moderate closed head injury is one where the episode of loss of con- sciousness is 30 minutes or greater, though less than 24 hours in dura- tion, or the anterograde amnesia or confusion is one hour or greater but less than 24 hours in duration. Severe closed head injury is one where the episode of unconsciousness or amnesia/confusion is 24 hours or greater in duration. (Note: Minimal closed head injury, which will not be discussed further here, is considered one in which no loss of conscious- ness, anterograde amnesia or signifi- cant confusion or cognitive impair- ment occurs.)

Based on these categories, a research program has been developed to further study head injury as it relates to aeromedical disposition. The hypotheses for this planned study are as follows:

a) A subset of mild CHI aviators have cognitive slowing, precluding a safe early return to flying status. (The present practice is to return these aviators following a 30-day

observation period and no specific evaluation.);

b) The subset referred to in a) can be identified with neuropsychological testing;

c) A subset of severe CHI aviators and a subset of moderate CHI aviators have a better prognosis and, specifically, a reduced seizure risk than that reflected by the groups of severe and moderate CHI populations at large;

d) The subsets referred to in c) can be determined by the use of currently available neuroanatomic and neuro-physiologic testing modalities, to include CT, MRI, PET, MEG, EEG and other modalities.

This study will be conducted as follows:

First, at the time of the closed head injury, the aviator's flight surgeon will contact the ACS to coordinate the evaluation. Locally, the aviator will receive the standard of care. In most cases, this will involve at least overnight observation. In all cases of moderate and severe closed head injury, a CT also will be performed as well as an MRI and EEG as soon as possible. The initial Glasgow Coma Scale will be documented at the initial medical treatment facility. Within the first 30 days, all aviators with mild, moderate or severe closed head injuries will have neuropsychological screening evaluations, e.g., Cogscreen, Microcog and Multidimensional Aptitude Battery. Mild head-injured individuals who perform adequately in accordance with aviator norms on these neuropsycho-logical screening tests, provided everything else including standard physical and neurological exams are normal, will be returned to flying status at 30 days. Those who do not satisfactorily perform on this testing regimen will undergo more formal neuropsychological evaluation locally. If they perform satisfactorily on that evaluation they will be returned to flying status at 30 days. If they do not perform satisfactorily, they will be managed aeromedically as a moderate closed head injury.

Moderate and severe CHI individuals will also receive the same early neuropsychological screening tests.

Poor performance on these tests, however, will not require additional, more extensive neuropsychological evaluation at that point as they will not be returning to flying status at that time. Rather, they will be evaluated at the ACS at approximately the 6 month point. At the ACS, they will undergo evaluations by flight medicine, neurology, ophthalmology, psychiatry, psychology, and ENT. Also, they will undergo extensive studies, to include:

a) EEGs, routine and sleep deprived;

b) special senses laboratory evaluation including rotational chair testing, eye tracking analysis, vestibular testing, brainstem auditory evoked potentials, full audiometry and posturography;

c) ECG;

d) neuropsychological testing.

They will also undergo an MEG, to be performed at the New Mexico Institute of NeuroImaging in Albuquerque, New Mexico. PET will be performed at the Research Imaging Center at the University of Texas Health Sciences Center, San Antonio, Texas.

Aviators with moderate closed head injuries in whom all of these studies are normal will be returned to flying status at 6 months or when all the studies are completed and results analyzed, whichever is later. Avia-tors in whom some studies are not normal will be managed similarly to the severe CHI individuals.

The severe CHI individuals will also be seen at the ACS at 6 months and undergo the same evaluation as that discussed above for the moderate CHI individuals. The severe CHI individ-uals and the mild and moderate CHI individuals who had abnormalities on prior testing will return at the 2-year point. At this time any previous testing which was abnormal will be repeated and the EEGs and MEG will be repeated regardless of previ-ous results (as there is a potential for these to become abnormal, even if previously normal). Those aviators in whom all studies are normal will be returned to flying status at that point. Those in whom some of the

studies are abnormal will be re-evaluated at the 5-year point. As at 2 years, they will undergo all studies which were previously abnormal and also EEGs and an MEG. Upon completion of these results, appropriate aeromedical disposition will be made. Also, as with the present waiver process, if certain specific studies are abnormal, such as an MRI revealing gliosis or hemosiderin in the cortex, such aviators are returned to flying after this 5-year period of observation.

Questionnaires will be sent to all participants annually for 10 years and at the 15- and 20-year points from the date of their accident. These questionnaires will request information on commonly occuring post-traumatic sequelae such as slowed cognition, dizziness, headaches, and lightheaded-ness, and also will query whether any seizures have occurred.

Collaborators in this study include the New Mexico Institute of NeuroImaging in Albuquerque, New Mexico, the Research Imaging Center at the University of Texas Health Sciences Center, San Antonio, Texas, and the School of Public Health, at the University of Texas at Houston.

The duration of the study is expected to be 10 years in order to achieve statistically significant results for the common categories of closed head injury at a $p=0.05$ level of signifi-cance.

A computerized data entry and reporting system is currently being constructed so that individuals at all collaborat-ing institutions and others who may want to participate in the future will record common information regarding the characteristics of the head injuries, the results of subsequent studies and any sequelae which occur. It is hoped that within 3 months this database format will be available on a disk and shared to any others who are interested in collecting data on CHI subjects which they see. Through collaboration, it is hoped that an increase in the number of subjects will be achieved so that statistically significant results will be obtained as early as possible.

Any further questions on the study should be directed to Dr William Drew at the given address.

SECONDARY INJURY AFTER SEVERE TRAUMATIC BRAIN INJURY: MECHANISMS TOWARDS WHICH CLINICAL TRIALS ARE TARGETED

J. PAUL MUIZELAAR, M.D., Ph.D.
Professor of Neurosurgery
Director, Institute for Neurotrauma
Wayne State University, School of Medicine
4201 St. Antoine 6E
Detroit, Michigan 48201, USA

SUMMARY

In this paper, we cite literature showing that after traumatic brain injury (TBI) much of the damage is done well after the impact, even though the morphological appearance might suggest otherwise. The biochemical cascades leading to this secondary or delayed injury are demonstrated. Drugs are available to interfere with specific pathways or steps in these biochemical cascades. The general principals of clinical trials to test the safety and efficacy of these drugs are described: Double-blind, randomized, placebo-controlled design; Entry criteria, concerning the severity of the injury, mostly based on the Glasgow Coma Scale; Outcome measurement, mostly based on the Glasgow Outcome Scale. Specific drugs and the status of their clinical trials are also described: Oxygen radical scavengers and lipid peroxidase inhibitors have failed in large scale, phase III trials; NMDA receptor antagonists are currently in phase III trials. Different types of calcium channel blockers have been tested or are ready to enter into phase III trials. Some trials with drugs with different mechanisms or trials with new management strategies (hypothermia) are also mentioned.

INTRODUCTION

Many findings in the pathology of (severe) head injury were thought to have occurred at the moment of impact, and thus not amenable to treatment. Modern research, however, has proven this is not to be true in many cases. One of the most striking examples is that of "axonal snap" : Sudden, extreme motion of part of the brain was assumed to stretch the long axons (traveling from one side of the brain to the other through the corpus callosum or from the cortex to the spinal cord through the capsula interna or the brain stem) beyond their limit of elasticity, and consequently they would snap (Strich, 1956 and 1961). Now it is generally accepted though that immediately after the impact, the axons are still intact but undergo various morphological changes over the ensuing 24 hours, finally resulting in the appearance of a "snap" with the subsequent formation of retraction balls (Povlishock, et. al., 1985; Erb, et. al., 1988; Gennarelli, et. al., 1989). Autopsy findings in brains of humans who died between 9 and 48 hours post-injury confirm a similar time course. The time it takes between the impact and the final morphological or functional result provides a window of opportunity for therapeutic intervention.

An outline of known biochemical cascades ultimately leading to neuronal dysfunction or death is provided below (Siësjö, 1985). It is of interest that this cascade of cellular

Modified After Siësjö
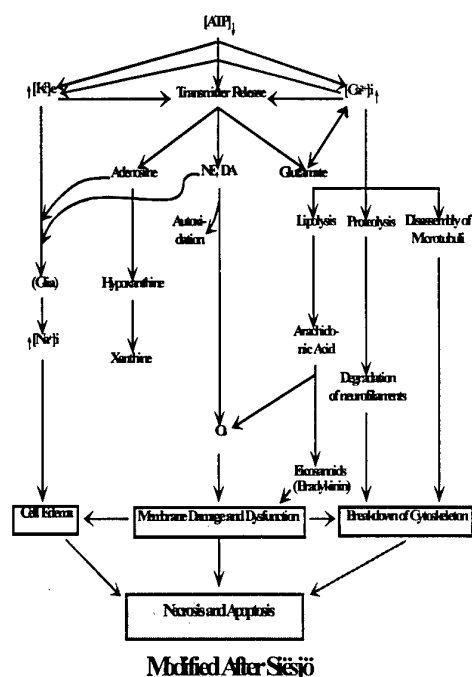
biochemical events is similar for stroke and traumatic injury, which also leads to similar therapeutic interventions in this cascade for stroke and injury. Separate from this, however, it has also been shown that ⅓ of severely brain injured patients suffer from cerebral ischemia in the first 12 hours after their injury (Muizelaar, et. al., 1984, Bouma, et. al., 1991, 1992) and an even larger percentage of patients suffer brief periods of cerebral ischemia between the first and fifth day after injury (Gopinath, et. al. 1994). This, then not only provides opportunities for neuroprotection similar as in stroke, but also for therapeutic interventions that relate to the pathology of blood vessels involved in this cerebral ischemia. Indeed, many of the processes in the schedule above also occur in non-neuronal cells, especially in the blood vessels such as endothelium, and in some cases drugs may exert their effects mostly on these non-neuronal cells even if they were "designed" with neuronal effects in mind.

DESIGN OF CLINICAL TRIALS IN SEVERE HEAD INJURY

Clinical trials with drugs are often divided into three phases: Phase I, which often tests the drugs in increasing doses ("dose escalation study") for side effects and pharmacokinetics in volunteers or small numbers of patients with varying diseases (if the drug is to be used for more than one indication); Phase II is usually a larger scale study (± 100 patients) in a more clearly defined population of patients, randomized and placebo controlled, but often still testing more than one dose and now looking for an indication of efficacy either in clinical outcome or in some other parameter that might ultimately be beneficial for the patient. Phase III trials are designed to give a definite answer as to whether a drug is improving clinical outcome and often demand enrollment of 400-1,200 patients. The trials using clinical outcome endpoints such as increased life span, lower mortality, less neurological or mental deficits are called "pragmatic", while those using surrogate endpoints, such as lower intracranial pressure (ICP) or less or smaller lesions on a CT scan, are called "explanatory" (Schwartz, et. al. 1967).

In severe head injury, the phase III pharmaceutic clinical trials are randomized, placebo-controlled and double-blind. Randomization is probably the most important prerequisite for a good clinical trial (Nowak, 1994). A chance imbalance in the severity of injury between the placebo and verum drug groups dooms a trial, and presently more and more prerandomization stratification is used to insure against this problem. The entry criteria are rather similar for most studies: Patients with a Glasgow Coma Score (Teasdale, et. al., 1961, see below) of between 3 or 4 and 8 (coma) or 12 (disturbed consciousness but not coma), and with a greater than approximately 10% chance of survival (exclusion of patients with bilateral unresponsive pupils, or with blood pressure below 90 mm. Hg. systolic, or arterial oxygenation below 60 mm. Hg., or age above 70, etcetera), and in whom the experimental treatment can be initiated within 8-12 hours after injury are eligible.

GLASGOW COMA SCORE

MOTOR		EYE OPENING		VERBAL	
Flacid	1	None	1	None	1
Extension	1	To pain	2	Incomprehensible	
Abnormal		To voice	3	Sounds	2
Flexion	3	Spontaneous	4	Inappropriate	
Normal flexion	4			Words	3
Localizing	5			Disoriented	4
Following				Oriented	5
Commands	6				

Practically all studies have used the Glasgow Outcome Scale (GOS Jennett, et. al., 1975, see below) at three or six months post-injury as the primary endpoint

GLASGOW OUTCOME SCORE

1. Dead
2. Vegetative
3. Severely disabled
4. Moderately disabled
5. Good

Severely disabled is defined as conscious, but dependent on others for most activities of daily living; moderately disabled is independent for most activities, but not being able to return to former occupational or social activities; good means going back to those former activities with or without neurologic deficits. Often 4 and 5 are combined into "favorable", while 1, 2 or 3 together are considered "unfavorable". A typical study will aim to increase favorable outcome from 45% placebo to 55% in the drug group at three months, or from 50% to 60% at 6 months, which calls for approximately 300 patients per group.

Although pharmaceutical companies do not divulge much financial information on this subject, this author estimates the cost to bring a new drug for this indication to the market at $30-60 million.

SPECIFIC MECHANISMS

Oxygen Radicals and Lipid Peroxidation

PEG-SOD (Sanofi-Winthrop) and Tirilizad (Pharmacia-Upjohn) were the first ones to be tested in large scale (phase III) clinical trials. They are both oxygen radical scavengers. Tirilizad is also a lipid peroxydation inhibitor. As can be seen in Figure 1, oxygen radical formation is the final step in a number of reactions, in turn leading to cell membrane or

organelle membrane damage through lipid peroxydation. Interfering with the final steps was thought to offer the largest time window, which appears important in most animal studies. Although PEG-SOD has consistently led to an increase in patients with a favorable outcome (from 47% to 51%), this has never reached statistical significance, and the company has abandoned the drug. (Muizelaar, et al., 1993 Young, et. al., 1996) The Tirilizad trial in head injury was terminated just before its targeted number of patients (1,080) was reached because of an excess-mortality in the drug group. Subsequently, this turned out to be due to an imbalance in the number of patients with extremely severe injury randomized to received verum drug, but it seems extremely unlikely that this trial will be repeated, although Tirilizad is still in trials in spinal cord injury and subarachnoid hemorrhage. (Data presented at meetings, but not published as yet)

Glutamate

Selfotel (Ciba-Geigy), Cerestat (Cambridge Pharmaceuticals) and EAA494 (Sandoz) are all glutamate (NMDA) receptor antagonists. Glutamate is the ubiquitous excitatory neurotransmitter in the central nervous system. Glutamate is released from its presynaptic terminals in large amounts after experimental trauma and stroke, and its release after human head injury or during secondary insults (high ICP, low blood pressure) has also been shown using microdialysis. Activation of the NMDA receptor leads, amongst others, to influx of calcium setting in motion a number of processes, including proteolysis, mitochondrial dysfunction and finally cell death.

The prototype of NMDA receptor antagonist is animal experiment has been MK-801 but due to its side effects (severe sedation, hallucinations) it cannot be used in humans. The other NMDA receptors antagonists have the same side effects but to a (much) lesser degree.

Selfotel has been tested in two phase III trials in head injury and two in stroke, both in the U.S.A. and Europe. In an interim analysis of all 400 patients entered so far in the four trials, no benefit was found and, apparently the likelihood to find any was small, and all four trials were terminated. The phase III trials with EAA494 and Cerestat are ongoing, but still in their early phases.

Another (putative) inhibitor of glutamate is the kappa-opioid agonist Enadoline (Parke Davis). Its neuroprotective effects and glutamate release inhibiting effects have only been shown in models of stroke, but phase in-II trials in head injury are presently conducted with this drug.

Calcium

The case of the calcium channel blocker Nimodipine (Bayer) is somewhat special. Nimodipine was originally developed to prevent or treat vasospasm after subarachnoid hemorrhage from ruptured cerebral aneurysm (elevation of intracellular free calcium is the final event leading to contraction of the smooth muscles in the vascular wall). However, in clinical trials of aneurysmal rupture, it was found not to affect vasospasm but still improve outcome, probably on the basis of being a neuronal protectant. With this in mind, it was now tried after severe and moderately severe head injury: Overall it turned out not to be effective, but in subgroup analysis it appeared promising in those patients who had subarachnoid blood on their initial CT scan after head injury (± 35%). (Braakman, et al., 1993) Now a new trial was done, focusing on patients with traumatic subarachnoid hemorrhage: Favorable outcome at six months increased from 54% in placebo to 75% in the verum group (total 121 patients). (Harders et., al., 1996) Based on these reports, it now seems reasonable to administer Nimodipine to most patients with traumatic subarachnoid hemorrhage. However, in the trials, Nimodipine was administered by continuous I.V. infusion, which is not possible in the U.S.A. (the I.V. solution of Nimodipine in alcohol and polyethylene glycol is not available in the U.S.A.).

As mentioned earlier, and seen in the diagram, calcium plays a crucial role in mediating neuronal cell dysfunction and damage. One of its effects is mediated by the influx of calcium through the N-type channels into the presynaptic terminals, in turn releasing glutamate, but probably also having other effects. There is a neuronal specific N type calcium channel blocker, SNX III (Neurex Corporation). A unique property of SNX-III compared, to other drugs is that it is still effective when administered 24 hours after experimental stroke induction in certain models. Our own research with this drug in experimental traumatic brain injury even shows its peak effect if given four hours post injury, rather than earlier or (much) later. Phase II trials with a SNX III are being carried out presently, while phase III trials in the U.S.A. and Europe are planned (Neurex and Parke Davis).

Arachidonic Acid

Although the arachidonic acid cascade, resulting in bradykinin formation plays a role in neuronal processes, it is probably even more important in mediating vascular endothelial damage. Endothelial damage may have multiple effects, increased cerebral edema, secondary bleeding into the brain, vasospasm or vascular narrowing, increased leukodiapedesis and others. A phase II trial of a bradykinin-antagonist (SB238592, SmithKline Beecham, Bradycor) showed a greatly decreased incidence of contusion/hematoma expansion necessitating later surgical intervention. Another phase II trial with this compound is underway.

Others

A mechanism of secondary brain injury not shown in the diagram is the formation of lactic acid, because pyruvate can not be oxidized in the Krebs cycle to form ATP. The reason for this is not clear, our own investigations make it likely that it is secondary to calcium absorption to the mitochondrial membrane. There is a simple molecule, dichloroacetate or

DCA (CPC-211, Cypros) that has been used to prevent lactate formation and increase pyruvate metabolism by stimulating Pyruvate Dehydrogenase, in shock. It has been shown to be effective for biochemical markers but also for functional end-points in animal models of brain ischemia. It is now slated for testing in severe head injuries.

It should be emphasized that this overview is not complete. A number of drugs which have been shown to be effective in experimental ischemia or even in clinical stroke, are slated to be tested also in head injury. For some drugs, the mechanisms are actually unknown e.g. Lubelozole (Janssen) is possibly an intracellular NO synthase inhibitor, but this is mostly speculative.

Hypothermia

Finally, a large, phase III trial sponsored by the NIH (PI: Guy Clifton, M.D.) is ongoing, testing the effect of moderate hypothermia (33°C) for 48 hours after severe head injury. In three, small preliminary but randomized trials with a total of 118 patients, favorable outcome at six months increased from 28% in the normothermic group to 52% in the hypothermic group. (Marion, et. al., 1993; Clifton, et al. 1993; Shiozaki, et al., 1993). The mechanism is not known, but with micro dialysis, hypothermia has been shown to suppress secondary surges of glutamate release.

REFERENCES

1. Bouma, JG, Muizelaar, JP, Scringer, WA, et al. Ultra-early evaluation of regional cerebral blood flow in severely head-injured patients using xenon-enhanced computed tomography. J Neurosurg 1992; 77(3):360-368.

2. Bouma, JG, Muizelaar, JP, Choi, SC, et. al. Cerebral circulation and metabolism after severe traumatic brain injury. The elusive role of ischemia. J Neurosurg 1991;75(5): 685-693.

3. Braakman, R. For the European Study Group on Nimodipine in Severe Head Injury. A multicenter trial of the efficacy of nimodipine on outcome after severe head injury. J Neurosurg 1994; 80: 797-804.

4. Clifton, GL, Allen, S, Barrodale, P. et. al. A phase II study of moderate hypothermia in severe brain injury. J. Neurotrauma 1993; 10(3) 263-271.

5. Erb, DE, Povlishock, JT Axonal damage in severe traumatic brain injury: An experimental study in cat. Acta Neuropathol 1991; 76: 347-358.

6. Gennarelli, TA, Thibault, LE, Tipperman, R, et. al. Axonal injury in the optic nerve: A model stimulating diffuse axonal injury in the brain. J. Neurosurg 1989; 71: 244-253.

7. Gopinath, SP, Robertson, CS, Contant, CF, et. al. Jugular venous desaturation and outcome after head injury. J. Neurol Neurosurg. Psychiatry 1994; 57(6): 717-723.

8. Harders, A. et. al. Traumatic subarachnoid hemorrhage and its treatment with nimodipine. J. Neurosurg 1996; 85: 82-89.

9. Jennett, B, Bond M. Assessment of coutcome after severe brain damage: A practical scale. Lancet 1975; 1: 480-484.

10. Marion DW, Obrist, WD, Carlier, PM, et al. The use of moderate therapeutic hypothermia for patients with severe head injuries: A preliminary report. J Neurosurg 1993; 79(3): 354-362.

11. Muizelaar, JP, Becker, DP, Lutz, HA, et. al. Cerebral ischemia after severe head injury: Its role in determining clinical status and its possible treatment. In: Villani R. Ed: Advances in Neurotramatology. Amsterdam: Excerpta Medica. 1984, pp 92-98.

12. Muizelaar, JP, Marmarou, A, Young, HF, et. al. Improving the outcome of severe head injury with the oxygen free radical scavenger PEG-SOD: A phase II trial. J Neurosurg 1993 78: 375-382.

13. Nowak R. Problems in clinical trials go far beyond misconduct. Science 1994; 264: 1538-1541.

14. Povlishock, JT, Becker, DP. Fate of reactive axonal swellings induced by head injury. Lab Invest 1985; 52(5) 540-552.

15. Schwartz, D. et. al. Explanatory and pragmatic attitudes in therapeutic trials. J. Chronic Dis. 1967; 20: 637-648.

16. Shiozaki, T. Sugimoto, H. Taneda, M. et. al. Effect of mild hypothermia on uncomfortable intracranial hypertensioin after severe head injury. J Neurosurg 1993; 79:354-362.

17. Strich, SJ Diffuse degeneration of cerebral white matter in severe dementia following head injury. J. Neurol Neurosurg Psychiatry 1956; 19: 163-185

18. Strich, SJ Shearing of nerve fibres as a cause of brain damage due to head injury. A pathological study of twenty cases. Lancet 1961; 2: 443-448.

19. Teasdale, G, Jennett, B. Assessment of coma and impaired consciousness: A practical scale. Lancet, 1974; 2:81-84.

20. Young, B., Runge, J.W., Waxman, K.D., Harrington, T., Wilberger J., Muizelaar, J.P. A Multicenter Phase III Trial of the Oxygen Radical Scavenger PEG-SOD in Patients with Severe Head Injury. JAMA, 276: 538-543, 1996.

HEAD PROTECTION: MOTOR CYCLISTS, SPORTS AND INDUSTRY

D. Doyle
K. Sturrock
Institute of Neurological Sciences, Southern General Hospital
Glasgow, G51 4TF Scotland, UK

Introduction

Protection against brain injury has been the major concern of those who have been involved in the design of head wear for participants in dangerous pursuits. Various forms of head gear have been available throughout the ages for horsemen and those concerned with military pursuits. The development of engine driven vehicles and aircraft has led to empirically designed protective hats and helmets but, relatively recently, the scientific input into the design of helmets has become more noticeable. These have led to the creation of national and international standards for the design of helmets for various activities. One of the purposes of the studies, in which we have been involved, has been the evaluation of causes of brain injuries. Looking at these, with a view to brain protection, has led to a number of observations which seem relevant to the development of protective helmets.

Head Protection

Pedal Cyclists
Motor Cyclists
Horse Riders
Vehicle Occupants
Pilots
Industrial Workers

We have had the opportunity to study accidents and injuries in pedal cyclists, motor cyclists, horse riders, vehicle occupants, pilots and industrial workers, all of which groups have had helmets specifically designed for their use. An attempt is being made to provide information on mechanisms of brain injury in humans and to provide information on the value and performance of helmets.

Materials and Methods

Motor cyclists have given us opportunities to study correlations between accidents and injuries. The main purpose of this paper is to study head injuries. Of the 306 motor cycle accidents we have studied, to date, head injuries have been the main cause of death in at least half of the cases.

Motor Cyclists' Injuries

Total Cases Studied	- 306
Fatal	- 116
Non Fatal	- 190

116 fatal accidents have been studied and 190 non-fatal accidents. The causes of death have been analysed. In half of the fatal cases the head injuries were more important than body injuries. In a small proportion, body and head injuries were of equal severity and in roughly 1/3 of the fatal cases the injuries to the body were more severe than those to the head.

Motor Cyclists' Injuries

Causes of Death	
AIS Body > Head	39
Body = Head	19
Body < Head	58
(DAI - 5 cases)	

The injuries have all been assessed according to the Abbreviated Injury Scoring (AIS90) system. Of the fatal cases, 20% had irrecoverable injuries with AIS scores of 6. Almost 50% had extremely severe injuries, with AIS scores of 5 and around 20% died although their maximum AIS scores were 4 or less. Among those who survived their accidents a few had very severe injuries at AIS 5 but the majority had much lower scores and some, although involved in significant accidents, escaped unscathed.

Motor Cyclists' Injuries

AIS (1990) Scores			
Fatals	36	AIS	6
	53		5
	26		3-4
	1		2
Non-Fatals	15	AIS	5
	16		4
	65		3
	69		2
	22		1
	3		0

We have been fortunate in having the full co-operation of the Strathclyde Police and Department of Transport Vehicle Inspectors who have provided information about the accidents and allowed us to examine accident sites, damaged vehicles and damaged safety equipment. The Scottish Crown Office and the forensic pathology services of the west of Scotland have given us full co-operation and we have been able to study the fatal cases in great depth. The brains have usually been available to us. In some non-fatal cases, neuroradiological imaging has shown the positions of major brain injuries. Observations from the neuropathological examinations of these cases are presented in this paper.

Studies of helmets are going on simultaneously. Helmets have been obtained

from most of the accidents - fatal and non-fatal. These are inspected and diagrams prepared. Photographic records are also made of major lesions. We have made radiological studies of helmets in an attempt to increase the information available and have also attempted CT scanning of helmets. The information about the helmets and the neuropathology is reviewed with Police and Vehicle Inspectors to create as full a picture as possible of how injuries were sustained.

Studies of Helmets

Visual inspection - diagrams
Photographic record
Radiology
CT scans
Case reviews with police and vehicle inspectors for accident parameters (helmet damage reconstructions)

Neuropathology studies have included the conduct of many full autopsies or the availability of extremely detailed reports prepared by senior forensic pathologists.

Neuropathology

Full autopsies
Skull diagrams for fractures
CT of uncut brains
Macroscopic lesions on diagrams
Microscopy of brain stem, cerebellum and cerebrum - standardised survey and special sites

Skull fractures are logged on prepared diagrams and these are related to external evidence of impact damage. Such external evidence may only come from examination of the helmets.

Motor Cyclists' Injuries

Skull Fractures
  Fatals   46
  Non Fatals   21
Neck Fractures
  Fatals   1
  Non Fatals   0

Examination of the brains has, occasionally, included CT scanning of the intact brains. Macroscopic lesions are recorded on diagrams and are photographed. Extensive microscopy has been undertaken on all cases including microscopy of the brain stem, cerebellum and a standardised survey of the cerebral hemispheres.

Results

Least Evidence of Head Injury

Least Evidence of Head Injury

Ventricular Angle Rupture (VAR)
- Acute
- Intermediate
- Late
(Severity: minimal to hemisphere dissection)

If a motor cyclist dies immediately after an accident, there may be little evidence of brain injury. Some lesions take time to declare themselves and survival is required for the development of most of the lesions commonly associated with brain injury. There are also motor cyclists whose cause of death is in another part of the body and may appear to have suffered little brain damage on a hurried examination of the brain. Such individuals may, however, have evidence, from their helmets, of severe impacts. There are instances in which the brain has only been minimally damaged. Examination of all of these categories of brains has shown 2 main features - subarachnoid haemorrhage and ventricular angle rupture.

Fig. 1.
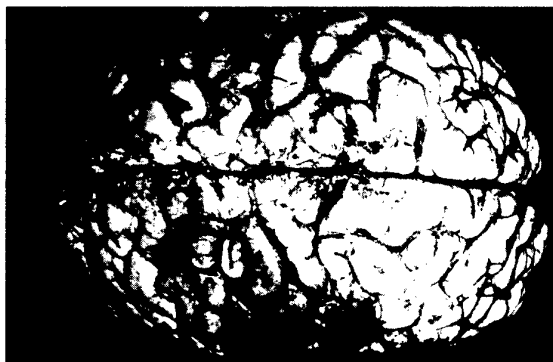
Subarachnoid haemorrhage overlying the left parietal and right fronto-parietal regions may be coup and contrecoup lesions.

Subarachnoid haemorrhage is often present in small amounts on one or both sides of the brain. This feature may not have been given due consideration in post mortem studies where larger lesions were being sought. The locations of the subarachnoid haemorrhage may, however, have importance for the directional input of energy to the head in an accident situation. The concept of true coup and contrecoup injuries to the brain has been explored in many studies and its incidence can rarely be proven in relation to larger haemorrhages and contusions within the substance of the brain. It is possible that some patches of subarachnoid haemorrhage may be coup and contrecoup lesions as small, unsupported vessels in the arachnoid may be subjected to disruptive forces at impacts.

Fig. 2-3.

Ventricular Angle Rupture (VAR) has
occurred at the upper angles of both
lateral ventricles. There is more tissue
disruption on the left where there is also
ventricular rupture below the caudate
nucleus. VAR often affects the full length
of the ventricular wall and as with
ventricular rupture, the depth of the
disruption may vary.

Fig. 4.

Ventricular rupture is less frequently seen
than VAR but may occur without VAR.

Fig. 5.

VAR may also affect the angles of the
fourth ventricle symmetrically or, as shown
in this section of pons, more on one side.

*Ventricular rupture or ventricular angle
rupture* (VAR) has been found in virtually
all of the brains examined. This
disruption at the upper angles of the
lateral ventricles, the angles of the
temporal horns of the lateral ventricles,
the lateral walls of these ventricles and
at constant positions in the walls of the
fourth ventricle, probably result from
movement of brain components and disruption
of the ependyma and underlying tissues.
These lesions occur in varying degrees of
severity from minimal ependymal tears to
deep dissections into one or both cerebral
hemispheres. Haemorrhage always occurs
with these tears and the position of
haemorrhage among tissue components makes
it clear that these are real lesions and
not post mortem artefacts. The acute
lesions are haemorrhagic. Lesions of
intermediate age have macrophages and blood
degradation products in them while late
lesions show glial scarring. Disruption of
the ependyma is not necessarily localised
to the ventricular angles but haemorrhage
is more frequently seen there than in other
parts of the ventricular walls. These
lesions cause bleeding into the cerebro-
spinal fluid in the lateral ventricles.
They may occur without there having been
disruption of the septum lucidum or any
other cause of bleeding into the
ventricles. They are probably the cause of
the transient CT scan evidence of bleeding
into the lateral ventricles after head
injury.

Subarachnoid haemorrhage and ventricular
angle rupture may be used as evidence that
a head injury has occurred and may be the
least evidence of head injury when more
severe lesions have not been caused.

Contusions

Contusions

Conventional Sites - Frontal
**   - Temporal**
Sparing Occipital Lobes
Fracture Contusions
Contre-coup

Cerebral contusions have occurred in these
cases in the conventional sites of the
anterior and under aspects of the frontal
lobes and the under and lateral aspects of
the temporal lobes. In common with all
other types of head injury studies, the
occipital lobes are spared except in
certain conditions, such as beneath
fractures. The sparing of the occipital
lobes in a population of the individuals
whose head injuries have often resulted
from severe frontal impacts makes the
contrecoup theory difficult to accept. The
occipital lobes are, however, protected,
anatomically, while the frontal and
temporal lobes are more liable to
deformation from internal vascular events
at impact.

Fig. 6.

**Tentorial Contusions in the uncal cortex of
both temporal lobes often appear, as here,
more severe on one side.**

Tentorial contusions, consequences of
impacts between the under surfaces of the
temporal lobes and the tentorial margins
are often unilateral or more severe on one
side. They may give evidence of impact
direction. These lesions have,
occasionally, been misinterpreted as signs
of increased intracranial pressure but can
be distinguished from herniae by their
haemorrhagic character and by time factors.

Diffuse Vascular Injury (DVI)

Contusions
Basal Ganglionic Haemorrhage
Microscopic Haemorrhage
Time Development
Vulnerability in Alcoholics

Diffuse Vascular Injury is a unifying concept which can explain cerebral contusions, basal ganglionic haemorrhages, haemorrhages in other parts of the nervous system, microscopic haemorrhages and blood vessel dysfunction. The surge of intra-vascular pressure - transmitted in arteries and the veins - will cause sudden vascular distension throughout the cerebral hemispheres and, particularly, in parts of the brain which have room to expand, notably the frontal polar regions and the temporal lobes.

Diffuse Vascular Injury (DVI)

Loading of Cerebral Vessels at Impact
Diffuse Damage to Vessel Walls by Stretching and Straightening
sequelae   - Fluid leakage (ICC proven)
              - Haemorrhages (major and minor
              - Microglial Activation (stars and scars)
              - Axonal Injuries

The distension and straightening of blood vessels may cause damage to vessel walls such that haemorrhage may occur or that the normal functioning of vessel walls will be compromised. This will allow the development of haemorrhages and of brain swelling. Other theories of the causation of contusions as impact interactions between the surface of the brain and the interior of the skull would seem likely to place the damage on the surface of the brain and also to imply that damage would be evident on the surface of the brain immediately after impact. The facts that the haemorrhages develop into contusions in the days after impact and that the haemorrhages lie within the substance of the cortex makes it as likely that these have been caused by disruptive forces from within the vessels.

The concept of diffuse vascular injury proposes that cerebral vessels are subjected to loading forces at impacts and that, in addition to disturbance of the integrity and the function of the vessel walls, axonal injuries may be caused in particular anatomical situations as axons and myelin are damaged by distortion caused by the deformation of blood vessels.

Diffuse Axonal Injury (DAI)

Causes:
Brain Movement - Stretching Axons
                - Vulnerable Axons
                - Confusion from Secondary Neuronal Damage
Forces Required - Heights of Falls
                - Speeds of Impacts
                - Direction of Induced Movement

Diffuse Axonal Injury is also an important concept which has attracted academic interest in terms of its causation and prevention. It is believed to be the result of movement of the brain and distortion of axons.

Diffuse Axonal Injury (DAI)

DAI Complex
- DLQ - Dorso Lateral Quadrant of Upper Brain Stem
- CC - Corpus Callosum lesions
- GC - Gliding Contusions
- ARB - Axonal Retraction/Regeneration Bulbs
- VA - Varicose Axons

Microscopic
- ARBs - Silver Impregnation, Immunocytochemistry, (Routine Stains)
Time and development of macroscopic and microscopic features

The diffuse axonal injury complex, pathologically, comprises haemorrhagic injuries to the dorso-lateral quadrant of the upper brain stem, corpus callosum lesions, usually also gliding contusions and the microscopic demonstration of axonal regeneration bulbs and varicose axons.
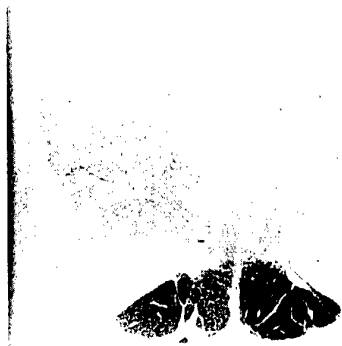
Fig. 7.
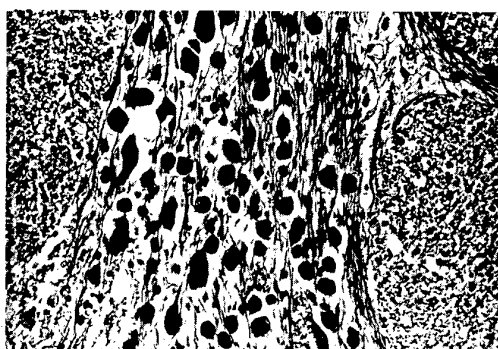
Axonal transection retraction/regeneration bulbs in a bundle of axons. There is no axonal injury in bundles running at right angles. (Palmgren Silver).

Fig. 8.
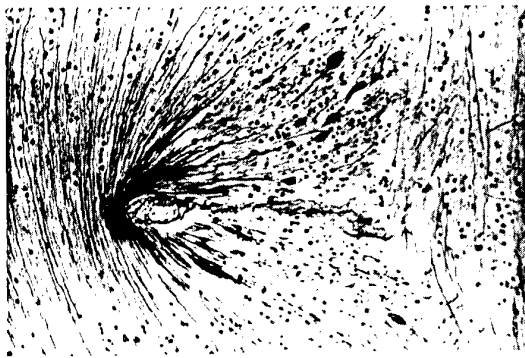
Axonal transection bulbs and varicose axons
where distortion has occurred around a
blood vessel. (Palmgren Silver).

Fig. 9.

Cortico-spinal tract degeneration may
follow cerebral trauma and may show greater
damage, as here, on one side (Marchi
technique) where myelin degeneration has
occurred after axonal damage.

Damage to axons, microscopically, can be
demonstrated in less severe injury
situations and may be the substrate of post
traumatic syndromes. The microscopic
lesions cannot usually be demonstrated
until several days have elapsed after an
accident. This means that microscopic
axonal damage cannot be demonstrated in
those who die very soon after impact. The
naked eye features may, however, be
demonstrable in some cases and it is likely
that these are the results of movement of
the brain relative to the skull and
intracranial structures. Skull deformation
and consequent deformation of the
intracranial dural partitions may also
account for some of the lesions in
particular anatomical situations. These
movements may cause stretching of axons in
vulnerable situations or local forces may
be generated, sufficient to disrupt myelin
and axons. In long surviving cases, with
the clinical counterpart of the diffuse
axonal injury complex, there may be
confusion with long tract damage which may

follow secondary neuronal damage. Diffuse
axonal injury may occur in falls from
varying heights, including a simple fall
from a person's own height, in impacts at
varying speeds and may be more frequently
induced by particular directions of
movement which would be thought likely to
increase intracranial movements.

Evidence of Brain Movement
Causing Brain Injury

Ventricular Angle Rupture
Supra-callosal Dissection
Tentorial Contusions
Cingulate Contusions
Gliding Contusions
Bridging Vein Rupture
Corpus Callosum Tears
Ponto-midbrain Tears
Ponto-medullary Tears

_Evidence of brain movement and the
direction of induced movement_ may be
deduced from several features. _Ventricular
angle rupture_ may be unilateral or more
severe in some locations.

Fig. 10.

Supracallosal Dissection, on the right,
between the upper surface of the corpus
callosum and the lower cingulate area.

Supra-callosal dissection , the disruption
of tissues between the cingulate gyrus and
the upper surface of the corpus callosum
may also be unilateral or more severe on
one side or in particular locations.
Tentorial contusions result from collision
between the under surface of the temporal
lobe and the margin of the tentorium. This
may be caused by the brain being thrust
against the tentorium, the brain expanding
by the vascular pul se of impact or by
tension induced in the tentorium during
skull deformation.

Fig. 11.

Cingulate contusions are usually unilateral as the free falcine margin and the cingulate cortex collide at impact.

Cingulate cortex contusions have similar connotations. They are more likely to be unilateral than the tentorial contusions but tentorial contusions may be either unilateral or more severe on one side than the other.

Gliding contusions may occur because brain movement stretches vessels passing to the bridging veins. Such movements would associate gliding contusions with the amount of movement thought likely to cause diffuse axonal injury. Gliding contusions may relate to bridging vein rupture, a major cause of subdural haemorrhage.

Corpus callosum tears may result from movement of the cerebral hemispheres causing stretching of the corpus callosum but some lesions of the corpus callosum are predominantly haemorrhagic and may be consequences of vascular mechanisms such as the proposed diffuse vascular injury.

Brain stem tears such as the transverse tears at the pons mid brain and pons medullary junctions are usually associated with skull base fractures but they imply longitudinal stretching of the brain stem causing disruption above and below the basis pontis.

Summary

The evaluation of motor cyclists' injuries has been conducted in fatal and non-fatal accidents. Brain damage has been evaluated by CT scanning and other forms of imaging in a small number of the surviving individuals but the greater part of the information has been gained from the neuropathological examination of fatal accidents. Evidence of movement between the brain, the skull and the intracranial partitions has been deduced. Correlations between impacts to helmets and heads (some motor cyclists had not worn helmets or their helmets had become detached) are continuing with the Department of Transport. Experience has been gained of injuries in other groups for which helmets are available. The evaluation of the motor cyclists' head injuries has suggested that the least evidence of head injury may be subarachnoid haemorrhage and ventricular

angle rupture. A concept of diffuse vascular injury is proposed to explain the generation of intracerebral haemorrhages and contusions, including tentorial and cingulate contusions. The possibility that vascular distortion may also cause axonal injury, is described.

Implications for helmet design

The prevention of movement between the brain, skull and intracranial partitions may be improved by increasing the rigidity and closeness of fit of helmets. The prevention of diffuse vascular injury could be minimised by reducing acceleration parameters at the time of impact and also by prevention of the transmission of a pulse of increased intravascular pressure through the major neck vessels.

Conclusion

Much has yet to be learned by the study of real world accidents. Although the motor cycle is diminishing as a form of transport in many countries, there still is a large requirement for head protection in motor cyclists, world-wide, and in motor cycle sports. This group does, unfortunately, provide us with an opportunity to make detailed studies which are proving profitable although it takes many years to provide cases for comparison. Information gained from motor cyclists can be applied to the design of protective helmets for other groups and it is hoped that the publication of information from this data base will be valued. It may be that the production of helmets for vehicle occupants will be seriously considered as deaths from head injuries in vehicle occupants is numerically vastly greater than the motor cycle problem.

Head Injury Risk in US Army Rotary-wing Mishaps: Changes since 1980.

Samuel G. Shannon, DrPH
John P. Albano, MAJ, MC
Joseph R. Licina, MS

Aircrew Protection Division
US Army Aeromedical Research Laboratory
USAARL, MCMR-UAD-CI, P.O. Box 620577
Fort Rucker, Alabama 36362-0577, USA

1. SUMMARY

Over the past several decades, data have been collected on U.S. Army aircraft mishaps defining the environment within an aircraft during a mishap, injuries suffered by the occupants, and the cause (or causes) of the mishap, if known. An analysis of these data indicates 60% of the occupants are injured, one-third fatally, if the mishap concludes with the aircraft impacting the ground. More significantly, despite improvements in helicopter design, restraint systems, and personal protective equipment, 68% of all fatalities had at least one fatal injury to the head. After adjusting for differences in mishaps, including the aircraft series, and the occupant's station within the aircraft, the authors concluded that an occupant's injury risk in a helicopter mishap had decreased significantly between 1980-84 and 1990-94. One factor in this was a decline in the risk of head injury, which declined by 50%. Injury risks to the face and brain, critical anatomical regions of the head, also showed a significant decline. Risks of injury to the neck, torso, and upper extremities were not significantly different between the two time intervals. Although the authors could not identify causative factors with clear implications for preventive strategies, the proportion of new, crashworthy helicopters in the U.S. Army fleet have risen steadily since 1980 and a new flyer's helmet with improved impact protection, the SPH-4B, was fielded by the U.S. Army in the 1990's.

2. INTRODUCTION

One of the first investigations of occupant injury in U.S. Army rotary-wing aircraft mishaps was conducted by Shanahan and Shanahan [1] in 1989. The authors presented statistics on crash velocity, type of injury, and injury characteristics in rotary-wing mishaps that occurred between 1980 to 1985. Of the 1,060 occupants in these mishaps, 136 were killed and another 475 suffered significant, but nonfatal injuries. More significant to this investigation, Shanahan and Shanahan differentiated between those injuries induced by acceleration and those injuries resulting from contact. According to Shanahan, acceleration-induced injuries result from the occupant's inertial response to acceleration force. Contact injuries, on the other hand, result from the occupant striking or being struck during the crash sequence. They reported a high prevalence of contact injuries to the head, prompting renewed developmental efforts in this area.

Concerns about contact injury prompted Raddin [2] to conduct a similar study using U.S. Air Force mishaps. Among the 620 occupants in Raddin's study, 126 were killed, while 100 more sustained injuries which resulted in lost days away from work or restricted duty. As in Shanahan and Shanahan's research, head injuries pre- dominate among the fatalities. Among survivors, spinal injuries are the predominate injury. It is likely that the high incidences of spinal injuries in USAF mishaps reflect acceleration-induced injuries during ejection and the parachute landing that follows.

This study expands on Shanahan and Shanahan's foundation, the authors examining historical data from U.S. Army rotary-wing aircraft mishaps that occurred during the 15-year period between 1 January 1980 and 31 December 1994. The toll during this period was 441 fatalities and 1,112 days lost/restricted duty injuries, ranking rotary-wing aircraft mishaps as one of the leading causes of mortality and morbidity among U.S. Army personnel. If Shanahan and Shanahan's assessment of injury causation are correct, as many as one-third of these fatalities and days lost/ restricted duty injuries resulted from contact injury to the head, many of which were preventable.

This study investigates injury to determine if the prevalence of contact injury to the head has changed since 1985. Since 1985, the U.S. Army has fielded thousands of SPH-4Bs, a new version of its SPH-4 flyer's helmet, and has upgraded the impact protection of thousands of older SPH-4s. Additionally, old aircraft have been replaced by new aircraft with improved crashworthiness, From an academic viewpoint, this study compares the distribution of injury for three 5-year intervals: 1980-84, 1985-89, and 1990-94. It provides quality benchmark data (that can be used for numerical analysis) on the prevalence of traumatic injury in U.S. Army rotary-wing mishaps.

3. MATERIALS AND METHODS

Selection of mishaps

The U.S. Army Safety Management Information System (ASMIS) was queried to identify all rotary-wing mishaps involving AH-1 (Cobra), AH-64 (Apache), CH-47 (Chinook), OH-58 (Kiowa) OH-6 (Cayuse), UH-1 (Iroquois), and UH-60 (Black Hawk) series helicopters that occurred between 1 January 1980 and 31 December 1994. Although other aircraft series were operated by the U.S. Army during this period, these mishaps were not included because of differences in operational use of the aircraft and the small percentage of the overall fleet represented.

The Army's aircraft mishap classification schema, defined in DA PAM 385-40 [3], is based on cost of the property damage or the level of injury sustained by the occupants, whichever is greater. Criteria are revised periodically, the last revision being in November 1994. Table 1 provides an overview of the cost and injury criteria contained in this revision of DA PAM 385-40. Because of its focus, the study was restricted to Class A, B, or C, mishaps where injury was likely to have occurred.

Mishaps also are classified by *survivability*. Survivability is defined in the Aircraft Crash Survival Design Guide [4]. A mishap is said to have been survivable only if the impact forces involved are within limits of human tolerance and the occupied space within the helicopter was sufficiently maintained throughout the crash sequence to permit each occupant's survival. If none of the occupied stations within a helicopter meet these criteria, the mishap is said to have been nonsurvivable. If some, but not all, of the occupied stations within the helicopter met these criteria, the mishap was said to be partially survivable. This determination of survivability is independent of actual survival, therefore, a mishap could have no survivors but be classified survivable. Likewise, a mishap could result in no injuries but be classified as nonsurvivable.

The initial query of the ASMIS database identified 1,296 aircraft (AH-1, AH-64, CH-47, OH-58, OH-6, UH-1, and UH-60) in 1,268 rotary-wing mishaps (Class A, B, or C) which occurred between 1 January 1980 and 31 December 1994. Narrative summaries and kinematic data (impact velocities, impact angles, and terrain characteristics) were then reviewed to identify those mishaps in which the helicopter did not impact the earth, i.e., wire or blade-strikes where the helicopter subsequently landed safely, aircraft fires that occurred during refueling, mishaps where the occupant fell from the helicopter during flight but the helicopter was not damaged, mishaps where individuals were struck by rotor blades while the helicopter was on the ground, mishaps where the helicopter was damaged by wind while taxiing, and mishaps where damage was limited to a load suspended from the helicopter, were excluded. After exclusions, the final data set consisted of 672 mishaps involving 683 helicopters. (The number of aircraft exceeds the number of mishaps because of mishaps with more than one aircraft.) For clarity, these are said to be *ground-impact mishaps*.

Table 2 provides a summary of the 672 ground-impact mishaps in the final data set. Station and degree of injury (DEGINJ) also are provided for the 2,337 occupants in these helicopters. Two occupants were coded as "missing." As several years have passed since their mishap, these occupants were presumed dead.

Creation of injury profiles
Since Shanahan and Shanahan first described the high frequency of head injury in U.S. Army helicopter mishaps, ASMIS has provided important insights into the determinants of traumatic injury. Developed to provide researchers with a simple method of describing environmental, social, and mechanical aspects of a mishap, ASMIS currently lists up to seven injuries to each occupant in a mishap. If an occupant receives more than seven, injuries are ranked by severity and the seven most serious are recorded in the database. A U.S. Army flight surgeon, participating in the accident investigation, determines the ranking.

The goal of this study was to describe any changes in occupant injury patterns since 1980. More specifically, we would like to be able to determine the distribution of injuries to each occupant and describe any changes to this distribution over time. The distribution of injuries was determined by an aggregate of four ASMIS fields: BREG (body region), INJTYPRS (injury type), CAUDEA (cause of death), and DEGINJ (degree of injury).

ASMIS conceptualizes the human body as composed of 5 major anatomical regions: Head, neck, torso (chest, abdomen, and pelvis), upper extremities (arms), and lower extremities (legs). These regions are identified by the first digit in the field, **BREG**. The next two digits in BREG identify specific anatomic structures within each region. Injuries involving more than one anatomical region are grouped into a single, catchall classification "General body injury." An example of such injuries would be a thermal burn, extending over 75% of the individual's body. As this code does not provide specific information on an injury and is virtually useless for comparative purposes, a concerted effort was made to minimize this code. This was done using a combination of the flight surgeon's notes in the case file, cause of death in ASMIS, and mishaps narratives. For example, the cause of death was 'decapitation', the injury was coded as either an injury to the head or neck depending on whether the cervical spine was transected. Likewise, if the injury was a 'concussion,' the injury was coded to reflect injury to the brain. Coding 'loss of consciousness' proved to be more difficult. The consensus among the investigators was that loss of consciousness could reflect the occupant's 'blacking-out' due to pooling of blood in the extremities or movement of the brain within the skull in response to contact partially mediated by the helmet. The decision criteria

used was that if the narrative cited confusion or disorientation confirmed by another observer, loss of consciousness was an indicator of brain trauma. Otherwise, it was not. This coding is consistent with the instructions for categorizing loss of consciousness by the Association for the Advancement of Automotive Medicine in the Abbreviated Injury Scale 1990 Revision (AIS 90) [5].

When appropriate, major anatomical regions of the occupant's body were divided into smaller subregion. This was accomplished by using the second and third digits of the ASMIS field, BREG. The head, because of its clinical importance, was divided into three subregions: Face, brain, and skull. Similarly, the cervical spine was broken out of the neck. Because of its size and complexity, the torso was divided into 4 subregions: Major organ systems, thoracic spine (T1-T12 vertebrae and their related IVD), lumbar spine (L1-L5 vertebrae and their related IVD), and the spinal cord. Injuries within a region not identified as within to a specific subregion were simply classified as 'any other structure.'

During the next step, injuries were summed for each body region (and subregions). A profile of injuries, based on the number of regions with traumatic injuries, was created. The profile of body regions with injuries was called an occupant's *injury profile*. An occupant was considered injured if they suffered one or more injuries to any body region. Likewise, the occupant was considered killed if any injury was fatal. *DEGINJ* was coded as "A" (Killed) or "H" (Missing, presumed dead), or a 'cause of death' was present.

The final step in analysis of ASMIS injury data was to estimate an occupant's injury severity score (ISS). In 1984, ASMIS was modified to allow coding of severity for individual injuries. A field, INJSEV, was added which described injury severity using a six-point scale from first aid (1) to fatal (6). This coding schema is compatible, to the extent possible, with the scoring schema used in AIS 90 to describe injury severity. Using the method described by Baker et al. [6], an ISS was computed for each occupant in the mishap. Computationally, ISS is the sums of squares of the highest score for the three most seriously injured body regions. Since the body regions used to calculate an ISS do not coincide with ASMIS body regions (nor with AIS 90 body regions), this necessitated further coding. ISS divide the body into six anatomical regions: Head/neck, face, chest, abdomen, extremities, and external. We elected not to code external injuries (lacerations, abrasions, contusions, and burns) separately but to retain these injuries within the body region affected. In accordance with the Injury Scaling Committee's instructing in AIS 90, loss of consciousness was given an injury severity score of '2' if it was witnessed, resulted in confusion or disorientation, and was less than 1 hour in duration. Finally, any individual with one or more fatal injuries was automatically assigned an ISS of 75.

Classification of mishaps
Mishaps were divided into two groups based on the survivability of the aircraft: Potentially-survivable and nonsurvivable. A potentially-survivable mishap is one where any occupied station was potentially survivable, i.e., a survivable or partially-survivable mishap. Nonsurvivable mishaps are those where no occupied stations were said to be survivable; that is, all occupied stations were classified as nonsurvivable. In general, non-survivable mishaps are catastrophic events with multiple fatal injury producing mechanisms. Less that 15% of occupants in nonsurvivable mishaps survived the mishap, less than 1% were uninjured in the mishap.

Mishaps also were categorized according to their date of occurrence. The 15-year study interval was divided into three 5-year

1984), Period II (1 January 1985 through 31 December 1989), and Period III (1 January 1900 through 31 December 1994). The 5-year intervals were chosen because Period I roughly replicate the interval described in Shanahan and Shanahan's study [1].

Classification of occupant station
Within an aircraft, an occupant's location within the helicopter is said to be their 'station.' To simplify analyzes, all occupants were assigned to one of three stations: Pilot/copilot (PC), crew chief/engineer/aerial gunner (CEG), and passengers (PAC). (In a tandem-seat attack helicopter the gunner station is the copilot station, therefore the gunner station in these aircraft was coded as PC.) The PC station is well documented and the protective equipment worn by occupants of this station are generally standardized, therefore, it was decided to classify all occupants into two stations: PC and all others. This change affected only the occupants of the crew chief/engineer/ aerial gunner station who were combined with passengers.

Statistical analyses
Analyses were conducted in three stages. First, traumatic injury to each body region was examined by comparing the frequency distribution of injury counts. Next, we formally tested the null hypothesis that injury risks have declined in comparing injuries in Period I with injuries in Period III. Clinically, the body is divided into several anatomical regions. Therefore, in comparing injury rates we divided the body into five anatomical regions. This provided an estimate of the effect of time on the risk of acceleration and contact injury. We previously reported that new, high performance helicopters exhibit higher injury rates possibly related to a distinct tendency for these helicopters to impact with high vertical velocity. Therefore, relative risks were estimated using multivariate logistic regression to adjust for survivability, occupant station, and helicopter type. For all relative risk estimates, we provide 95 percent test-based confidence intervals (CI_{95}) when appropriate. Student's T Tests (or multivariate Analysis of Variance (ANOVA) when appropriate) were used to compare ISS values. As the calculation of ISS values was possible only after 1983, these comparisons were limited to mishaps which occurred after January 1, 1985 (Periods II and III). P-values, based on 95% confidence intervals are provided for these estimates.

4. RESULTS
Over the 15-years of the study, 1,226 aircraft of the seven helicopter series previously discussed were involved in Class A, B, or C mishaps. Six hundred and eight-three of these mishaps involved the aircraft actually striking the ground (55.7%), that is, a ground-impact mishap. Acquisition and retirement of aircraft have changed the Army helicopter fleet significantly over the past decade. A breakdown of the distribution of the 683 'study' aircraft is provided for each of the three time intervals in the study as Table 3. As the AH-64 Apache entered the U.S. Army fleet in 1984; no Apaches crashed during the first five years of the study.

Of the 2,337 occupants in the 683 aircraft, 1,395 were reported as being injured (59.7%), 401 fatally (17.2%). Table 4 provides a survey of injuries and fatalities by helicopter series.

In Table 4, the first column reflects the helicopter series, the second the number of occupants in mishaps involving this series, the third the number of occupants injured, and the last the number of occupants killed. For example, there were 188 individuals in 94 AH-1 aircraft. Of these 165 suffered at least one injury (87.8%) and 33 (17.6%) were killed. By comparison, 48 of the 62 (77.4%) individuals in AH-64 mishaps were injured, 9 (14.5%) fatally.

A summary of traumatic injury by body region is provided as Table 5. The first column defines the body region affected (or subregion, if appropriate). The next represent the number of injured occupants for each region or sub-region. The third column displays a percentage. For regions, this value represents the percentage of injured occupants. For subregions, the percentage reflects the percentage of occupants with injuries to a specific subregion within that region. The fourth represents the ranking of the region within major body regions or subregions within a major region. Columns 5 through 7 describe injury profiles for all occupants for each of the three 5-year periods. The risk of traumatic injury rose during the second 5-year period, before falling during the third. If this trend continues, statistical significance will eventually be reached.

Thirteen hundred and eighty-five of the 2,337 occupants in the study aircraft were injured. Of these, 638 (27.3%) suffered at least one injury to the head. Head injuries ranked second in terms of most frequently body region injured behind the torso. Analysis of subregions, reveals that 264 (41.4%) of individuals with head injuries suffered at least one injury to the face. Of clinical importance is that while 254 injured occupants (39.8%) suffered brain injuries (mostly concussions), only 142 (22.3%) had fractures of the bony components of the head. Between Period I and Period II, the prevalence of head injury rose by 35% (33.6/24.8=1.354), including a 70.4%(15.65/9.18=1.704) increase in brain injury. Fortunately, during Period III the prevalence of brain injury declined to 7.2% of the overall study population, 30.9% of occupants with head injury.

The unadjusted relative risk estimates for all occupants, grouped by body region, are shown in Table 6. These estimates were derived by comparing the injury risk in Period III with the injury risk in Period I (defined as baseline). None of these estimates were statistically significant, although many showed marked improvement Readers who have not had experience with the relative risk and its estimation are referred to Hosmer and Lemeshow [8].

Subgroup analysis of injury trends revealed a pattern of very high injury prevalence among occupants in nonsurvivable mishaps. In nonsurvivable mishaps, 86.3% (328 of 380) of the occupants were killed. Over the 15-years of the study, only three occupants in nonsurvivable crashes were uninjured. Moreover, injury trends suggest possible reporting bias for head injury in nonsurvivable crashes. That is, a flight surgeon was more likely to include head injuries among the seven injuries in ASMIS than injuries to other body regions. To assess the impact of a reporting bias, injury profiles in occupants in potentially-survivable mishaps were developed. Other than dropping the occupants in nonsurvivable crashes, Table 7 duplicates Table 5.

Table 7 is important because it suggests a declining trend for head injury. The prevalence of head-injured occupants in potentially survivable helicopter mishaps fell by 26% between Period I and Period III. Most of this decline seems to be related to a reduction in the number of occupants with brain injury. Prior to Period III, 31% of all head injured occupants suffered at least one brain injury; during Period III this number fell to 19%. The decline in the proportion of head-injured occupants with brain injury resulted in a rise in the proportion with facial injury (s). Overall, however, the proportion of crash occupants with facial injury declined slightly from 10.3% in Period I to 9.4% in Period III. The proportion of crash occupants who suffered torso injuries remained fairly constant over the 15-years of the study at 27.8-29.5%. However, the proportion of torso injury involving the major organ systems dropped significantly from 32.6% to 16.0%. Unadjusted relative risk estimates were calculated from these data. Presented as Table 8, the relative risk estimates suggest a linear trend of declining risk. Within specific anatomical regions,

the risk of head injury declined significantly, driven by a significant decline in the risk of brain injury. There was no decline in the risk of neck, torso, or upper extremity injury. However, within the torso, the risk of major organ system injury declined. As expected, this decline was matched by an increase in the risk of other injuries to the torso, predominately minor strains and contusions to the back. Perhaps more significant, there was a decline in the risk of lower extremity injuries. This is important because it tends to refute the hypothesis of a reporting bias in head injury previously discussed.

A crewmember's station has been used in accident investigations for years; but it was not until recently that differences in injury risk between crew stations was fully appreciated. In this study, crew stations were either classified as pilot/copilot (PC) or other. The distribution of occupants stratified by crew station and ASMIS survivability are provided as Table 9. These data reveal that 59% of the occupants in potentially survivable crashes were in the PC station versus 51% in nonsurvivable crashes.

Table 10 presents injury patterns for occupants in the pilot/copilot station, limited to potentially survivable mishap. The data in Table 10 are presented in the same format as Tables 5 and 7 with the first columns representing the overall study and the last columns representing the 3 5-year intervals.

Fifty-two percent of PCs in potentially survivable crashes were injured, 3.8% killed, over the 15 years of the study. Ranking body regions from most frequently injured to least frequently injured, the torso was most the frequently injured body region and the neck the least. The head region ranked third behind the lower extremities, with 20.5% of all PCs suffering at least one head injury.

Comparing injury profiles across 5-year intervals, the proportion of injured PCs fell from 55.6% in Period I to 47.3% in Period III. More significantly, mortality fell from 5.7% to 2.1% over the same period. Many of the lives saved may be attributable to a reduction in head injury risk also observed. The risk of head injury fell from 20.6 in Period I to 15.4% in Period II, a decline of by 25.3%. More significantly, the risk of brain injury fell from 7.3% (36 of 491) to 2.7% (8 of 292). Likewise, the risk of skull fractures fell from 5.1% in Period I to 3.76% in Period III. As a proportion of head injuries, the risk of facial injury and skull fracture remain relative constant throughout the study.

The risk of torso injury remained relatively flat, beginning at 28.3% and ending at 26.3%. Within the region, the prevalence of vertebral fractures and spinal injury was essentially unchanged, although the risk of injury to the major organ systems declined significantly from 30.2% of torso injuries to only 13.2% of torso injuries. As a percentage of the population, crew members with major organ system injury declined from 8.6% to 3.4% in a decade.

In Table 11, the unadjusted relative risks for the PC in potentially survivable injuries are presented. As before, the overall risk of injury decreased. The decline in head injury was only borderline in significance, with a reduction in brain injury possibly the primary factor in this change. As before, there was no decline in the risk of injury to the neck, torso, and upper extremities. Although injuries to the major organ system(s) of the chest and abdomen declined significantly, possibly related to changes in helicopter design, the risk of leg injury also declined.

Again, comparing ISS values for Period II with ISS values for Period III yielded significant declines. The mean ISS value for

PCs in Period II was 10.516 declining to 7.39 in Period III (Student's T=2.45, $p=0.0125$). Restricting the comparison to injured PCs, the mean ISS in Period II was 20.47 versus 15.59 in Period III (Student's T=2.31, $p=0.02$).

A potential confounder which could mask injury trends in U.S. Army helicopter mishaps is the phenomenon of replacement, wherein older aircraft series are replaced by newer designs. Within the Army's helicopter fleet, AH-64 Apaches have largely replaced the AH-1 Cobra in the attack role and the UH-60 Black Hawk is rapidly replacing the UH-1 Iroquois in the Army's utility helicopter role. Historically, high-performance helicopters have exhibited high ground and sink speeds during crashes. In view of these findings, it is likely that some of the results observed in Table 10 are distorted by replacement.

The approach we took to investigate replacement was to divide the U.S. Army helicopter fleet into old (AH-1, CH-47, OH-58, OH-6, and UH-1) and new (AH-64 and UH-60) aircraft. For replacement to be a confounder, it must have an effect; that is, occupants of new aircraft must have a different injury profile. The overall risk of injury to the PC was significantly higher in the new aircraft group. Sixty-seven percent of PCs were injured in new helicopter mishaps versus only 48% of PCs in crashes of helicopters of older designs.

Table 12 compares injury profiles, restricted to PC station occupants, in potentially survivable crashes for old and new helicopter series by 5-year group. The proportion of injured crew members declined significantly in both old and new helicopters. In the older helicopter series, the proportion of injured crew members declined from 54.3% to 42.1%. While injuries to all body regions declined, the decline in head injury from 19.2% to only 10.9% possibly was causative in the decline in fatality risk from 5.3% to 2.3%. In the new aircraft, the number of mishaps during Period I was too small for the authors to draw any valid conclusions. However, overall injury rates fell from 68.3% in Period II to 63.4% in Period III. More significantly, the fatality rate fell between Period II and Period III.

After confirming that replacement was indeed confounding, its effect was controlled by the use of multiple logistic regression methods. Table 13 shows the results of multiple logistic regression models to adjust for helicopter type (old versus new), survivability (potentially survivable versus nonsurvivable), and occupant station (PC versus Other). Based on these models, we estimate a 42% decline in the overall injury risk between Periods I and II (1-0.578=0.422). The risk of head injury also declined by more than 51%, driven by statistically significant reductions in both face and brain injury. There was no significant decline in neck injury. Overall, the risk of torso injury also was unchanged but the risk of major organ injury did decline. This reflects a rise in the occurrence of back strains and strains since Period I. Interestingly, lower extremity injuries declined but not upper extremity injury.

To determine whether there had been a decline in injury severity, multivariate Analysis of Variance (ANOVA) methods were used to evaluate trends in the ISS. Controlling for occupant station, helicopter type, and survivability, the 5-year interval during which the crash occurred was statistically significant in the model. This was interpreted to demonstrate statistically difference in the ISS values between Period II and Period III. When the ANOVA models were used to predict the mean ISS for each Period, Period III was 5.1 points lower than Period II, controlling for helicopter type, survivability, and the occupant station.

The final analysis was to compare ISS scores. Since the 1980s, investigators have compared groups of injured patients in the

context of the ISS. The ISS provides especially useful information on the impact of injury severity on survival. Table 14 compares the ISS values for each station in potentially survivable and nonsurvivable mishaps.

Results were analyzed using ANOVA procedures. This revealed a significant difference in the ISS values between Period II and III for pilot/copilot station in potentially-survivable mishaps. No differences were observed in the ISS values other occupants nor for the pilot/copilot in nonsurvivable mishaps. Subsequent analyzes demonstrated that the mean ISS for the pilot/copilot station occupant in potentially survivable mishaps declined from 14.15 to 10.10 in new aircraft and from 9.25 to 6.30 in old aircraft between Periods II and III. For other occupants, the ISS rose from 8.05 to 19.55 in new aircraft and fell from 10.70 to 4.84 in old aircraft.

5. DISCUSSION

Today, the U.S. Armed Services are forced to operate under extremely tight budget constraints when fielding new aircraft. As crashworthiness does not improve an aircraft's performance, increase its range, or reduce its operational cost, program managers are often hard pressed to justify its long-term benefits against the added cost and weight. We believe that crashworthiness is best justified by reductions in morbidity and mortality, but we needed a method of reliably predicting injury patterns in new helicopters--before they were built. To do this, we compared the injury patterns in ground-impact mishaps over the past 15 years. After controlling for key characteristics known to be associated with injury risk, clear trends emerged. We found that after adjusting for helicopter type, survivability, and occupant station, the risk of any injury had declined by 42% between 1980-84 and 1990-94. To our knowledge, this is the first cohort study conducted on U.S. Army helicopter mishaps which reports a decline in injury risks. This decline was found particularly for head injury, which declined by more than 50%.

But there is a question begged in all of this: what are the factors accounting for these differences? To investigate, we compared both injury profile and severity for all occupants. We determined that two factors played a role in the lack of significance in Table 6. The first was the severity of injury in nonsurvivable mishaps. Most, if not all, occupants in nonsurvivable mishaps are injured. The second was replacement. Newer aircraft have significantly higher injury risks. Therefore, as AH-64 and UH-60 helicopters entered the fleet, injury risk increased although the adjusted injury risk continued to fall.

These findings are confirmed by analysis of the ISS. There was a significant decline in the injury severity of the average pilot/copilot between 1985-89 and 1990-94. The overall ISS declined by 3.4 points while the ISS in potentially survivable mishaps declined by 2.8 points. Other occupants did not fare so well. The overall ISS for other occupants declined by 6.5 points while the ISS for other occupants in potentially survivable mishaps declined by only 0.07 points. A number of factors may be responsible for these differences. The U.S. Army began to field an improved version of its SPH-4 flyer's helmet, the SPH-4B, in 1990. The SPH-4B provides improved impact protection and is lighter than the helmet it replaced. As concussions have declined significantly, it is likely that the SPH-4B has played a role in the decline of head injuries previously cited. A second factor in the equation is the replacement of the earlier PVS-5 night vision goggle with the ANVIS. The ANVIS mount features a breakaway feature not found on the PVS-5. This feature virtually eliminated facial injuries associated with night vision goggle use.

It has been suggested that to be successful, programs must reduce mortality as well as morbidity. We estimate that by reducing the mortality risk from 4.6% in 1980-84, to 2.5% in 1985-89, and finally to 3.8% in 1990-94, 17 lives have been saved.

(611*4.6=28.1 -15=13.1; 449*4.6=20.7-17=3.7; 13.1+3.7=16.8)

6. CONCLUSIONS

This study has demonstrated that it is possible to reduce the risk of morbidity and mortality in rotary-wing mishaps. The most important cause of mortality, head injury, fell by more than 50%. Likewise, the risk of brain injury fell by 49%. While many possible causes of this decline are possible, major consideration should be given to improvements in helmet design and the Army's fielding of an improved flyer's helmet in 1990. Many of the changes in the SPH-4B were incorporated quickly into the existing SPH-4 helmet, which may explain the reduction in brain injury without a reduction in skull fractures.

7. REFERENCES

1. Shanahan, D.F., and Shanahan, M.O., "Injury in U.S. Army Helicopter Crashes: October 1979 through September 1985". Journal of Trauma, Vol 29 (4), April 1989.

2. Raddin, J.H., "Adapting the Adam Manikin Technology for Injury Probability Assessment," Wright-Patterson AFB, OH: Armstrong Laboratory Report No.AL-TR-1992-0062, February 1992.

3. Department of the Army. "Army Accident Investigation and Reporting," Washington DC: Department of the Army Headquarters, November 1994.

4. Desjardins, S.P., Zimmermann, R.E., Bolukbasi, O., and Merritt, N.A., "Aircraft Crash Survival Design Guide," Fort Eustis, VA: Aviation Applied Technology Directorate, U.S. Army Aviation Research and Technology Activity (AVSCOM), USAAVSCOM TR-89-D-22, December 1989.

5. The Abbreviated Injury Scale, Des Plaines, IL: Association for the Advancement of Automotive Medicine, 1990 revision.

6. Baker, S.P., O'Neill, B., Haddon, W., Long, W.B., "The Injury Severity Score: A Method for describing patients with multiple injuries and evaluating emergency care," Journal of Trauma, 14: 187-196, 1974.

7. Shanahan, D.F., Shannon, S.G., and Bruckart, J.E., "Projected Effectiveness of Airbag Supplemental Restraint Systems in U.S. Army Helicopter Cockpits," Fort Rucker, AL: U.S. Army Aeromedical Research Laboratory, USAARL Report No. 93-31, September 1993.

8. Hosmer, D.W., and Lemeshow, S., "Applied Logistic Regression," New York: John Wiley & Sons, 1989.

Table 1. Criteria for categorizing U.S. Army aircraft mishaps in DA PAM 385-40.

Class	Total cost	Injury/cost threshold
A	More than	Fatality or total permanent
B	$200,000 to	1 permanent partial
C	$10,000 to	Loss of time from work

Table 2. Survey of U.S. Army Class A, B, and C ground-strike rotary-wing mishaps (1 January 1980 - 31 December 1994).

Total Mishaps		672	*Total Aircraft*		683
	Class A	430		Survivable	506
	Class B	111		Partially survivable	70
	Class C	142		Non-survivable	99
				Unclassified	8
Aircraft Series			*Aircraft occupants*		2,337
	AH-1	94		Pilot/Copilot/Gunner	1,342
	AH-64	31		All other	995
	CH-47	24			
	OH-58	190	*Injuries*		1,395
	OH-6	45			
	UH-1	235		Fatalities	401
	UH-60	64		Disabling	64
				Non-disabling	930

Table 3. Summary of study aircraft by time interval.

Series	Period I 80-84	Period II 85-89	Period III 90-94	Overall 80-94
AH-1	39	40	15	94
AH-64	0	10	21	31
CH-47	12	7	5	24
OH-6	16	17	12	45
OH-58	74	53	64	190
UH-1	125	69	41	235
UH-60	14	30	20	64
All	280	226	177	683

Table 4. Distribution of injuries and fatalities by aircraft series.

Aircraft	N	Injured	Killed
AH-1	188	165	33
AH-64	62	48	9
CH-47	243	156	81
OH-6	103	60	13
OH-58	413	254	53
UH-1	1,000	553	125
UH-60	328	223	87
Total	2,337	1,395	401

Table 5. Injury profiles in all aircraft: Overall (Jan. 1980 - Dec. 1994), Period I (Jan. 1980 - Dec. 1984), Period II (Jan. 1985 - Dec. 1989), and Period III (Jan. 1990 - Dec. 1994).

	Overall			Period I		Period II		Period III	
Population size	2,337			1,034		773		530	
	N	%	Rank	N	%	N	%	N	%
General (Multiple sites)	198	8.5	6	103	10.0	65	8.4	30	5.7
Head	638	27.3	2	256	24.8	259	33.5	123	23.2
Face	264	44.4	i	108	42.2	103	39.8	53	43.1
Skull	142	22.3	iii	63	24.6	44	17.0	35	28.5
Brain	254	39.8	ii	95	37.1	121	46.7	38	30.9
Neck	263	11.3	5	112	10.8	92	11.9	59	11.1
Cervical Spine	90	34.2		44	39.3	23	25.0	23	39.0
Torso	868	37.1	1	348	33.7	324	41.9	196	37.0
Thoracic Spine	112	12.9	ii	45	12.9	33	10.2	34	17.3
Lumbar Spine	86	9.9	iii	40	11.5	34	10.5	12	6.1
Spinal cord	47	5.4	iv	24	6.9	18	5.6	5	2.6
Major Organ System	395	45.5	i	156	44.8	164	50.6	75	38.3
Upper Extremities	435	18.6	4	189	18.3	168	21.7	87	16.4
Lower Extremities	578	24.7	3	246	23.8	214	27.7	118	22.2
Any Injury	1,385	59.3		619	59.9	475	61.4	291	54.9
Any Fatal Injury	401	17.2		159	15.4	154	19.9	88	16.6

Table 6. Estimates of the relative risk contrasting Periods I and III.

Injury	RR	CI_{95}	
Any Injury	0.816	0.661,	1.009
Head	0.918	0.718,	1.175
Face	0.953	0.674,	1.348
Skull	1.090	0.711,	1.670
Brain	0.763	0.516,	1.249
Neck	1.031	0.738,	1.440
Torso	1.031	0.930,	1.439
Major Organ System	0.928	0.687,	1.249
Upper Extremities	0.932	0.704,	1.233
Lower Extremities	0.917	0.715,	1.178

Table 7. Injury profiles, potentially survivable aircraft mishaps only: Overall (Jan. 1980 - Dec. 1994), Period I (Jan. 1980 - Dec. 1984), Period II (Jan. 1985 - Dec. 1989), and Period III (Jan. 1990 - Dec. 1994).

Sample size	Overall 1,957			Period I 897		Period II 611		Period III 449	
	N	%	Rank	N	%	N	%	N	%
General (Multiple sites)	68	3.5	6	36	4.0	16	2.6	16	3.6
Head	366	18.7	3	170	19.0	133	21.8	63	14.0
Face	225	61.5	i	92	54.1	91	68.4	42	66.7
Skull	72	19.7	iii	37	21.8	21	15.8	14	22.2
Brain	112	30.6	ii	56	32.9	44	33.1	12	19.0
Neck	187	9.6	5	86	9.6	60	9.8	41	9.1
Cervical Spine	35	18.7		22	22.9	5	8.3	8	19.5
Torso	563	28.8	1	258	28.8	180	29.4	125	27.8
Thoracic Spine	56	9.9	ii	30	11.6	10	5.6	16	12.8
Lumbar Spine	77	13.7	ii	37	14.3	29	16.1	11	8.8
Spinal cord	13	2.3	iv	10	3.9	2	1.1	1	0.8
Major Organ System	152	27.0	i	84	32.6	48	26.7	20	16.0
Upper Extremities	353	18.0	4	158	17.6	125	20.5	70	15.6
Lower Extremities	459	23.4	2	223	24.9	145	23.7	91	20.3
Injury	1,008	51.5		483	53.8	314	51.4	211	47.0
Fatality	73	3.7		41	4.6	15	2.5	17	3.8

Table 8. Relative risk estimates, traumatic injury for all occupants in potentially survivable U.S. Army rotary-wing mishaps.

Injury	RR	CI$_{95}$	
Head	0.683*	0.499,	0.936
Face	0.886	0.603,	1.301
Skull	0.735	0.393,	1.374
Brain	0.405*	0.215,	0.764
Neck	0.930	0.629,	1.375
Torso	0.923	0.725,	1.201
Major Organ	0.442	0.268,	0.731
Upper Extremities	0.846	0.622,	1.151
Lower Extremities	0.751*	0.570,	0.989
Any Injury	0.742*	0.591,	0.932
Fatal Injury	0.807	0.453,	1.438

* Statistically significant

Table 9. Population size: Pilot/copilot versus all other occupants stratified by survivability (ASMIS variable: SURV).

	Potentially	Non-survivable
Pilot/copilot	1,147	195
Other occupants	810	185

Table 10. Injury profiles, PC in potentially survivable aircraft mishaps only: Overall (Jan. 1980 - Dec. 1994), Period I (Jan. 1980 - Dec. 1984), Period II (Jan. 1985 -- Dec.1989), and Period III (Jan. 1990 - Dec. 1994).

	Overall			Period I		Period II		Period III	
Population size	1,147			491		364		292	
	N	%	Rank	N	%	N	%	N	%
General	33	2.9	6	14	2.9	11	3.0	8	2.7
Head	235	20.5	3	101	20.6	89	24.4	45	15.4
Face	156	66.4	I	54	53.5	67	75.3	35	77.8
Skull	49	20.9	iii	25	24.8	13	14.6	11	24.4
Brain	73	31.1	ii	36	35.6	29	32.6	8	17.8
Neck	123	10.7	5	59	12.0	39	10.7	25	8.6
Cervical Spine	23	18.7		16	27.1	5	12.8	2	0.8
Torso	323	28.2	1	139	28.3	108	29.7	76	26.0
Thoracic Spine	36	11.1	iii	19	13.7	8	7.4	9	11.8
Lumbar Spine	56	17.3	ii	22	15.8	23	21.3	11	14.5
Spinal cord	8	2.5	iv	6	4.3	1	0.9	1	1.3
Major Organ System	79	24.5	I	42	30.2	27	25.0	10	13.2
Upper Extremities	225	19.6	4	99	20.2	74	20.3	52	17.8
Lower Extremities	307	26.8	2	143	29.1	99	27.1	65	22.3
Any Injury	597	52.0		273	55.6	187	51.4	138	47.3
Fatal Injury	44	3.8		28	5.7	10	2.7	6	2.1

Table 11. Relative risk estimates for traumatic injury for PC station for potentially survivable rotary-wing mishaps only.

Injury	RR	CI$_{95}$	
Any Injury	0.692	0.516,	0.927
Head	0.681	0.468,	1.002
Face	1.071	0.681,	1.684
Skull	0.710	0.334,	1.466
Brain	0.346	0.159,	0.756
Neck	0.666	0.407,	1.089
Torso	0.860	0.619,	1.193
Major Organ System	0.369	0.182,	0.747
Upper Extremities	0.831	0.572,	1.206
Lower Extremities	0.673	0.410,	0.942

Table 12. Injury profiles among pilot/copilot station occupants in potentially survivable rotary-wing aircraft mishaps, stratified by aircraft class and year group of the mishap.

	Old Aircraft						New Aircraft					
	Period I		Period II		Period III		Period I		Period II		Period III	
Sample size	473		304		221		18		60		71	
	N	%	N	%	N	%	N	%	N	%	N	%
General	12	2.5	7	2.3	5	2.3	2	11.1	4	6.7	3	4.2
Head	91	19.2	60	19.7	24	10.9	10	55.6	29	48.3	21	29.6
Neck	59	12.5	27	8.9	15	6.8	0	0.0	12	20.0	10	14.1
Torso	129	27.3	86	28.3	50	22.6	10	55.6	22	36.7	26	36.6
Upper Extremities	92	19.5	53	17.4	29	13.1	7	38.9	21	35.0	23	32.4
Lower Extremities	136	28.8	74	24.3	42	19.0	7	38.9	25	41.7	23	32.4
Injury	257	54.3	146	48.0	93	42.1	15	83.3	41	68.3	45	63.4
Fatality	25	5.3	8	2.6	5	2.3	3	16.7	2	3.3	1	1.4

Table 13. Multivariate relative risk estimates for injury in US Army helicopter mishaps controlling for survivability, aircraft type, and occupant station.

Injury	RR	CI$_{95}$	
Any Injury	0.578	0.451,	0.741
Head	0.486	0.355,	0.665
Face	0.616	0.411,	0.923
Skull	0.816	0.521,	1.279
Brain	0.510	0.313,	0.831
Neck	0.707	0.474,	1.055
Torso	0.796	0.609,	1.042
Major Organ System	0.547	0.350,	0.858
Upper Extremities	0.748	0.547,	1.024
Lower Extremities	0.736	0.553,	0.979

Table 14. A comparison of ISS values: Pilot/copilot versus all other occupied stations by survivability.

Period	Station	Mishap Class	Mean	STD
2	Pilot/ Copilot	Overall	20.65	27.92
		Potentially	10.07	16.51
		Non survivable	67.62	17.95
	Other	Overall	24.30	30.19
		Potentially	9.87	16.10
		Non survivable	68.88	17.0
3	Pilot/ Copilot	Overall	17.20	26.89
		Potentially	7.23	13.58
		Non survivable	70.13	15.74
	Other	Overall	17.77	27.93
		Potentially	9.80	19.87
		Non survivable	65.85	20.37

Standards for Protective Helmets

'Declare ye among nations, and publish, and set up standards, publish and
conceal not'. Jeremiah, Ch 50, v2.

Dr D H Glaister O StJ PhD MB BS FFOM   Gp Capt RAF (Ret[d])
RAF School of Aviation Medicine Farnborough Hants GU14 6SZ UK

As commanded by the prophet Jeremiah, the author has been struggling for the past 7 years to set up standards and to have them published as ENs (for European Normalisation), in his capacity as chairman of CEN (European Committee for Standardisation) Technical Committee 158, Head Protection.

One of the four planks of the single European market as defined by the European Community Act of 1972 was the achievement of the free movement of goods (the others being the free movement of services, capital and labour). In May, 1985, European Community Ministers agreed on a 'New Approach to Technical Harmonisation and Standards' to fulfil this objective and outlined Essential Requirements for Personal Protective Equipment (PPE) which must be satisfied before any product can be supplied throughout the Community. European Standards (ENs) fill in the details of these essential requirements specific to any particular PPE (such as a protective helmet) and compliance with these requirements is then indicated by a CE mark.

The applicability of harmonised standards has been widened under a combined EC/EFTA (European Free Trade Association) mandate and the addition of Switzerland, Iceland and Norway, provides a market of 18 countries with a population of 378 million potential helmet users.

It should be clear from the foregoing that the primary objective of CE marking is free trade and that ENs only define the minimum levels of protection considered essential. While there is nothing to stop a manufacturer from offering higher levels of protection - against impact, for example - he will have a hard time convincing prospective purchasers to meet the higher implicit cost and other possible drawbacks such as greater weight and decreased comfort. As one manufacturer of motorcyclist's helmets said to the author, 'safety does not sell helmets'. It is, therefore, the responsibility of the standards making bodies and their individual members to ensure that they achieve the maximum protection possible for the public at risk, whilst still ensuring the 71% positive response from the EC's population weighted formal vote required prior to the standard becoming mandated. This is no mean task when one considers the diversity of cultures, climates and, in some instances, philosophies of helmet usage, together with the often conflicting demands of manufacturers, accident investigators, medical specialists and user organisations. Potential solutions used to achieve consensus have been to offer an additional 'high level of protection' standard which need not be enforced, and to include optional clauses for items such as electrical insulation, flame resistance or ventilation which may not be considered essential by all countries needing to adopt the standard. Such devices, whilst effective, create a potential minefield when it comes to the interpretation of CE marks, national legislation and enforcement.

A penetrating impact is an obvious and easily understood mechanism for brain injury. Standard helmet test methods currently use an impactor fitted with a 60° cone and 0.5mm radius tip, either placed against the helmet shell and struck by a falling hammer, or being allowed to freefall on to the shell. The helmet is fitted to a headform and failure is expressed either as a minimum permitted clearance, or actual physical contact between striker tip and headform. Higher performance is achieved by increasing the impact energy, the maximum currently used being a 3.0kg striker dropped vertically 3.0m with failure designated by even momentary electrical contact with the headform surface. This requirement comes from a racing driver's helmet specification, though it is applied at lower energy levels to many helmet types. Field experience shows such injury mechanisms to be extremely rare in road users, but attempts to delete the requirement and so to permit lighter helmets (with attendant reductions in associated neck injuries) have been thwarted, as have attempts to introduce an alternative load distribution test. This test, devised by Aldman (1984) impacts the helmet with a hemispherical (25 mm radius) striker and measures the force transmitted to a circular area of headform surface (100mm^2) directly in line with the striker. The proposed pass/fail criterion is a transmitted force greater than 1.0kN. In independent tests on 8 makes of cyclists' helmets, the method was found to be both reproducible and reliable (Glaister, 1990). It offers many advantages over a penetration test since it represents a known, definable and realistic injury mechanism, it permits ventilation holes without being design restrictive and it can lead to a reduction in helmet mass. It has obvious relevance to any helmet used in active sports such as cycling, canoeing, ice hockey or even for moped riders in hot climates.

Several papers already presented at this meeting have addressed head injury mechanisms. While the controversy over linear versus angular forces being the more relevant is set to continue for many years to come, it is immaterial to the helmet designer whether the shock absorbing liner acts by reducing the peak translational force per se or, through an off-axis lever arm, by reducing the peak rotational force. Likewise, specific injury thresholds are less important than the basic tenet that any reduction in transmitted forces can only be beneficial.

Although test methods have developed over the years, the basic principle has remained constant - a helmet mounted on a headform is struck against an anvil and the resulting force (or its reaction) measured to determine whether or not a specified pass/fail criterion has been exceeded. Many 'linear' impact devices have been used - fixed headform, swingaway headform, a headform in guided free-fall and a biodynamic, rather than rigid, headform - and many anvil configurations - flat (wood or metal), ball, hemispherical, kerbstone, edge etc, depending upon the helmet's intended use. A recently developed test rig drops a helmet in guided free-fall, measures the resultant force at its centre of mass by tri-axial accelerometry and allows the helmeted headform free motion immediately following impact.

Pass/fail criteria have been based on peak impactor deceleration, transmitted force, or headform acceleration and time dependancy has also been applied to some standards - either in the form that certain force levels must not be exceeded for more than specified time periods, or by use of the Head Injury Criterion (HIC) or Gadd Severity Index (GSI). It is important to note that in the very brief timescale of a head impact, the helmet shell becomes an independant mass and the forces recorded from the striker and

headform are not necessarily equal and opposite (Glaister, 1979). Clearly it is the headform measurement which more closely represents what a real head would have experienced. An AGARD Advisory Report, shortly to be published (Anthropomorphic Dummies for Crash and Escape System Testing) summarises 29 current helmet standards in which the pass/fail criteria for transmitted forces are 4.4kN, 5.0kN, 8.2kN or 15.0kN, and those for accelerations as 100G, 150G, 200G, 250G, 300G or 400G. An HIC of 1,500 and GSI of 1,500 are also listed. Suffice it to say that, regardless of helmet type or application, the brains being protected are the same and should share a common injury threshold. There must be a strong case for standardising the Standards, but this should be preceded by a better definition of the injury mechanics and human brain injury thresholds.

It has already been pointed out that a reduction in the linear force applied to the head will, pari passu, reduce any resulting angular acceleration so that the need for a specific rotational test for helmets is arguable. However, all the current linear impact test methods take great care to direct the force vector towards the centre of mass of the headform and to eliminate any induced rotation as far as possible. Such impacts must be rare events in the real world of accidents. Furthermore, helmet surface effects are ignored in the linear tests and quite different results can be expected if the impact is directed off-axis. As early as 1976, Aldman and colleagues developed a test for non-perpendicular impacts and subsequently showed that modifications to helmet design could prove extremely effective in reducing induced rotational forces (Aldman et al, 1978). A similar, but much simpler test method was developed for the British Standards Institution (Glaister, 1982) and has been applied in BS 6658, specification for protective helmets for vehicle users, since 1985. Its chief benefit has been to make BS 6658 less design restrictive than comparable standards since surface features, textures and profiles can be evaluated, so need not be specified.

This 'oblique impact test' drops a helmeted headform in guided free-fall as in the linear impact test, but the anvil is inclined and offset so that the helmet is struck obliquely and rotation induced. To save the cost and complexity of angular accelerometry, reactive forces were measured on the anvil and pass/fail values based on the best current helmet performance. The chosen criteria were the peak tangential force (to equate with peak induced angular acceleration, assuming simple Newtonian mechanics) and its integral with time (to equate with the induced angular velocity), these being the two parameters proposed by Löwenhielm (1977) to define brain tolerance.

Attempts to get this test adopted by the International Organisation for Standardisation (ISO) or CEN were thwarted by divergent national interests and, in the latter case, by the eventual withdrawal of the proposed motorcyclist's helmet standard (prEN 398) from the EC's new approach directives. This left the United Nations Economic Commission for Europe's Regulation 22 (ECE Reg. 22) as the most widely adopted standard for motorcyclists' helmets (including 11 EC nations) and an oblique impact test has formed a significant part of the relevant committee's work programme for the past several years. Although the need for a rotational test has been accepted, contentious issues were that the BS 6658 procedure measured reactive forces rather than headform accelerations per se, so took little account of helmet/headform interactions, and that the pass/fail criteria had been derived ad hoc, not based on human brain tolerance data. On behalf of the UK Department of Transport, the Transport Research Laboratory at Crowthorne

(TRL) has conducted tests using the BSI rig, together with a headform instrumented with a 9 accelerometer array to permit computation of angular accelerations and velocities in all three axes. Acceptable correlations between anvil and headform dynamics have been demonstrated and the BS 6658 pass/fail criteria have been shown to be in acceptable agreement with Löwenhielm's (1977) and other published human brain tolerance levels. It is not unduly optimistic to assume that an oblique impact test will be adopted in the 05 series of amendments to ECE Reg. 22 and the door will finally be open for the test procedure to be made gradually more stringent and for manufacturers to design helmets specifically to reduce the rotational forces transmitted to the head, and so to reduce further the mortality and morbidity of road traffic accidents.

Because of wide variations in the shape and size of human heads, it is probably true to say that the only way to ensure that a helmet is retained in an accident is to fit it to the wearer's head and to demonstrate that it cannot be displaced by whatever means attempted. Failing such a representative, but potentially injurious demonstration, test methods have been introduced into helmet standards to ensure adequate chinstrap strength (in BS 6658 the strap must not break nor stretch unduly under a snatch load of some 4.5kN), to preclude inertial release of quick fastening attachments in accidental impacts, and to limit buckle slippage and strap wear over the anticipated lifetime of the helmet. Thus, a chinstrap may have to retain its strength and a fastening remain functional after 5,000 cycles of operation and salt corrosion. Many helmet standards now include a roll-off test in which a snatch load is applied to the helmet brim in an attempt to roll it off a standard headform, and this may even have hair and a deformable neck to make it more human like. However, this test is too dependent on the fit, or misfit, of the helmet to eliminate all but the very worst helmet designs.

The lifing of protective helmets poses a problem in standardisation in that some helmet materials are extremely durable - a glass reinforced plastic (GRP) helmet can retain its original performance after 20 or more years of careful use - while some thermoplastics may become embrittled by exposure to ultraviolet light or solvents such that they can fail catastrophically under impact while still appearing 'as new'. Certain road racing organisations, the Royal Automobile Club and Motor Cycle Union for example, put a limited life (such as 3 years) on a competition helmet, but this is impracticable for the general public and for the sale of helmets which may have spent a year or more in storage prior to reaching a retail outlet. It would also discriminate against the purchase of expensive high-performance GRP helmets.

A solvent conditioning test was developed for the earlier BSI standards for road users' helmets (BS 2495 and BS 5361) in 1980 and has been shown to be extremely effective in eradicating susceptible materials. In this procedure, 25ml of a 50/50 iso-octane toluene mixture is applied to the entire outer surface of the helmet shell at least 30 min prior to all the specified impact tests. Any area of stress caused by drill holes or too rapid mould cooling, for example, could have developed microcracks and these will be sought out and propagated by the solvent so leading to catastrophic failure during the chinstrap, shock absorption or penetration testing. This test has been accepted into ECE Reg. 22.

Prolonged sunlight exposure tests (even in the UK) have demonstrated that some thermoplastic materials can become degraded, with certain shell colours appearing more susceptible

than others. Obviously it is not practical to age helmets in this way prior to routine performance testing, but accelerated ageing using a powerful UV light source is of some value in type approval tests. ECE Reg. 22 exposes the outer surface of the shell to UV irradiation from a 125W xenon-filled quartz lamp for 48 hr at a range of 25cm, followed by 4-6 hr of water spray and subsequent shock absorbing tests. While this test is unrepresentative of the UV exposure which could be attained after several years of outdoor wear, a more severe test procedure had been proposed for prEN 398 in which an exposure of $1GJ/m^2$ was to be applied in the wavelength range of 280 to 800mm. However, suitable apparatus in which to apply these conditions is not widely available and, as mentioned earlier, prEN 398 is no longer being pursued.

Undoubtably, the protection afforded by helmets for sporting activities, the workplace and the military has improved over the years, but at a somewhat modest pace. Many published reports attest to the benefits of helmet wear in most applications, but equally show that brain damage and death can still occur despite the wearing of approved headgear, and not always under conditions of massive 'unsurvivable' impact. A better understanding of the mechanics of brain injury, the continued application of accident data, the development of more appropriate helmet test methods and the availability of new materials, together with a growing public awareness of safety, should allow the makers of standards to demand further improvements from helmet manufacturers and ensure a continuing fall in morbidity and death from head injury.

References

1. Aldman, A. "A method for the assessment of the load distributing capacity of protective helmets proposed to replace the current resistance-to-penetration test". Chalmers University of Technology, Göteborg, Sweden,1984.

2. Aldman, B, B Lundell and L Thorngren "Non-perpendicular impacts, an experimental study on crash helmets". *In* Proceedings IRCOBI 1st International Meeting on Biomechanics of Injury to Pedestrians, Cyclists and Motorcyclists, 1976, pp 322-331.

3. Aldman, B, B Lundell, C Thorngren and T Turbell. "Helmet attentuation of the head response in oblique impacts to the ground". *In* Proceedings IRCOBI 3rd International Meeting on Simulation and Reconstruction of Impacts in Collisions,1978, pp 118-128.

4. Glaister, D H. "Measurement of impact forces and accelerations in human crash simulation and protection". *In* Proceedings of the Conference on Weighing and Force Measurement. Institute of Measurement and Control, London, September 1979, pp 48-65.

5. Glaister, D H. " The development and initial evaluation of an oblique-impact test for protective helmets". *In* Impact Injury Caused by Linear Acceleration: Mechanisms, Prevention and Cost AGARD Conference Proceedings No 322, October 1982, Paper 33.

6. Glaister, D H. " A method for the assessment of the load distributing capacity of protective helmets". IAM Report No 694. Farnborough, RAF Institute of Aviation Medicine, July, 1990.

7. Löwenhielm, C G P. "On Bridging Vein Disruption and Rotational Cerebral Injuries due to Head Impact". Department of Forensic Medicine and Division of Solid Mechanics, University of Lund, Sweden, 1977.

U.S. Army Aircrew Helmets: Head Injury Mitigation Technology

B. Joseph McEntire
U.S. Army Aeromedical Research Laboratory
USAARL, MCMR-UAD-CI, P.O. Box 620577
Fort Rucker, AL 36362-0577, USA

1. SUMMARY

Head injury remains the predominant cause of severe and fatal injuries to Army aircrew involved in helicopter mishaps. As a means to prevent injuries or reduce their severity, the U.S. Army has continuously sought improvements to aviator helmets. Numerous improvements have resulted from analysis of helmets involved in aviation accidents and the wearer's injuries. It is believed that the newest Army aviator helmet, the HGU-56/P, offers significant improvements over earlier designs. This paper presents a chronology of Army aviator helmets with descriptions defining their differences and improvements.

2. LIST OF SYMBOLS

cm   Centimeter
dB   Decibel
G   Acceleration, gravity constant (32.17 ft/sec^2 or 9.81 m/sec^2)
gm   Gram
hz   Hertz
m   Mass
ml   Milliliter
N   Newtons

3. SUBJECT MATTER KEYWORDS

Helmets
Protective headgear
Impact protection
SPH-4
SPH-4B
IHADSS
HGU-56/P
Head injury

4. INTRODUCTION

The high frequency of head injury in U.S. Army helicopter mishaps is well documented by Bezreh [1], Berner [2], Shanahan [3], and Shannon [4]. Aircrew helmets have played an important role in mitigating injury in survivable mishaps. The Army has strived to improve the crashworthiness of helicopters by requiring energy-absorbing seats and landing gear, and crashworthy fuel systems in modern aircraft [5]. Aircrew helmets have received several improvements to increase impact protection. Yet, head injury remains the leading cause of contact related fatal and severe injury in Army helicopter mishaps [3].

Several helmet types have been used by Army aircrew in the rotary wing environment. A brief chronology is presented in Table 1. The Army aircrew protective helmet #5 (APH-5), shown in Figure 1, was widely fielded in 1960 with significant reductions in head injury within 4 years [1]. Yet, the APH-5 provided minimal hearing protection from ambient cockpit noise.

To increase sound attenuation, the Army accepted the sound protective helmet #4 (SPH-4), shown in Figure 2, as a new standard helmet in 1969. This design was a derivative of the U.S. Navy SPH-3 helmet which offered increased noise attenuation for the helicopter sonar operators. The SPH-4 was based on a new shell design which accommodated large volume rigid earcups with state-of-the-art noise attenuation.

Table 1. Army aviation helmet chronology.

Year	Helmet	Characteristic
1960	APH-5	Navy design, general purpose
1969	SPH-4	New shell contour, improved sound attenuation, general purpose
1974	SPH-4	35% thicker foam liner
1982	SPH-4	Thinner shell
1984	IHADSS	Equivalent to SPH-4, specific to AH-64 aircraft
1989	SPH-4B	New shell material, liner, fitting, retention, earcup, and visor systems (Lower weight)
1995	HGU-56/P	All new, general purpose and aircraft unique design (Improved impact protection)

Several improvements were made to the basic SPH-4 helmet. In 1974, the foam liner was changed from 0.375 inches to 0.5 inches in thickness. In 1982, the helmet shell was reduced in thickness to reduce helmet weight. This helmet was a general purpose helmet and variants are still in use by some active and reserve Army aircrew.

The introduction of the AH-64 Apache helicopter to the Army helicopter fleet in 1984 resulted in an aircraft specific helmet. This helmet is the integrated helmet and display sighting system (IHADSS), shown in Figure 3. The IHADSS utilizes a unique shell design which houses infra-red sensors for slewing pilotage and weaponry systems. It is also designed to receive a helmet display unit (HDU) which can deliver weapon targeting, forward looking infra-red (FLIR), and flight instrumentation symbology to each crewmember.

Figure 1. APH-5 aircrew helmet.
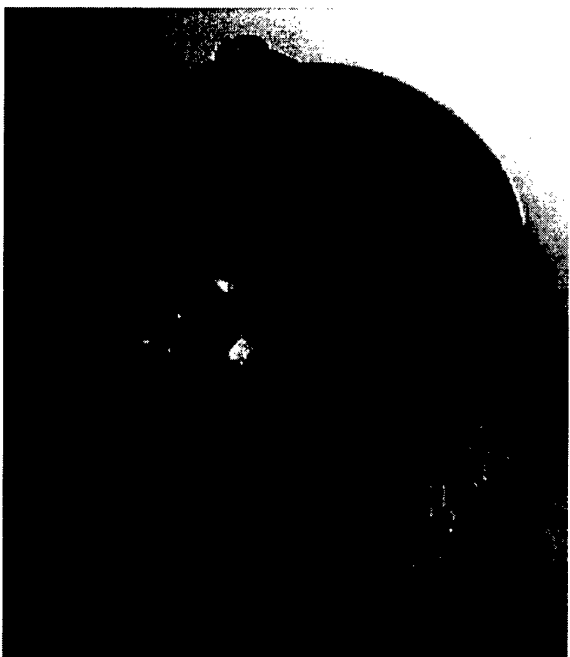
Figure 2. SPH-4 aircrew helmet.

constructed of different shell material, energy liners, retention system, earcups, and visor system.
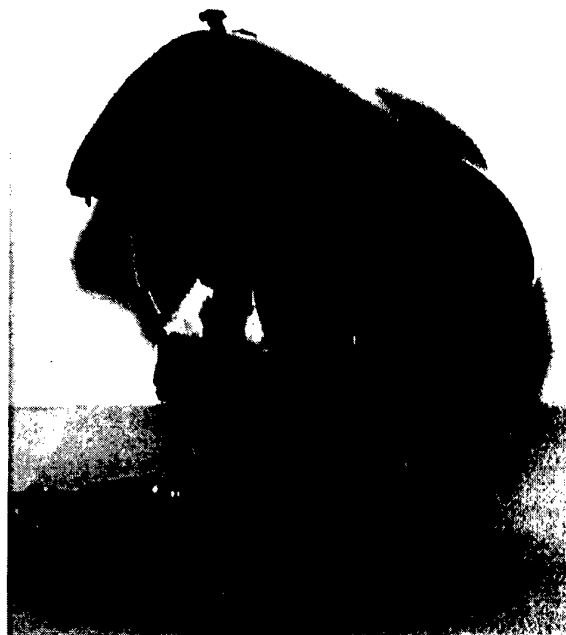
Figure 3. IHADSS aircrew helmet.

Figure 4. SPH-4B aircrew helmet.

At the U.S. Army Aeromedical Research Laboratory (USAARL), personal protective equipment involved in Army aviation mishaps are evaluated to determine its effectiveness at reducing and preventing injuries. This program is formally recognized as ALSERP, the Aviation Life Support Equipment Retrieval Program. As a result of the findings of this program and through collaboration with the SPH-4 helmet program manager and the Gentex Corporation, design improvements were made to the SPH-4, and the SPH-4B was introduced in 1989. The SPH-4B, shown in Figure 4, utilizes the same shell contour, but is

In 1983, the Army initiated a development program to develop a completely new Army aircrew helmet, the head gear unit #56, personal (HGU-56/P). The original HGU-56/P configuration was evaluated by the Army in 1985, but did not receive favorable reviews. The program was resurrected in 1988 with revised requirements. The revised HGU-56/P, shown in Figure 5, was finally introduced in 1995 and is currently in full production. This helmet possesses greater impact protection than previously available in aviation helmets and is intended to become a standard helmet platform for all Army helicopters.

Another helmet currently being developed is aircraft specific. This is the RAH-66 Comanche helicopter helmet, shown in Figure 6. The RAH-66 helicopter is unique from other helicopters in that it demands high man-machine integration for transfer of flight, mission, and targeting data to be highly effective. The original intent of the prime contractor for the RAH-66 was to develop a specific helmet unique to the Comanche to achieve the desired man-machine interaction. An effort is currently funded to determine the feasibility of adopting the HGU-56/P helmet as a mounting platform for the RAH-66 unique avionics, thereby keeping the HGU-56/P as a common helmet across the Army helicopter community.
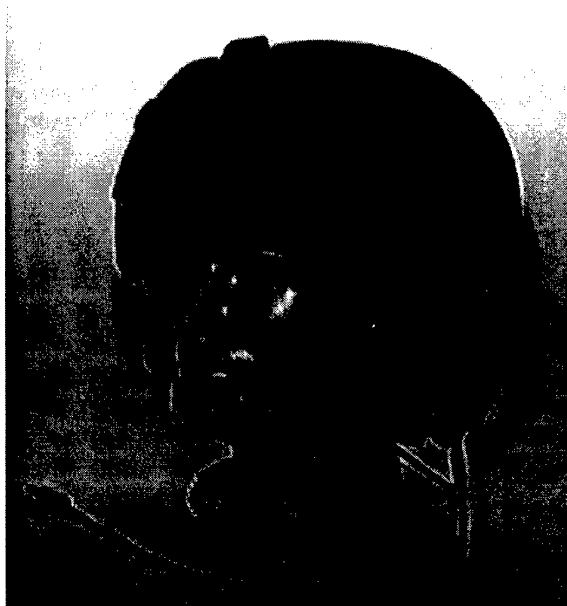
Figure 5. HGU-56/P aircrew helmet.

5. HELMET COMPONENTS
The helicopter aircrew helmet is best described as an assembly of subcomponents. Seven major subcomponents, shell, energy liner, fitting, retention, communication, visor, and mission or aircraft specific systems configure the HGU-56/P helmet assembly.

5.1 Shell
Brief descriptions of aircrew helmet shells are provided in Table 2. The HGU-56/P utilizes a hybrid construction of graphite and SPECTRA® 1000, embedded in an epoxy resin in its shell construction.

The graphite provides stiffness and rigidity to the shell for a stable platform of optical systems. The SPECTRA® is used to defeat a tear penetration requirement. This requirement was intended to ensure the final product was structurally tough and would withstand multiple impacts. This test is essentially a shear test of the composite laminate. Kevlar®, a very high tensile strength material, performs poorly in this test.

The helmet shell provides three primary purposes. First it is the structural member, or foundation, of the helmet used

Figure 6. Comanche aircrew helmet.

Table 2. Helmet shell materials.

Shell	Material
APH-5	Fiberglass
SPH-4	Fiberglass
SPH-4 (1982)	Fiberglass
IHADSS	Kevlar® & graphite
SPH-4B	Kevlar®
HGU-56/P	SPECTRA® & graphite

for mounting other systems. Second, it distributes impact loads over greater surface areas. This reduces the likelihood of receiving point contact loads. Third, it resists penetration from rigid contact surfaces.

It is important that the shell not be so stiff as to prevent flexure during impact. Shell deformation into the energy liner is an effective means of reducing the energy transmitted to the wearer as long as the shell does not permit a concentrated force or "bottoming."

5.2 Energy absorbing liner
From an impact protection perspective, the energy liner is the most critical component in the protective helmet. All of the Army aviator helmets utilize energy liners manufactured from expanded bead polystyrene. Differences between helmets are based on the energy liner thickness and its density. These differences are defined in Table 3.

Table 3. Helmet energy liner differences.

Helmet	Thickness (cm)	Density (gm/ml)
APH-5	1.27	0.08
SPH-4	0.96	0.08
SPH-4 (1974)	1.27	0.07
IHADSS	~1.4	0.07
SPH-4B	1.6	0.04
HGU-56/P	1.78	0.035

The noticeable trend in Table 3 is the increase in liner thickness and decreases in liner density. This follows USAARL's belief that head tolerance to blunt impacts is increased if the transmitted head acceleration is reduced. The increase in energy liner thickness provides an increased stopping distance, while the reduced density results in a lower force transmitted to the head.

5.3 Fitting systems
Significant advances in fitting system technology have been realized over the last 30 years. A brief description of the different technologies is provided in Table 4.

Table 4. Helmet fitting systems

Helmet	Fitting system discription
APH-5	Foam pads
SPH-4	Sling suspension
IHADSS	Basket & spacers
SPH-4B	Thermoplastic liner (TPL®)
HGU-56/P	Thermoplastic liner (TPL®)

The APH-5 utilized leather covered foam pads of various thicknesses to provide individual helmet fitting. These pads were provided with either self adhesive or hook and pile (Velcro®) backing. The SPH-4s were configured with a sling suspension, shown in Figure 7 with a cutaway helmet. Individual adjustments were accomplished by varying the lengths of the three cross straps and the headband. The IHADSS helmet is configured with an inner basket. This basket is shown in Figure 8. Individual fittings are made by adjusting the crown drawstring and placing Velcro® fitting pads in the brow and nape area. The SPH-4B and HGU-56/P both utilize the thermoplastic liner (TPL®). This is a multiple layer of thin thermoplastic sheets, each formed with egg carton type dimples covered with a washable cloth fabric. The pre-formed TPL® sheets are assembled by the manufacturer. Approximately 60 to 80 percent of individuals are fitted adequately with the preformed TPL®. Individual fitting is accomplished by heating the TPL® until the thermoplastic layers become

pliable, then having the individual don the TPL® and helmet until the TPL® has cooled and formed to the shape of the wearer's head.

Figure 7. SPH-4 sling suspension system.

Figure 8. IHADSS inner basket.

While helmet fitting systems are not intended as an energy absorbing material for impact protection, it does influence helmet performance in a laboratory setting. The SPH-4 sling suspension provided energy attenuation by plastic bending of the six metal attachment clips. The TPL® provides assistance by maintaining offset distances prior to impact except in those cases of custom fitting where the TPL® layers were compressed entirely. It also provides load distribution between the skull and energy liner.

5.4 Retention systems

The helmet retention system is critical for head impact safety by securing the helmet snugly to the wearer's head. Several improvements have been made in the helmet retention systems. Table 5 provides a brief discription of the different systems utilized in the Army aviation helmets.

Table 5. Helmet retention systems.

Helmet	Type system
APH-5	separate
SPH-4	harness
IHADSS	integral
SPH-4B	harness
HGU-56/P	integral

The APH-5 utilized separate straps for the chin and nape straps. Each of these attached separately to the helmet shell. This configuration is considered inadequate because retention system effectiveness is dependent on the helmet shell stiffness and the mounting locations of the strap to the shell.

The SPH-4 and SPH-4B helmets utilize a harness configuration which contain the earcups. These two harnesses are shown in Figures 9 and 10. The original SPH-4 design was poor because the chinstrap load was carried through four attachment tabs, the webbing containing the earcups, and finally to the chinstrap itself. Failures occurred at the tab and webbing or the chinstrap and webbing attachment points. The pull-the-dot chinstrap fasteners also caused helmet loss. The SPH-4B utilized an improved design by routing the chinstrap webbing directly to the helmet shell. Thus, chinstrap loading was through a continuous piece of material instead of multiple links. The harness material containing the earcups could also be adjusted in length to pull against the wearer's nape. When properly adjusted, the nape increased the helmet's stability and retention characteristics.
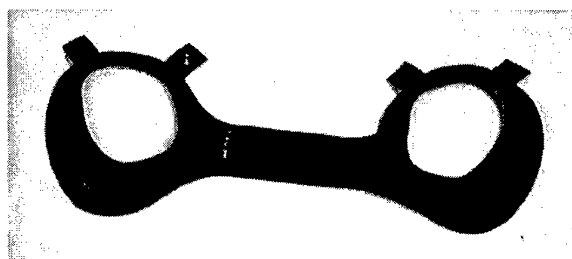
Figure 9. SPH-4 retention harness.
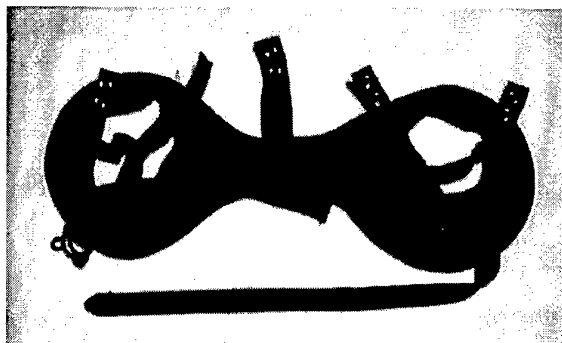
Figure 10. SPH-4B retention harness.

The IHADSS helmet retention system is similar to the SPH-4B system. Its chinstrap connects to the lower portion of a "V" strap. The upper legs of the "V" strap attach directly to the helmet shell and provide stability. The rearward strap weaves through the harness material which contains the earcups. This material wraps around the wearer's nape and can be adjusted snugly to improve helmet stability.

The HGU-56/P also utilizes a chinstrap which attaches to a "V" strap similar to the IHADSS and SPH-4B. The difference is that no harness is used to contain the eacups. The earcups are attached to the "V" straps with Velcro®. The "V" straps are also integrated with the nape strap pad with adjustable webbing. This configuration yields a low elongation chinstrap assembly and a stable helmet when properly adjusted.

The method used to attach the chinstrap is critical. Single snap fasteners, as used on the APH-5 and original SPH-4s, allowed frequent helmet loss in survivable mishaps [6,7]. Double snaps improved retention performance, but did not eliminate helmet loss. The SPH-4B and HGU-56/P both utilize only double D-rings for the attachment and adjustment of the chinstrap.

5.5 Earcups

The APH-5 helmet utilized foam earcups and provided little ambient noise attenuation. The SPH-4 provided much improved sound attenuation by utilizing thick and rigid earcups. A cross section view of a standard SPH-4 earcup is shown in Figure 11.

Through the USAARL ALSERP, it was recognized that aircrew basilar skull fractures were often accompanied with fractured earcups [8]. Static testing of the standard SPH-4 earcup revealed fracture occurred at over 22,000 Newtons. Yet, the temporoparietal region of the human skull can fracture under loads half as great [9].

The IHADSS helmet contains earcups that are rigid, but fracture at loads below the standard SPH-4 earcups. The SPH-4B and HGU-56/P helmets both contain crushable earcups which yield at loads below human threshold. Crosssectional views of these earcups are shown in Figures 12 and 13.
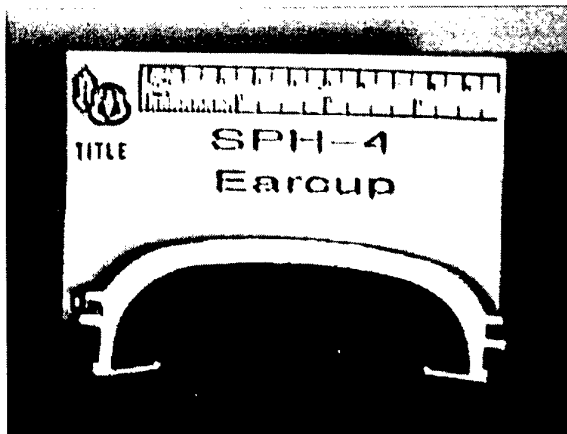
Figure 11. SPH-4 earcup, cross section.
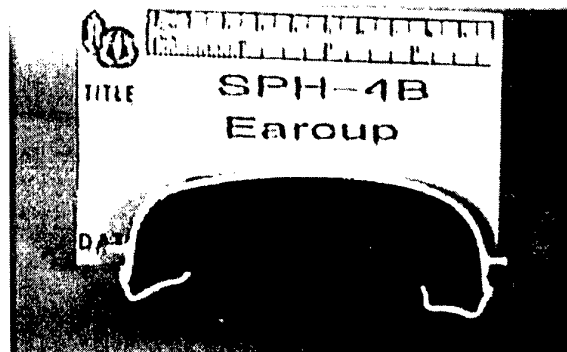
Figure 12. SPH-4B earcup, cross section.
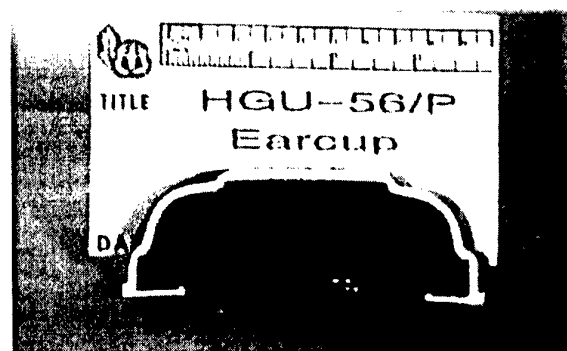
Figure 13. HGU-56/P earcup, cross section.

5.6 Visor systems

Visor systems have experienced little change except for graduating from a single visor design in the SPH-4 and IHADSS to a dual visor design in the SPH-4B and HGU-56/P. The dual visors are preferred by aircrew since it provides an option of a clear visor during low daylight situations and a smoke visor during daylight operations. Single visor design forced the aircrew to select a visor prior to flight or risk eye injury if they decide not to deploy the visor. Both the clear and the smoke visors filter at least 98 percent of ultraviolet rays [10]. Visor use is important as it protects the eyes from flash fires, flying debris, and impact during crashes. Early visors were made from acrylic and frequently fractured when impacted. Current visors are made from polycarbonate and rarely fracture.

5.7 Ancillary equipment

Depending on the mission and the aircraft being flown, various ancillary equipment can be used with aircrew helmets. Listed in Table 6 are the helmets and various compatible pieces of equipment.

The oxygen mask requirement is necessary because of high altitude missions (greater than 10,000 feet) in mountainous regions. Usually these missions are associated with the special operation forces and emergency rescues.

The PNVS-5 is an early generation night vision goggle which has been replaced with the ANVIS-6 goggle. These devices are necessary to reduce risk when missions are required to be conducted at night.

The threat of chemical and biological warfare necessitate the requirement for chemical and biological protective respirators (CBR mask).

Table 6. Helmet ancillary equipment.

Helmet	Compatible equipment
APH-5	Oxygen mask
SPH-4	AN/PVS-5, ANVIS-6, oxygen mask, CBR mask, AH-1 mechanical tracking& targeting system
IHADSS	AH-64 Infra-red head tracker & HDU, CBR mask, ANVIS-6
SPH-4B	PNVS-5, ANVIS-6, oxygen mask, CBR mask, AH-1 mechanical tracking& targeting system
HGU-56/P	ANVIS-6, oxygen mask, CBR mask, AH-1 mechanical tracking& targeting system, AH-64 Infra-red head tracker & HDU

The AH-1 and AH-64 helicopters both have weapon systems capable of being aimed by sensing the position of the helmet in the cockpit. The AH-1 Cobra uses a mechanical linkage attached directly to the helmet to measure the helmets position and orientation. The AH-64 Apache uses infra-red sensors mounted on the helmet to sense orientation.

6. PROTECTIVE REQUIREMENTS

The basic protective requirements for the Army helicopter aircrew helmet have become more stringent in an effort to improve aircrew safety. These requirements include impact, retention, tear resistance, and sound attenuation.

6.1 Impact protection

The helicoper aviator helmet protective requirements have

received considerable changes over the past 30 years. Table 7 provides some basic details on the requirements for each helmet. The APH-5 is not included in this table since its impact requirements were based on the "swing away" test method and are not comparable to the other helmets.

The HGU-56/P has the most stringent impact requirements. These requirements are also applicable to the RAH-66 Comanche helmet development efforts.

Table 7. Impact performance requirements.

Helmet	Impact site	Impact velocity (m/s)	Peak accel (G)
SPH-4			
flat	all	5.3	400
hemi	all	5.3	400
SPH-4 (1982)			
flat	all	5.3	300
IHADSS			
flat	all	5.3	300
SPH-4B			
flat	earcups	6.0	175
flat	other areas	6.0	250
HGU-56/P			
flat	crown	4.9	150
flat	earcup	6.0	150
flat	headband	6.0	175

The headband region acceleration threshold of 175 G was placed in order to prevent concussion to Army crewmembers in survivable mishaps [11]. Surviving a military mishap with a concussion is unacceptable due to potential hazards associated with military crash environments. Unconciousness could lead to an aviator's drowning or capture, depending on the crash location (water or enemy teritory) or burns in the presence of a postcrash fire. Aircrew must remain concious during survivable mishaps to quickly egress the crashed aircraft, provide assistance to fellow crewmembers, and evade hostile search parties.

The 150 G requirement for the crown and earcup region were established to reduce the potential of basilar skull fractures when impacted at those sites [11]. The impact velocity for the crown impact was reduced because direct blunt crown impact at the greater velocity rarely occurs in survivable mishaps.

Impact tests are required to be conducted on a guided freefall drop tower assembly configured in accordance with the American National Standards Institute ANSI Z90.1-1971 [12]. The USAARL helmet impact tower is shown in Figure 14.
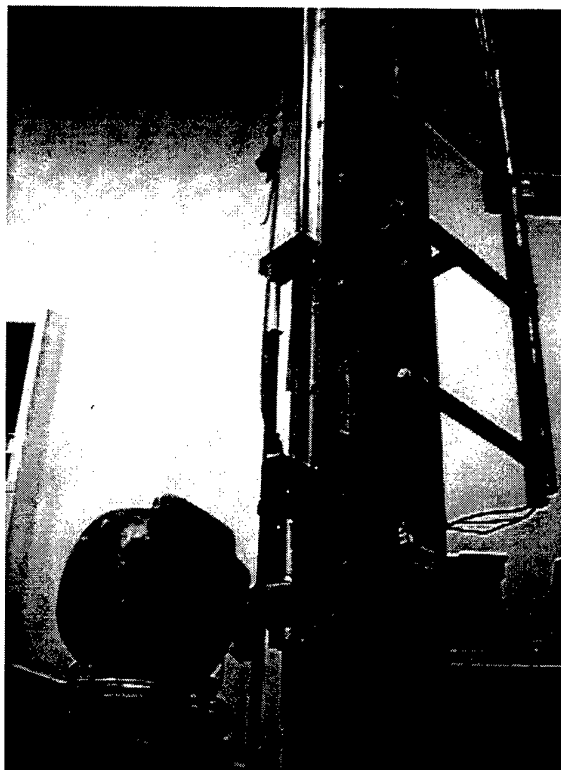
Figure 14. USAARL helmet impact tower.

For the crown and headband impacts, headforms conforming to the Department of Transportation (DOT 218) size B, C, and D are used. Impacts to the earcup region require use of a modified size C headform. This modification includes the downward extension of the headform in the earcup region to increase the contact surface area. Material is removed from the inner surface of the headform to maintain the mass requirement of the size C headform.

All impacts for performance assessments are conducted onto flat impact anvils. The hemispherical anvil was eliminated after ALSERP investigators revealed less than 3 percent of helmet impacts resulted from hemispherically shaped objects, while flat surfaces accounted for over 60 percent [6].

6.2 Helmet retention
Helmet retention assessments are necessary to ensure the basic helmet system, if fitted and worn as designed, will keep the helmet properly positioned on the wearer's head. The Army currently requires only a static strength assessment be performed. In addition to the static test, USAARL routinely conducts dynamic retention tests for comparative purposes.

6.2.1 Static
The static retention test is conducted in accordance with ANSI Z90.1-1979 [13] with one exception, the preweight is 25 pounds instead of 50 pounds. As illustrated in Figure 15, this test requires a static load be applied through a simulated chin onto the chinstrap. The maximum strength and elongation requirements are provided in Table 8. Inspection of Table 8 reveals an increase in static strength

requirements. Again, this is a result of ALSERP findings of chinstrap and harness failures in accident helmets [6,7].

Table 8. Static retention requirements.

Helmet	Static strength (pounds)	Maximum elongation (inches)
APH-5	150	no separation
SPH-4	150	no separation
SPH-4 (1982)	300	no separation
IHADSS	300	no separation
SPH-4B	440	1.5
HGU-56/P	440	1.5

Figure 15. Chin strap static pull test setup.

6.2.2 Dynamic

The dynamic retention tests are conducted on a pendulum test device which has a Hybrid II head attached to a Hybrid III manikin neck at the end of the pendulum. Triangular shaped impact pulses from 10 to 15 G up to 25 to 30 G are applied to the pendulum beam in a rearward direction to the headform (a forward impact). The dynamic response of the helmeted head is recorded on video at 1000 images per second. Digitization of this data reveal relative angular displacements between the helmet and head. The test setup

is shown in Figure 16. Graphical results of a prior study are provided in Figure 17. No absolute pass and fail criteria currently exist for dynamic retention performance. New systems and modifications are compared to the standard SPH-4B and HGU-56/P aircrew helmets.

Figure 16. Dynamic retention pendulum tower.

6.3 Shell tear penetration

As a measure of shell integrity, a helmet shell tear penetration test is required on the HGU-56/P [11]. This requirement was not placed on any other helmet configuration, but the performance levels were established by testing standard SPH-4 (fiberglass) helmet shells.

Figure 17. Dynamic retention test results.

Figure 18. Helmet tear test penetrator.

The requirement is to drop a tear penetrator (shown in Figure 18) weighing 5 kg from a drop height of 1.52 meters. If the penetrator creates a tear length (measured along the shell surface) greater than 5 cm, the shell fails. The SPH-4 fiberglass helmet shells performed at this level. The SPH-4B Kevlar® shell and the IHADSS composite shell both fail to meet this requirement. This setup essentially tests the shell material in shear, in which graphite and Kevlar® perform poorly. The SPECTRA® rarely allows

tearing to initiate, but allows the shell to buckle unless it is rigidly supported on its underside.

6.4 Sound attenuation

The ability of aviator helmets to reduce ambient noise levels remains a primary requirement. The performance requirements do not represent desired limits based on aircraft noise environments and human tolerance to exposure levels, but a reflection of state of the art performance. Table 9 provides the performance requirements of the HGU-56/P helmet when tested in accordance with ANSI S12.6-1984 [14]. To supplement the basic helmet performance, earplugs are required to be worn under the aviator helmets.

Table 9. Sound attenuation requirements.

Frequency (hz)	HGU-56/P (dB)
125	17
250	14
500	20
1000	21
2000	26
3150	38
4000	37
6300	44
8000	42

7. REFERENCES

1. Bezreh, A.A., "Helicopter versus fixed wing crash injuries," Aerospace medicine, Vol. 34, No. 1, January 1963.

2. Berner, W.H., and Sand, L.D., "Deaths in survivable aircraft accidents," Aerospace medicine Vol. 42, No. 10, October 1971.

3. Shanahan, D. F., and Shanahan, M.O., "Injury in U.S. Army helicopter crashes fiscal years October 1979-September 1985," Journal of trauma, 1989, 29(4):415-423.

4. Shannon, S.G., Albano, J.P., and Licina, J.R., Head injury risk in U.S. Army rotary-wing mishaps: Changes since 1980. AGARD Specialist Meeting on Impact Head Injury, 7-9 November 1996, Mescalero, New Mexico.

5. Department of Defense, "Light fixed- and rotary-wing aircraft crash resistance," Washington, DC, 26 September 1988, MIL-STD-1290A(AV).

6. Reading, T.E., Haley, J.L., Jr., Sippo, A.C., Licina, J. R., and Schopper, A.W. 1984. SPH-4 U.S. Army flight helmet performance, 1972-1983. Fort Rucker, AL: U.S. Army Aeromedical Research Laboratory. USAARL Report No. 85-1.

7. Vyrnwy-Jones, P., Lanoue, B., and Pritts, D. 1988. SPH-4 U.S. Army flight helmet performance, 1983-1987. Fort Rucker, AL: U.S. Army Aeromedical Research Laboratory. USAARL Report No. 88-15.

8. Shanahan, D.F., "Basilar skull fracture in U.S. Army aircraft accidents, Aviation, space, and environmental medicine. Vol. 54, No. 7, pp.628-631. July 1983.

9. Chamouard, F., Tarriere, C., Got, C., Guillon, F., Patel, A., and Hureau, J. 1986. Relationship between some biomechanical and dimensional characteristics of the skull and the risk of cerebral injuries. Zurich, Switzerland: International IRCOBI Conference on the Biomechanics of Impacts. International Research Council on Biokinetics of Impacts.

10. Department of Defense, "Visor, flying helmet, polycarbonate," Washington, D.C. Military Specification MIL-V-43511.

11. Fabrication specification, "Aircrew integrated helmet system fabrication specification," St. Louis, MO: U.S. Army Aviation and Troop Command. 1680-ALSE-101.

12. American National Standards Institute. 1971. Specification for protective headgear for vehicular users. New York: American National Standards Institute. ANSI Z90.1-1971.

13. American National Standards Institute. 1979. Specification for protective headgear for vehicular users. New York: American National Standards Institute. ANSI Z90.1-1979.

14. American National Standards Institute. 1984. Method for the measurement of the real-ear attenuation of hearing protectors. New York: American National Standards Institute. ANSI-S12.6-1984.

Mass Requirements for Helicopter Aircrew Helmets

B. Joseph McEntire
Dennis F. Shanahan
U.S. Army Aeromedical Research Laboratory
USAARL, MCMR-UAD-CI, P.O. Box 620577
Fort Rucker, AL 36362-0577, USA

1. SUMMARY

Helicopter aircrew helmets are becoming more sophisticated with increased mission requirements. This increase results in additional mass being supported on the aircrew's head. Ultimately, there is a limit to how much mass can be supported by the aircrew without increasing the fatigue rates and neck injury risk in accidents. This paper reviews the past mass property requirements of Army helicopter helmets. Current requirements for the RAH-66 Comanche helmet are also detailed with the rationale for their derivation.

2. LIST OF SYMBOLS

AH-64	Attack helicopter
CM	Center of mass
cm	Centimeter
HMD	Helmet mounted device
HSD	Head supported device
IHADSS	Integrated helmet and display sighting system
kg	Kilogram
kg-cm	Kilogram-centimeter
M	Moment
m	Mass
N	Newtons
N-cm	Newton-centimeter
NVG	Night vision goggle
PM	Program manager
PNVS	Pilot night vision system
RAH-66	Reconnaissance attack helicopter
SPH-4	Sound protective helmet #4

3. SUBJECT MATTER KEYWORDS

Aircrew
Helmets
Protective headgear
Mass
Mass requirements
Mass properties
Center of mass
Center of gravity
Head supported devices
Helmet mounted devices

4. INTRODUCTION

The mass of the flight helmet used by fixed-wing and rotary-wing pilots has been a concern since "hard shell" helmets first appeared in the 1950s. These helmets were introduced to provide increased head protection during a crash, but at a significant weight increase over the previously worn cloth caps. The total headborne mass increased from 0.5 kg for the leather or cloth cap to 1.5 kg for early hard shell helmets which included noise-attenuating earcups, earphones, microphone, and integral, adjustable visors. The hard shell helmet, lined with polystyrene foam, provided an order of magnitude improvement in impact protection.

In the 1980s, the introduction of various visual enhancement devices further increased the mass to 3 kg for the standard Army sound protective helmet No. 4 (SPH-4) equipped with the pilot night vision system No. 5 (PNVS-5). The increased mass of this helmet system is believed to have a detrimental effect on pilot performance due to neck muscle strain and fatigue and, also, to increase the risk of severe neck injury in crashes. The disadvantages of increased helmet mass, however, are offset by the enhanced visual capability for night flying and increased weapons aiming capability offered by helmet-mounted image intensification devices and other helmet-mounted displays. In order to permit the use of 3 kg helmets without overloading the neck in severe crashes, the U.S. Army's night vision laboratory at Fort Belvoir, VA, developed a spring-loaded, ball-socket mount which permits the latest generation night vision device (AN/AVS-6) to break free during a crash. The 0.6 kg night vision goggle (NVG) device was designed to break free of the helmet at a goggle deceleration of 10 to 15 times the acceleration of gravity (G) (Military specification, MIL-A-49425(CR))[1]. Although this approach may offer one solution to the problem of increased head-supported mass in Army aviation, little is known about the dynamic behavior of this device in a crash or of the physical limitations of the human neck to support these masses.

In an initial attempt to define a safe limit on flight helmet mass for the Army, the United States Army Aeromedical Research Laboratory (USAARL) in 1982 proposed a limit of 1.8 kg (3.96 lb) during the development of the AH-64 Apache flight helmet [2]. The helmet system subsequently developed met this mass limitation while providing the desired visionics and required impact protection. Nonetheless, the SPH-4 helmet with NVG attached used for night operations in all other Army helicopters continued to exceed the proposed 1.8 kg limit by more than a full kilogram. Although there have been anecdotal reports from aviators complaining of considerable discomfort with this system, particularly after long missions, the effects on pilot performance of bearing this much mass has never been systematically studied. Furthermore, the dynamic consequences of crashing with head-borne masses approximating 3 kg remain largely speculative.

5. BACKGROUND

5.1 Helicopter helmet functions

The functional requirements of the helicopter pilot helmet have grown considerably. Traditional helmet functions include head impact protection and service as a mounting platform for communication systems, hearing protection, eye protective visors, and on occasion, oxygen systems. Increases in threats and operational effectiveness demand the helmet also serve as a mounting platform for such systems as weapon targeting, night vision or image intensification devices, flight symbology displays, chemical

defense masks, and nuclear flash protection. These require-
ments demand more complex mounting devices on the
helmet and, ultimately, result in increased system weights
and potentially less than optimal center of mass (CM)
placement.

5.2 Prior helmet mass requirements

Historically, helmet mass and CM requirements have been
nonexistent or vague. These requirements were often
loosely written and based on existing designs. Language in
helmet development specifications often resembled "the
helmet CM must be located as close to the head CM as
possible," "lighter and CM no worse than current helmet
systems," "provide ease of head movement," and "reduced
bulkiness." These requirements provided little guidance to
the design teams and could not be quantitatively evaluated.

5.3 Mass properties

Seven parameters are required to fully define the mass
properties of helmet systems. As illustrated in Figure 1,
these include mass, the center of mass position along three
orthogonal axes, and the mass moment of inertia about the
three respective axes. The coordinate system used by the
Army aviation community is based on the head anatomical
coordinate system and is illustrated in Figure 2 [3]. The x-
axis is defined by the intersection of the mid sagittal and
Frankfort planes with the positive direction anterior of the
tragion notch. The y-axis is defined by the intersection of
the Frankfort and frontal planes with the positive y-axis
exiting through the left tragion notch. The z-axis is ori-
ented perpendicular to both, the x- and y-axes following the
right hand rule.
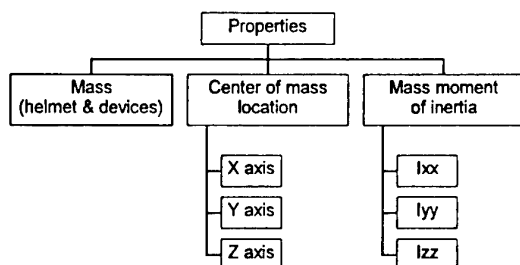
Figure 1. Parameters required to fully define helmet system
mass properties.

5.4 The need for mass property requirements

The reason for defining aviator helmet mass requirements
can be segregated into three areas; aircrew health, opera-
tional effectiveness, and user acceptance. Aircrew health
can be affected by both short- and long-term exposures of
head and neck loadings. Long term exposures are the result
of helmet mass and its mass center location in normal flight
conditions (vibration and 1 to 2 G flight environment).
These effects include discomfort from a sore or stiff neck
after normal missions. It is not uncommon to find Army
aircrew who admit "off-the-record" that they seek unauthor-
ized treatment for sore neck muscles. Treatments may in-
clude heat pads, topical ointments, neck rubs and massages
from spouses or masseuses, and chiropractic adjustments.

Short-term exposures may cause neck injuries resulting
from inertial loadings. Inertial neck loadings are created in
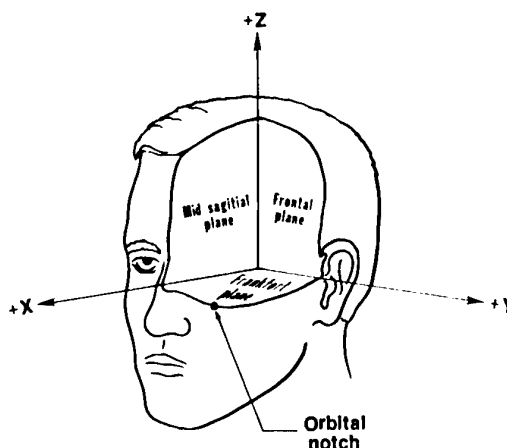
Figure 2. Head anatomical coordinate system.

high acceleration, short duration, dynamic crash environ-
ments. At high seat accelerations, neck loads are com-
pounded by helmet mass and improper center of mass
locations. These neck injuries can be low severity, such as
strains and muscle tears, or high severity, such as cervical
transections.

Aircraft crash environments also may cause direct and
indirect loading injuries to the neck. Direct loading injuries
are caused by objects physically striking the neck inflicting
tissue damage. Indirect loading neck injuries are caused by
the transfer of energy to the neck from a head impact. It is
assumed that neither direct nor indirect loading neck
injuries are influenced by the mass supported by the head.
Thus, these direct and indirect types of neck injuries are not
considered in the determination of allowable mass
properties for head supported devices.

The mass properties of head supported devices (HSD) also
can affect operational effectiveness by increasing aircrew
fatigue. Aircrew operating with high fatigue are less
efficient, have lower mental concentration ability, and are
more prone to commit mistakes. Little data is available on
fatigue effects in rotary-wing environments and is generally
based on small sample sizes and limited helmet mass and
CM positions.

Helmet stability also is affected by helmet mass and CM
placement. High helmet mass and misplaced center of mass
locations can result in helmet slippage relative to the
aircrew eye location. When helmet-mounted displays or
image intensification devices are used, helmet slippage
could effectively "blind" the aviator from receiving the
desired display information for effective aircraft control.

The final area which can be affected by head-supported
mass is user acceptance. The final configuration must be
acceptable to the final user prior to fielding to operational
units. Failure of a system to receive user acceptance will
result in misuse and abuse of the system and failure of the
system to achieve its desired operational capability. User
acceptability is difficult to define and quantify since each
aircrew has a subjective opinion. No data beyond anec-

dotal data on existing systems has been generated to quantify user acceptance of mass property limits.

6. APPROACH

The USAARL was asked to review head-supported weight requirements by the Program Manager, Comanche (PM-Comanche) of the Army Aviation and Troop Command (ATCOM) in St. Louis, MO. As a result of this review, a series of memoranda were submitted to PM-Comanche recommending changes to the mass property requirements of head-supported devices. Recommendations were made by USAARL to change the total allowable mass and the x- and z-axes CM locations. The recommended allowable mass requirement were based on neck tensile strength. The x-axis CM location was based on measured biodynamic responses of aviators wearing various helmet mass and CM combinations. The z-axis CM was based on maintaining a constant moment about the C7/T1 juncture resulting from the helmet mass and vertical CM position.

7. ANALYSIS

7.1 Inertia loading-neck injury mechanisms

It is important to define the mechanisms of neck injury when establishing mass limits on HMDs. McElhanney provides a good engineering description of neck loadings, which are reproduced in Figure 3 [4]. Two injury mechanisms are most likely to be affected by the mass properties of HMDs. These are axial tension and forward bending (flexion). Neck extension and neck compression injury mechanisms are not considered to be effected by HMD mass properties. This is based on current helicopter crew seat design requirements which include headrest and load limiting vertical energy absorption capabilities.

Shanahan and Shanahan, in a study of U.S. Army helicopter crash injuries from 1979-1985, found 82 reported spinal fractures [5]. Figure 4, taken from the Shanahan report illustrates the spinal fracture distribution by vertebral level. The cervical and upper thoracic vertebra with the highest frequency of fracture was the 7th cervical. The lower thoracic and the lumbar region experienced a higher frequency rate, but these injuries are believed due to compression loadings resulting from high vertical impact loads in precrashworthy seat designs. Cervical spine fractures comprise only 1.6 percent of the 1484 injuries sustained in survivable crashes. The cervical injuries were caused by either acceleration loadings or contact injury. No differentiation between these two injury mechanisms was made.

This review of helicopter crash injury indicates a lack of evidence supporting significant inertial neck injury for Army aviators wearing a 1.5-1.8 kg helmet. In some crashes, heavier helmets of 2.9 kg (including night vision components) have been worn, but the extra 1.1 to 1.4 kg mass of night vision goggles and counterbalance weights have broken free from the helmet and relieved the neck of this added loading. The non-documentation of inertial neck injury does not mean none occurred, but that the accident investigators failed to recognize this infrequent injury among the far more obvious contact, crushing, and spinal column injuries in the older, non load-limiting seats.
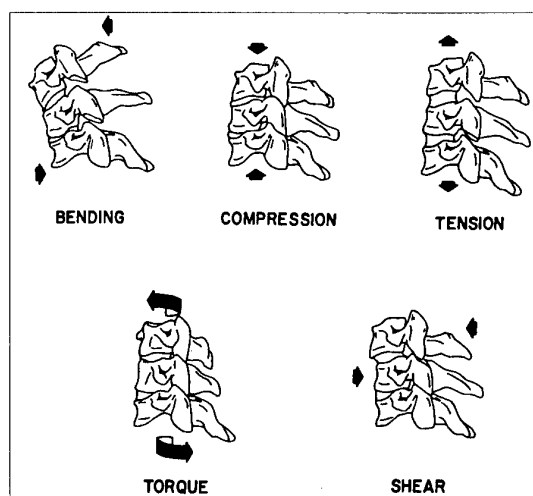
Figure 3. Engineering descriptions of neck loading.
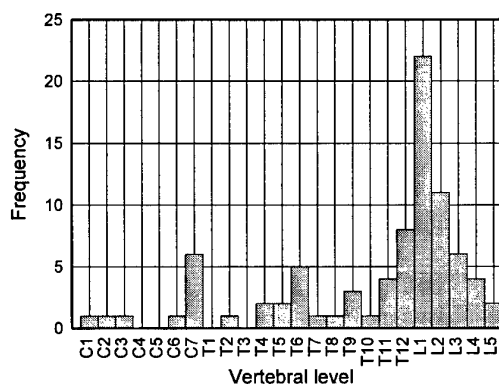
Figure 4. Frequency distribution of spinal fractures in class A and B survivable crashes as vertebral level.

7.2 Factors influencing inertial neck injury

Recent Army helicopter designs incorporate minimal levels of crashworthiness with specific performance levels for the crewseats. Helicopter crew seats are typically procured to military performance specifications with a 30G longitudinal static load requirement and a vertical energy absorption capability (Military specification, MIL-S-58095(AV)). [6] The 30 G longitudinal requirement is a structural integrity check of the seat and its mounting hardware to provide assurance that the seat will not be ripped from the floor. The vertical energy absorber is a mechanical device which restricts the vertical crashloads experienced by the occupant. The desired vertical load is an average of 14.5 G over the range of seat stroke. Peak loads of 18.3 G have been measured in anthropomorphic test dummies during seat qualification trials [7]. The worst case condition would be a seat experiencing 30 G longitudinally and stroking with a peak vertical load of 18.3 G. The resultant from these two loading vectors is 35 G directed 31.4 degrees downward from horizontal.

Aircrew restraint systems utilized in Army helicopters are either a traditional 4-point restraint system or a newer 5-point restraint. The primary difference between the two systems is that the 5-point system includes a center tie-down strap to reduce occupant submarining (movement of the pelvis under the lap belt). Dynamic tests with rigid seat structures have indicated a range of possible "dynamic overshoot" (the ratio of measured head or chest acceleration of a test dummy to the input floor or seat acceleration). This increase in acceleration results from harness slack, neck tissue stretch, and upper body compression (by contact with restraint harness) which allows a relative velocity to be created between the occupant and surrounding structure. The dynamic overshoot value is also dependent on when the shoulder strap inertia reel locks (which is activated by occupant motion). A dynamic overshoot value of 1.5 has been selected as the magnification of seat acceleration to the head acceleration; this is an average value based on dynamic tests of aircrew seats for the UH-60 Black Hawk helicopter.

7.3 Neck strength
A literature search was conducted to assess neck strength. This review (report is in draft form for USAARL publication) revealed data from military operational experiences [8], automotive accident injuries [9,10], volunteer [11,12], and cadaver test data [13,14], animal test data [15], and manikin injury assessment values [16]. Based on our analysis of this data, a neck tensile strength threshold of 4050 Newtons was selected as the maximum limit. It is believed that risk of serious neck injuries exist above this limit for the Army aviator population. This value is probably too great for populations other than military aviators since aviators generally are young and physically fit.

8. MASS PROPERTY LIMIT DETERMINATION

8.1 Mass requirements
The determination for maximum allowable HSD mass is based on Newton's second law; $F = ma$. This equation is used by considering the neck tensile strength threshold of 4050 Newtons and the acceleration environment of 35 G with a dynamic overshoot ratio of 1.5. The effective mass acting on the C7/T1 juncture can then be calculated as follows:

$$F = ma$$
$$m = F / a$$
$$m = 4050 / [(35) * (1.5) * (9.81)]$$
$$m = 7.86 \text{ kg}$$

The mass acting on the C7/T1 juncture includes the helmet, head, and neck. The total mass of the neck is included in this calculation to be conservative. By subtracting the head mass (4.32 kg) and neck mass (1.04 kg) from the above value, we arrive at the allowable helmet mass for the given impact condition.

$$m = m_{head} + m_{neck} + m_{helmet}$$
$$m_{helmet} = m - m_{head} - m_{neck}$$
$$m_{helmet} = 7.86 - 4.32 - 1.04$$
$$m_{helmet} = 2.5 \text{ kg}$$

8.2 Vertical CM requirements
The vertical center of mass limit is based on a constant

mass moment concept acting about the C7/T1 juncture. This rationale allows for greater helmet mass as the vertical CM location moves downward. The C7/T1 juncture was selected as the pivot point because, as noted by Shanahan [5], it is more frequently injured in helicopter accidents than upper cervical vertebra. Application of this theory requires selection of a HSD mass and vertical CM position to use as a constant mass moment. Lack of emperical data necessitated the selection of the "worst case" fielded helmet system, the AH-1 cobra helmet configuration, to establish an acceptable constant mass moment. This helmet configuration has a mass of 1.74 kg and a vertical CM location of 5.2 cm above the tragion notch. The final variable needed to determine the constant mass moment is the vertical distance between the C7/T1 juncture to the tragion notch [17]. A value of 11.94 cm was selected which represents the 95th percentile female and the 85th percentile male.

To determine the constant mass moment, the definition of a mass moment is used: $M = md$. The mass is the helmet mass of 1.74 kg and the distance is the total distance of the helmet vertical CM position above the C7/T1 juncture (11.94 cm + 5.2 cm). This is calculated as follows:

$$M = md$$
$$M = (1.74) * (11.94 + 5.2)$$
$$M = 29.8 \text{ kg-cm}$$

This moment value can be used to establish a relationship between the vertical CM position and mass by rearranging the above equation as follows:

$$29.8 = m_{helmet} * (11.94 + Z_{helmet\ cm})$$
$$Z_{helmet\ cm} = (29.8 / m_{helmet}) - 11.94$$

Plotting this relationship results in the curve shown in Figure 5. The allowable mass is limited to 2.5 kg as determined above. Additionally, the allowable vertical CM position is limited to 5.2 cm since biodynamic reactions to higher CM locations are unknown. Plotting specific HSD mass and vertical CM values on the graph allows acceptability assessment.
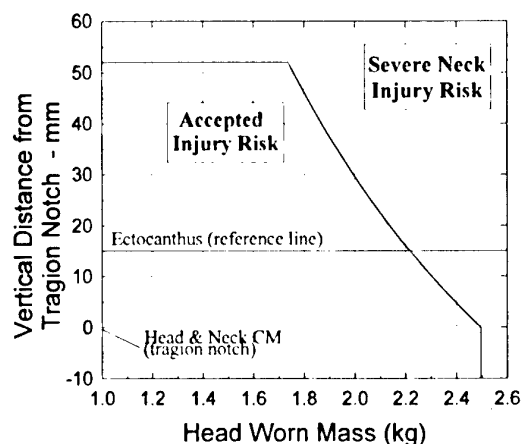
Figure 5. Vertical center of mass placement as a function of head worn mass.

8.3 Longitudinal CM requirements

The longitudinal CM locations of HSDs are believed to have greater effects on wearer fatigue and performance decrements than crash induced injury. Efforts have been conducted by Butler [18] to assess these effects by exposing volunteers to controlled helicopter ride environments with various helmet mass and CM configurations. During his study, Butler measured both physiological and biomechanical responses to the changes in HSD mass properties. The property changes included three masses (2, 3, & 4 kg) and four longitudinal CM positions (-2, 0, 2, & 4 cm) measured relative to the head center of mass. A head supported weight moment of 82.8 ± 22.8 N-cm, measured about the occipital condyles, was recommended based on changes in head pitch accelerations and posterior neck myoelectric responses. It was also recommended that negative moments be avoided. By using the recomended weight moment, including the tolerance (105.6 N-cm total), this value can be converted into a mass moment relative to the tragion notch and plotted. This relationship is shown in Figure 6. The rearward CM location was limited at -2 cm based on Butler's recommendation [18] that negative moment be avoided. Mass was limited at 2.5 kg as determined earlier. The forward limit was arbitarly set at 9.5cm.
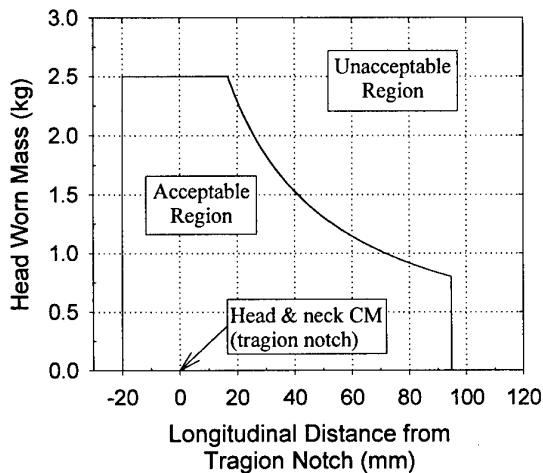
Figure 6. Allowable head-worn mass as a function of longitudinal center of mass placement.

8.4 Lateral CM requirements

No data has been identified to warrant changing the lateral CM requirements from 1.9 cm off the mid-sagittal plane. Operationally, the IHADSS helmet, which is used in the AH-64 Apache helicopter, possesses an off sagittal CM position when the monocular helmet-mounted display is attached. No neck injuries to the occupants involved in mishaps have been attributed to the lateral CM locations. This may be attributed to the breakaway capability of the HDU when exposed to contact forces and high accelerations.

9. RECOMMENDATIONS

The mass and center of mass requirements presented are based on limited data. Future efforts should be expended to increase the available human tolerance data and subsequently refine or change the presented mass requirements. These efforts should include defining human neck strength to various loading mechanisms, defining user tolerance to mass properties of head-supported devices, and defining fatigue affects of HSD mass properties. Epidemiological studies should be conducted to determine the incidence of chronic neck injury among aging and retired aircrew and its correlation to flight experience. Finally, numerical simulations of occupant loads in crash situations should be conducted to validate the presented HSD mass requirements.

10. ACKNOWLEDGMENTS

11. REFERENCES

1. Military Specification. Aviator's night vision imaging system, AN/AVS-6(V)1, AN/AVS-6(V)2. Fort Monmouth, NJ: HQ, U.S. Army Communications-Electronics Command. MIL-A-49425(CR).

2. Knapp, Charles. 1982. Letter to AAH Program Manager, subject: Production tolerances permissible for weight and center-of-gravity aspects of the IHADSS helmet. Fort Rucker, AL: U.S. Army Aeromedical Research Laboratory. February.

3. Rash, Clarence E., Mozo, Ben T., McLean, William T., McEntire, B. Joseph, Haley, Joseph L., Licina, Joseph R., and Richardson, L. Wayne. 1996. Assessment methodology for integrated helmet and display systems in rotary-wing aircraft. Fort Rucker, AL: U.S. Army Aeromedical Research Laboratory. Report No. 96-1. June 1996.

4. McElhanney, James H. 1993. Biomechanical aspects of cervical trauma. Accidental injury: Biomechanics and prevention, Nahum, Alan M., and Melvin, John W., eds. New York, NY: Springer-Verlag

5 Shanahan, D. F., and Shanahan, M. O. 1989. Injury in U.S. Army helicopter crashes fiscal years October 1979-September 1985. Journal of trauma. 29(4):415-423.

6. Military Specification. Seat system: Crashworthy, nonejection, aricrew, general specification for. Fort Eustis, VA: U.S. Air Mobility Research and Development Laboratory. MIL-S-58095(AV).

7   Melvin, J. W., and Alem, N. M. 1985. <u>Analysis of impact data from a series of UH-60 "Black Hawk" pilot seat tests</u>. Columbus, OH: Battelle Columbus Laboratories, Contract No. DAAG29-81-D-0100.

8. Schall, D. G. 1989. Nonejection cervical spine injuries due to +Gz in high performance aircraft. <u>Aviation, space, and environmental medicine</u>. Washington, DC: Aerospace Medical Association. May 1989. Vol. 60, p. 445.

9. Foret-Bruno, J. Y., Tarriere, C., LeCoz, J. Y., Got, C., and Guillon, F. 1990. Risk of cervical lesions in real world and sumulated collisions. In: <u>34th annual proceedings: Association for the advancement of automotive medicine</u>. Des Plaines, IL: AAAM. pp. 373-389.

10. Larder, D. R., Twiss, M. K., and MacKay, G. M. 1985. Neck injury in car occupants using seat belts. In: <u>American association for the advancement of automotive medicine</u>. Des Plaines, IL: AAAM. Pp. 153-168.

11. Ewing, C. L., Thomas, D. J., Sances, A., Jr., and Larson, S. J., Eds. 1983. <u>Impact injury of the head and spine</u>. Springfield, IL: C. C. Thomas.

12. Hearon, Bernard F., and Brinkley, James W. 1985. Psychomotor performance after forward-facing impact. <u>Aviation, space, and environmental medicine</u>. Vol. 56, No. 11, pp. 1043, 1051. November.

13. Cheng, R., Yang, K.H., Levine, R.S., King, A.I., and Morgan, R. 1982. Injuries to the cervical spine caused by a distributed frontal load to the chest. In: <u>Proceedings of the 26th Stapp car crash conference</u>. Warrendale, PA: Society of Automotive Engineers. SAE paper No. 821155. October. pp. 1-40.

14. Walsh, Michael J., and Kelleher, Barbara, J. 1978. Evaluation of air cushion and belt restraint systems in identical crash situations using dummies and cadavers. In: <u>Proceedings of the 22nd Stapp car crash conference</u>. Warrendale, PA: Society of Automotive Engineers.

15. Clarke, T.D., Smedley, D.C., Muzzy, W.H., Gragg, C.D., Schmidt, R.E., and Trout, E.M., 1972. Impact tolerance and resulting injury patterns in the baboon: Air Force shoulder harness-lap belt restraint. In: <u>Proceedings of the 16th Stapp car crash conference</u>. Warrendale, PA: Society of Automotive Engineers. SAE paper No. 720974.

16. Mertz, Harold J. 1993. Anthropomorphic test devices. <u>Accidental Injury: Biomechanics and prevention</u>. Nahum, Alan M. And Melvin, John W., eds. New York, NY: Springer-Verlag.

17. Donelson, Sarah M., and Gordon, Claire C. 1991. <u>1988 Anthropometric survey of U.S. Army personnel: Pilot summary statistics</u>. Natick, MA: U.S. Army Natick Research, Development, and Engineering Center. Technical report No. TR-91/040. July 1991.

18. Butler, B.P. 1992. <u>Helmeted-head and neck dynamics under whole-body vibration</u>. Ph.D. Dissertation, University of Michigan, Ann Arbor, MI.

Inflatable Restraint Systems for Reducing Head Injury

Richard E. Zimmermann
Gershon Yaniv
Simula, Inc., 10016 S. 51st Street
Phoenix, AZ 85044, USA

1. SUMMARY

Inflatable restraint systems, in the form of "air bags," are widely recognized as an effective means of reducing crash injury in automobiles. In order to provide similar crash injury protection in both commercial and military aircraft, a variety of inflatable restraint systems are now being developed.

For commercial aircraft, the Passenger Air Bag System, (PABS) will provide protection for occupants in seats positioned behind bulkheads, galleys, or restrooms. The first application of PABS will be on the Jetstream J-41 aircraft.

For military aircraft, a number of inflatable restraint systems are also being developed for the special conditions found in their crewstations. In addition to the Cockpit Air Bag System (CABS) that has similarities to automotive air bags, there is the Inflatable Body and Head Restraint System (IBAHRS) for use in some attack helicopters, and the Inflatable Tubular Structure (ITS) for use in small helicopters.

2. INTRODUCTION

Although air bags are now commonplace in automobiles, the development and acceptance of the product took many years. In 1953, John W. Hetrick was awarded U.S. Patent No. 2,649,349 for an automobile air bag system. However, this patent had been expired for nearly 20 years before Government regulations finally required air bags to appear as standard equipment in new U.S. automobiles.

The application of air bags in aircraft has taken even longer. However, recently developed air bag systems will be installed in some commercial and military aircraft within the next year.

3. SPECIAL DESIGN REQUIREMENTS FOR AIRCRAFT APPLICATIONS

Although the basic technology of automotive air bags is applicable, there are many special design requirements for aircraft applications. For example, aircraft instruments and controls are quite different from those used in automobiles, and less space is available for air bag modules.

The design of inflatable restraints for aircraft is also more complex than for automobiles because of the more complex crash dynamics. Aircraft typically crash with vertical, lateral, and forward velocity components. There may also be angular velocities about all axes. Aircraft crashes frequently involve several severe impacts. Sometimes an aircraft will strike trees or other large objects before it hits the ground. Helicopters, which are often quite narrow and top-heavy, can roll and experience a side impact after the initial impact. Therefore, inflatable restraints must be designed to protect the occupant in a lateral as well as a forward impact, and must remain inflated over a more extended period of time.

The design of a crash sensor for aircraft also becomes appreciably more complex. For an automobile, a single-axis sensor may be adequate. For helicopters, the sensor should be capable of multi-axis impact sensing. Ideally, it should respond with the proper sensitivity for all possible impact attitudes with any combination of forward, lateral, and downward velocities.

Components for aircraft usually have stringent environmental test requirements, which include high- and low-temperature, humidity, salt, fog, vibration, and EMI testing. Exposure to high levels of electromagnetic radiation is also a concern, as is exposure to severe electrostatic discharges. The latter requirements have a particularly significant impact on the system design. All components and cables must be protected with shielding. Equipment operating onboard an aircraft may also be subjected to unique environments caused by severe maneuvers, turbulence, hard landings, gunfire vibration, and rocket launching. The crash sensor must be designed to avoid inadvertent activation under all such conditions.

The design of an inflatable restraint may also be influenced by the equipment worn by military crewmembers. Aircrew members may wear a variety of equipment, including, but not limited to, survival vests, body armor, life vests, exposure suits, parachutes, and helmets. This equipment increases the bulk and mass of the occupant, and may complicate the effectiveness of an

inflatable restraint. Direct interaction between the bag and the crewmember's gear may also present unique design problems, such as those caused by snagging of the air bag during deployment or puncturing of the air bag after deployment.

Combustible materials used in commercial aircraft must comply with FAA flammability requirements. Specifications for military aircraft often include similar requirements. To comply with FAA flammability requirements, aircraft air bag systems must be made from different materials than those used in automotive air bags.

4. PRIOR DEVELOPMENT WORK

The idea of using an inflatable restraint to enhance survivability in an aircraft crash has been explored intermittently for more than 50 years. In a 1976 AGARD paper, Snyder summarized some of the early explorations of this idea. Although the earliest concepts for inflatable restraints for aircraft required pre-inflation before the crash, the self-inflating feature has been under consideration for nearly 40 years.

In particular, Snyder cited a 20-year-old (in 1976) engineering research study conducted for the FAA to develop a concept for an inflatable restraint for general aviation aircraft. He also cited three international conferences on aircraft air bags conducted between 1967 and 1976. An example of some of the past work on inflatable restraint applications is a prototype air transport seat air bag designed and fabricated in 1973. The prototype air bag was designed for the McDonnell Douglas DC-10, and was mounted in the back of the seat. Several working prototypes were fabricated, but there is no indication that they were ever dynamically tested.

5. NEED FOR AIRCRAFT AIR BAGS

The frequent and severe head injuries that occur in aircraft crashes provided the motivation for recent efforts to apply air bags in aircraft. For commercial aircraft, Government regulations required enhanced passenger protection, and industry has explored various ways of achieving it. In the case of military aircraft, the U.S. Army and the U.S. Navy sought ways to reduce serious head injury to highly trained crewmembers. The development of inflatable restraints eventually became the approach selected for achieving this goal.

In 1988, aviation regulations in the U.S. and Europe were amended to upgrade passenger protection in a crash (Amendment 25-64 to FAR 25 and Change 13 to JAR 25). These amendments require dynamic impact certification tests of seat structure, and impose a limit on the severity of head impact with other seats or aircraft structure. Compliance with the limitations on head

impact for passengers seated immediately behind bulkheads, lavatories, galleys, and class dividers was particularly difficult because of the large relative velocities which can develop prior to head impact with the rigid, fixed surfaces. A means of reducing this impact severity was required.

Head injury is the most frequent injury in crashes of the UH-60 Black Hawk and the AH-64 Apache helicopters, even though both aircraft have optimized five-point restraint systems developed in accordance with the general specification for crash resistant aircrew seat systems, MIL-S-58095A (AV). In a practical crewstation, where space is limited, a MIL-S-58095 restraint cannot prevent head injury in all survivable crashes. Neither can all possible contact surfaces be delethalized to the extent required to prevent injury in all survivable crashes.

Figure 1, reproduced from the Aircraft Crash Survival Design Guide (Reference 1), shows head motion with a double shoulder harness restraint in a 30-G forward impact. As shown, 20 in. of forward head displacement is possible. Even greater head motion may occur if the deceleration includes a downward component that will cause more compression of the body, and therefore, more slack in the restraint system. Since existing restraints cannot prevent head injury in all survivable crashes, some form of enhanced head and/or body restraint is needed. Therefore, there is a need for effective inflatable restraint systems that can prevent or at least reduce the severity of occupant impact with lethal structure and/or objects inside the crewstation.
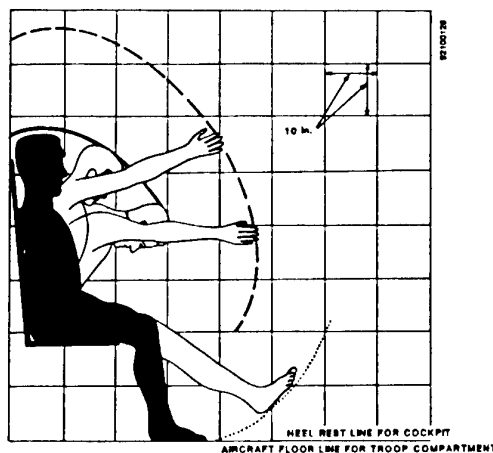
Figure 1.
Full-restraint extremity strike envelope (10-in. squares).

6. SYSTEMS AND APPLICATIONS

A number of inflatable restraint systems are or will soon be available for commercial and military aircraft. For commercial aircraft, the first product available will be the Passenger Air Bag System (PABS). For military aircraft, the Cockpit Air Bag System (CABS), the Inflatable Body and Head Restraint System (IBAHRS), and the Inflatable Tubular Structure (ITS) are being introduced.

6.1 Passenger Air Bag System (PABS)

Simula explored various means for reducing the severity of passenger head impact with an aircraft bulkhead. Among the possibilities were padded bulkheads, shoulder harnesses, and special seat structures designed to reduce the forward motion of the body. Simula determined that an air bag system would provide the most effective protection in most applications, and proceeded to develop such a system.

Figure 2 shows the air bag system concept with air bag modules mounted on the bulkhead and a crash sensor subsystem mounted on proximate and rigid airframe structure. Because the occupants are restrained by only a lap belt, and because of the significant distance between the bulkhead and the occupants, the design of an effective bulkhead-mounted air bag system was a particular challenge. After considerable analysis, development, and testing, an air bag design evolved which performed as required. This air bag is inflated by a gas generator specifically designed for the system. The gas generator uses materials which are non-toxic both before and during inflation. Individual air bags are provided for each occupant to provide adequate protection even if the sizes of the occupants vary greatly.

The performance of a prototype bulkhead system was first evaluated at Simula's dynamic test facilities in Phoenix, Arizona. After appropriate adjustments were made to optimize system performance, a second-generation prototype system was fabricated. This prototype was dynamically tested in the FAA's Civil Aeromedical Institute (CAMI) in Oklahoma City, Oklahoma.

The CAMI test setup is shown in Figure 3. A panel mounted on a steel truss simulated the bulkhead, and the air bag module was mounted on it in the appropriate position. The simulated bulkhead and a seat were mounted to the dynamic test facility with a 35-in. setback
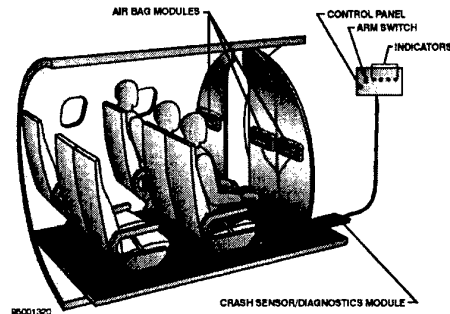
Figure 2.
Bulkhead air bag system.

distance, and an instrumented anthropomorphic test dummy (ATD) was secured in the seat with the conventional lap belt restraint system. The ATD's instrumentation included a triaxial accelerometer in the head to provide data for the calculation of the Head Injury Criterion (HIC).

The dynamic test facility applied the longitudinal deceleration pulse shown at the top of Figure 4 in accordance with the relevant aviation regulations. The air bag system functioned as intended, and the maximum excursion of the ATD during the deceleration is shown in Figure 5. Two tests were conducted with 0 degrees of yaw, and two tests were conducted with 10 degrees of yaw. The resulting data is shown in Table 1. All HIC values were well below the maximum allowable value of 1,000 and showed that the system performs as well as or better than required.

Table 1. CAMI Sled Test Results			
Yaw (Deg)	Target Crash Pulse Peak Accel. (G)	Actual Crash Pulse Peak Accel. (G)	HIC
0	16	16.9	874
0	16	16.7	658
10	16	16.6	811
10	16	16.3	788
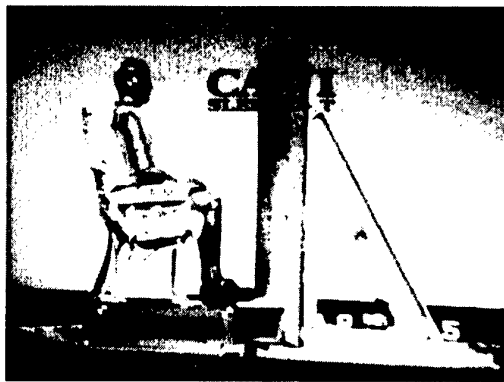
Figure 3.
CAMI Test Setup.

Figure 5.
Maximum displacement of anthropomorphic test dummy (ATD).
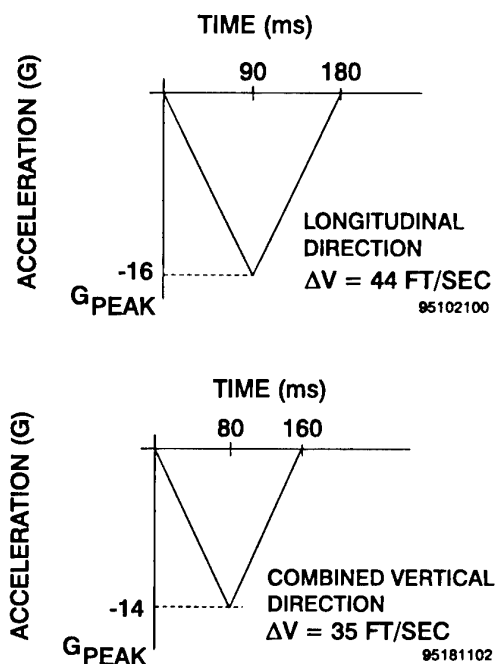
Figure 4.
Dynamic Crash Pulses.

Following the successful prototype development program, Simula offered the bulkhead air bag system to the airline industry. Simula subsequently entered into a contract with a launch customer, Jetstream. Consequently, development of the production design for the first bulkhead air bag system is nearing completion at this time. It is expected that certified systems will be installed in Jetstream's J-41 commuter aircraft in early 1997.

In the J-41, the seat-reference-point-to-bulkhead setback distance is just 29 in. The system designed for this application performed even better than the prototype did. Four tests were performed with the double-occupant seat behind the starboard wardrobe, and one was performed with the single seat behind the port-side partition.

The results are shown in Table 2, and all the HIC values are below 550, except for Test No. 4. In that test, there was no air bag installed in the left-hand seat. Because there was no air bag in the left-hand seat, the dummy in the right-hand seat slipped off of the air bag due to the yaw, and its head hit the bulkhead in front of the left-hand seat. The deployment of a complete three-bag system will prevent this result, because the adjacent bag will not allow the head to slip off the primary bag.

The performance-proven bulkhead air bag system now provides the most space-efficient means of complying with current aviation regulations for seats installed behind bulkheads.

6.2 Inflatable Body and Head Restraint System (IBAHRS)

Exploratory development of the concept for IBAHRS was conducted at the Naval Air Development Center (now the Naval Air Warfare Center) in Warminister, Pennsylvania, under a jointly sponsored U.S. Army/ U.S. Navy program. Simula was subsequently awarded a contract to develop an IBAHRS for the AH-1F Cobra and AH-1W Super Cobra attack helicopters.

The IBAHRS includes a MIL-S-58095 restraint system with air bags attached to the shoulder harness straps. Each air bag contains a pyrotechnic gas generator which inflates the bag when activated by the crash sensor. The components of the system are illustrated in Figure 6.

| | | Seat Occupancy (Part 572 ATD) Port/Starboard | | Impact Conditions Peak G | | HIC Port/Starboard | |
Test	Test Configuration	L/H	R/H	AP (G)	DV (ft/sec)	L/H	R/H
1	Starboard Wardrobe L/H Air Bag Only	- X -		164 (10° Left Yaw)	44.7	- 386.6	-
2	Starboard Wardrobe L/H Air Bag R/H Air Bag	- X	X	17.2 (10° Left Yaw)	44.9	- 278.8	534.5
3	Starboard Wardrobe Mock-up L/H Air Bag R/H Air Bag	- X	X	16.4 (10° Right Yaw)	44.6	- 242.4	366.1
4	Starboard Wardrobe Mock-up (R/H Air Bag Only)	- -	X	16.0 (10° Right Yaw)	44.2	- -	939.2
5	Port Partition	X	- -	16.5 (10° Right Yaw)	44.9	274.3	- -

Table 2.
Dynamic Test Results Summary
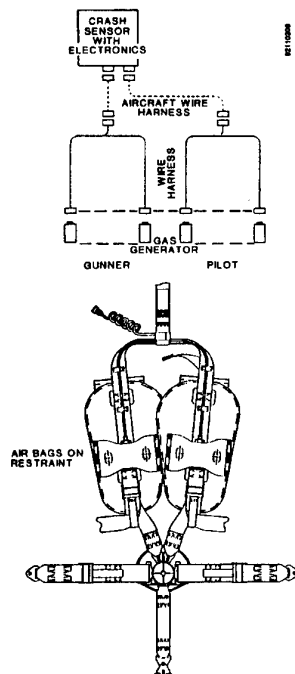
Figure 6.
Inflatable Body and Head Restraint System components.

The Simula program included design and development tasks to solve bag deployment problems identified during exploratory development work conducted by the U.S. Navy. Those problems included failure of the air bags to retain adequate pressure, as well as failure to remain in their proper position under the shoulder straps in every deployment. Satisfactory and reliable deployment was achieved through refinements of the air bag stowage and gas manifolding techniques, and was verified through dynamic testing at Simula and at NAWC-Warminster, Pennsylvania.

The pre-deployed and the deployed configurations of the IBAHRS are shown in Figures 7 and 8. In the present patented design, the air bags are attached to the back side of the shoulder harness strap, but the folded portion of each air bag is stowed on the front of the strap so that the bags can deploy reliably without interference from contact pressure between the strap and the occupant.

The deployed IBAHRS air bags remove slack from the restraint by occupying the space between the shoulder harness strap and the occupant. The top ends of the bags also support the head and neck, and reduce head motion relative to the torso. Both effects reduce the total head

Figure 7.
Stowed Inflatable Body and
Head Restraint System.

Figure 8.
Deployed Inflatable Body and
Head Restraint System.

occupant motion in a crash and make it less likely that the occupant's head will strike equipment or structure within the aircraft. Even if a head strike does occur, the severity of injury will probably be reduced.

The crash sensor is an integrated assembly including the acceleration sensor, firing circuit, and diagnostic, (self-check) circuitry. The sensor is connected to the aircraft power supply and the gas generators through a wiring harness installed in the aircraft for that purpose.

The sensing element and crash sensor electronics are mounted in the same case, along with capacitors which provide a reserve energy source. This enclosure is mounted on a rigid structure behind the copilot/gunner seat to ensure proper discrimination between crash and non-crash events.

The gas generators use a sodium azide propellant and are configured to fit within the stowed IBAHRS. They are mounted in manifolds on the front side of the system and distribute gas to both sides of the air bags to ensure that they inflate uniformly and remain properly positioned under the straps during deployment.

Simula-conducted system integration development tests consisted of dynamic tests with an ATD in a seat equipped with the IBAHRS. The tests were conducted using Simula's drop tower. They demonstrated that the design features meant to satisfy the Government-requested performance enhancements functioned as intended. The Simula air bag and manifold design resulted in optimal and reliable deployment, with the air bags remaining in their proper position under the straps.

The dynamic test criteria for the IBAHRS established by U.S. Navy specifications were selected to be consistent with the structural capabilities of the AH-1W Cobra helicopter (see Figure 9). After the production configuraton was finalized, 22 dynamic impact tests were conducted at the NSWC in Warminster, Pennsylvania, to verify compliance with performance specifications. The testing showed the system reduces the head trajectory by over 5 in., and prevents head impact with weapons sighting equipment in the AH-1 Cobra. Because the system included electronically actuated pyrotechnic devices, many specialized test facilities (listed in Table 3) were utilized during the entire qualification test program.

6.3 Cockpit Air Bag System (CABS)
A CABS is being developed for both the U.S. Army attack and utility helicopter crewstations. Attack helicopters, such as the AH-64 Apache manufactured by McDonnell Douglas Helicopters, typically have tandem

Dynamic Test Requirements (Forward)

CHANGE IN VELOCITY = 42 FPS

15 G

0.050 SEC
0.083 SEC
0.140 SEC

**Dynamic Test Requirements
(Combined Veritcal Drop)**

CHANGE IN VELOCITY= 38.5 FPS

23 G

0.025 SEC
0.048 SEC
0.081 SEC
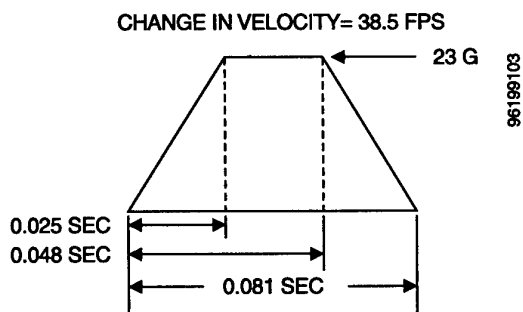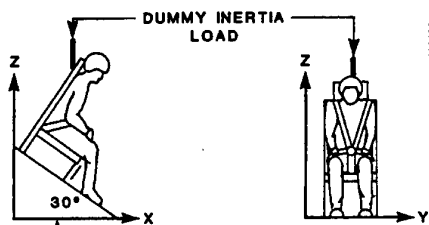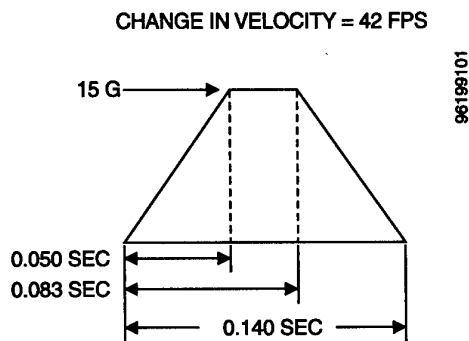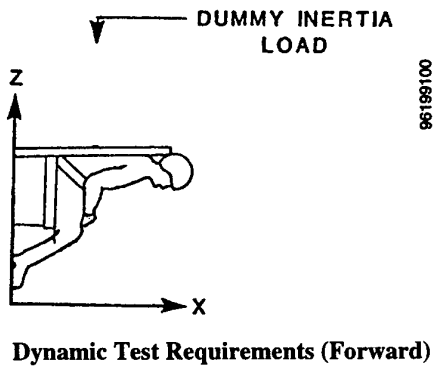
**Figure 9.
Dynamic Test Condition for Inflatable Body and
Head Restraint System.**

seating. Utility helicopters, such as the UH-60 Black Hawk manufactured by Sikorsky Aircraft, typically have side-by-side seating.

A prototype inflatable restraint system for an attack helicopter is illustrated in Figure 10. A prototype CABS installed in a crewstation mock-up in a dynamic test fixture is shown in Figure 11. The concept includes the use of three air bags to provide lateral and forward restraint. Lateral support is considered to be critical in attack helicopters because of their narrow cockpits and their tendency for post-crash rollover.

**Figure 10.
Three-air-bag system for attack helicopter.**

95128-08

**Figure 11.
AH-64 Apache helicopter crewstation mock-up
mounted in the dynamic test facility.**

Table 3. Government-Conducted Qualification Tests	
Test	**Agency/Location**
Inflator Service Release Test (SRT)	NOS, Indian Head, MD
Development Test (DT)	ATTC, Fort Rucker, AL
Hazards of Electromagnetic Radiation to Ordnance (HERO)	NSWC, Dahlgren, VA
Electromagnetic Environmental Effects	NAWC, Patuxent River, MD
Environmental Tests per MIL-STD-810	NAWC, Warminster, PA (Dayton T. Brown)
Dynamic Sled Tests	NAWC, Warminster, PA
Initial Operational Test and Evaluation (IOT & E)	TEXCOM/USAR, Minneapolis, MN

The aggressive performance criteria selected for the CABS are consistent with the upper limits of survivability expected in newly designed crashworthy helicopters.

Testing conducted at Simula has demonstated that it is possible to design a CABS to provide the desired head protection for these aggressive criteria. The criteria are expected to become a part of the requirements of a specification for the production CABS, and are illustrated in Figure 12.
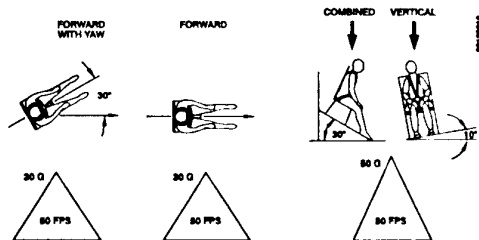
Figure 12.
Cockpit air bag system test conditions.

Inadvertent deployment tests were performed because of the frequently expressed concern that such a deployment could interfere with the pilot's ability to control the aircraft and lead to disastrous consequences. These tests were conducted in the AH-64 Apache Combat Mission Simulator at Fort Rucker, Alabama. The air bags were inflated with pyrotechnic gas generators to make the evaluation as realistic as possible. The tests were conducted with four different aviators. Each aviator was subjected to three deployments while flying a realistic

mission in the simulator. A total of seven different flight conditions were used, including high- and low-altitude flight, contour and nap-of-the-earth flying, hovering in and out of ground effect, and transitioning from forward flight to hover. A typical simulated flight maneuver is shown in Figure 13.
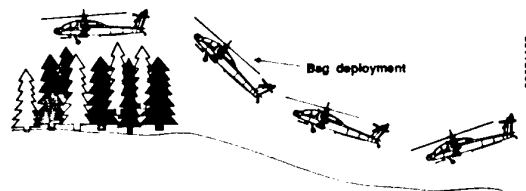
Figure 13.
Quick-stop and hover-flight maneuver.

The missions for each aviator were conducted in the order of increasing difficulty and were selected to approximate worst-case conditions for the influence of the deployment on the ability of the aviator to control the aircraft.

The inflation of the air bags produced no loss of control of the simulated aircraft. The aviators felt a mild sting on their arms and sometimes on their faces as the bags deployed, but there was no evidence of contusions or other injuries. They also sensed the heat from the hot gas, but no discomfort was noted because of the short duration. Furthermore, the deployments did not adversely affect the crewmember's fields of view. The tests demonstrated that an inadvertent deployment should not be a problem for an aviator, even if it occurs under difficult conditions.

The crash protection performance of the CABS concept was evaluated through multiple dynamic drop tests conducted at Simula. The dynamic tests were conducted in helicopter cockpit mock-ups. The mock-up

crewstations were equipped with transparencies and simulated consoles. The mock-up for an attack helicopter (Figure 11), also included a simulated weapons sight as a forward strike hazard. The crewstation mock-up used in conducting the dynamic tests for the Black Hawk helicopter CABS and a close-up of the interior are shown in Figures 14A and 14B.

Table 4 shows the typical performance capability of the CABS. It shows that serious or fatal head impact will be avoided by use of the CABS.

The CABS and the IBAHRS were also included in a crash test of an AH-1 Cobra attack helicopter that was conducted at the NASA Langley Research Center in Hampton, Virginia. There, the crash test was conducted by swinging an aircraft suspended by cables into a prepared impact surface. Just before impact, pyrotechnic guillotines cut the cables, so they would not interfere with the impact dynamics. Figure 15A shows the aircraft in the pre-test condition, and Figure 15B shows the aircraft at impact.

95050-16

Figure 14B.
Close-up of UH-60 Black Hawk crewstation mock-up.

Table 4. Typical Test Results		
Deceleration pulse: 30 G, 50 ft/sec		
		Impact direction: Forward
MAX Head Acceleration (G)	HIC	Comments
Without Air Bags 300	2,500	Chin hit weapons sight
With Air Bags 55	580	No headstrike
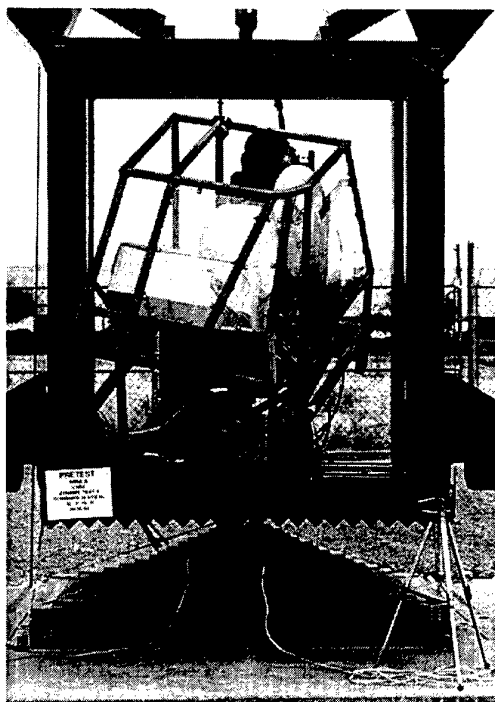
94123-14A

Figure 14A.
Half UH-60 Black Hawk helicopter
crewstation mock-up in dynamics test fixture.
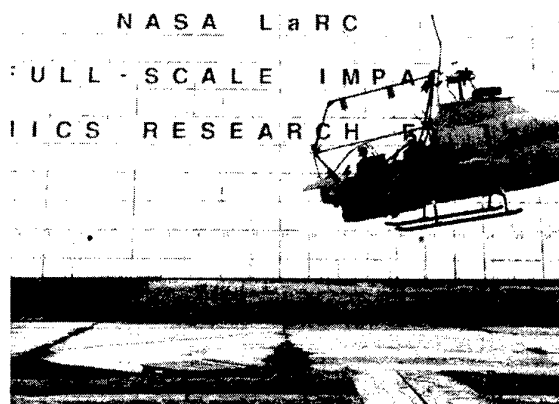
93148-03

Figure 15A.
Pre-test photo of AH-1 Cobra helicopter.
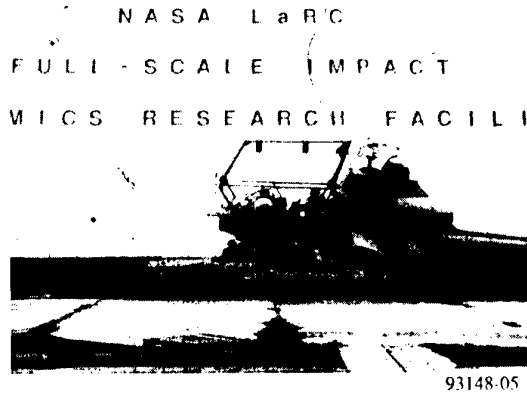
Figure 15B.
AH-1 Cobra helicopter at impact.

6.4 Inflatable Tubular Structure (ITS)

The ITS is a device developed to be fixed to an automobile's "A" pillar at one end, and to the roof rail aft of the "B" pillar at the other end, as shown in Figure 16.
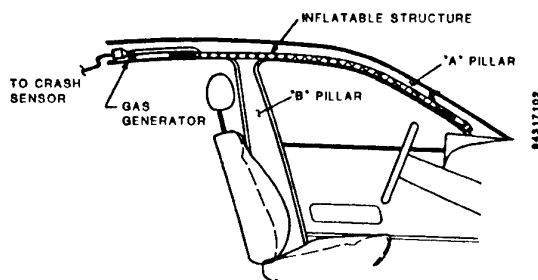
Figure 16.
The Inflatable Tubular Structure in a stored position.

It is inflated by a gas generator initiated by a side-impact crash sensor if the impact intensity exceeds a predetermined level.

The detailed packaging and the specific location of the gas generator are vehicle-dependent to facilitate optimum integration. In the event of a side impact, the gas generator fills the tubular structure with gas. As the tube inflates, it gets bigger in diameter and shorter in length (Figure 17), and pulls itself out from under the headliner. The ITS positions itself between the head of the occupant and the side of the vehicle and any intruding objects. (Figure 18).
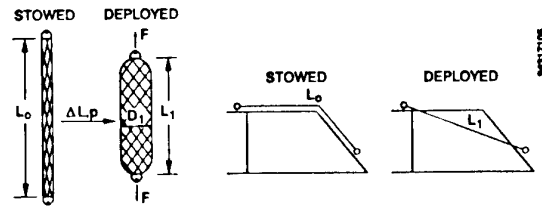
Figure 17.
Inflatable Tubular Structure principle of operation.
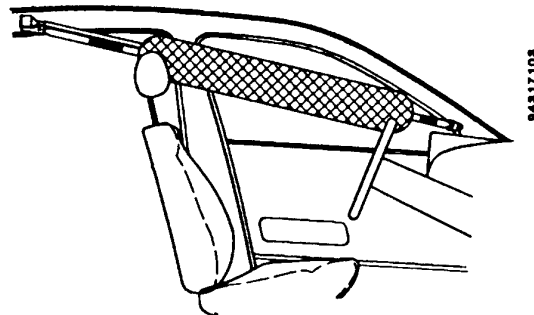
Figure 18.
The Inflatable Tubular Structure in a deployed position.

The location of the ITS end points at the "A" pillar and the roof rail determine the protection zone of coverage. The position and the orientation of the ITS were selected to protect a wide range of occupant sizes. Figure 19 shows how both 5th-percentile and 95th-percentile occupants would be protected without the need to perform any adjustments to the ITS.
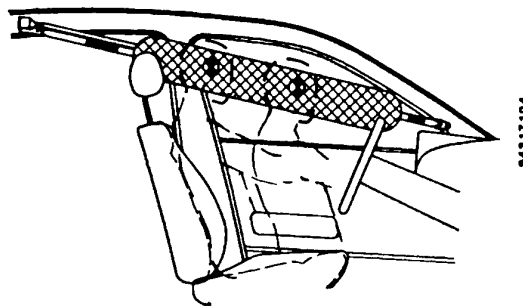
Figure 19.
Inflatable Tubular Structure protection for
5th- through 95th-percentile occupants.

The ITS performs two main functions:

1. In the absence of a bearing surface, the tension indirectly provides the reaction force. This way, the ITS can prevent the head from flailing out through the window plane, reducing the hazard of hitting external objects and of laceration from broken glass.

2. The pressurized, inflated ITS provides a cushion to blunt the impact of the head against hard objects such as the "B" pillar or window frame, and intruding objects, such as poles and trees.

Unlike conventional air bags, which deflate after about 150 msec from the start of deployment, the ITS is not vented immediately after deployment. Since the pressure of the ITS is well over one (1) bar, the relatively slow reduction in gas volume due to cooling allows the ITS to provide protection for several seconds. Should a roll-over occur following a side-impact accident, the ITS would still provide protection. The deployed ITS would also reduce the potential of the occupant's ejection through the window.

A significant number of static deployments, sled tests, and several full-scale crash tests have been conducted to examine the performance and kinematics of the ITS and the response of an instrumented test dummy.

Sled tests include impacts of the dummy's head with the car interior (e.g., the "B" pillar), and with a simulated intruding pole. Sled tests were also conducted with the dummy's head passing through the window (no head impact). These sled tests were conducted at different impact velocities.

Figure 20 shows the inherent benefits of the ITS in reducing head injury as demonstrated in a full-scale pole intrusion side impact crash test. The test was conducted with an impact velocity of 40 km/h with a resulting deceleration pulse. A Eurosid instrumented test dummy was used. When tested without the ITS, the maximum resultant head acceleration due to contact with the intruding pole was about 340 G, which translated to a Head Injury Criterion (HIC) of 1,600. Repeating the test with an ITS resulted in a significant reduction of the resultant head acceleration to about 80 G and a HIC of less than 500. The obvious conclusion, based on the measured head deceleration time-histories, is that the impact without the ITS would probably have resulted in a fatality; whereas, the impact with the ITS would probably not have been injurious.

POLE INTRUSION - FULL-SCALE SIDE IMPACT CRASH TEST
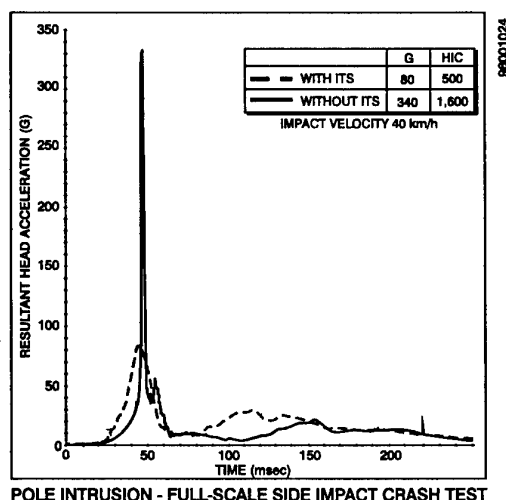
Figure 20.
Typical sled tests results with and without the
Inflatable Tubular Structure.
Head impact target - "B" Pillar.

The ITS also has the potential to solve unique restraint problems in aircraft. For example, in very small and lightweight helicopters, there is either insufficient room for a conventional side air bag to deploy and/or there is not enough structure to provide a surface to react the air bag restraining loads. The ITS however, can provide protection in such helicopters. The concept for a small helicopter application is illustrated in Figure 21. Two ITS assemblies are shown installed in combination with more-conventional frontal air bags.
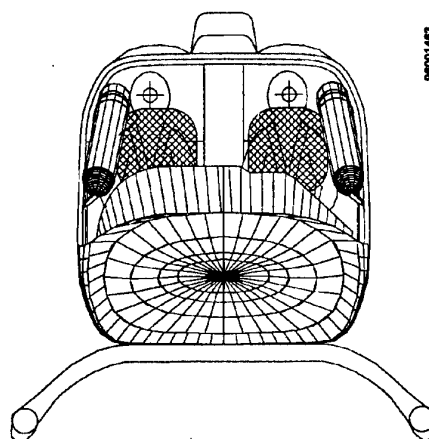
Figure 21.
ITS/CABS in small
helicopter-front view.

7. CONCLUSION

The IBAHRS, CABS, PABS, and ITS are all through or nearly through the development process and kits will soon be installed in various aircraft and automobiles. It is anticipated that future statistics will show a marked reduction in head injury resulting from the application of these systems.

REFERENCES

1. Aircraft Crash Survival Design Guide, Volume II, Aircraft Design, Crash Impact Conditions and Human Tolerance, Volume III, Aircraft Structural Crash Resistance, Volume IV, Aircraft Seats, Restraints, Litters, and Cockpit/Cabin Delethalization, TR-89-D-22-B, C, D, Aviation Applied Technology Laboratories (AVRADCOM), Fort Eustis, Virginia, December 1989.

BIBLIOGRAPHY
Inflatable Restraints (Aircraft Only)

1. Alem, N. A., Shanahan, D. F., Barson, J., Muzzy, W., The Air Bag as a Supplement to Standard Restraint Systems in the AH-1 and AH-64 Attack Helicopters and its Role in Reducing Head Strikes of the Copilot/Gunner, U.S. Army Aeromedical Research Laboratory, Fort Rucker, Alabama, USAARL Report No. 91-6, January, 1991.

2. Bark, L. W., Schmickley, D. L., "Optical Flash Effects of Inadvertent Cockpit Air Bag Deployment on an Aviator's Night Vision Imaging System," paper presented at the American Helicopter Society (AHS) National Technical Specialists Meeting on Avionics, Crew Systems Integration, and Simulation Technology, Bridgeport, Connecticut, October 6-7, 1993.

3. Bark, L. W., Zimmermann, R. E., Smith, K. F., "Inadvertent Helicopter Air Bag Deployment - Evaluation of the Effects in a Flight Simulator," paper presented at the 49th Annual American Helicopter Society Forum, St. Louis, Missouri, May 19-21, 1993.

4. Barth, T. H., "Air Bag Systems in Aircraft," paper presented at the International Conference on Cabin Safety Research, Atlantic City, New Jersey, November 15, 1995.

5. Barth, T. H., "The Bulkhead Air Bag System - Head Strike Protection for Passenger Aircraft," paper presented at the SAE General, Corporate, and Regional Aviation Meeting and Exposition, Wichita, Kansas, May 3-5, 1995.

6. Barth, T. H., Cote, G. "Development of a Passenger Aircraft Air Bag System," paper presented at the 1995 SAFE Symposium, Reno, Nevada, 1995.

7. Domzalski, L., Inflatable Body and Head Restraint System (IBAHRS): Dynamic Gx Crash Simulation Test Program, NADC-84140-60, Aircraft and Crew Systems and Technology Directorate, Naval Air Development Center (NADC), Warminster, Pennsylvania, June 1984.

8. Domzalski, L., Inflatable Body and Head Restraint System (IBAHRS): YAH-63 Crash Test, NADC-84141-60, Aircraft and Crew Systems Technology Directorate, Naval Air Development Center (NADC), Warminster, Pennsylvania, June 1984.

9. Gragg, C. D., et al, "Evaluation of the Lap Belt, Air Bag and Air Force Restraint Systems During Impact with Living Human Sled Subjects," SAE, Proceedings of the 14th Stapp Car Crash Conference Report No. 700904, November 1970.

10. Gragg, C. D., et al, "Human Weight Distribution During Impact - Lap Belt, Air Bag and Air Force Harness Restraint Systems," Institute of Environmental Science Proceedings, 17th Annual Tech. Meet, Living in Our Environment, April 1971.

11. Greth, R. L., Shope, W. E., Pfaff, M. S., Smith, K. F., "Concept Feasibility Demonstration for Army Cockpit Delethalization Program." Paper presented at the American Helicopter Society 48th Annual Forum and Technology Display, Washington, DC, June 3, 1992.

12. Lorch, D., "Development of a Supported Air Bag Ejection Restraint (SABER) for Windblast Protection." U.S. Naval Air Development Center, Airtask No. F 414000. AD A109807, November 1981.

13. Loushine, T. M., Air Bag Protection of the Gunner in the U.S. Army Cobra AH-1Q, AD-A009-421, Army Material Command, Texarkana, Texas, April 1975.

14. McElhenney, J., Bohmueller, B., "Dynamic Performance of the Inflatable Body and Head Restraint System (IBAHRS)." Paper presented at the 1995 SAFE Symposium, Reno, Nevada, 1995.

15. Schultz, M., Bohmueller, B., "Dynamic Performance of the Inflatable Body and Head Restraint System (IBAHRS)." Paper presented at the American Helicopter Society 51st Annual Forum, Fort Worth, Texas, May 9-11, 1995.

16. Schwartz, M., "Feasibility Testing of a Body Inflatable Bladder (BIB) Restraint Device." U.S. Naval Air Development Center, Airtask No. WF-41-400-000, AD A078881, April 1979.

17. Shaffer, J. T., Brinkley, J. W., "Lateral (-Gy) Impact Tests with Inflatable Restraint Systems for Air Force Crew Escape Module Applications." Paper No. 740043, presented at the Society for Automotive Engineers (SAE) Automotive Engineering Congress, Detroit, Michigan, February 25 - March 1, 1974.

18. Shyulman, M., and McBinenny, J., "Inflatable Body and Head Restraint." U.S. Naval Air Development Center, Airtask No. WF-41-451-403, AD AO 46477, September 1977.

19. Smith, K. F., Bark, L. W., Zimmermann, R. E., "Crash-Protective Performance of a Helicopter Cockpit Air Bag System (CABS)." Paper presented at the American Helicopter Society 50th Annual Forum and Technology Display, Washington, D.C., May 11-13, 1994.

20. Snyder, R. G., "Advanced Technologies in Crash Impact Protection and Emergency Egress from Air Transport Aircraft," AGARD-AG-221, Advisory Group for Aerospace Research and Development (AGARD), Neuilly sur Seine, France, June 1976.

21. Snyder, R. G., "Evaluation of Inflatable ("Air Bag") Occupant Restraint Systems for Aircraft Application," A77-49951, Proceedings of the Survival and Flight Equipment Association's 14th Annual Symposium, San Diego, California, September 13-16, 1976.

22. Zenobi, J. T., "Development of an Inflatable Head/Neck Restraint System for Ejection Seats." U.S. Naval Air Development Center, Airtask No. WF41-451-403, AD AO 57124, December 1978.

23. Zimmermann, R. E., "Inflatable Restraint Systems for Aircraft," SAFE Journal, Volume 23, No. 4, July-August 1993.

24. Zimmermann, R. E., Rogers, J. P., "Crash Sensors for Inflatable Restraint Systems." Paper presented at the 1995 SAFE Symposium, Reno, Nevada, 1995.

25. Zimmermann, R. E., Smith, K. F., Vincenc, T. F., "Recent Helicopter Inflatable Restraint Developments." Paper presented at the 1995 SAFE Symposium, Reno, Nevada, 1993.

SIMULATIONS OF HEAD STRIKES IN HELICOPTERS AND THE ROLES OF RESTRAINTS, SEAT STROKE AND AIRBAGS ON THEIR REDUCTION

Nabih M. Alem
Amir A. Mobasher*
Frederick T. Brozoski*
David G. Beale**
U.S. Army Aeromedical Research Laboratory
USAARL, MCMR-UAD-CI, P.O. Box 620577
Fort Rucker, Alabama 36362-0577 USA
*UES, Inc.
Fort Rucker, Alabama, 36362-0577 USA
**Department of Mechanical Engineering
202 Ross Hall, Auburn University, Alabama 36849-5341 USA

1. SUMMARY

Injuries from head strikes remain the leading cause of fatalities in U.S. Army helicopter mishaps. The roles of the restraint system, energy absorbing seat stroke and airbags in preventing or reducing the severity of head strikes are explored in this paper using mathematical simulations. Starting with a baseline simulation of an actual AH-64 survivable mishap in which the pilot received fatal basilar skull injury, the effects of three parameters were examined: timing of inertia reel locking, stroking of the energy absorbing seat, and the presence of an airbag mounted at the instrument panel. Results of the simulations suggested that delay of inertia reel in locking at the appropriate time together with obstruction of seat stroking may have caused the pilot's head to strike the glare shield. When a head strike was unavoidable, simulations indicated that an airbag would have reduced its severity.

2. INTRODUCTION

The crashworthy design of modern Army helicopters has resulted in fewer injuries from the impact acceleration in survivable crashes. The injury reduction, primarily to the spinal column, may be attributed to the energy-absorbing seat design which limits the forces transmitted to the seated pilot. Head and upper torso injuries also have been addressed with various design concepts to cockpit interior components, such as the breakaway optical relay tube used by the gunner in the AH-64 Apache helicopter. Following the introduction of these energy-absorbing devices into the U.S. Army Apache and Black Hawk helicopters, the injuries sustained in Army helicopter crashes between 1980 and 1985 due to excessive accelerations have dropped relative to other helicopters [1]. Ten years later, the risk of injury to U.S. Army helicopters occupants during the 1990-94 period was reduced significantly, primarily due to a 50% drop in head injuries [2]. Despite the success of the crashworthy design of modern helicopters, flail injuries continue to occur and, in fact, outnumber acceleration injuries. Contact or flail injuries are produced in secondary collisions which result from inadequate restraints, collapsing structure, or a combination of both.

Total delethalization of U.S. Army helicopter interior systems is impossible because of operational requirements and design constraints. Further, current restraints systems are unable to prevent secondary impacts [3]. The use of some airbag protection for the gunner has been suggested for many years [4], but no acceptable system ever was

introduced into Army helicopters. More recently, the U.S. Army Aeromedical Research Laboratory (USAARL), Fort Rucker, Alabama, has demonstrated the effectiveness of airbags in reducing the severity of head injury [5], and evaluated the projected effectiveness of airbag supplemental restraint systems in Army helicopters [6]. These studies and other factors convinced the Army of the need to introduce airbag technology as a method of delethalizing the cockpit interior of its helicopters. As part of a development program by the Aviation Applied Technology Directorate to reduce the likelihood that aviators will be injured seriously by cockpit strikes [7, 8], Simula, Inc. developed a multi-airbag system [9] which will inflate during a crash to protect the aviator.

2.1 Objectives

In this paper, the roles of the inertia reel, energy absorbing seat, and airbags in preventing or reducing the severity of head strikes in helicopter crashes are explored by performing biodynamic simulations of crashes under various crash scenarios.

2.2 Baseline scenario

The simulations revolve around a baseline scenario in which a U.S. Army Apache helicopter crashed during a training mission at Fort Rucker, Alabama. The mishap resulted in fatal injuries to the rear seat pilot and survivable injuries to the front seat co-pilot. The seating configuration of the two pilots within an Apache is shown in Figure 1. An accident investigation team from the U.S. Army Safety Center gathered data of damage to the aircraft and cockpit, and medical assessment of the injuries sustained by the two pilots were made. The helmets, inertia reels, restraint harnesses, and crashworthy seats also were retrieved and examined by investigators from U.S. Army Aeromedical Research Laboratory to assess whether these life saving equipment functioned as expected. This allowed the investigators to infer kinematics of the aircraft prior to ground impact and to estimate the motion of the restrained pilots during the mishap. It was theorized that excessive extension of the shoulder harness may have been due to delay of the inertia reel in locking early in the mishap. The energy-absorbing seat stroked only about 2.5 cm due to distortion in the cockpit structure. These factors may have contributed to the head strike of the pilot with the instrument panel-mounted glare shield. The positions of the glare shield relative the pilot's head are shown in Figure 2 prior to and after impact with the ground.

3. BIODYNAMIC SIMULATIONS

A widely used tool for accident reconstruction is the articulated total body (ATB) simulation software [10, 11]. Given a number of body segments connected by mathematical models at common joints, the ATB automatically formulates the differential equations that govern the motion of the body segments.

The model is driven by acceleration pulses which approximate the crash profiles. The ATB then integrates those equations to compute the kinematics of every body segment and to calculate the forces at all joints. The software can be requested to produce time histories of forces and accelerations of body segments which are used to predict injuries. In this study, the simulations were performed using an interactive version of the ATB, called DYNAMAN [12]. Both DYNAMAN and ATB are inexpensive tools that provide approximate answers to approximate questions.

3.1 Baseline simulation

A detailed description of the simulation of the baseline scenario is given in a previous study [13]. In this baseline simulation, the following features were modeled:

Figure 1 - Seating positions for the pilot (rear) and copilot (front) in the Apache helicopter.

Figure 2 - Likely scenario of a head strike showing pre- and post-crash position of the head relative to the glare shield.

- A vertical acceleration profile to represent the floor acceleration estimated at the rear seat location (Figure 3). The first part of the pulse represents the collapse of the landing gears in the Apache helicopter.

- A mid-size pilot represented by the 50th percentile male Hybrid III manikin data set. The ATB data set for this occupant has been validated extensively.

- A large helmet size simulating the IHADSS helmet worn by the Apache pilots. A small protrusion was modeled to represent the visor knob which is believed to have been caught under the glare shield. The weight of the simulated helmet was 2.7 kg.

- An energy-absorbing seat element that limited the forces transmitted through the seat to the spinal column to no more than 18 kN by stroking. The seat stroke was limited to 2.5 cm travel to simulate the obstruction caused by deformation of the cockpit floor and bulkhead structures.

- A four-point restraint system in which the shoulder harness was not locked until 150 ms into the crash. This simulated a failure of the inertia reel to lock early in the crash because of the low level accelerations during the collapse of the landing gears.

- A rectangular panel was placed in front of the occupant at the same location where the glare shield was mounted in the actual helicopter. Its mechanical properties were estimated from similar panels found in other vehicles.

3.2 Alternate scenarios

Starting from the baseline simulation, alternate "what if" scenarios were simulated. In these scenarios, all parameters were kept as in the baseline except for the following modifications.

3.2.1 Shoulder harness

To explore what would have occurred if the restraint system functioned as expected, the shoulder harness was prevented from excessive extension by locking it at 80 ms into the crash. That is, it was locked when the inertia reel should have sensed the second rise of the pulse after the landing gears had bottomed out.
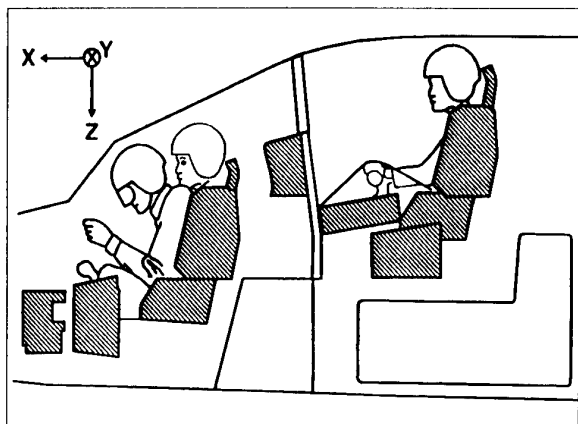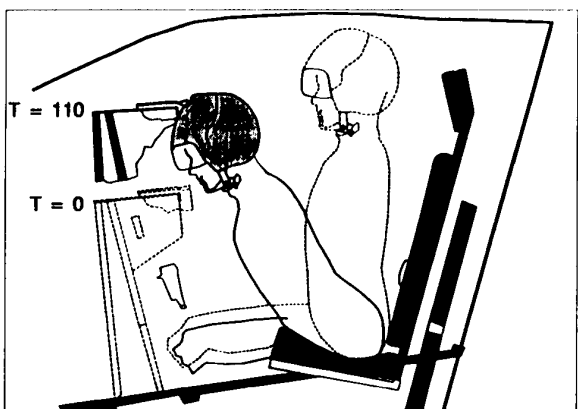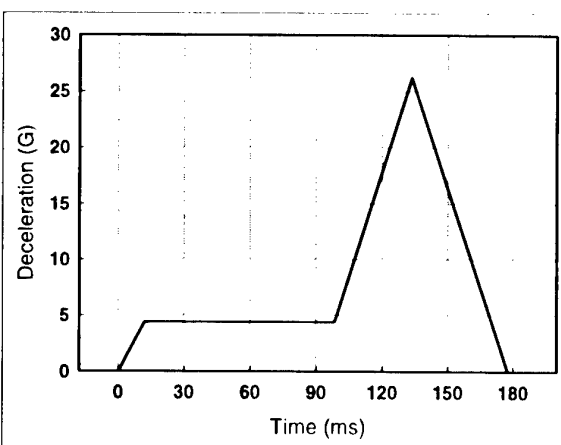
Figure 3 - Vertical deceleration profile estimated at the floor under the rear seat pilot.

3.2.2 Seat stroke

Although stroking of the seat is intended to dissipate energy and limit the forces, it will affect the kinematics of the upper body motion and the excursion of the head during the crash. To explore these effects, the seat was allowed to stroke to 25 cm. The energy-absorbing element in the Apache helicopter seat is designed for a 30-cm stroke.

3.2.3 Airbag model

A multi-airbag system was introduced in the simulations to attenuate the severity of a head strike, when such event occurs. The airbags were represented by ellipsoids with simple geometry and deployment characteristics. The detailed description of the airbags, the panel definition, airbag geometry, deployment history, thermodynamic properties, position and sizes of each airbag were presented elsewhere [14].

The geometry of the airbags and the relative positions of their respective reaction panels, deployment point, and deployment direction are depicted in Figures 4 and 5. Although three airbags (front, left, and right) were available, only the frontal airbag interacted with the pilot because of the nature of the mishap.

3.3 Injury assessment

Injury assessment generally requires the use of crash dummies in actual crash tests to determine if the human body can tolerate the forces of impact. The method of assessment is to compare the magnitudes and durations of individual force and acceleration pulses, measured at strategic locations in the dummy, to acceptable tolerance limits. Given the time history graph of a load, prominent pulses are examined by plotting magnitudes (N, or N·m) within each pulse versus the width of the pulse (ms) at that loading level. Assessment reference values are well defined for the Hybrid III type dummies [15]. In this study, the same assessment methods and reference values were applied to time histories generated by the ATB simulations.

The focus of this study was head and neck injury. In this case, the head injury criterion (HIC) and neck loads at the head-neck interface are commonly used as injury predictors. Since an airbag was used, direct head contacts did not occur in all simulations, making comparisons of HIC values not useful. This leaves neck forces and moments as the only reasonable injury parameters which may be examined. Furthermore, because the simulated motion was primarily in the mid-sagittal plane, the analysis was limited to neck compression and tension forces ($\pm Fz$), to fore-aft shear forces ($\pm Fx$), and to the extension-flexion moment about the lateral axis ($\pm My$).

4. RESULTS

Results of paired simulations are given in Table 1 as peaks of relevant response parameters. These parameters are the compression-tension axial force, the fore-aft shear force and the flexion-extension moment, all computed at the head-neck interface. The listed peaks are exactly as determined from time histories without regard to pulse width. Therefore, one should be cautious in interpreting the differences between the results of different test conditions.

Time histories of response parameters at the head-neck interface are shown in Figures 5, 6, and 7 for simulations in which the harness did not work. Results where the harness locked properly are shown in Figures 8, 9, and 10. In all these simulations, the seat stroke was limited to 2.5 cm travel.
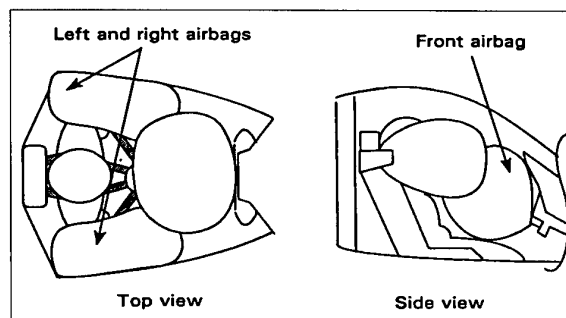
Figure 4 - Top and side views of a simulated multi-airbag system for the Apache helicopter.
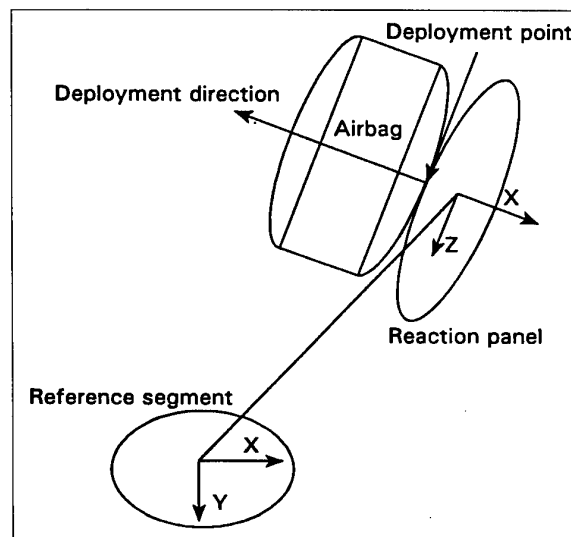
Figure 5 - Geometry of simulated frontal airbag.

Evaluation of the effects of the locking of the harness (vs. not locking), the seat fully stroking to 25 cm (vs. stroking only 2.5 cm), and the presence of the airbag (vs. not having an airbag) was done by using injury assessment techniques described earlier. It should be noted that this assessment method is used here only as a comparative tool to allow evaluation of results of paired simulations without inferring any injury outcome.

Injury assessment graphs are shown in Figures 11, 12, and 13 for simulations where the harness was allowed to fail by delaying its locking, and in Figures 14, 15, and 16 for the same simulations but with the harness locking as expected. These correspond to the time histories shown in Figures 5 through 10. Again, these results are for runs where the seat stroke was limited to 2.5 cm.

5. DISCUSSION

The peak loads listed in Table 1 are for simulations with 2.5-cm and 25-cm seat strokes. Discussions involving peak loads apply to both seat strokes. However, the discussion of time histories (Figures 5 through 10) and injury assessment (Figures 11 through 16) will be limited in this section to the 2.5-cm seat stroke simulations. We will discuss the results of the baseline simulation, then discuss the effects of the seat stroke, harness failure and the introduction of a frontal airbag on the neck injury response parameters.

Table 1
Peaks of relevant response parameters computed at the head-neck interface.

Response Parameter	Seat stroke (cm)	Harness malfunctions		Harness functions	
		Without airbag	With airbag	Without airbag	With airbag
Rearward shear force (N)	2.5	8646	912	4308	1744
	25	9020	1495	2011	1015
Forward shear force (N)	2.5	2799	2523	2893	1896
	25	3017	814	2345	841
Compressive force (N)	2.5	7805	1994	7894	2852
	25	6635	2924	3716	1121
Tensile force (N)	2.5	16647	3315	7418	2456
	25	17346	721	3435	1268
Flexion moment (Nm)	2.5	1022	87	588	223
	25	894	215	238	87
Extension moment (Nm)	2.5	658	84	254	146
	25	303	68	324	47

In all these discussions, keep in mind that only the 50th percentile male aviator was simulated. Results will be different for other aviator sizes, particularly for a small size female. It should be noted also that the airbag model used in these simulations is a simple representation of a complex system. Other more sophisticated airbag models have been developed using computational fluid dynamics and finite element methods. These models, which require extensive computational capabilities and resources, were not used in this study.

5.1 Baseline simulation
In the baseline simulations, Beale showed that pilot's helmet became wedged under the glare shield, as displayed in Figure 2. Further forward motion of the neck and body, while the head essentially remained motionless under the glare shield, would have allowed forces of such magnitude, direction, and duration to produce the observed basilar skull fracture.

5.2 Effects of seat stroke
In all simulations where the harness functioned properly, the peak magnitudes of neck loads (shown in Table 1) were reduced by as much as 68% when the seat was allowed to fully stroke. This was true regardless of the presence of an airbag in the simulation. An exception to this observation is the extension moment without airbag which increased slightly when the stroke was increased. In this case, however, the increased moment did not exceed acceptable reference values. The same observations could not be made when the harness malfunctions. That is, no correlation could be found between the seat stroke and peak loads when the harness is simulated to fail.

5.3 Effects of harness
The failure of the inertia reel to lock was simulated by allowing excessive extension. The effects of harness failure can be observed by comparing the injury assessment diagrams of the three response parameters of simulations where the harness worked as expected (Figures 11, 12, and 13) to those where the harness failed to work properly (Figures 14, 15 and 16).

It is clear prominent pulses were reduced significantly when the harness was simulated to work. For cases without airbags, however, prominent pulses in all three response loads remained near borderlines of the assessment corridors, as shown in solid bullets in Figures 14 and 15. When an airbag was introduced along with a working harness, the prominent pulses moved further away from the borderlines and toward the center of the corridors, as shown in the hollow circles of Figures 14 and 15.

Another observation may be made from the time histories of Figures 8, 9, and 10. Even with a working harness but without an airbag, a significant impact with the head rest occurred on rebound (at approximately 325 ms) causing high forces and moments which exceed the corresponding reference values.

5.4 Effects of an airbag
In addition to the airbag-related observations made in the previous paragraphs, two additional observations must be made about the role of the airbag. First, examination of time histories in Figures 5 through 10 shows that all prominent peaks were greatly reduced by the introduction of an airbag. Second, the injury assessments shown in Figures 11, 12 and 13 demonstrate that, even in the absence of a working harness, the airbag reduced magnitudes of prominent pulses to levels that are well within acceptable injury assessment corridors.

6. CONCLUSIONS
In this study, we examined the effects of seat stroke, shoulder restraint and airbags on reducing the severity of potential neck injury to the aircrew during a helicopter crash. For this purpose, we performed mathematical simulations of the pilot's biodynamics to examine the internal loads at the head-neck interface. The simulations demonstrated that, when the harness functioned properly, the peak magnitudes of neck loads were reduced significantly. In the absence of a working harness, results indicated the airbag reduced magnitudes of prominent pulses to levels that are well within acceptable injury assessment corridors.

7. REFERENCES

1. Shanahan, D.F., "Injury in U.S. Army helicopter crashes: October 1979 - September 1989," Journal of trauma, 1989, 29:415-423.

2. Shannon, S.G., Albano, J.P., and Licina, J.R., "Head Injury Risk in U.S. Army Rotary-wing Mishaps: Changes since 1980," AGARD Specialist Meeting on Impact Head Injury, 7-9 November 1996, Mescalero, New Mexico.

3. McEntire, B. J., "U.S. Army helicopter inertia reel locking failures," Neuilly-sur-Seine, France: AGARD-CP-532-92, 1992, pp. 43-1 to 43-6.

4. Loushine, T. M., "Airbag protection of the gunner in the U.S. Army Cobra AH-1Q," Texarkana, TX: Army Material Command, AD-A009-421, 1975.

5. Alem, N. M., Shanahan, D. F., Barson, J. V., and Muzzy, W. H., III., "The effectiveness of airbags in reducing the severity of head injury from gunsight strikes in attack helicopters," Neuilly-sur-Seine, France: AGARD-CP-532-92, 1992, pp. 44-1 to 44-9.

6. Shanahan, D. F., Shannon, S. G., and Bruckart, J. E., "Projected effectiveness of airbag supplemental restraint systems in U.S. Army helicopter cockpits," Fort Rucker, AL: U.S. Army Aeromedical Research Laboratory, USAARL Report No. 93-31.

7. Smith, K. F., "Future of the Army's cockpit crash protection," U.S. Army aviation digest. September/October 1993, pp 18-23.

8. Greth R. L., Shope, W. B., Pfaff, M. S., and Smith, K. F., "Concept feasibility demonstration for Army cockpit delethalization program," Washington, DC: American Helicopter Society 48th Annual Forum & Technology Display, 3 Jun 92.

9. Zimmerman, R. E., "Inflatable restraint systems for aircraft," SAFE J, Volume 23, Number 4 & 5, 1993, pp 16-28.

10. Obergefell, L. A., Fleck, J. T., Kaleps, I., and Gardner, T. R., "Articulated total body model enhancements," Wright-Patterson Air Force Base, OH: Harry G. Armstrong Aerospace Medical Research Laboratory. AAMRL-TR-88-009.

11. Fleck, J.T., Butler, F.E., and Vogel, S.L., "An Improved Three-Dimensional Computer Simulation of Crash Victims," Washington, DC: Department of Transportation, NHTSA, 1975, Report No. DOT-HS-801-507 through 510.

12. GESAC, Inc., DYNMAN 4.0 (Beta version) user's manual. Kearneysville, WV: GESAC Inc., 1996.

13. Beale, David, Alem, Nabih M., and Butler, Barclay P., "A correlative investigation of simulated occupant motion and accident report in a helicopter crash," Aviation, Space, and Environmental Medecine, Col. 67, No. 1. January 1996.

14. Strawn, G., Alem N., "Biodynamic simulation of pilot interaction with helicopter multi-airbag restraint system," Fort Rucker, AL: U.S. Army Aeromedical Research Laboratory. USAARL Report No. 95-3. 1995.

15. Mertz, H.J. "Anthropomorphic test devices," in Accidental Injury: Biomechanics and prevention, Nahum, A.M. and Melvin, J.M., eds. Springer-Verlag, New York, NY: 1993.

8. ACKNOWLEDGMENTS
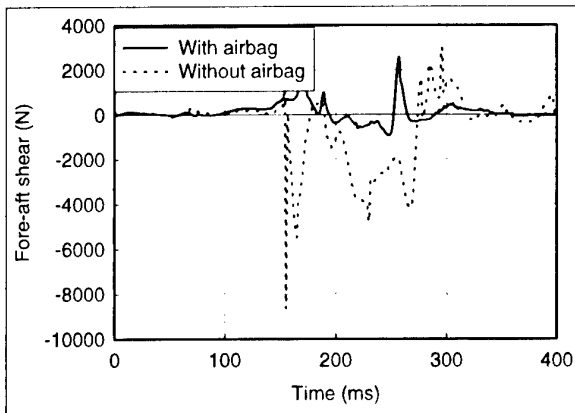
Figure 5 - Fore-aft shear force at the head neck joint in two simulations where the harness did not function as expected.
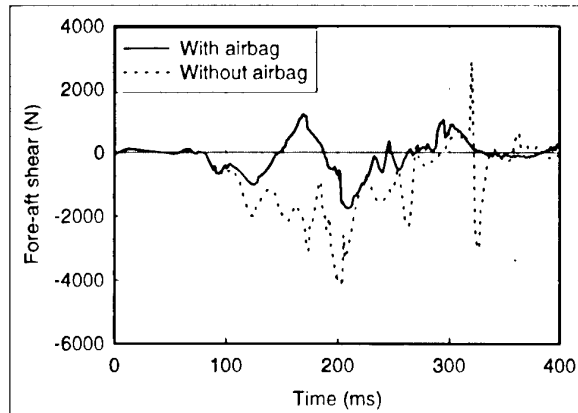
Figure 8 - Fore-aft shear force at the head-neck joint for simulations where the harness worked properly.
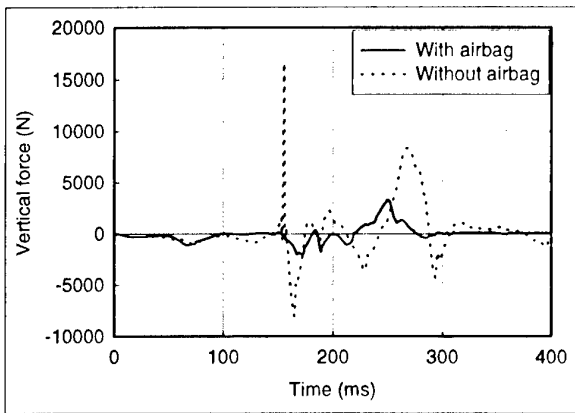
Figure 6 - Axial compression-extension force at the head-neck interface from simulations where the harness did not function properly.
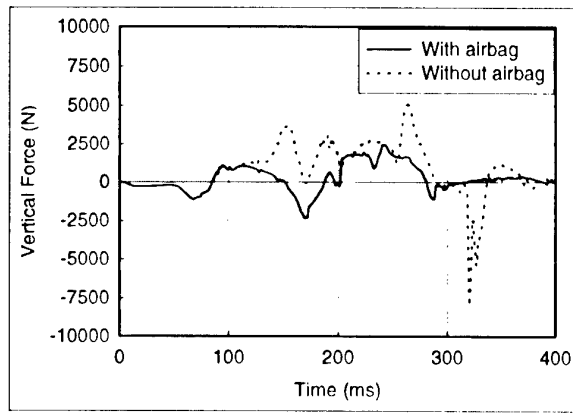
Figure 9 - Compression-extension axial force at the head-neck joint for which the harness worked properly.
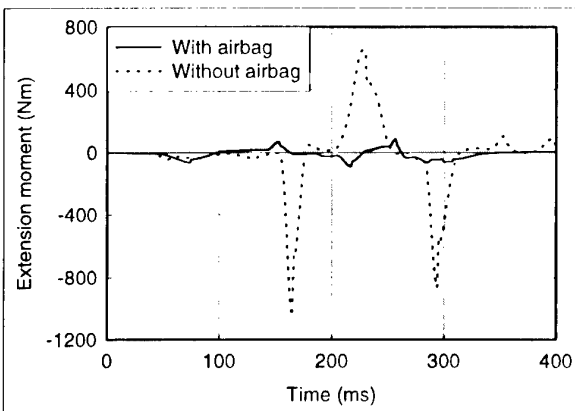
Figure 7 - Extension-flexion moment at the neck joint in two simulations where the harness failed to lock as expected.
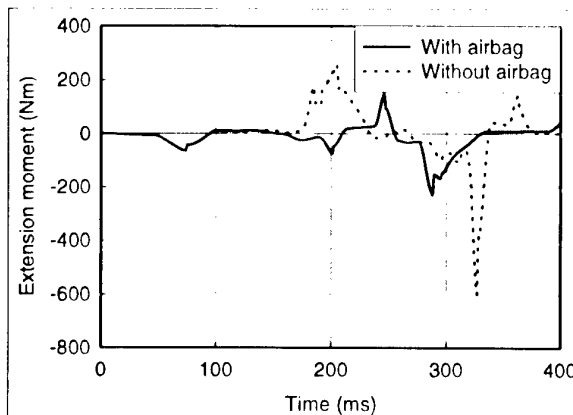
Figure 10. Extension-flexion moment at the head-neck joint for two simulations where the harness functioned as expected.
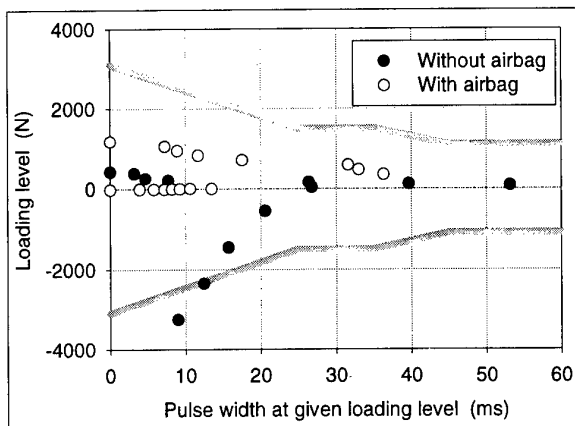
Figure 11 - Injury assessment of neck fore-aft shear from simulated harness malfunction.
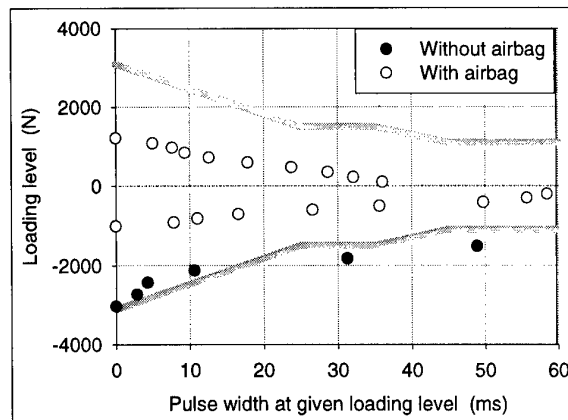
Figure 14 - Injury assessment of neck fore-aft shear from simulations in which the harness functioned properly.
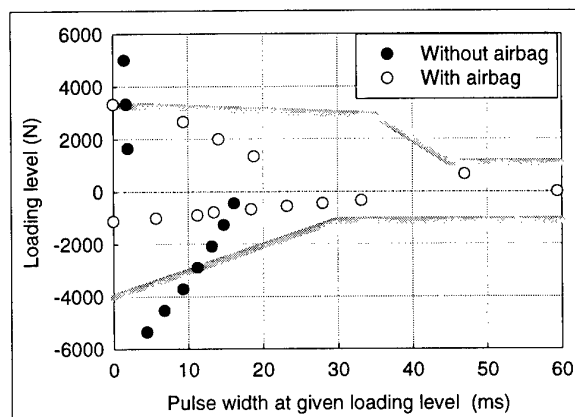
Figure 12 - Injury assessment of neck axial force for simulated malfunctioned harness.
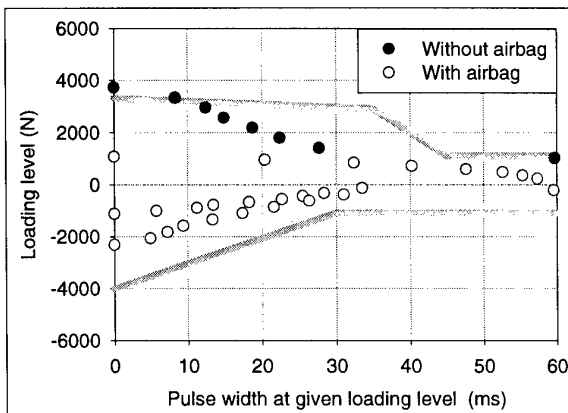
Figure 15 - Injury assessment of neck axial force for simulations where the harness worked properly.
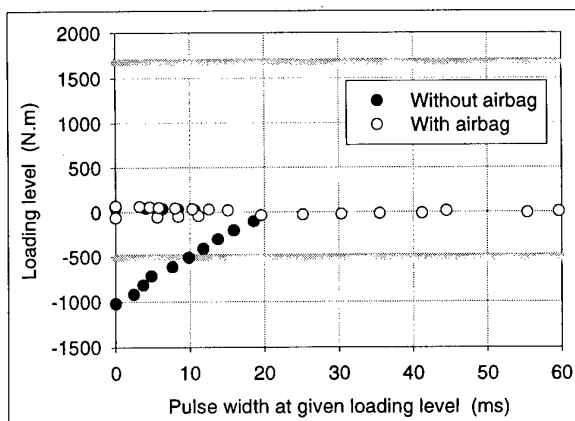
Figure 13 - Injury assessment of neck extension-flexion moment for cases where harness was simulated to malfunction.
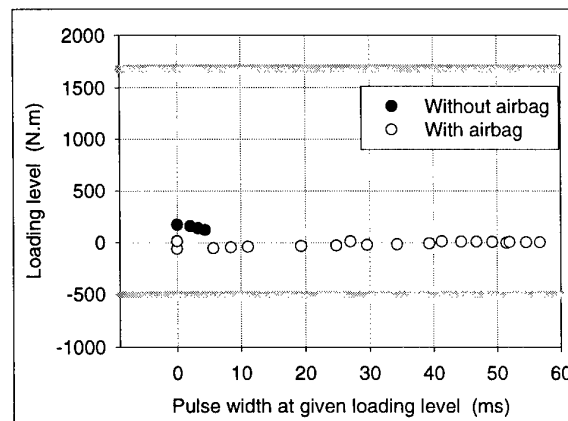
Figure 16 - Injury assessment of neck moment for cases where the shoulder harness was simulated to work properly.

ADDRESSING FRONT ROW HIC REQUIREMENTS IN COMMERCIAL AIRPLANES

J.R. McCarthy*
K.H. Yang**
M.T. Shanahan*
A.I. King**
*BTS Consulting Engineers
1725 North Talbot Road, R.R. #1
Windsor, Ontario, N9A 6J3, Canada
**Wayne State University
Bioengineering Center
Detroit, Michigan, USA

1. SUMMARY

Changes to the Federal Aviation Administration (FAA) regulation regarding occupant crash protection in commercial airplanes has created new design considerations for each occupant position. In particular, addressing front row seating positions to meet the head injury criteria can be a challenging design assignment involving numerous considerations. Various design approaches to meet this requirement are discussed. Particular attention is given to the articulating seat pan approach. Results of prototype testing are presented with recommendations regarding further development.

2. INTRODUCTION

In 1988, the FAA increased the impact protection requirements for many aircraft, including those used by commercial airlines. The new airworthiness standards required two dynamic tests to assess the crashworthiness of an aircraft seat.

The intent of the standard is to decrease the injury potential for an occupant, particularly in the area of head, chest, spine, and lower extremities. The two Federal documents which pertain to this area are:

- Federal Aviation Regulation Part 5.562: Airworthiness Standard, and
- FAA Advisory Circular 25.562-1: Dynamic Evaluation of Seat Restraint System and Occupant Protection on Transport Airplanes.

One of the first commercial planes required to comply with FAA Regulation Part 25.562 was the Boeing 777. The regulation applies to all seating positions; however, the aircraft industry, as a whole, believes that the most difficult aspect of the standard is in meeting the head injury criterion for front row occupants. Front row occupants are passengers who are seated directly behind an interior structure other than a row of passenger seats. The structure located in front of the passenger could be a lavatory bulkhead, a bustle, or a partition wall separating the different sections of the aircraft (i.e., Executive, Business, and Economy Classes). For a typical "Tri-Class" configuration, approximately 36 seating positions (out of 320) may involve such a forward structure.

Prior to the application of the new standard, the typical dynamic performance of an airline seat resulted in the head of a front row passenger forcibly striking the bulkhead structure

with a velocity of approximately 46 fps (31 mph or 50 km/h) or higher during a 30 mph (48 km/h) horizontal crash test [1]. In sled tests conducted without a forward structure, the forward head trajectory exceeded the imaginary plane of the bulkhead by approximately 7 inches (0.178 m). A typical head trajectory is illustrated in Figure 1. These tests were conducted assuming minimal seat dynamic deflection. The head trajectory would increase for a test incorporating a seat which is less stiff and deflects further forward.

Figure 1
TYPICAL FRONT ROW HEAD TRAJECTORY

Ref.—CAMI Test A91082
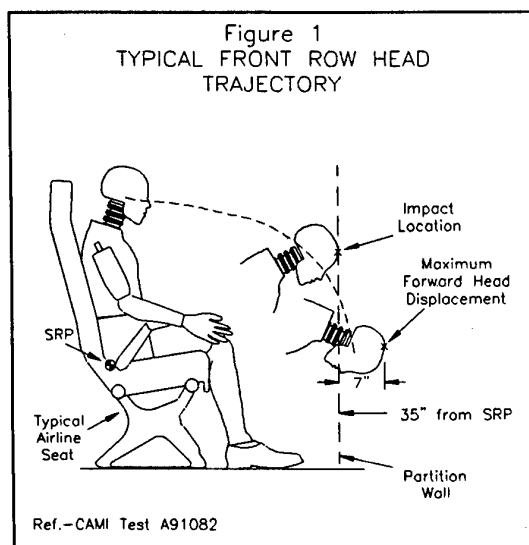
Knee contact with the bulkhead structure does not generally occur. Therefore, compressive loading of the upper legs (femurs) was not expected to be a concern in complying with this portion of the regulation. The main focus, then, was in reducing forward head trajectory during a horizontal crash test and to achieve acceptable HIC values.

The dynamic testing requirements were specified in the FAA Regulation composed of two crash tests with each incorporating a triangular crash pulse [2]. The first dynamic test requirement involved a crash pulse which resulted in the dummy's inertia loading being forward and downward at an angle of 60 degrees from the horizontal (Figure 2). The minimum change in velocity was 35 fps (24 mph or 38.4

km/h). The minimum deceleration was 14 g's at 0.08 seconds (80 ms).

Figure 2
DYNAMIC TEST REQUIREMENTS

	TEST 1	TEST 2
Illustrations shows a forward facing seat		
Dummy inertial load shown by arrow		
Minimum Impact Velocity (fps)	35	44
Maximum Rise Time = tr (sec)	0.08	0.09
Minimum Deceleration (g)	14	16
Floor Deformation degree roll	0	10
degree pitch	0	10
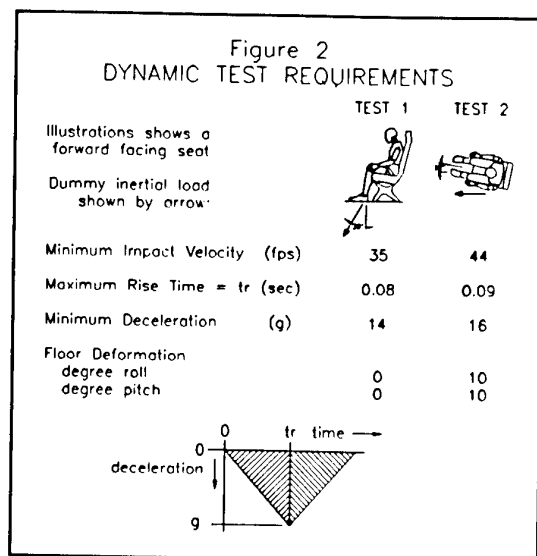
The second test requirement involved a crash pulse which resulted in inertia loading of the dummy while the seat was positioned at a 10 degree yaw (Figure 2). The minimum change in velocity was 44 fps (30 mph or 48 km/h). The minimum deceleration was 16 g's at 0.09 seconds (90 ms).

3. INJURY ASSESSMENT

To assess the level of impact protection to a passenger, an anthropomorphic test device (ATD or crash dummy) is used which incorporates instrumentation to collect data regarding the ATD's response to the applied crash pulse. The dummy response data are then used to assess the potential for injury based on currently accepted injury criteria. The Federal Regulations address the dummy's response using criteria to evaluate the potential for injury to the head, chest, spine, and upper legs [3].

To assess the potential for head injury, the Head Injury Criteria (HIC) is used. HIC is based upon the Wayne State Tolerance Curve which was interpreted by Gadd [4] and later by Versace [5]. A HIC value below 1000 is required to comply with the Federal Regulation. A HIC value of 1000 is believed to be the value at which 1 in 6 occupants may sustain a life threatening skull fracture or brain injury [6].

Comparatively, for a resultant HIC value of approximately 400 or less, the likelihood of injury to the head or brain is virtually 0. For a HIC value of 2500 or more, it is believed that nearly all crash victims may experience life-threatening head injuries with probable death or long-term disability.

To assess the threat of thoracic injury when a shoulder belt is used to restrain a passenger, a shoulder belt load criterion is used [3]. For a single shoulder belt, the belt tension must not exceed 7784 N (1750 lbs). If two shoulder belts are used, the sum of the tensions in each belt must be less than 8896 N (2000 lbs).

To assess the likelihood of spinal injury during compressive spinal loading, a lumbar load cell is used in the ATD. The peak compressive force must be below 6672 N (1500 lbs).

This is the value at which spinal injury is considered to be unlikely [3].

The last criterion involves the upper legs in which the femur loading criterion is used. The compressive loading of the femur must not exceed 10000 N (2250 lbs) to meet the criterion [3].

4. METHODS FOR ADDRESSING FRONT ROW HIC REQUIREMENTS

To achieve compliance with the HIC requirement during the horizontal crash test, four methods have been researched and tested by various institutions and industry. These methods are:

a) Air bags
b) Shoulder harnesses
c) Energy absorbing panels on the impacted surfaces.
d) Articulating seats.

A fifth possible method would be to increase the setback of the front row seat from the forward structure. The setback would be determined such that head contact with the forward structure would not occur. This method may cause a reduction in the number of passenger seats available, depending on the extent of the additional seat setback. To maintain the same number of available passenger seats, the pitch between subsequent rows of seats could be reduced to compensate for the additional pitch of the front row seat.

Implementation of the air bag would require the installation of large automotive-type air bags into the bulkhead or partition wall structure. This method is advantageous since air bag technology is currently available. However, the development and application of this technology has been predominantly for automotive use, and development work would be required to ensure proper installation and deployment in commercial airplanes. Crash sensor locations, analysis, and triggering sequence would have to be determined. Inadvertent deployment of air bags would also have to be prevented. If a crash involves multiple impacts, the air bag may not provide sufficient protection on impacts following the impact initiating deployment. Variations in the pre-impact brace instructions to the passengers would likely be required. Effects on cabin structure, post-crash evacuation concerns, significant changes in cabin pressure during deployment, and excessive sound levels are other factors which must be addressed to obtain the practical installation of air bags into commercial airplanes.

Some of the above issues were studied in the Bulkhead Air Bag System developed and researched by Simula [7]. The prototype system incorporated crash sensing elements which respond to accelerations and velocity changes of the aircraft. Preset thresholds were established to prevent inadvertent deployment during non-crash conditions. If the aircraft sensors detected accelerations indicative of a crash impact, then the air bag would be deployed from the air bag module located on the forward cabin structure. The air bag shape was established to provide a sufficient level of occupant protection, while minimizing the risks associated with rapid air bag deployment and rapid egress from the aircraft. Under the various test conditions, the system demonstrated compliance with the head injury aspect of the regulation.

The utilization of shoulder belts to limit the forward excursion of an occupant's torso and head has been considered and could prevent head strike to the surface in front of the occupant. However, the use of shoulder belts would require strengthening the seat belt anchor location(s) which may cause

increases in the weight of the seat and seat structure or the cabin structure. If the shoulder belt(s) is connected to the seat, the structure of the seatback would have to be strengthened to withstand shoulder belt loading. Depending on how the seat is strengthened to accommodate the additional loads, a potential hazard may now exist to passengers sitting behind this row of seats. Attaching the shoulder belt(s) to the seatback would also require eliminating the forward seatback pivot to limit the forward excursion of the occupant. Shoulder belts attached to the seatback connected to the seat would also result in substantial increases in floor loading which may not be acceptable under the current maximum allowable interface loads.

The implementation of energy absorbing material by attachment to a surface in the head strike zone is another option which has been investigated to minimize injury associated with head contact. Various rigid, semi-rigid, and non-rigid foams (last-a-foam, dytherm, ensolite) were evaluated, as were as honeycomb material (aluminum Hexcell and Nomex), without satisfactory results. Satisfactory results were achieved with aluminum Hexcell covered with 0.25 (6 mm) inches of rigid foam [8]. Further testing is required to determine whether the depth of foam or energy absorbing material could create other injuries due to pocketing of the head as the material is crushed. Facial lacerations are also another consideration.

The fourth method being considered is articulating seats. These involve the forward and rotational movement of the seat pan during a crash event. The rotation of the seat pan provides lower torso restraint which minimizes the forward excursion of the lower torso. This, in turn, reduces the forward excursion of the head and has resulted in head excursions which would not strike the vertical interior structure located 900 mm (35 inches) in front of the seat reference point.

Research and testing were conducted to assess the feasibility of utilizing an articulating seat to achieve the compliance with the HIC requirement during the horizontal crash test of the FAA Regulation Part 25.562.

5. ARTICULATING SEATS

Articulating seats date back to the 1930's with many new concepts emerging in the late 1950's and early 1960's. The intent of the seats was to provide restraint to the occupant through the seat's motion, without the use of a seat belt system. The articulation of the seat was either passive or controlled by intricate springs and/or hydraulic systems to assist in the articulation.

The particular articulating seat used in our study was developed and patented by a company in St. Louis, Missouri. The motion of this articulating seat is such that the front portion of the seat pan is displaced forward and upward. The rear portion of the seat pan is also displaced forward. The seatback can either remain stationary or articulate with the seat pan.

The trajectory of the seat is controlled by rollers located at the front and rear sides of the seat pan. The trajectory of the rollers is controlled by either slots or ramps integrated into the side structure of the seat base (Figure 3). The geometry of these slots or ramps can be altered to achieve different seat pan motions. The motion of the seat results from the longitudinal deceleration of the aircraft. The inertia of the seat and its interaction with the occupant results in the forward motion of the seat relative to the vehicle during a longitudinal crash pulse. The extent of seat motion along its

trajectory is dependent upon the severity of the crash pulse, the geometry of the slots and ramps, and the position of the occupant on the seat.

Figure 3
ARTICULATING
SEAT PAN
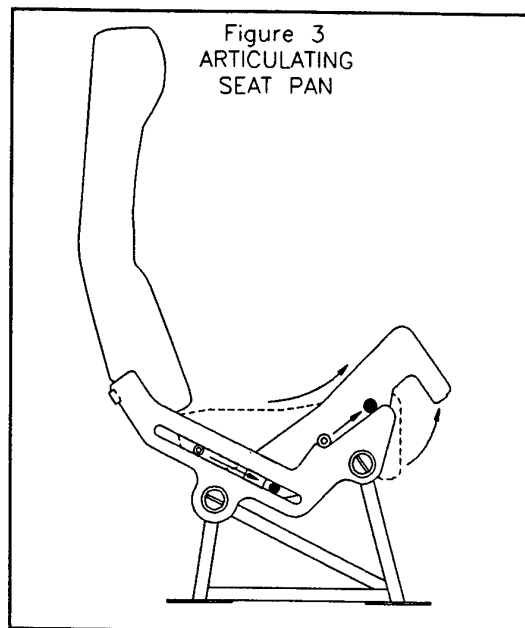
The design intent of the seat is to be crash pulse sensitive. The greater the deceleration, the greater the resulting seat motion, and the greater the restraint provided to the occupant. In the current (non-articulating) commercial airline seat, a lap belt is used to restrain the occupant to the seat. The lap belt provides virtually all of the restraint to the occupant. The articulating seat pan concept attempts to transfer energy into the seat cushion to provide an additional load path to restrain the occupant. In doing so, a reduction in the pelvic displacement will be achieved which will result in the reduction of the maximum forward displacement of the head. Furthermore, the upward motion of the front of the seat pan will result in earlier thigh-to-chest contact which is believed to reduce the forward velocity of the torso, and subsequently the head.

To comply with the Federal Regulations, the design goal for the seat is to provide sufficient occupant restraint such that head and knee contact of a 50th percentile male ATD do not occur with the structure located forward of the occupant during a longitudinal crash pulse. The dynamic requirements for HIC and femur loading would then be met simply by eliminating contact.

Design features used to minimize the forward displacement of the occupant included:

- rigid seat frame
- low elongation, polyester lap belt
- Energy Absorbing Foam in the seat cushion (optional)
- movable belt anchors to maintain optimal belt geometry and to assist in the initial articulation of the seat pan
- an articulating seat pan.

The seat trajectory was established using a 3-dimensional computer simulation. The simulation program used was the Articulated Total Body (ATB) model. This program was developed in the early 1970's by Calspan Corporation and was

originally called the Calspan 3-Dimensional Crash Victim Simulation (CVS-3D or CAL-3D) program. It was subsequently enhanced by the Air Force Aerospace Medical Research Laboratory (AFAMRL) and renamed the ATB program.

This model is a rigid body dynamics program capable of simulating gross human body motion resulting from interaction with applied forces resulting from either a body segment contacting the vehicle interior or a body segment interacting with a restraint or air bag. The simulation program is capable of providing the user with numerous output data.

The prototype articulating seat was constructed with a rigid steel seat base. Attached to the seat base were aluminum side plates which incorporated slots and/or ramps to control the trajectory of the seat pan. Rollers were attached to the sides of the seat pan at the front and back corner locations. Rollers interacted with the slots or ramps to control the seat pan's motion. The seatback was rigidly attached to the aluminum side plates and did not articulate with the seat pan. Seatback break-over could still occur if desired; however, for the purpose of this testing, the seatback was rigidly attached. The seat pan consisted of an aluminum sheet metal pan with aluminum plate side structures. The rollers were attached to the aluminum plate side structures. The rear portion of the seat cushion was composed of commonly available open cell foam. The forward portion consisted of "Confor," an energy absorbing foam. This particular seat also included a moving belt anchor. The belt anchor block moved along the same path as the rear roller for the seat. The belt anchor block could not move forward unless the seat pan also underwent a similar forward displacement. However, the seat pan could be displaced further forward without the belt anchor block moving along with it. Attached to the belt anchor block was a polyester lap belt.

Two prototype seats were constructed incorporating the above features. The first seat was initially tested at Wayne State University (WSU) Bioengineering Center in Detroit, Michigan, and then at the FAA Civil Aeromedical Institute (CAMI) in Oklahoma City, Oklahoma. The last prototype was tested only at CAMI. Sled tests conducted at WSU were performed using the Hybrid III dummy. The CAMI tests were conducted with the Hybrid II. Figure 4 illustrates the configuration of the second prototype.

Three tests were conducted at CAMI. Each test achieved approximately 1 inch (25 mm) of head clearance. The second test had a peak sled deceleration of 16.2 g's (7340N), and the average belt force was approximately 1650 lbs. The maximum belt angle was 54 degrees upwards from the horizontal, and the seat rotation was approximately 36 degrees. This is illustrated in Figure 5.

Based upon the results of the sled tests, the use of seat articulation with a moving belt anchor appears to be a feasible means of achieving compliance with the HIC requirement in a horizontal crash pulse.

Review of the high speed film revealed that the seat articulated smoothly. The belt anchor moved forward and downward along its path and maintained good lap belt geometry. It appears that the seat provided substantial restraint of the lower torso from forward displacement. The lap belt also appears to provide some restraint in the forward direction as well as providing a downward restraint to maintain the lower torso contact with the seat cushion.

Figure 4
PROTOTYPE SEAT-
SEAT PAN ASSEMBLY

Figure 5
CAMI TEST RESULTS
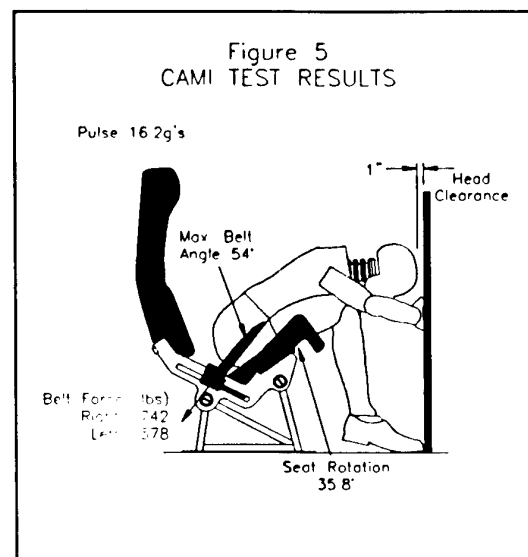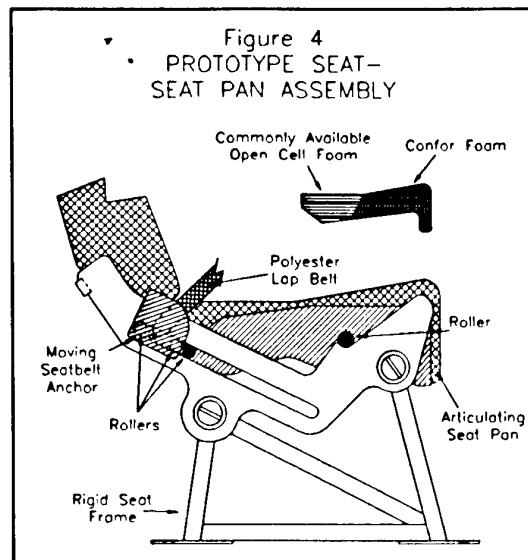
Other versions of articulating seats have been developed and tested by industry with various degrees of success. Predominantly all of the other articulating seat concepts incorporate non-moving or rigid belt anchors. In some designs, the belt anchor locations have been raised with respect to the seat reference point causing shallow lap belt angles. The resulting lap belt angles fell substantially below, or outside of, the range typically recommended for airline design [9, 10] (Figure 6). Sled tests have shown that the head path can be reduced by incorporating higher belt anchors. The use of higher belt angles have resulted in sometimes non-repeatable results with varying head trajectories. The higher belt anchor configuration appears to be very sensitive to the initial location of the lap belt across the iliac spines of the dummy's pelvis.

Figure 6
LAP BELT GEOMETRY
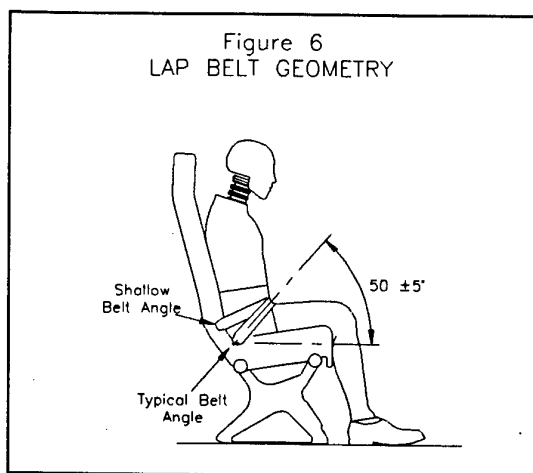
The concerns for such a design is, firstly, the potential, or increased potential, for submarining. Similar belt anchor configurations would most likely result in submarining within an automotive environment. However, some differences do exist between a commercial aircraft seat and a typical automotive seat which may minimize the increase in potential for submarining with a shallower belt angle. The two predominant factors are the upright seating posture due to the upright seat back angles as well as seat pan and seat cushion combinations which are very stiff relative to automotive seat systems.

Regardless of what is demonstrated in 50th percentile dummy tests, a shallower lap belt angle will increase the potential for submarining for smaller occupants such as many females and children. A shallow belt angle also provides the occupant little margin of error or forgiveness in the initial positioning and adjustment of the lap belt. The margin between good belt performance and serious lap belt-induced abdominal injury becomes narrower.

6. DISCUSSION

It should be noted that an increased potential for submarining is not the only issue at hand. Some of the variability in head trajectory may be the result of the reduction in forward pelvic rotation. It is believed that the higher belt anchors reduce the forward rotation of the pelvis about the H-point. In doing so, additional flexion and shear loads are applied to the base of the spine. Neither forward bending moments or shear loads in the lumbar spine are monitored during routine sled testing. The question now becomes, is a reduction in head injury potential achieved at the expense of an increase in injury potential to the lumbar spine. Further research in this area is recommended.

7. CONCLUSIONS

An articulating seat with a moving belt anchor appears to be a feasible means of achieving compliance with the HIC requirement of the FAA regulation during a horizontal crash pulse.

Caution should be used in all seat designs incorporating lap belt anchors which fall outside the range typically recommended in automotive and aerospace environments.

The authors would like to caution that, even though numerous sled tests have been conducted to test articulating seat pans,

the biomechanics involved are still not fully understood. Caution should be used in extrapolating laboratory sled test results with ATDs to real world crashes with humans since numerous differences exist.

REFERENCES

1. Gowdy, V., DeWeese, R., "Evaluation of Head Impact Kinematics For Passengers Seated Behind Interior Walls," Final Report, AD-A252 651, Civil Aeromedical Institute, Federal Aviation Administration, Oklahoma City, Oklahoma, May, 1992.

2. Federal Aviation Administration Advisory Circular AC-25.562-1, "Dynamic Evaluation of Seat Restraint Systems and Occupant Protection On Transport Airplanes," June 3, 1990.

3. Marcus, J.H., "Dummy and Injury Criteria for Aircraft Crashworthiness," Society of Automotive Engineers, SAE paper No. 951167, May 1995.

4. Gadd, C.W., "Use of a Weighted Impulse Criterion for Estimating Injury Hazard," Tenth Stapp Car Crash Conference, Society of Automotive Engineers SAE Paper 660793, 1996.

5. Versace, J., "A Review of the Severity Index," Fifteeth Stapp Car Crash Conference, Society of Automotive Engineers, SAE Paper No. 710881, 1971.

6. Prasad, P., Mertz, H.S., "The Position of the United States Delegation to the ISO Working Group 6 on the Use of HIC in the Automotive Environment," Society of Automotive Engineers, SAE Paper No. 851246, 1985.

7. Barth, T.H., "The Bulkhead Air bag System - Head Strike Protection for Passenger Aircraft," Society of Automotive Engineers, SAE Paper No. 951169, 1995.

8. "Seat-to-Bulkhead HIC Assessment," ATA/FAA Meeting Presentation Outline, February 28, 1992.

9. "Aircraft Crash Survival Design Guide," Volume IV, Aircraft Seats, Pg. 140 - 144.

10. Aerospace Recommended Practice, "Safety Lap Belts (For Civil Transport Aircraft)." Society of Automotive Engineers, ARP 682B, 1979.

INVESTIGATION OF INDY CAR CRASHES USING IMPACT RECORDERS [1]

J.W. Melvin, K.J. Baron and W.C. Little
Safety Research Department, General Motors R&D Center
30500 Mound Road, Warren, MI 48090-9055, USA

J. Pierce
GM Motorsports

T.R. Trammell
CART Safety Team

ABSTRACT
This paper describes the initial phases of an ongoing project in the GM Motorsports Safety Technology Research Program to investigate Indy car crashes using an on-board impact recorder as the primary data collection tool. The development of a database consisting of crash investigation data patterned after national highway crash databases is discussed. The data gathered and coded includes track and incident scene information, vehicle damage, and driver injuries, as well as the vehicle decelerations measured by the impact recorder. The paper discusses the development of specifications for the impact device, the selection of the specific recorder and its implementation on a routine basis in Indy car racing. The results from incidents that produced significant data during the 1993, 1994 and 1995 racing seasons are summarized.

INTRODUCTION
The investigation of automobile crashes for the purpose of understanding the various factors involved in the production of occupant injuries has been a well-proven method for developing countermeasures for injury mitigation. The methods for organizing and cataloging the sometimes voluminous information from such investigations of highway crashes in the US were formalized in the 1960s and 70s. During that time, computerization of the databases became viable and coding methods were developed to allow categorization of crash conditions, vehicle damage and occupant injuries in codes that could be searched and retrieved by computer. That capability greatly expanded the ability of researchers to analyze mass accident data by statistical means.

In 1991, during the planning of the GM Motorsports Safety Technology Research Program (MSTRP) it was concluded that there was a need for a similar methodology to enhance the collection of racing car crash data. The goal of the MSTRP is to improve the safety of both racing cars and passenger cars through the application of the methods of crash protection research to racing car crashes. The program is presently focused on

Indianapolis-type (Indy car) racing car crash investigation, because of the extensive records of such crashes kept by one of the authors (T.R.T.) for the prior eight years. This paper will discuss the enhancements and additions that have been made to the accident investigation process and present examples of the results to date.

METHODS
Investigations of highway crashes result in data that typically consist of a description of the accident scene and conditions at the time of the crash; estimates of the vehicle trajectories and speeds; a description of the nature of the impact and the exterior damage to the vehicle; a description of the damage to the interior of the vehicle, including possible contact points with the occupants; and detailed information on the occupant injuries. Usually, these items are not determined on scene but, rather, the next day or so

---

after the crash has occurred. In addition, not all crashes in a geographic region are investigated in depth. Instead, statistical selection of crashes to be investigated, or attention to a few types of crashes, is used to provide a manageable work load for the investigators.

Investigation of Indy car crashes allows for some significant differences in methodology in comparison to highway crashes. In contrast to the highway driver population, the Indy car driving population is well defined, being limited in any one season to about 50 drivers. Similarly, if a crash during a race occurs, its location is also well-defined and limited to one of 17 or less tracks in the 1992-1995 time period covered by this paper. The structural designs of all the Indy cars are similar and controlled by the sanctioning bodies. There is often video coverage of the vehicle crash trajectory and vehicle impact attitude. The response of the emergency crews is very rapid and treatment is available at the track. That eliminates the time between the occurrence of the injuries and subsequent treatment as a variable in injury outcome, a significant factor in many highway crashes. Given the tight space for an Indy car driver and the mandatory and universal use of multi-point belt restraints thereare no questions concerning driver position and restraint use at the time of a crash. All of these factors present significant advantages in conducting an investigation, and in the accuracy and detail of data when compared to a highway crash investigation.

Examination of video coverage of typical Indy car crashes into walls indicates that the actual impact takes place in about two video frames (about 66 msec). That makes it very difficult to estimate peak deceleration levels from video motion analysis. It became evident in the early development of the MSTRP activities that the only way to accurately determine the vehicle decelerations associated with Indy car crashes was to use impact recorders. Since the number of cars used in the races is limited to about 50 to 60 vehicles which are known in advance of a race, then the only cars which could be possibly involved in crashes are contained within this known population. This fact makes it possible and reasonable to consider the use of impact recorders to record vehicle decelerations during a crash.

The initial phase of the MSTRP crash investigation study was divided into two projects. The first was to refine and expand the crash investigation methods used for Indy cars to provide more detail, particularly on the vehicle, and to allow computerized coding of the vehicle deformations and the driver injury data. The second project was to investigate the feasibility of installing impact recorders in Indy cars, define their performance requirements, and identify a source capable of supplying the appropriate equipment.

REFINEMENT OF CRASH INVESTIGATION PROCEDURES - Many of the basic aspects of investigating racing car incidents (crashes) were already in place, in some form or another, with the sanctioning bodies for Indy car racing, the United States Auto Club (USAC) and the Championship Automobile Racing Teams (CART). These include incident reports from track observers, photographs of crash damage to the vehicle, and injury information from the medical teams.

The package of data being gathered for the MSTRP consists of sections with general information, car deformation, crash description, driver information, driver injury, photographic coverage, and an overall summary. An example of the data sheets developed for this purpose are given in the Appendix to this paper.

The general information section contains data on the race event, race car type, track type and conditions, crash classification and comments. The car deformation is indicated on a drawing of an open-wheeled race car. The crash description has an overall drawing of the track and a place for a detailed sketch of the incident site. The driver information consists of the anthropometry of the driver previously determined by the MSTRP (Andrzejak, et al., 1994) and information on driver posture, restraint type, and initial post-crash status and treatment. The driver injury section contains detailed injury information as determined by the medical team. The photographic coverage section documents the existence and location of the various photographic records of the car, the incident site, car kinematics (video) and any other photographic records (such as still photographs of the impact by trackside photographers). The summary sheet contains subsets of the data in the other sections for quick review.

We chose to expand the photographic coverage through cooperation with the individuals charged with taking the photographs and, in 1994, added

documentation of the crash scene. This was accomplished by adding a high resolution 8 mm video camera and recorder to each of the safety vehicles to view the track scene as the vehicle approaches the incident. The cameras and recorders were modified to automatically operate when the emergency lights on the vehicle are turned on. This allowed documentation of the incident site in terms of skid marks, impact point, and car resting position without any effort on the part of the safety team or additional personnel.

The usefulness of the information gathered from an incident is enhanced greatly if it can be organized and analyzed in such a manner that it is possible to code the major characteristics for storage in a computerized relational database. The coding ranges from using a simple scheme for indicating the year, the sanctioning body, the race track and the incident, up to more complex coding schemes for characterizing vehicle damage and driver injury.

The most specialized revision of standard crash investigation coding methods involves vehicle damage. Highway crash investigation studies use a method called the Collision Deformation Classification (CDC) for this purpose (SAE, 1996). The CDC uses a seven character alphanumeric code to describe the crash force direction (using clock directions), general area of damage, specific horizontal or lateral area, specific vertical or lateral area, type of damage distribution and, finally a damage extent code. We have taken the CDC method and specialized it for the case of open-wheeled Indy-type racing cars. This is shown in the Appendix as Figure A-1 for the first six characters, and in Figure A-2 for the damage extent code. We have also added driver injury coding to the investigation records. Both the Abbreviated Injury Scale (AIS) code, used in highway crash investigation, and the ICD-9CM discharge diagnosis code, used by hospitals, are recorded for each driver injury.

The goal of the MSTRP database is to move from individual physical files, containing the information outlined above, to a completely computerized database with all the information stored in a form that can be easily searched by computer. That phase of the work is presently in progress.

IMPACT RECORDER DEFINITION - Early in 1992, it was determined that an impact recorder was the only way to obtain accurate information on the deceleration-time histories and peak deceleration levels associated with an Indy car crash. The next steps were to define the specifications for the recorder and, in many ways more importantly, to investigate how such a device could be implemented on a regular basis on all competing cars in a race. The initial specifications were very general and included the requirements of measuring triaxial accelerations in the ±50 to ±100 G range, a sampling rate of 2000 samples/sec/channel,and the ability to record multiple impacts or, alternatively, record for 7 to 8 seconds.

Two prototype recorders were designed and built for the program through a contract with the Cranfield Impact Centre (UK). Following discussions with racing team personnel on the physical location and operation of the recorder in a typical Indy car, we concluded that stand-alone battery operation was very desirable. This was both for isolation from the vehicle electrical system to prevent any possible interference and for proper functioning in the event of an impact that compromised the vehicle's electrical system. Small size and low weight were also important, as was low power consumption since the recorder is battery-powered. The recorder should be able to remain in a car without any attention by the race car crew for at least the typical four days of a race weekend. Although the prototype recorders were never installed in a car during a race, they were installed in practice and testing sessions. Verification of their proper impact functioning for accuracy and resolution was determined by sled tests Actual in-car functioning was achieved by setting the recorder in the car to trigger on vertical impacts associated with the chassis bottoming on the race track.

By the end of the 1992 Indy car racing season we had obtained enough experience with the realities of interfacing a piece of impact recording hardware with a racing car team to establish a set of necessary requirements for an impact recorder that could be installed in all competing Indy cars. They were:
- Small, lightweight (about 1.0 kg), and self-contained with long (up to a week) battery life
- Capable of triaxial acceleration measurement (fore/aft, lateral and vertical)
- ±100 G measurement capability
- 2000 samples/second/per channel minimum digitization rate
- Multiple impact recording capability

The recording system that met all these requirements and was chosen for use in this study was an IST Model EDR-3 Environmental Shock and Vibration Recorder (Instrumented Sensor Technology, Okemos, MI) shown in Figure 1. This unit is a rectangular box (107 X 112 X 56 mm) and weighs 1.14 kg with its full complement of eight 9-volt batteries. It has three internal piezoresistive accelerometers and a temperature sensor for temperature compensation of the accelerometer signals. In operation, it

Figure 1 Impact Recorder Chosen for Use in the MSTRP Indy Car Crash Investigation Study.

continuously samples all three channels at 2000 samples/second/channel and if a predetermined trigger condition is sensed it digitally stores the data (12 bit resolution with 412 Hz anti-aliasing filtering) and then resets itself for another impact. At the chosen sampling rate it can record up to 10 separate impacts with each recording lasting for 2.0 seconds. The IST EDR-3 has been used as designed except for some firmware modifications for trigger sensing. During the first year of use, it was found that the high lateral vibration of the racing engines, which is transmitted to the rigidly mounted impact recorder, were producing some physical electronic component failures. These failures have been eliminated by potting the electronic components in silicone gel.

The triggering mode that we have used requires that the deceleration level be above a given level for a given duration of time. The values of these parameters were initially set at above 7 G for at least 10 msec. This was later changed to above 5 G for at least 5 msec. This corresponds to a minimum velocity change of 0.25 m/sec. When the unit triggers it is set to save the data from 0.5 seconds prior to the trigger point to 1.5 seconds after the trigger point, for a total recording of 2 seconds. The recorder then resets itself after one digitized sample (0.5 msec) and is ready for the next impact event. It can record up to

10 such events and then begins to overwrite the least significant event if a more severe impact takes place. Typically, most significant impacts disable the car and are the last recorded event. Occasionally, there are secondary impacts following the main impact. If a car is bottoming severely it is possible to trigger the recorder many times during a race. These impacts do not usually disable a car and represent threshold velocity changes. The repeated triggering will not affect the recording of a crash-related impact, however, because of the greater overall severity of crash impacts in terms of duration and deceleration level.

IMPACT RECORDER IMPLEMENTATION - The recorders were first installed in Indy cars in May 1993, at the Indianapolis Motor Speedway, and were used in increasing numbers of cars throughout the remainder of the 1993 season. In 1994 and 1995, the recorders were installed in virtually every Indy car in every race of the season. The use of the impact recorders is required by the rules of CART and are strongly recommended by USAC. The preferred location for the recorders is mounted on the floor of the car, below the driver's knees. This puts the recorder as near the driver as possible while remaining accessible and easy to install. The recorder must be attached with four bolts to provide a rigid coupling to the car chassis.

Cooperation from the sanctioning bodies (CART and USAC) solved the major logistics problems related to implementing the recorders in as many as 50 racing cars during a racing event. Prior to the racing car technical inspection by the sanctioning body, the recorders are loaded with fresh batteries and programmed for the upcoming days of the event by MSTRP staff. They are programmed to turn on before the first practice and to turn off one day after the race. The turn-off time is chosen to allow for the possibility of rain-delayed oval track races. As the cars pass through technical inspection, the sanctioning body technical staff assigns a recorder to each team for installation . After the race is completed, or if there is an incident in which a car is damaged, technical observers from the sanctioning body obtain the recorders from the teams and return them to the MSTRP staff for analysis and/or storage. This support from the sanctioning bodies has proven to be extremely helpful in avoiding time delays in distributing the recorders, minimizing mistakes in recorder assignment and retrieval, and allowing

MSTRP staff to concentrate on analyzing the information from the recorders and the overall task of documenting the other information associated with an incident. Two MSTRP staff members are present at each race to insure the timely and accurate acquisition of all the available photographic, video, impact recorder and medical information for each incident.

RESULTS

CRASH INVESTIGATION - The MSTRP crash investigation effort has gathered information on a total of 316 incidents from 1992 through the end of the 1995 season. For the purposes of this program an incident is defined as an impact in which the car has to be brought in "on a hook", that is, the car cannot be rolled in due to damage. This is analogous to the tow-away definition used in the national highway crash databases. Table 1 lists the number of incidents for each of the four years as well as the number of major

injuries produced and the number of impact recordings obtained for each year. There have been no fatal injuries sustained during the time period (1993-5) that the recorders have been installed in the cars.

The first year for impact recording, 1993, had a lower number of incident recordings than the subsequent years because the installation of the recorders did not start until mid-season and they did not have a high implementation rate at first. The first year with all cars in all races having impact recorders was 1994. Since not all incidents are severe enough to trigger the recorders, the total number of recordings is always less than the number of incidents. Over the years, there have been a few incidents in which the recorders have failed to capture data, primarily due to human errors or component fatigue failures (before potting was instituted), but these situations are very rare.

Table 1 MSTRP Crash Investigation Summary

Season	1992	1993	1994	1995	Total
Number of Incidents	67	82	83	84	316
Number of Major Injuries	11	14	11	5	41
Number of Recordings	*	16	44	55	115

* No Recorders Installed in 1992

ANALYSIS OF CRASH VIDEOS - In 1992, before impact recording and while the feasibility of onboard impact recording was being studied, there were two similar frontal crashes that produced severe lower leg injuries and had video coverage that could allow estimation of vehicle path and speed at the time of impact with the track wall. The MSTRP analyzed the two crashes and was able to estimate the motion of the center of mass of the car to obtain the velocity changes associated with motion into and along the wall. Additional information on the degree of crushing of the noses of the cars and the data from the required nosecone tests were used to estimate average car deceleration levels for the two crashes.

The severity of an impact can be described by the velocity change the car undergoes during the impact and the resulting deceleration level. The velocity change is not usually the speed of the car, but is rather some smaller value that is a function of the impact direction and crush of the car. Similarly, the

deceleration level depends on the crush behavior of the car. Racing car impacts, especially on oval tracks, take place at vehicle speeds that are high (170 to 230 mph) but with the velocity of the center of mass of the vehicle usually traveling at a shallow angle relative to the track walls.

In a typical wall impact, the object impacted by the car does not move and the component of car velocity along the wall does not change significantly. Accordingly, if there is little rebound of the car from the wall, the velocity change of the car is equal to the component of the center of mass velocity perpendicular to the wall. This appears to be the case in most Indy car wall impacts because the crushing of the composite structures involves permanent deformation with little elastic recovery. Even though the attitude of the car may be such that the front of the car is aimed directly towards the wall at the time of contact, as was the case in both the analyzed impacts, the motion of the center of mass of the car is

predominantly along the wall, with a lesser component into the wall. The MSTRP experience to date indicates that this is typical in impacts on high speed ovals.

The results of the analysis of the impact with the clearest video coverage are given in Table 2 below.

This analysis provided an insight into the dynamics of an Indy car/wall interaction and showed that the impact angle was shallow and the resulting velocity change was much less than the vehicle speed. The estimated average deceleration level of 53 G during the chassis crush phase of the crash was significant new information on human tolerance. Since there were no internal organ injuries in either of the two drivers, it appeared that the crush force levels of the nosecone could be raised significantly without increasing the risk of deceleration-related internal injuries. This was done by the sanctioning bodies for the 1993 season. There have been no frontal crash intrusion injuries to the lower legs and no significant internal injuries in frontal crashes since that change.

Table 2. Impact Analysis of a Video of an Indy Car Crash

Vehicle Speed at time of Impact	307 km/hr (190 mph)
Center of Mass Velocity Components Before Impact	288 km/hr (179 mph) Along Wall 101 km/hr (63 mph) Into Wall
Center of Mass Velocity Components After Impact	288 km/hr (179 mph) Along Wall 0 km/hr (mph) Into Wall
Angle of Impact with Wall	19 Degrees
Impact Duration	< 2 Video Frames (<67 msec)
Attitude of Car at Impact	Nose-First
Crash Velocity Change	101 km/hr (63 mph)
Overall Car Crush	1.1 m (3.6 ft)
Estimated Average Deceleration	First 0.38 m (1.25 ft) Nose Crush - 14 G followed by: 0.72 m (2.35 ft) Chassis Crush - 53 G

DISTRIBUTION OF CRASHES BY IMPACT
DIRECTION - The direction of impact to the car
depends on the attitude of the car at the instant of
impact and the pre-impact motions of the car
(especially rotations). As a result, the point of impact
and the direction of impact can vary greatly. The
impact directions, in terms of principal direction of
force, for the 115 incidents in which an impact
recording was obtained, have been analyzed. The
categories chosen were front, left or right front, left or
right side, left or right rear, rear and rollover.

The results of this analysis are shown in Figure 2 as a
distribution around the car in a clockwise manner.
The most frequent impact direction was the right side
(19%), followed closely by the left front (18.3%) and
the right front (16.5%). The left rear was involved
next most frequently (14.8%) and the other directions
were all below 10% with left side at 9.5%, right rear
at 8.7%, front at 6% and rear at 5.2%. Rollovers were
the least frequent occurrence at 1.7%.
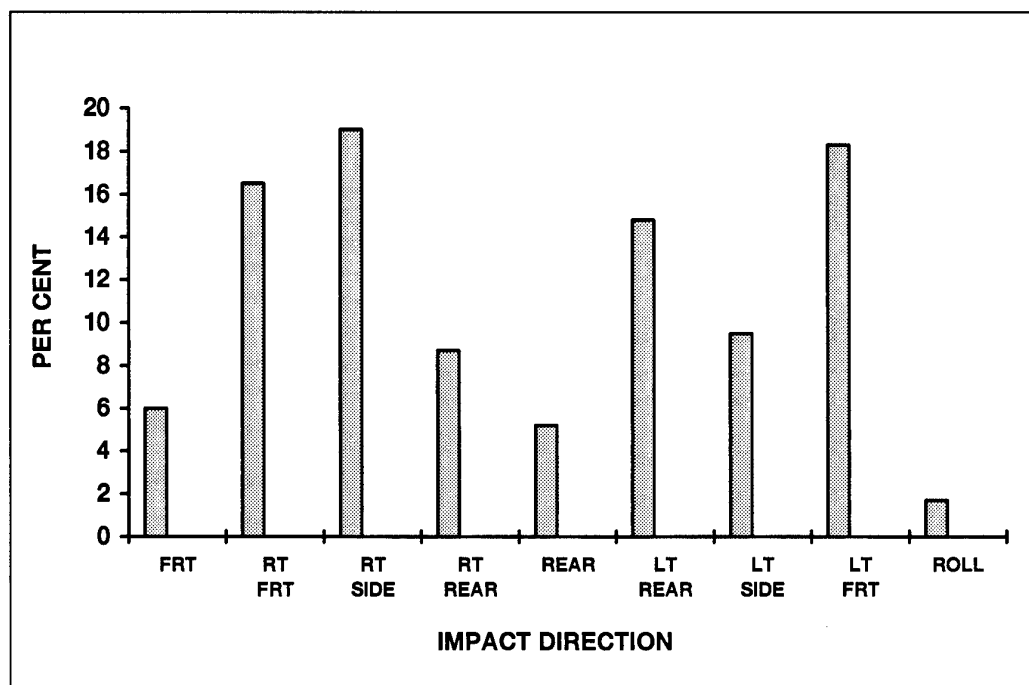
Figure 2. Distribution of Impact Direction for Impacts with Recordings. 1993-1995 Seasons (115 Cases).

EXAMPLES OF MOST SEVERE CRASHES

The following are examples of the most severe impacts recorder during the 1993 through 1995 racing seasons,

FRONTAL IMPACT - The most severe frontal impact that has been recorded is shown in Figure 3. The velocity change was 61 km/hr (38 mph) and the peak deceleration was 62 G. The driver lost control of the car and it contacted the outside wall of the track with a nose-first attitude. The nosecone of the car was completely crushed, but the front bulkhead was not damaged. The driver suffered only minor pains and scrapes. His helmeted head struck the steering wheel, but there were no head or neck injuries. This crash demonstrated the effectiveness of the nosecone performance changes initiated by the sanctioning bodies in 1993.

SIDE IMPACT - The most severe side impact recorded is shown in Figure 4. The lateral velocity change was 104 km/hr (64.5 mph) and the peak lateral deceleration was 120 G. The driver lost control of the car at the apex of a turn and the car spun 180 degrees and struck the outside wall of the track first with its left rear wheel. This contact rapidly rotated the car into the wall, striking the front wheel and then the entire left side of the car against the wall. The suspension and side structure crushed significantly during the impact, but there was no intrusion into the cockpit. The driver was rendered unconscious for a brief time, as his helmeted head struck the side edge of the cockpit during the impact. There were no internal torso or skeletal injuries.

REAR IMPACT - The most severe rear impact recorded is shown in Figure 5. The rearward velocity change was 70 km/hr (29 mph) and the peak rearward deceleration was 82 G. The driver lost control of the car at the apex of a turn, the car spun 90 degrees counterclockwise and struck the outside wall of the track rear-first with both its rear wheels, followed quickly by the gearbox which was crushed severely. This car had a transverse gearbox. The car had an onboard video camera which showed that the driver leaned his head forward prior to the impact. The driver suffered no significant injuries and continued to compete that same weekend
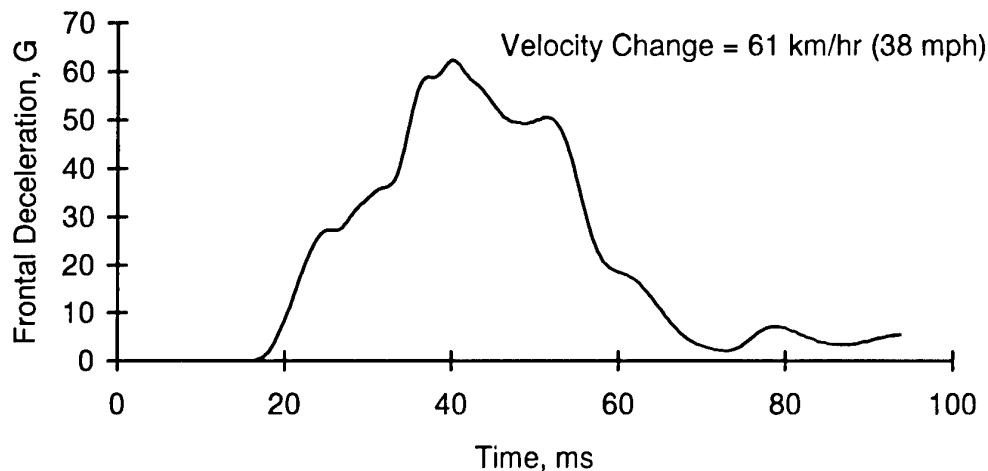
Figure 3. Most Severe Frontal Impact Deceleration-Time History Recorded During 1993-1995.
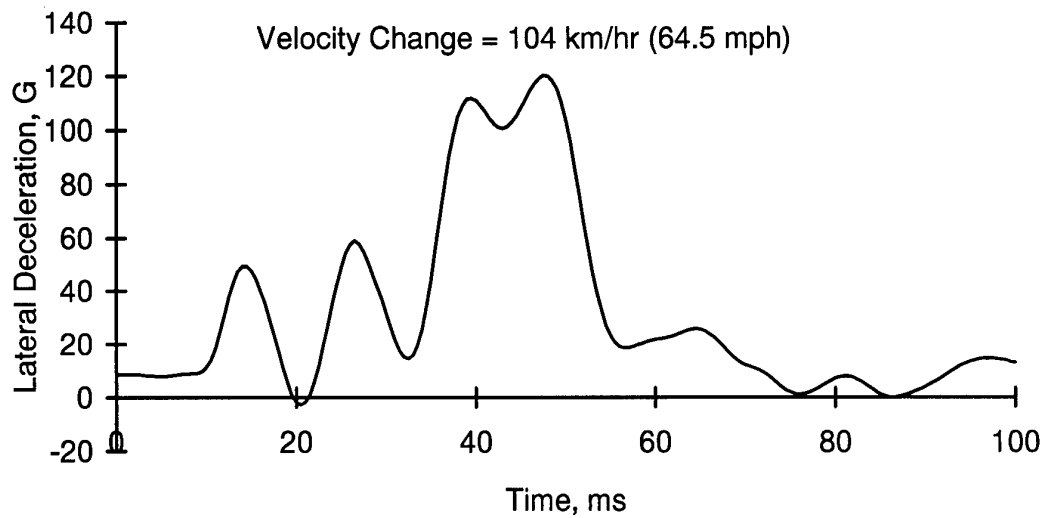
Figure 4. Most Severe Lateral Impact Deceleration-Time History Recorded During 1993-1995.
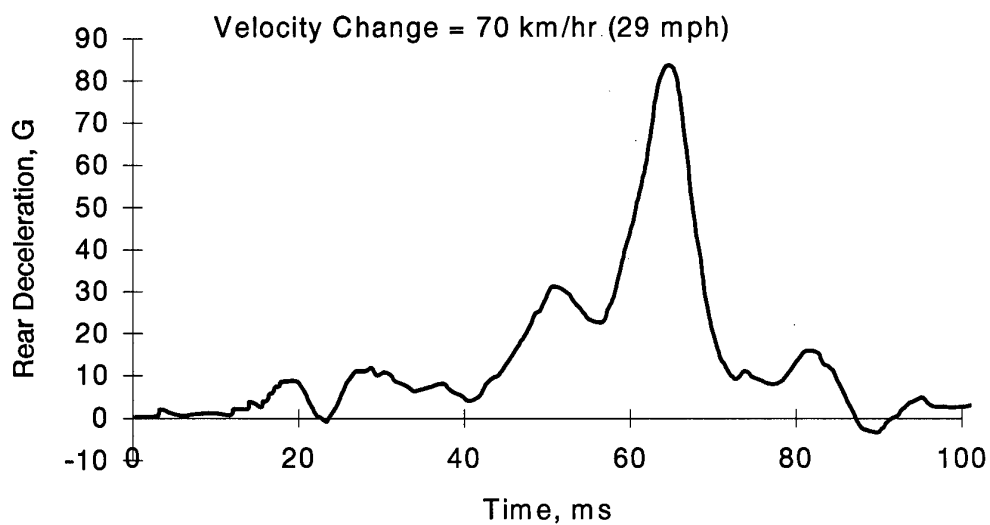
Figure 5. Most Severe Rear Impact Deceleration - Time History Recorded During 1993-1995.

DISCUSSION

The methods described above are the result of a number of trials and refinements of procedures that allow the efficient and effective performance of routine crash investigation in the difficult setting of a competitive automobile racing event. Four years of investigation of Indy car crashes has provided a number of insights into the dynamics of racing car crashes. What began as a program to investigate racing car crashes to improve the safety of racing cars has had the additional benefit of providing new information on the tolerance of the human body to crash decelerations.

The focus on Indy car crashes has proven to provide an almost laboratory-like setting due to the similarity of the cars and to the relative simplicity of the crashes (predominantly planar crashes involving single car impacts against well-defined impact surfaces). The recording of the vehicle decelerations in real racing car crashes has added immeasurably to our knowledge. The examples of impact recordings given above are remarkable in terms of the severity of crashes and the resulting lack of significant injuries. Subsequent study of these crash conditions using instrumented test dummies and mathematical models will provide even greater insight into the tolerance of the human body to impact loading as well as into ways to improve protection for both racing drivers and passenger car occupants. An example of such a study of racing car restraint systems in frontal crashes was given in a previous paper from the MSTRP in 1994 (Melvin, et al., 1994)

ACKNOWLEDGMENTS

REFERENCES

Andrzejak, D.V., Baron, K.J., and Roegner, J., "Anthropometry of Indy Car Drivers", Proceedings of the 1994 Motorsports Engineering Conference, Volume 1: Vehicle Design Issues, pp. 367 -379, December 1994, SAE Paper No. 942547, SAE, Warrendale, PA

Melvin, J.W, Little, W.C., Jedrzejczak, E.A.,and Pierce, J., "Racing Car Restraint Frontal Crash Performance Testing", Proceedings of the 1994 Motorsports Engineering Conference, Volume 1: Vehicle Design Issues, pp. 73 - 80, December 1994, SAE Paper No. 942482, SAE, Warrendale, PA

SAE Handbook, "Collision Deformation Classification - SAE J224 MAR80", SAE Recommended Practice, 1996, SAE, Warrendale, PA

APPENDIX A - MSTRP Crash Investigation Forms

[GM] Collision Deformation Classification - Open Wheel

FRONT

(Seven Character Code)

```
1  2  3  4  5  6  7
```

FORCE DIRECTION
GENERAL AREA OF DAMAGE
SPECIFIC HORIZONTAL OR LATERAL AREA
SPECIFIC VERTICAL OR LATERAL AREA
TYPE OF DAMAGE DISTRIBUTION
EXTENT CODE
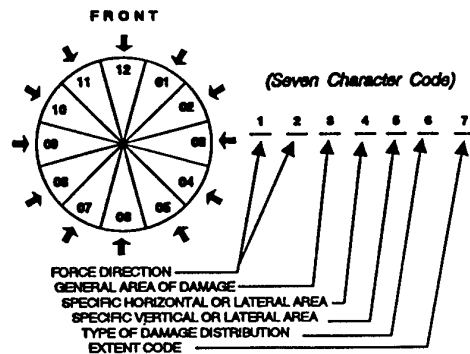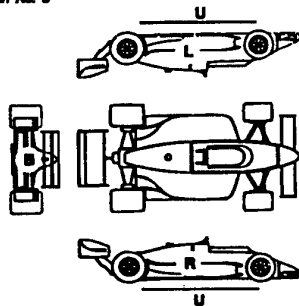
Column No. 3

F - FRONT
R - RIGHT SIDE
B - BACK SIDE
L - LEFT SIDE
T - TOP
U - UNDERSIDE
X - UNCLASSIFIABLE

	F, B LAT VERT	L, R LONG VERT	T, U
Col 3			
Col 4	LAT	LONG	LONG
Col 5	VERT	VERT	LAT
Col 7	LONG	LAT	VERT

Choices for 4, 5 & 7 are based on choice for 3.

Column No. 4
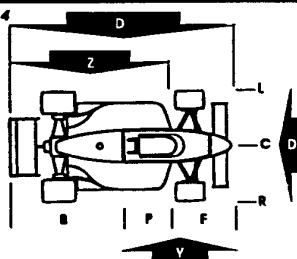
LATERAL CHOICES

D - DISTRIBUTED
L - LEFT FRONT OR REAR
C - CENTER - FRONT OR REAR
R - RIGHT - FRONT OR REAR

LONGITUDINAL CHOICES

D - DISTRIBUTED
F - SIDE FRONT - LEFT OR RIGHT
P - SIDE CENTER SECTION - LT OR R
B - SIDE REAR - LEFT OR RIGHT
Y - SIDE OR END (F+P OR L+C)
Z - SIDE OR END (B+P OR R+C)

Column No. 5
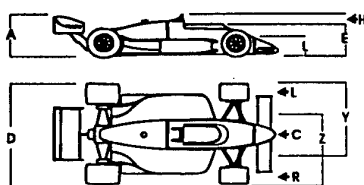
VERTICAL CHOICES
(FRONT, REAR OR LAT)

A - ALL
E - TOP OF COCKPIT & BELOW
L - NOSE CONE
H - TOP OF COCKPIT & ABOVE
W - WHEELS, TIRES, SUSPENSION

LATERAL CHOICES
(TOP & UNDERSIDE)

C - CENTER
R - RIGHT
Y - L & C
Z - R & C
D - DISTRIBUTED
L - LEFT

Column No. 6
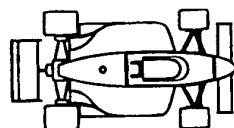
W - WIDE IMPACT AREA > 16'
N - NARROW IMPACT AREA <= 16'
S - SIDE SWIPE
O - ROLLOVER (INCL ONTO SIDE)

A - OVERHANGING STRUCTURE
E - CORNER
U - NO RESIDUAL DEFORMATION
K - CONVERSION
T - TORN OFF

CDC Extent Code Grids
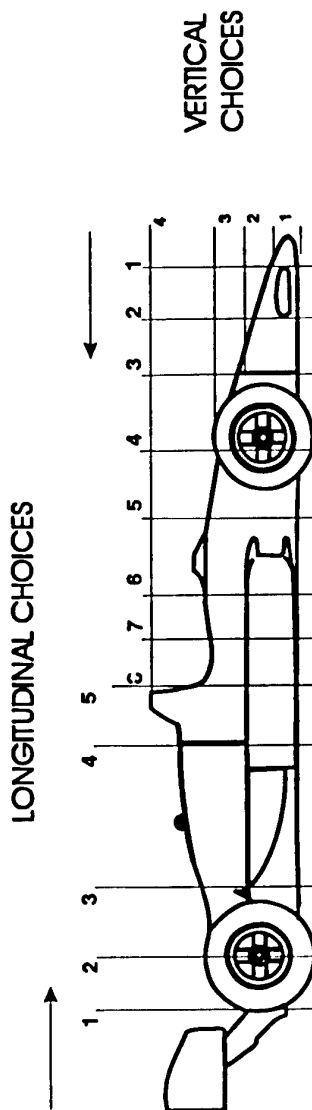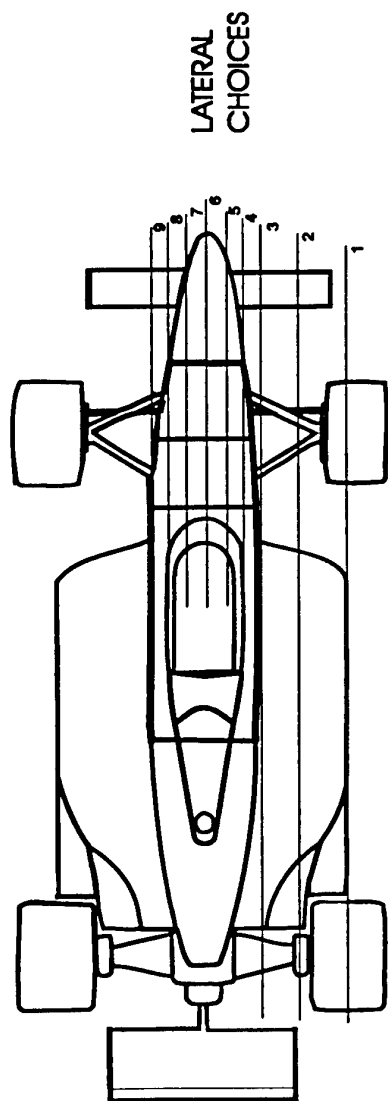
LATERAL CHOICES

VERTICAL CHOICES

LONGITUDINAL CHOICES

GM

GM **MARS**

Motorsports Accident Reporting System

Summary

Case No. ☐☐–☐☐–☐☐–☐☐

Summary

Diagram section of track, and sketch motion of car from pre- thru post-crash.

right side   left side

OIC _____

_____

CDC _____

_____

MARS

GM
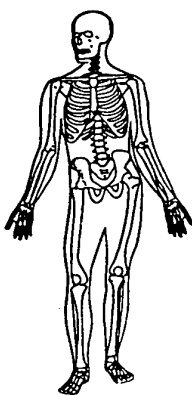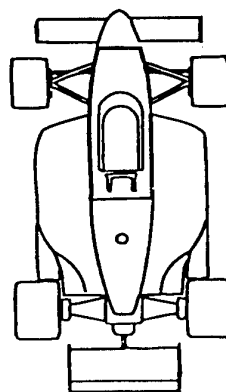
General Information

Motorsports Accident Reporting System

Case No. ☐☐ ☐☐ ☐☐ ☐☐

Race Car

Class	_____
Chassis	_____
Model	_____
Average track speed	_____ (mph)
Speed at crash	_____ (mph)
Wt (w/fuel) at crash	_____ (lbs)

Race

Sanctioning body	_____
Date of crash (mm/dd/yy)	_____

Track

Type	☐ oval	☐ city	☐ road	☐ other:_____
Condition at crash	☐ dry	☐ oily	☐ wet	☐ other:_____
Flag at crash	☐ green	☐ yellow	☐ red	☐ none
Ambient temperature	_____ °F			

Crash Classification

Car contacted	☐ another car ☐ concrete wall ☐ tire barrier ☐ armco ☐ nothing ☐ other:_____
Pre-crash motion	☐ skid ☐ spin_____ degrees ☐ loss of control w/o skid or spin
Activity	☐ practice ☐ qualifying ☐ race
Location on track	_____

Comments

_____

_____

_____

_____

_____

_____

_____

_____

GM **MARS**

Motorsports Accident Reporting System

Crash Description

Case No. ☐☐–☐☐–☐☐☐–☐☐

Summary

Diagram section of track, and sketch motion of car from pre- thru post-crash.

Track: Indianapolis 500
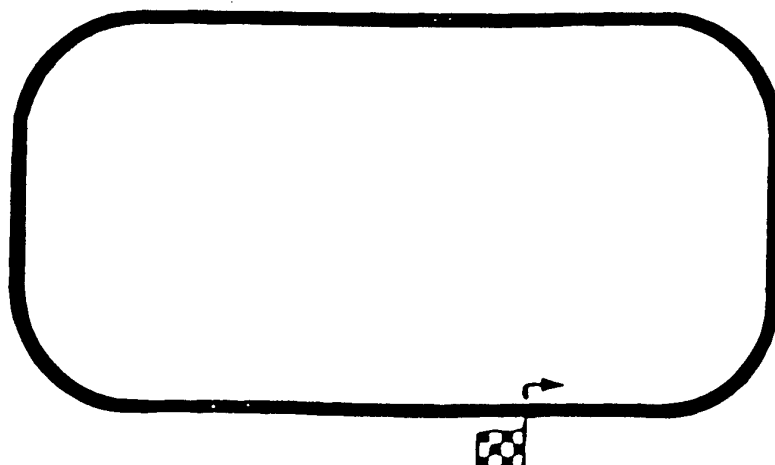
Car Deformation

Case No.

1	2	3	4	5	6	7

Open wheel race car crash deformation code

Motorsports Accident Reporting System

MARS

GM

GM MARS — Driver Information

Motorsports Accident Reporting System

Case No. ☐☐ ☐☐ ☐☐☐ ☐☐

(Units of length in inches)		
Sex	Male	☐
	Female	☐
Age		
Stature		
Weight (lbs)		
Upper leg Length		

Seated Length	
Hip Width	
Shoulder Width	
Seated Height	
Seated Eye Length	
Upper Arm Length	

Forearm Length	
Chair Height	
Knee Height	

Ejection	☐ no ☐ yes { ☐ completely / ☐ partially
Posture at time of crash	☐ normally seated ☐ other:_____
Harness type	☐ 5 point ☐ 6 pt w/forward / ☐ 6 pt w/rearward
Injured	☐ no ☐ minor ☐ major
Unconscious	☐ no ☐ yes, how long: ____ ☐ min / ☐ hrs coma scale (0-15): _____
Treatment	☐ none ☐ first aid ☐ hospital, not ☐ hospital, admitted outpatient ☐ hospital, ____ # ☐ fatal

MARS

GM

Motorsports Accident Reporting System

Driver Injury
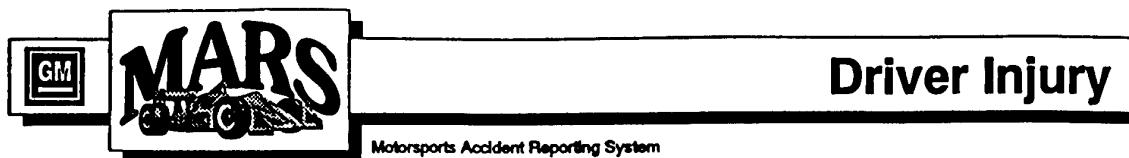
Case No. ☐☐ ☐☐ ☐☐ ☐☐

- Write all injuries (minor & major) on occupant diagram.
- Write type of injury, severity or injury & any specific treatment of each injury.
- Number each injury for use on chart below.

right side   left side
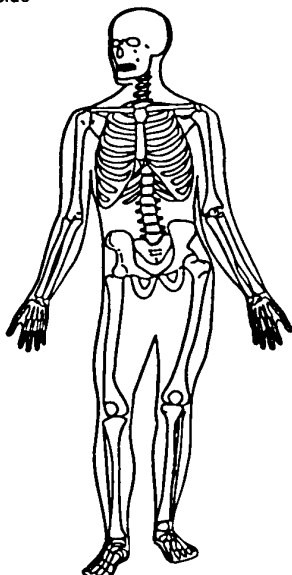
- Write possible source of contact for each injury.
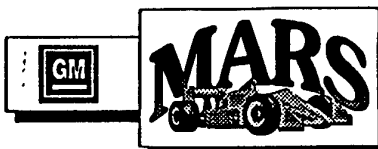
Injury #	Most Likely Source	AIS	ICD9	Rt.	Lt.
				☐	☐
				☐	☐
				☐	☐
				☐	☐
				☐	☐
				☐	☐

Photo Coverage

GM MARS

Motorsports Accident Reporting System

Case No.

● *Video* ☐ none

Format	Provided by	Where stored	Label / ID / number

| Identify location on tape | | | copy |
| | | | org |

Format	Provided by	Where stored	Label / ID / number

| Identify location on tape | | | copy |
| | | | org |

● *Other* ☐ none

Media	Provided by	Where stored	Label / ID / number	copy	org

Comments	

Modelling Head Injury Countermeasures: a 3D helmet model.

D.W.A. Brands, J.G.M. Thunnissen, and J.S.H.M. Wismans

TNO Crash Safety research Center
Schoemakerstraat 97
P.O. Box 6033
2600 JA Delft
The Netherlands

ABSTRACT

A three dimensional Finite Element Model of an existing full-face motorcycle helmet mounted on a headform has been developed. Material parameters were obtained from literature data and from component tests. The model is validated by simulating impacts at different locations using the headform acceleration time histories. From this it can be concluded that the headform response is predicted in a realistic way. The simulations showed two phenomena that influence the headform response, i.e. the behaviour of the material between the headform and the point of impact, and the dynamic response of the outer regions of the outer shell. It is believed that the current model describes most of the phenomena observed during an impact and, therefore, is suitable for future optimization studies. The application of the current model is limited to impacts on a flat anvil at points in the median plane of the headform. Recommendations for further model enhancements will be presented.

1. INTRODUCTION AND OBJECTIVES

The head and spine of the human body are considered the most critical body parts in crash situations because of the often irreversible nature of injuries to the central nervous system. Basically four different strategies for head injury mitigation can be distinguished:

- Influencing the <u>accident conditions</u> by changing the environment of the crashing vehicle. An example of such a measure is a deformable guard rail.
- Improvement of the <u>crashworthiness</u> of the vehicle by means of the design of the vehicle construction like the crush zone.
- Control of the <u>occupant motion</u> during the crash. The seat belt is based on this principle. The primary function of the seat belt is to connect the motion of the occupant to the vehicle motion in order to use the built-in deceleration properties of the vehicle (crashworthiness) and to control the motion of the passenger within the free space between occupant and vehicle interior.
- Control of the <u>impact contact</u> between the body and environment. A safety helmet is based on this principle. The function of a safety helmet is the reduction of the impact load (energy absorption) as well as the distribution of the load over a larger contact area (pressure distribution). In addition the hard outer shell of a helmet prevents penetration of sharp objects.

For a specific accident situation often a combination of above strategies will offer the optimal effect.

Several kinds of numerical models are available in support of the development of measures based on the above strategies. Examples are models for the interaction between vehicle and road furniture, models describing the crash response of the vehicle structure itself, models describing the occupant response in interaction with restraint systems and models describing the head impact with a surface and the effect of countermeasures such as crash helmets.

In literature, two types of helmet models were found, Lumped Mass Models [1],[2] and Finite Element Models [3],[4]. The Lumped Mass Models are suitable for trend studies. However they do not allow to calculate the stiffness of the individual helmet parts by their shapes, dimensions and material properties as can be done when using a Finite Element Model. So far, the Finite Element Models described in literature were not validated and neglected the effect of the soft comfort liner that provides the fit of the helmet on the head.

Objectives

Approximately 30% of the traffic accidents in the Netherlands result in head injuries [5]. A direct method of reducing head injuries is the use of (crash) helmets. In practice, helmets have proven their effectiveness, it is shown that for direct impact situations, an injury risk reduction of circa 30% to 90% can be achieved [6]. However, a fundamental understanding of its protective function is still lacking. For this reason, the objective of this paper is specifically the development and validation of a numerical model for helmet design optimization.

2. METHODS

In this study, a three dimensional model of an existing, certified full-face motorcycle helmet of consumer size 59-60 (L) was developed in the Multibody-Finite Element package MADYMO version 5.2 [7].

The model has been validated by simulating free fall impact absorption tests as specified under ECE-Regulation 022/04 (R.22 impact tests) using a flat, fixed steel anvil [8]. During the impact the acceleration time histories of the headform are recorded in three directions of a local headform coordinate system (x_l, y_l, z_l) with its origin in the centre of gravity (cg) of the headform, as

shown in Figure 1. Simulations of impact absorption tests have been conducted on four different impact points and the recorded headform acceleration has been used for validating the model. In case of the frontal impact the anvil reaction forces are also used for validation of the model.
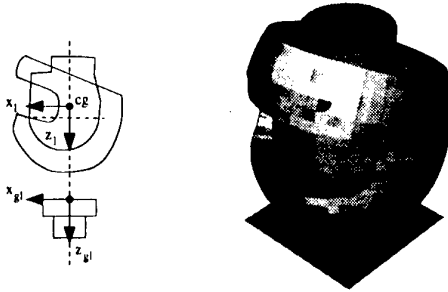
Modelling assumptions

Figure 1   *A helmeted headform in an ECE-R022 impact test and the definition of the coordinate systems used.*

The model in R.22 test setup is shown in Figure 1. The helmet model consists of an outer shell, a protective padding liner, a chin strap and accounts for a comfort liner. The chin parts of the inner liner are not included in the model. Table 1 summarizes the most important material parameters and modelling assumptions. These will be discussed for each component individually.

The *outer shell* is modelled by 880 shell elements and it's geometry has been digitized by a 3-D coordinate measuring device with an accuracy of approximately 0.01 *mm*. The thickness of the outer shell is assumed to be constant. In reality its thickness varies between 2.2 and 3.9 *mm*.

During an impact onto a flat surface the deformation of glassfibre reinforced shells is small and no visual delamination will occur [9]. Furthermore it is assumed that the material behaviour of the outer shell is isotropic because the glass fibres in the outer shell are randomly orientated. For these reasons an elastic material model will be used.

Since the exact composition of the outer shell is unknown, an estimation of the Young's modulus has to be made. For this reason static stiffness tests as described in [8] are conducted in three directions on the outer shell only. The test setup for the transverse loading direction is illustrated in Figure 2 together with the experimental determined force deflection curve and the simulation result.

The *protective padding liner* is modelled by 636 brick elements that are connected to the shell elements of the outer shell. The geometry of the inside of this liner has also been digitized.

In the impact conditions modelled, the material behaviour of this liner is strain rate independent [4]. It is modelled using an elasto-plastic material model that uses an isotropic hardening law based on the Von Mises yield
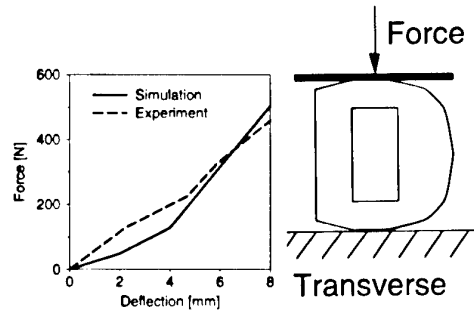

Figure 2   *Force deflection curve of outer shell only, in transverse loading direction, and test setup used.*

criterion [7]. The assumption has been made that the density of the Expanded Poly-Styrene (EPS) used in the liner is constant. The stress-strain relation that defines the yield function used in the elasto-plastic material model is shown in Figure 3 together with two stress-strain relations obtained from compression tests by [3] and [10]. It must be noted that the curve obtained from [10] yields for logarithmic strain values with absolute values less than 1.2. By extrapolating this curve using the slope of the stiffest part of [3] the remainder of the stress-strain relation used in the model is obtained. Figure 3 shows variations in literature data of the stress-strain behaviour of Expanded Poly-Styrene. The influence of these variations will be examined in a parametric study.
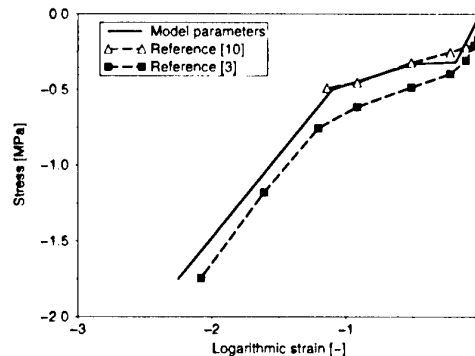

Figure 3   *Experimental and modelled stress-strain behaviour of the protective padding liner.*

The *comfort padding liner* consists of urethane foam faced with a nylon cloth layer. This liner has a strain rate dependent stiffness. This stiffness is very low but rises rapidly for compressive strains above 80% [1],[2]. It can be concluded that the comfort liner has no energy absorbing properties by itself [6] but effects on the headform acceleration time history were observed [2],[11]. These effects are accounted for by assuming a gap between the headform and the inner surface of the protective padding liner. This approach prevents numerical instabilities, due to large deformations as a result of the very low stiffness of the comfort liner to

Table 1 *Materials and modelling assumptions for the model of a full-face helmet and the test setup.*

Component	Material	Element type	Model	E [GPa]	v [-]	ρ [kg/m³]	Comment
Helmet							
Outer shell	Fibreglass and polyester resin*	shell	Linear elastic	8.54	0.325	2082**	thickness = 3 [mm]
Protective padding	Expanded polystyrene	brick	elasto-plastic	$1.8 \cdot 10^{-3}$	0.0	58.7**	σ_{yield}= 0.32 [MPa]
Comfort liner	Nylon cloth, Urethane foam	--	gap	--	--	--	--
Chin strap	Nylon webbing	--	Madymo belt model+	--	--	--	½ stiffness function by [11].
Test setup							
Anvil	Steel	--	Rigid plane+	--	--	--	--
Headform	Aluminium	shell	Rigid	70++	0.3++	--	mass = 5.6 [kg]+

*   *Exact composition unknown.*   **   *Densities include also mass of components not modelled.*
\+   *Multibody model.*   \+\+   *Parameters used by contact algorithm only.*

occur.

The *chin strap* is included in the model to prevent excessive headform rotations relative to the helmet during an impact. The chin strap is modelled by connecting the helmet to the headform using two MADYMO belt segment elements as can be seen in Figure 4. The stiffness of these elements is determined by a force-elongation curve that has to be given as input. This curve is obtained by dividing in two the values of a force elongation function of a car safety belt [12].

The steel *anvil* is modelled by a multibody plane that is assumed to behave rigidly.

The *headform* consists of aluminium and its stiffness is large compared to the stiffness of the protective padding liner. For this reason the headform is modelled by an arbitrarily surface that consists of 352 rigid shell elements. The mass, position of the centre of gravity and the geometry of the headform comply the provisions of the ECE Regulation [8]. The rotational inertia, however, are not prescribed in this regulation, therefore the rotational inertia values of the 50th percentile Hybrid III dummy head have been used [13].

The helmet is mounted on the headform conform the ECE-R022/04 requirements. However, the requirement that the helmet has to be mounted on the headform using a pre-load of 50 N, could not be met due to the fact that the comfort liner is modelled by a gap.

The contact between the headform and the helmet is modelled by a contact definition based on a penalty formulation using a low coefficient of friction. The contact between the outer shell and the anvil multibody plane, is modelled using a contact definition based on an impulse formulation with a low coefficient of friction applied.

A simulation of an impact on the top area of the helmet has been used for fine tuning the model parameters of the protective padding liner. Then impacts at the frontal, lateral and rear impact points (impact points B, X and R in [8]) have been used for model validation. The impact points are shown in Figure 4 and the test conditions are summarized in Table 2.

Top impact point (P)   Frontal impact point (B)

Rear impact point (R)   Lateral impact point (X)
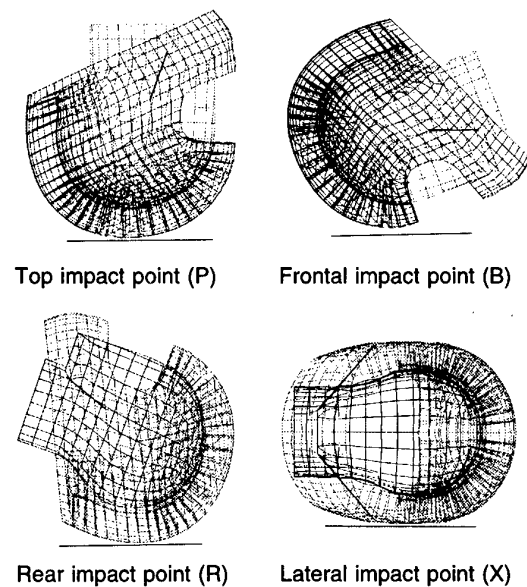
Figure 4   *Impact points modelled conform ECE-R022*

3. SIMULATION RESULTS

Top impact

Figure 5 shows the headform acceleration time history for an impact at the top area of both the experiment and the simulation after fine tuning the material parameters of the

Table 2 *Impact test conditions simulated.*

Impact point	Velocity	Anvil type	Purpose
Top	7.5 [m/s]	Flat	Fine tuning material parameters innerliner
Frontal	7.5 [m/s]	Flat	Validation
Rear	7.5 [m/s]	Flat	Validation
Lateral	7.0 [m/s]*	Flat	Validation

* ECE-Regulation 022/03

protectivé padding liner. Simulating this 12 *ms* impact needed approximately 13 minutes computational time on a Silicon Graphics computer with a 180 *Mhz*, R-5000 SC, processor.

Figure 6 *The deformation stages during an impact at the top area of the helmet.*

Figure 5 *Simulation results of an impact at top-area (impact point P) of a helmeted headform.*

Figure 5 shows that the simulation results resemble the experimental results quite well. The model gives a very good description of the shape of the acceleration peak which indicates that the model describes most of the phenomena that influence the headform acceleration during an impact. Still some differences can be observed,

* The peak acceleration levels are overestimated by approximately 12% of the experimental values.
* The acceleration peak lasts too long.

Deformation stages

For better understanding the contribution of the various components of the helmet to the dynamic response of the headform, the velocity of the headform is compared with the velocity of a node situated on the outer region of the helmet. From this analysis it can be concluded that in fact six different deformation stages can be observed during an impact on the top area of a helmeted headform. These are illustrated in Figure 6 and Figure 7.

-1- Both helmet and headform move towards the impactor plane. The helmet hits the impactor plane and its velocity decreases to zero while the velocity of the headform is constant.

-2- The amount of force applied on the headform by the

Figure 7 *Schematic overview of the dynamical behaviour of a helmeted headform. V_{sh}= velocity outer regions, V_{hf}= velocity headform.*

protective padding liner increases due to increasing compression of the protective liner and due to the outer regions of the helmet pressing the liner more firmly against the headform by its inertia. As a result the headform acceleration increases until the helmet velocity becomes zero.

-3- The outer regions of the helmet then move back towards the impactor plane. The protective padding liner will be pressed less firmly against the headform causing the headform acceleration to decrease.

When the simulated time reaches 4.6 *ms* the headform acceleration starts to increase again. This is due to the fact that the mechanical behaviour of the protective padding liner predominates the dynamical effect of the moving helmet part as a result of the firm compression of the protective padding liner.

-4- The inertia of the moving helmet part increases the

effect of the compression of the protective padding liner and the headform acceleration increases further until maximum compression of the protective padding liner is reached.

-5- The headform moves away from the impactor plane causing the protective padding liner to become less compressed. As a result the headform acceleration decreases.

-6- The moving helmet part now also bounces back from the impactor plane. This results in a helmet velocity even larger than the headform velocity. The helmet now pushes the headform away from the impactor plane causing the headform acceleration to decrease less for a while.

From this it may be concluded that the phenomena observed are mainly two dimensional. This is actually not true. The magnitude of the deformation of the outer shell perpendicular to the anvil's surface (global z-direction) equals approximately 18 mm, but in global x- and y-direction magnitudes of 10 mm and 5 mm respectively can be observed. However, the effects of the deformations in global x- and y-direction are not investigated in detail yet.

Energy absorption

For impacts at the top area the headform rotations stay low. For this reason the energy absorption can be obtained by

$$E_{absorbed} = \frac{1}{2} m_{headform} \left(v_{before}^2 - v_{after}^2 \right) \qquad (1)$$

in which $E_{absorbed}$ represents the energy absorption of the helmet, v_{before} and v_{after} resemble the headform velocity before and after the impact and $m_{headform}$ resembles the headform mass. It can be concluded that the energy absorption in the model (89 J for top-impact) is lower than in the real helmet (150 J for top-impact).

Different impact points

The impact points are shown in Figure 4.

Frontal impact

The simulation results obtained from the *frontal impact* are compared with results of experiments conducted by Beusenberg *et al.* [6]. They tested four helmets of the same type as the one modelled in this paper but with a lower impact velocity (7.0 m/s instead of 7.5 m/s). In these experiments, the headform accelerations with respect to the local headform coordinate system were measured together with the anvil reaction forces (see Figure 1).

The headform accelerations and anvil reaction forces for each direction separately, can be found in the Annex. The computed resultant headform acceleration is shown in Figure 8 together with the mean ± the standard deviation of the experimental results (dotted). This figure shows that the model predicts the maximum headform acceleration quite good, although it appears at a later moment in time than the experimental peak value.
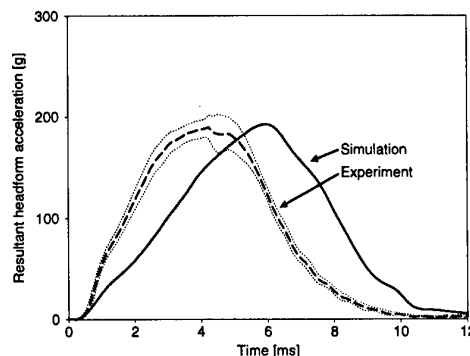

Figure 8   *Resultant headform accelerations for frontal impact point (B). Experimental corridors (dotted) defined as mean ± standard deviation.*

Rear impact

The simulation and experimental results of the *rear impact* at 7.5 m/s are shown in Figure 9. The model response is similar to the response of the frontal impact, in that the maximum acceleration value is predicted correctly but its appearance is later than in the experimental result. However, the initial loading slope of the predicted acceleration time history is good. During the unloading part of the headform acceleration a delay can be seen at 95 g that is not present in the experimental results. In the analysis of the top impact it was observed that this is caused by the helmet bouncing back from the impactor plane, hitting the headform.
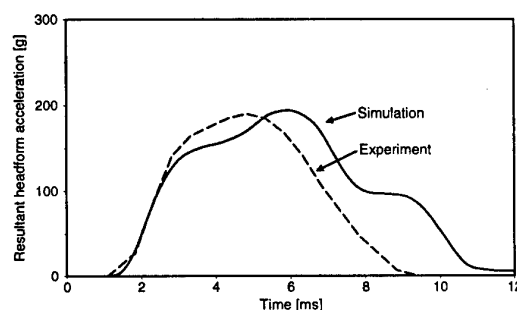

Figure 9   *Resultant headform accelerations for rear impact (R) according to ECE-R022/04.*

Lateral impact

Simulating a *lateral impact* was not possible with the current model. The reason is the excessive headform rotation with respect to the helmet. This is probably caused by the large gap between the headform and helmet that exists as a result of not modelling the comfort

foam and the chin parts of the helmet.

Parametric study

The top impact condition has been used in a parametric study to gain more insight on the sensitivity of both the resulting headform acceleration and the energy absorption of the model, to certain material parameters. The quantities observed are:

- The maxima of the first and second acceleration peaks in Figure 5 (a_{peak1}, a_{peak2}).
- The energy absorption ($E_{absorbed}$) by the helmet as is determined in Equation (1).

The parameters varied are:

- The Young's modulus (E) of both outer shell and protective padding liner.
- The thickness of the comfort liner, by varying the size of the gap between the headform and the inside of the protective padding liner.
- The density (ρ) of the outer shell.
- The yield stress (σ_{yield}) of the protective padding.

From an experimentally determined relationship between the yield stress of the Expanded Poly-Styrene and its density in [2] it can be found that

$$\sigma(\rho_1) = \left(\frac{\rho_1}{\rho_2}\right)^{1.5} \cdot \sigma(\rho_2) \tag{2}$$

in which $\sigma(\rho_i)$ resembles the yield stress of foam i with density ρ_i. From this relation is can be concluded that varying the yield stress of the Expanded Poly-Styrene by 30% complies a variation of the density by approximately 19%.

Table 3 *Results of parametric study for top impact.*

Parameter	Level %	a_{peak1}	a_{peak2}	Energy absorbtion
Protective padding				
E	±30	+	+	+
σ_{yield}	±30	++	++	-
Outer shell				
E	±30	o	o	o
ρ	±30	++	o	o
gap	±33	-	-	o

Change of observed quantity when parameter is increased from lowest to highest value:
o   *less than 5%*
-/+   *decrease/increase with more than 5%*
--/++   *decrease/increase with more than 15%*

The results in Table 3 show that varying material parameters of the protective padding liner has the largest effect on both the peak headform accelerations as well as the amount of energy absorbed. Of the material parameters of the outer shell only the density parameter

has effect on the value of the first peak. Increasing the gap size leads to lower peak acceleration values. Similar tendencies are found in experimental results in which a full-face thermoplastic shelled helmet was impacted with a flat striker, when loosely mounted on a headform instead of well strapped down [11].

4. DISCUSSION OF THE RESULTS

The model proves to be capable of giving quite good predictions of the *headform response* for impacts at points situated on the median headform plane. Experimental peak values of the resultant headform acceleration are computed within a 12% range for impacts at the top area of the helmet. For frontal and rear impacts these predictions are even better. However, the timing of the acceleration peaks can be improved by abandoning the assumption that the mass density of the protective padding liner is constant. In reality the densities applied in the real helmet are slightly lower at the top area of the helmet and higher on the edges of the protective padding liner. It was not possible to simulate lateral impacts because excessive headform rotation with respect to the helmet occurred. This is probably caused by the assumption that the effect of the comfort padding liner has been estimated by applying a gap between the headform and the protective padding liner. As a result there is no fixation of the helmet on the headform by means of friction at areas remote from the point of impact.

The parametric study showed that the headform response is sensitive to the material properties of the protective padding liner. Increasing the yield stress of the this liner, which resembles increasing the actual density of the expanded Poly-Styrene used, leads to higher acceleration peak values. Increasing the Young's modulus of this liner has similar effects.

Increasing the mass density of the outer shell leads to increasing headform acceleration peak values. Although experimental results in [14] indicate that increasing the outer shell stiffness leads to higher peak acceleration values, only minor effects on the headform response can be seen in Table 3.

The difference in *energy absorption* between the real helmet and the model, is caused by the choice of the material models used. The outer shell of the helmet is assumed to behave linear elastic. In reality the Fibre Reinforced Plastic outer shell will show hysteresis behaviour [1] and a strain rate dependent stiffness [9], thus contributing to the energy absorption.

The elasto-plastic material model, used for the protective padding liner, assumes incompressible material behaviour during Yielding. In reality Expanded Poly-Styrene behaves highly compressible until bottoming out occurs [15]. As a result, the computed stress in the direction of the largest compression will be larger than in reality. This implies that the computed stiffness of the protective padding liner will be too high, thus causing the headform accelerations to become too large. However during the elastic part of the deformation a compressible material behaviour, using a Poisson ratio of zero, can be applied.

To obtain realistic maximum headform acceleration values this elastic part is assumed to be larger than in reality using a low Young's modulus (80% of the lowest value found in literature [16]) and a relative high Yield stress (18% higher than the highest value found in literature [9]). As a result less foam of the protective padding liner will yield in the model than in reality, thus decreasing the amount of impact energy absorbed by the model. This effect is confirmed by the results of the parametric study that show that the energy absorption of the helmet can be improved by raising the Young's modulus and lowering the Yield stress of the protective padding liner which causes more padding to yield.

5. SUMMARY AND CONCLUSIONS

The three dimensional Finite Element Model of an existing full-face helmet mounted on a headform proved to be capable of giving quite good simulation results for impacts in the median headform plane on a flat anvil. Maximum headform acceleration values were predicted within a 12% range for impacts at the top area. The maximum headform accelerations for frontal and rear impacts lie within a 3% range.

Analysing the simulation results of an impact on the top area of the helmet confirms the observations by [2] that the impact load is applied on the headform via two mechanisms. These are the crushing of the foam material in the protective padding liner directly between the headform and the impact point, and the dynamical behaviour of the outer regions of the outer shell. This latter effect is strongly influenced by the three dimensional geometry of the model. High speed film recordings of a frontal impact by [6] confirmed that such dynamic behaviour of the outer regions of the helmet is actually present during an impact.

It can also be concluded that the model complies experimental findings in that lower density foams have to be used in the protective padding liner, for improving helmets performance in impact tests on flat anvils [14]. However, the influence of the stiffness of the outer shell in the parametric study showed to be too small compared to literature findings in [14].

Future directions

The energy absorption computed by the present model is lower than in reality as can be seen by the duration of the acceleration peaks. Improvements in this area are expected by the inclusion of a different material model of the Poly-Styrene foam in protective padding liner that is capable of describing the highly compressible behaviour of this foam during crushing.

The material parameters in the current model are mainly based on literature data. During the project this data proved to be non-available or not accurate enough. The parametric study showed that the headform response is very sensitive to variation in certain material properties of e.g. the protective padding liner. For this reason material tests of the helmet type to be modelled under well prescribed boundary conditions are necessary.

The current model was not capable of simulating a lateral impact due to the estimated gap between the protective padding liner and the headform. It is expected that the addition of a comfort padding liner model represents a solution to this problem by introducing friction at areas remote from the point of impact.

Also the current model needs additional validation. For this reason extra parameters such as headform rotations and deformation of the outer shell should be recorded during an impact test.

For obtaining more insight into the basic (bio)mechanical processes involved in helmeted head impact, combining this three dimensional mathematical helmet model with a human head model can be the starting point. By coupling these models to the human neck model by [17] realistic boundary conditions for head motion as a result of impacts can be achieved.
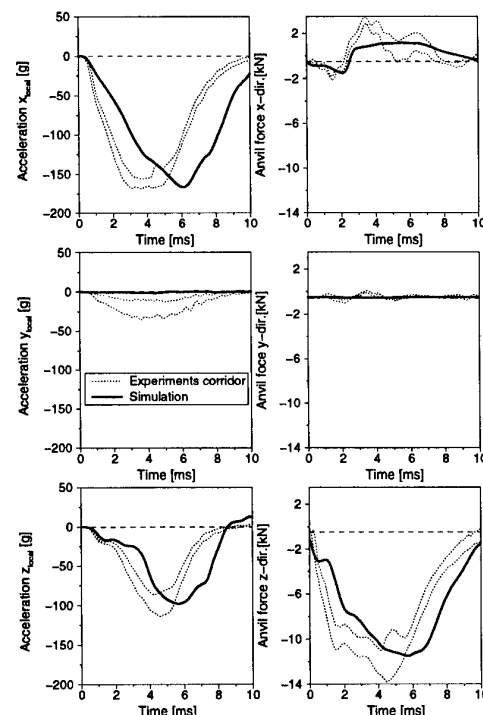
ACKNOWLEDGEMENTS

ANNEX

Figure 10   *Headform accelerations (local coor.syst.) and anvil reaction forces (global coor. syst.) for frontal impact, Experimental corridors (dotted): mean ± standard deviation.*

REFERENCES

1. Mills, N.J. and A. Gilchrist, "Mathematical modelling of the effectiveness of helmets in head protection", IRCOBI conference, Bergisch Gladbach, Germany, 1988, pp 215-226.

2. Gilchrist, A. and N.J. Mills, "Deformation analysis for motorcycle helmets", IRCOBI conference, Eindhoven, The Netherlands, 1993, pp 269-281.

3. Köstner, H. and U.W. Stöcker, "Improvement of the protective effects of motorcycle helmets based on a mathematical study", IRCOBI conference, Bergisch Gladbach, Germany, 1988, pp 195-213.

4. Yettram A.L., N.P.M. Godfrey and B.P. Chinn, "Materials for motorcycle crash helmets - a finite element parametric study",*in* "Plastics, Rubber and Composites Processing and Applications 22, 1994, pp 215-221.

5. Blokspoel, A., "De verkeersonveiligheid in 1988", in Dutch, report R-89-34, Institute for Road Safety Research, SWOV, The Netherlands, 1989.

6. Beusenberg, M.C. and R. Happee, "An experimental evaluation of crash helmet design and effectiveness in standard impact tests", IRCOBI conference, Eindhoven, The Netherlands, 1993, pp 308-323.

7. TNO Crash-Safety Research Centre, "MADYMO user's manual version 5.2", Delft, The Netherlands, 1986.

8. United Nations, "Regulation No.22:' Uniform provisions concerning the approval of protective helmets and their visors for drivers and passengers of motorcycles and mopeds; including 04 series of amendments', Geneva, SUI, 1994.

9. Mills, N.J. and A. Gilchrist, "The effectiveness of foams in bicycle and motorcycle helmets", in "Accid. Anal. & Prev.", Vol 23, Nos. 2/3, 1991, pp 153-163.

10. Miltz, J., O. Ramon and S. Mizrahi, "Mechanical behaviour of closed cell plastic foams used as cushioning materials", Journal of applied polymer science, vol.28, 1989, pp 281-290.

11. Mills, N.J. and A. Gilchrist, "Motorcycle helmet shell optimisation", Proc. Association for Advancement of Automotive Medicine conference, Portland, Oregon, 1992, pp 149-162.

12. TNO Crash-Safety Research Centre, "MADYMO Database Manual, Version 5.2", Delft, The Netherlands, 1996, p 18.

13. Philippens M., J.J. Nieboer and J. Wismans, TNO Road-Vehicles Research Institute "An Advanced Database of the 50th Percentile Hybrid III Dummy", SAE Int. Congress and Exposition, Detroit, 1991, SAE 910813.

14. Hopes, P.D. and B.P. Chin, "Helmets: a new look at design and possible protection", IRCOBI conference, Stockholm, 1989, pp 39-54.

15. Van Dorp, T., "Solid foundations with styrocell expanded polystyrene", Shell, Preprint South Asian Building, 1989, pp 36-43.

16. Ramon, O. and J. Miltz, "Prediction of dynamic properties of plastic foams from constant-strain rate measurements", Journal of applied polymer science, vol. 40, 1990, p 1686.

17. De Jager M., A. Sauren, J. Thunnissen and J. Wismans, "A Global and a Detailed Mathematical Model for Head-Neck Dynamics", STAPP Car Crash Conference Proceedings, 1996, pp 269-281.

REPORT DOCUMENTATION PAGE

1. Recipient's Reference	2. Originator's Reference AGARD-CP-597	3. Further Reference ISBN 92-836-1062-8	4. Security Classification of Document UNCLASSIFIED/ UNLIMITED

5. Originator Advisory Group for Aerospace Research and Development
North Atlantic Treaty Organization
7 rue Ancelle, 92200 Neuilly-sur-Seine, France

6. Title Impact Head Injury: Responses, Mechanisms, Tolerance, Treatment and
Countermeasures

7. Presented at/sponsored by
The Aerospace Medical Panel Specialists' Meeting held in Mescalero,
New Mexico, USA, 7-9 November 1996.

8. Author(s)/Editor(s) Multiple	9. Date November 1997
10. Author's/Editor's Address Multiple	**11. Pages** 242

12. Distribution Statement There are no restrictions on the distribution of this document.
Information about the availability of this and other AGARD
unclassified publications is given on the back cover.

13. Keywords/Descriptors

Head (anatomy)	Risk	Constraints
Injuries	Evaluation	Countermeasures
Brain damage	Acceleration stresses (physiology)	Computerized simulation
Impact	Helmets	Aviation accidents
Biodynamics	Headgear	Motor vehicle accidents
Skull	Protective clothing	Dynamic response
Bone fractures	Epidemiology	Treatment
Models	Flight crews	Tolerances (physiology)
Finite element analysis	Standards	Energy absorption
		Design

14. Abstract

These proceedings include the Technical Evaluation Report, a Keynote Address, and 23 invited papers, of the Specialists' Meeting sponsored jointly by the AGARD Aerospace Medical Panel, the Stapp Car Crash Conference Advisory Committee and the Society of Automotive Engineers. It was held at Mescalero, NM, from 7-9 November 1996.

Severe head injury resulting from vehicular accidents is a major concern to military and civilian health care workers. Significant advances have been made in the understanding of the causes of severe brain injury and in the factors, both direct and indirect, that contribute to the pathophysiological changes that follow from a severe head injury. Moreover, advances in design and the proper use of countermeasures can significantly reduce head injuries causing death. This Specialists' Meeting addressed the issues of severe head injury from the point of view of:
(a) the dynamic response of the head during impacts; (b) brain injury mechanisms in diffuse axonal injury; (c) physical and computer models for assessing injury severity; (d) human tolerance and injury criteria; (e) head injury assessment and treatment; (f) epidemiology in head injury mishaps; (g) harmonization and enforcement of standards for protective head gear; (h) personal protective systems in aircraft; and (i) computer simulations for optimizing head impact protective designs.

These proceedings will be of interest to military and civilian medical professionals, accident investigators, safety engineers and research scientists concerned with safety issues in vehicular crash protection. They will also benefit the research manager and scientist or flight surgeon requiring a state-of-the-art review of relevant research in the field of impact head protection.